STATE-DEPENDENT CORTICAL NETWORK DYNAMICS

Kristin K. Sellers

A dissertation submitted to the faculty of the University of North Carolina at Chapel Hill in partial fulfillment of the requirements for the degree of Doctor of Philosophy in the Curriculum of Neurobiology of the School of Medicine.

Chapel Hill
2016

Approved by:

Regina Carelli

Flavio Frohlich

John Gilmore

Joseph Hopfinger

Ben Philpot

Garret Stuber

ABSTRACT

Kristin K. Sellers: State-dependent cortical network dynamics
(Under the direction of Flavio Frohlich)

Neuropsychiatric illness represents a major health burden in the United States with a paucity of effective treatment. Many neuropsychiatric illnesses are network disorders, exhibiting aberrant organization of coordinated activity within and between brain areas. Cortical oscillations, arising from the synchronized activity of groups of neurons, are important in mediating both local and long-range communication in the brain and are particularly affected in neuropsychiatric diseases. A promising treatment approach for such network disorders entails 'correcting' abnormal oscillatory activity through non-invasive brain stimulation. However, we lack a clear understanding of the functional role of oscillatory activity in both health and disease. Thus, basic science and translational work is needed to elucidate the role of oscillatory activity and other network dynamics in neuronal processing and behavior.

Organized activity in the brain occurs at many spatial and temporal scales, ranging from the millisecond duration of individual action potentials to the daily circadian rhythm. The studies comprising this dissertation focused on organization in cortex at the time scale of milliseconds, assessing local field potential and spiking activity, and contribute to understanding (1) the effects of non-invasive brain stimulation on behavioral responses, (2) network dynamics within and across cortical areas during different states, and (3) how oscillatory activity organizes spiking activity locally and long-range during sustained attention. Taken together, this work provides insight into the physiological organization of network dynamics and can provide the basis for future rational design of non-invasive brain stimulation treatments.

To my parents, who taught me that hard work is not always rewarded, but that it is worth it. Who taught me to never settle. Who showed me passion.

ACKNOWLEDGEMENTS

This was only made possible by the mentors, colleagues, collaborators, and live-balancing friends and family that encouraged me through graduate school. First and foremost, I thank my mentor and advisor Flavio Frohlich. You showed me how to do science from the ground up and devoted your life energy to my success. Thank you for helping me find my scientific voice. I thank the present and past members of the Frohlich Lab. In particular, the ferret team of Chunxiu Yu, Yuhui Li, Iain Stitt, and Charles Zhou has been integral to my growth as a scientist. I thank other members of the Frohlich lab, Sankar Alagapan, Morgan Alexander, Michael Boyle, Franz Hamilton, Guoshi Li, Courtney Lugo, Caroline Lustenberger, Philipp Lustenberger, Juliann Mellin, Jessica Page, Betsy Price, and Steve Schmidt, I could always count on you for helpful input or a good laugh.

I would like to thank my committee, Regina Carelli, John Gilmore, Joseph Hopfinger, Ben Philpot, and Garret Stuber, for your guidance and knowledgeable perspective. I thank my collaborators, Jennifer Bizley, Susi Radke-Schuller, Bradley Vaughn, Michael Wibral, James Williams, Eric Youngstrom, Axel Hutt, Angel Peterchev, and Won Hee Lee, for your generous contribution to my work. I would also like to thank an enabler of great science, Vladimir Ghukasyan.

Thank you to the undergraduate and post-baccalaureate research assistants who committed to the Frohlich Lab and generously gave of their time to help with the less glamorous aspects of experimental science, Carrington Merritt, Matthew Wilson, Jeffrey Saelens, Taylor Rosenfeld, Davis Bennett, Jinghao Lu, Amanda Kramer, Molly Cowen, Helen Powell, Stephanie Belhorn; I hope the spark of curiosity about how things works grows stronger. Thank you to Nikki Crowley, Elliott Robinson, and Michael Goy for your scientific and personal encouragement. A special thank you to my running friends, Marley Lawrence, Lauren Osborne, Becca Krouse, Mariana Lucena, and Jay Smith for the many early morning and late night miles.

I thank my parents for their unwavering support and love. Just as you taught me, I kept asking questions. Finally, I thank Pavel Krajcevski. You were there from day one and held my hand through the best of it and the worst. This wouldn't have been possible without you.

TABLE OF CONTENTS

LIST OF TABLES

LIST OF FIGURES

LIST OF ABBREVIATIONS

ADHD	Attention deficit hyperactivity disorder
BDNF	Brain-derived neurotrophic factor
CNS	Central nervous system
CSD	Current source density
DLPFC	Dorsolateral prefrontal cortex
DSM	Diagnostic and Statistical Manual of Mental Disorders
ECoG	Electrocorticography
EEG	Electroencephalogram
fMRI	Functional magnetic resonance imaging
FSIQ	Full-scale IQ
IRB	Institutional Review Board
IQ	Intelligence quotient
ITPC	Inter-trial phase coherence
LFP	Local field potential
MEP	Motor-evoked potential
MRI	Magnetic resonance imaging
MU	Multi-unit
NIH	National Institute of Health
NIMH	National Institute of Mental Health
PFC	Prefrontal cortex
PLV	Phase-locking value
PPC	Posterior parietal cortex
PRI	Perceptual reasoning index
PSI	Processing speed index
RDoC	Research Domain Criteria
so-tDCS	Slow-oscillating transcranial direct current stimulation

SFC	Spike-field coherence
SU	Single unit
tACS	Transcranial alternating current stimulation
TCS	Transcranial current stimulation
tDCS	Transcranial direct current stimulation
TMS	Transcranial magnetic stimulation
tRNS	Transcranial random noise stimulation
USDA	United States Department of Agriculture
VCI	Verbal comprehension index
V1	Primary visual cortex
WAIS-IV	Wechsler Adult Intelligence Scale, Fourth Edition
WM	Working memory
WMI	Working memory index

CHAPTER 1: INTRODUCTION

Mental illness is estimated to affect approximately 20 - 32% of adults in the United States (Bagalman & Napili, 2015; T. Insel, 2015). Along with devastating burden on individuals and families, the estimated U.S. national expenditure for mental health care in 2012 was $467 billion (including direct costs, loss of earnings, and disability benefits, excluding incarceration, homelessness, comorbid conditions, and early mortality) (T. Insel, 2015; T. R. Insel, 2008). Substantial efforts in research and development have led to only relatively minor improvements in managing symptoms. Two key challenges in developing effective treatments have been unknown mechanisms underlying the diseases and the diverse symptomology associated with these conditions. In recognition that most of these conditions stem from altered biology, the term 'neuropsychiatric disorders' has come to refer to mental or neurological disorders that stem from a neurobiological component (Miyoshi, 2011). This definition includes a large and diverse set of illnesses, including but not limited to Alzheimer's disease, schizophrenia, depression, bipolar disorder, traumatic brain injury, brain tumor, cognitive disorders, seizure disorder, psychosis, and attentional disorders. While progress has been made in identifying the pathophysiology in these diseases, there are no complete models of the disease process. Relatedly, no identifiable biomarkers, or measurable entity to indicate the presence of disease, have been identified. These limitations have precluded adoption of the standard treatment-development approaches used by other branches of medicine. Furthermore, overlapping categories of neuropsychiatric, neuropsychological, and neurological symptoms often manifest concurrently. Symptoms include alteration to cognition, affect and behavior, language, reflexes, motor and sensory functions, and the manifestation of hallucinations and delusions. The complexity of symptoms in multiple domains (cognition, mood, social interaction) has complicated treatment development.

To facilitate studying neuropsychiatric illnesses, the National Institute of Mental Health established the Research Domain Criteria (RDoC). This research framework creates categories, or domains, of

functioning which are biologically valid. In essence, the goal of this framework is to provide a system for understanding and diagnosing mental illnesses based on the (ab)normal functioning of the brain. At the core of this approach is a mechanistic understanding of brain function underlying behavior. Thus, looking at activity in the healthy brain is a fruitful first step towards developing treatments for neuropsychiatric disorders.

In the brain, populations of neurons in individual areas are specialized to perform a set of functions or computations. Specialization is mediated by factors such as connectivity both locally and with other brain areas, organization of neurons, neuron species, and density. For example, visual cortex is optimized to represent the spatial world around us; thus, the neurons are organized in a retinotopic map to form a 2D representation of the visual image formed on the retina (Daniel & Whitteridge, 1961; Tootell, Silverman, Switkes, & De Valois, 1982). Multiple, specialized areas work together and form networks which can mediate complex processes and behavior (Sporns, Tononi, & Edelman, 2000). Elaborating on the above example of visual cortex, multiple features of an object are processed in parallel by different specialized areas; these visual features can then be integrated with input from other sensory modalities, as well as previous experience, expectancy, and higher-order factors such as attention (Uhlhaas & Singer, 2006).

The brain is organized into both structural and functional networks. Structural networks are defined by anatomical connections, or the synapsing of neurons and the physical connections of axons. These networks can change over time, but at a relatively slow time scale (hours to days) (Sporns, 2013). In contrast, functional networks are defined by coordinated activity. Functional networks can be assessed using functional connectivity or effective connectivity metrics. Functional connectivity assesses the statistical relationship of recorded brain activity between areas to determine if the activity is correlated. Effective connectivity assesses directed effects between brain areas, in essence trying to determine a causal ‘direction’ of action. Both functional connectivity and effective connectivity are highly time-dependent, and can change over tens to hundreds of milliseconds.

The consideration of functional brain networks is intimately related to abundant evidence for the importance of coordinated activity within and across networks for brain functioning. This coordination exists at multiple temporal and spatial scales. In this body of work, I focus on organization in the cortex at

the time scales of millisecond, relating fluctuations in the electrical potential in the extracellular space around neurons (local field potential, LFP) with action potential firing (single unit , SU, and multiunit, MU, activity). A key feature of the LFP recorded in the brain is the rhythmic fluctuation in voltage; when converted to the frequency domain, this allows for investigation of oscillations. Interactions of oscillations at multiple frequencies (commonly measured in Hz, or cycles per second) as well as with spiking activity, can occur within brain regions (local areas, on the order of 100s of microns) and across regions (separated by millimeters to centimeters). Importantly, the activity in the brain changes over time, based on behavioral demands, context, and internal state; thus, all of the aforementioned interactions are nonstationary.

The first recordings of oscillatory activity in cortex were conducted by Hans Berger using electroencephalogram (EEG) (Berger, 1929). His initial observations that brain activity fluctuates in this coordinated way, and that a specific rhythm of activity was modulated when eyes were opened or closed, paved the way for a century of work following. Historically, oscillations have been grouped into discrete frequency bands (delta: 0.5 to 4 Hz, theta: 4-8 Hz, alpha: 8 – 12 Hz, beta: 12 – 30Hz, gamma: 30 - ~200 Hz). There remains debate as to whether distinct frequency cut-offs should be used, or whether the delimitation of oscillations should depend on a consistent biological mechanism of generation (Uhlhaas, Haenschel, Nikolic, & Singer, 2008). This debate aside, in general, synchronization of brain areas that are more distant occurs in lower frequencies (theta, alpha, and beta frequencies) whereas short-range synchronization is more commonly found in higher gamma frequencies (Kopell, Ermentrout, Whittington, & Traub, 2000; von Stein, Chiang, & Konig, 2000; von Stein & Sarnthein, 2000). In addition, lower frequency oscillations can aid in the organization of higher frequency activity, termed cross-frequency coupling (Canolty & Knight, 2010). Cross-frequency coupling between theta and gamma activity appears to act in a number of systems to encode units of information while preserving their order (J. Lisman, 2005; J. E. Lisman & Jensen, 2013). This is achieved because a set number of gamma cycles occur during each theta cycle. Ensembles of neurons encoding specific elements fire during each of the gamma cycles. Thus, the theta oscillation can act as an absolute reference for the serial organization of the set of represented items. Oscillations in a given frequency band can also encode information independently. In the hippocampus, spatial coding and the accurate representation of movement trajectories is facilitated by

place cells shifting their preferred phase of firing relative to the theta oscillation as a function of position in the physical environment (O'Keefe & Recce, 1993). Substantial work in visual cortex has demonstrated correlations between gamma oscillations and effective perceptual binding of multiple features of visual space (Engel & Singer, 2001; Honkanen, Rouhinen, Wang, Palva, & Palva, 2015; Tallon-Baudry & Bertrand, 1999). Taken together, a body of work has now convincingly demonstrated that oscillations (measured at the scalp level of the EEG or invasively at the LFP level) at different frequencies are correlated with a variety of cognitive and behavioral processes and may be critical for the organization of network activity.

More recent work modulating network dynamics or oscillatory activity has demonstrated causative links with behavior. Demonstrating causative links between brain activity and behavior requires perturbation of brain activity in a relatively targeted or known manner and corresponding measurement of behavioral outcomes. In animal models, the use of optogenetics and Designer Receptors Exclusively Activated by Designer Drugs (DREADDS) has greatly advanced the dissection of circuitry involved in multiple behaviors and processes (Deisseroth, 2014; Steinberg, Christoffel, Deisseroth, & Malenka, 2015; Urban & Roth, 2015). Pharmacological or genetic manipulations can also be applied to alter the behavior of neuronal populations which generate specific oscillatory activity. A comprehensive review of this literature is beyond the scope of this document. In humans where such methods are not appropriate, the use of non-invasive brain stimulation allows for the perturbation of brain activity. A number of different technologies exist: in transcranial direct current stimulation (tDCS), transcranial alternating current stimulation (tACS), and transcranial random noise stimulation (tRNS), a weak electric current is passed between two or more electrodes which are placed at the level of the scalp; with transcranial magnetic stimulation (TMS), a magnetic coil placed above the scalp generates an electric current. Because of technological limitations (e.g. electrical artifacts), the simultaneous acquisition of electrophysiological recordings during stimulation is difficult. However, electrophysiological recordings immediately following stimulation can also be used to provide useful information about the causal relationship of network dynamics and behavior. In the first demonstration of direct causality between a physiological oscillation and concurrent motor behavior in healthy humans, authors found that 20 Hz tACS entrained cortical activity in the beta frequency band and slowed voluntary movement (Pogosyan, Gaynor, Eusebio, &

Brown, 2009). In another investigation of oscillatory activity, EEG recordings showed that TMS caused local entrainment of natural alpha oscillations (Thut et al., 2011). 10 Hz tACS successfully increased local alpha activity and improved target detection accuracy in a visual perception task (Helfrich et al., 2014). Immediately following anodal tDCS of the left dorsolateral prefrontal cortex (DLPFC) and cathodal tDCS of the contralateral supraorbital region, participants showed reduced delta activity accompanied with improved working memory task performance (Keeser et al., 2011). Emerging with these developments has been the importance of context in shaping network dynamics. In a study where participants kept endogenous alpha oscillations low or high through keeping eyes open or closed, respectively, tACS was administered at the individual alpha frequency; investigators found that only in conditions of low endogenous power did tACS enhance alpha power, while there was no increase under conditions of high endogenous power (Neuling, Rach, & Herrmann, 2013).

Such consideration of context and current activity patterns has been referred to as ‘state’. The term ‘state’ has many meanings in neuroscience. This term was originally applied in relation to the sleep cycle; however, as different motifs of activity during wakefulness were discovered, the use of the term has expanded. Here, I adopt the conceptually broad definition of endogenously-generated processing modes which are modulated according to internal factors. In essence, the brain is not simply a stimulus-driven machine, but rather alters processing as a function of motivation, previous experience, expectancy, physiological status, and myriad other factors. Cortical LFP can reflect a continuum of states ranging from prominent low-frequency fluctuations during synchronized activity to the absence of these fluctuations in a desynchronized state (Harris & Thiele, 2011). Sensory responses to identical stimuli vary as a function of such state in visual cortex (Scholvinck, Saleem, Benucci, Harris, & Carandini, 2015), auditory cortex (Kisley & Gerstein, 1999), and somatosensory cortex (Poulet & Petersen, 2008). Based on the definition applied here, behavior can also define different states. Animals presented with the same tones during a passive period or an active discrimination task showed markedly greater modulation in firing rate in frontal cortex during the active discrimination task (Fritz, David, Radtke-Schuller, Yin, & Shamma, 2010). Differences in state such as awake stillness vs. locomotion also altered visual responses to identical stimuli (Niell & Stryker, 2010). In humans, passive listening vs. an auditory working memory task differentially evoked cross-frequency coupling between theta phase and high gamma amplitude (Canolty

et al., 2006). Substantial work has also been conducted looking at differences in responses during states of attention vs inattention, finding that gamma synchronization increases during attention (Desimone & Duncan, 1995; Fries, Reynolds, Rorie, & Desimone, 2001). As a whole, this field of work demonstrates that network dynamics are state-dependent, and state must actively be considered when assessing coordinated activity in the brain.

Of interest for elucidating the neurobiological mechanism of neuropsychiatric disorders, individuals with these diseases show abnormal coordination of network activity, both during rest and cognitive tasks. Schizophrenia is hypothesized to be related to impaired neural synchrony, particularly in the beta and gamma frequency oscillations (Uhlhaas & Singer, 2006). Individuals with autism were found to exhibit reduced functional connectivity between Wernicke's and Broca's language areas, possibly related to the disordered language observed in autism (Just, Cherkassky, Keller, & Minshew, 2004). Disease states can also be associated with an excess of synchrony; patients with Parkinson's disease exhibit increased beta oscillations, which are thought to relate to akinesia symptoms (Schnitzler & Gross, 2005). Other work has posited that it is not the excess beta oscillations per se that is problematic, but the disruption to the balance of synchronization and desynchronization (Courtemanche, Fujii, & Graybiel, 2003; Kuhn et al., 2004)

Overall, work conducted using computational models, animals, and recordings in humans has demonstrated that brain activity organizes within and across areas. These networks exhibit dynamics in activity at the level of action potential firing and oscillations. Taken together, the causative role of oscillations in behavior and the observation of abnormal oscillatory activity in neuropsychiatric illnesses has led to a broad hypothesis: If cortical oscillations are involved in organized processing and found to be abnormal in patients with neuropsychiatric diseases, can modulating these oscillations be effective at 'correcting' abnormal activity found in disease states, thereby alleviating disease-related symptoms? A number of questions stem from this broad hypothesis. How do oscillations relate to specific behaviors in healthy individuals? Do these oscillations and behaviors correlate with abnormal activity and symptoms in disease? What are the appropriate oscillations to target? What are the state-dependent effects? How can oscillations be modulated? The work composing this dissertation does not attempt to answer all these questions, but rather provides a small piece toward a final answer.

In these basic science and translational investigations, I conducted studies in an intermediate animal model and healthy human participants. Combinations of electrophysiology and behavior/psychophysics were used to assess cortical network dynamics in a variety of states. Ferrets were selected for invasive electrophysiology for a number of reasons. These animals exhibit a gyrencephalic cortex similar to humans, a highly developed visual system, and cortical association areas such as prefrontal cortex. Studies fell into one or more of the following three categories:

1) Assessment of the effects of non-invasive brain stimulation on behavioral responses.
2) Characterization of network dynamics within and across cortical areas during different states (awake, anesthetized, spontaneous activity, visual/auditory stimulation).
3) Investigation of network dynamics within and between cortical areas during a sustained attention task.

First, I present a study assessing the effect of tDCS on cognitive function, assessed by a common intelligence quotient (IQ) test (Chapter 2). We found that this form of modulation, which does not take into account the oscillations underlying cognitive processing or the state of the brain, was detrimental to performance compared to sham stimulation. I then provide a review of current studies using tACS to target cognitive systems, organized according to RDoC (Chapter 3). Given the established interest and importance of better understanding network dynamics for the rational design of non-invasive brain stimulation paradigms, I then present a set of studies looking at network dynamics in an animal model. Characterization of network dynamics was conducted in prefrontal cortex (PFC) and primary visual cortex (V1) to assess differences during states defined by wakefulness and anesthesia (Chapter 4), during sensory stimulation (Chapter 5), and in awake animals during rest or naturalistic visual stimulation (Chapter 6). I next present a study assessing the dynamics within and between two cortical regions (PFC and posterior parietal cortex, PPC) during a sustained attention task, in particular focusing on local and long-range organization of spiking activity by oscillatory activity (Chapter 7). I conclude with a brief general discussion (Chapter 8).

REFERENCES

Bagalman, E., & Napili, A. (2015). Prevalence of Mental Illness in the United States: Data Sources and Estimates: Congressional Research Service.

Berger, H. (1929). Über das Elektrenkephalogramm des Menschen. *Archiv für Psychiatrie und Nervenkrankheiten, 87*(1), 527-570.

Canolty, R. T., Edwards, E., Dalal, S. S., Soltani, M., Nagarajan, S. S., Kirsch, H. E., . . . Knight, R. T. (2006). High gamma power is phase-locked to theta oscillations in human neocortex. *Science, 313*(5793), 1626-1628. doi: 10.1126/science.1128115

Canolty, R. T., & Knight, R. T. (2010). The functional role of cross-frequency coupling. *Trends Cogn Sci, 14*(11), 506-515. doi: 10.1016/j.tics.2010.09.001

Courtemanche, R., Fujii, N., & Graybiel, A. M. (2003). Synchronous, focally modulated beta-band oscillations characterize local field potential activity in the striatum of awake behaving monkeys. *J Neurosci, 23*(37), 11741-11752.

Daniel, P. M., & Whitteridge, D. (1961). The representation of the visual field on the cerebral cortex in monkeys. *J Physiol, 159*, 203-221.

Deisseroth, K. (2014). Circuit dynamics of adaptive and maladaptive behaviour. *Nature, 505*(7483), 309-317. doi: 10.1038/nature12982

Desimone, R., & Duncan, J. (1995). Neural mechanisms of selective visual attention. *Annu Rev Neurosci, 18*, 193-222. doi: 10.1146/annurev.ne.18.030195.001205

Engel, A. K., & Singer, W. (2001). Temporal binding and the neural correlates of sensory awareness. *Trends Cogn Sci, 5*(1), 16-25.

Fries, P., Reynolds, J. H., Rorie, A. E., & Desimone, R. (2001). Modulation of oscillatory neuronal synchronization by selective visual attention. *Science, 291*(5508), 1560-1563. doi: 10.1126/science.291.5508.1560

Fritz, J. B., David, S. V., Radtke-Schuller, S., Yin, P., & Shamma, S. A. (2010). Adaptive, behaviorally gated, persistent encoding of task-relevant auditory information in ferret frontal cortex. *Nat Neurosci, 13*(8), 1011-1019. doi: 10.1038/nn.2598

Harris, K. D., & Thiele, A. (2011). Cortical state and attention. *Nat Rev Neurosci, 12*(9), 509-523. doi: 10.1038/nrn3084

Helfrich, R. F., Schneider, T. R., Rach, S., Trautmann-Lengsfeld, S. A., Engel, A. K., & Herrmann, C. S. (2014). Entrainment of brain oscillations by transcranial alternating current stimulation. *Curr Biol, 24*(3), 333-339. doi: 10.1016/j.cub.2013.12.041

Honkanen, R., Rouhinen, S., Wang, S. H., Palva, J. M., & Palva, S. (2015). Gamma Oscillations Underlie the Maintenance of Feature-Specific Information and the Contents of Visual Working Memory. *Cereb Cortex, 25*(10), 3788-3801. doi: 10.1093/cercor/bhu263

Insel, T. (2015). Director's Blog: Mental Health Awareness Month: By the Numbers.

Insel, T. R. (2008). Assessing the economic costs of serious mental illness. *Am J Psychiatry, 165*(6), 663-665. doi: 10.1176/appi.ajp.2008.08030366

Just, M. A., Cherkassky, V. L., Keller, T. A., & Minshew, N. J. (2004). Cortical activation and synchronization during sentence comprehension in high-functioning autism: evidence of underconnectivity. *Brain, 127*(Pt 8), 1811-1821. doi: 10.1093/brain/awh199

Keeser, D., Padberg, F., Reisinger, E., Pogarell, O., Kirsch, V., Palm, U., . . . Mulert, C. (2011). Prefrontal direct current stimulation modulates resting EEG and event-related potentials in healthy subjects: a standardized low resolution tomography (sLORETA) study. *Neuroimage, 55*(2), 644-657. doi: 10.1016/j.neuroimage.2010.12.004

Kisley, M. A., & Gerstein, G. L. (1999). Trial-to-trial variability and state-dependent modulation of auditory-evoked responses in cortex. *J Neurosci, 19*(23), 10451-10460.

Kopell, N., Ermentrout, G. B., Whittington, M. A., & Traub, R. D. (2000). Gamma rhythms and beta rhythms have different synchronization properties. *Proc Natl Acad Sci U S A, 97*(4), 1867-1872.

Kuhn, A. A., Williams, D., Kupsch, A., Limousin, P., Hariz, M., Schneider, G. H., . . . Brown, P. (2004). Event-related beta desynchronization in human subthalamic nucleus correlates with motor performance. *Brain, 127*(Pt 4), 735-746. doi: 10.1093/brain/awh106

Lisman, J. (2005). The theta/gamma discrete phase code occuring during the hippocampal phase precession may be a more general brain coding scheme. *Hippocampus, 15*(7), 913-922. doi: 10.1002/hipo.20121

Lisman, J. E., & Jensen, O. (2013). The theta-gamma neural code. *Neuron, 77*(6), 1002-1016. doi: 10.1016/j.neuron.2013.03.007

Miyoshi, K. (2011). Characteristics of Clinical Manifestations of Neuropsychiatric Disorders. *Psychiatry and the Neurosciences*, 87-92.

Neuling, T., Rach, S., & Herrmann, C. S. (2013). Orchestrating neuronal networks: sustained after-effects of transcranial alternating current stimulation depend upon brain states. *Front Hum Neurosci, 7*, 161. doi: 10.3389/fnhum.2013.00161

Niell, C. M., & Stryker, M. P. (2010). Modulation of visual responses by behavioral state in mouse visual cortex. *Neuron, 65*(4), 472-479. doi: 10.1016/j.neuron.2010.01.033

O'Keefe, J., & Recce, M. L. (1993). Phase relationship between hippocampal place units and the EEG theta rhythm. *Hippocampus, 3*(3), 317-330. doi: 10.1002/hipo.450030307

Pogosyan, A., Gaynor, L. D., Eusebio, A., & Brown, P. (2009). Boosting cortical activity at Beta-band frequencies slows movement in humans. *Curr Biol, 19*(19), 1637-1641. doi: 10.1016/j.cub.2009.07.074

Poulet, J. F., & Petersen, C. C. (2008). Internal brain state regulates membrane potential synchrony in barrel cortex of behaving mice. *Nature, 454*(7206), 881-885. doi: 10.1038/nature07150

Schnitzler, A., & Gross, J. (2005). Normal and pathological oscillatory communication in the brain. *Nat Rev Neurosci, 6*(4), 285-296. doi: 10.1038/nrn1650

Scholvinck, M. L., Saleem, A. B., Benucci, A., Harris, K. D., & Carandini, M. (2015). Cortical state determines global variability and correlations in visual cortex. *J Neurosci, 35*(1), 170-178. doi: 10.1523/JNEUROSCI.4994-13.2015

Sporns, O. (2013). Structure and function of complex brain networks. *Dialogues Clin Neurosci, 15*(3), 247-262.

Sporns, O., Tononi, G., & Edelman, G. M. (2000). Connectivity and complexity: the relationship between neuroanatomy and brain dynamics. *Neural networks : the official journal of the International Neural Network Society, 13*(8-9), 909-922.

Steinberg, E. E., Christoffel, D. J., Deisseroth, K., & Malenka, R. C. (2015). Illuminating circuitry relevant to psychiatric disorders with optogenetics. *Curr Opin Neurobiol, 30*, 9-16. doi: 10.1016/j.conb.2014.08.004

Tallon-Baudry, C., & Bertrand, O. (1999). Oscillatory gamma activity in humans and its role in object representation. *Trends Cogn Sci, 3*(4), 151-162.

Thut, G., Veniero, D., Romei, V., Miniussi, C., Schyns, P., & Gross, J. (2011). Rhythmic TMS causes local entrainment of natural oscillatory signatures. *Curr Biol, 21*(14), 1176-1185. doi: 10.1016/j.cub.2011.05.049

Tootell, R. B., Silverman, M. S., Switkes, E., & De Valois, R. L. (1982). Deoxyglucose analysis of retinotopic organization in primate striate cortex. *Science, 218*(4575), 902-904.

Uhlhaas, P. J., Haenschel, C., Nikolic, D., & Singer, W. (2008). The role of oscillations and synchrony in cortical networks and their putative relevance for the pathophysiology of schizophrenia. *Schizophr Bull, 34*(5), 927-943. doi: 10.1093/schbul/sbn062

Uhlhaas, P. J., & Singer, W. (2006). Neural synchrony in brain disorders: relevance for cognitive dysfunctions and pathophysiology. *Neuron, 52*(1), 155-168. doi: 10.1016/j.neuron.2006.09.020

Urban, D. J., & Roth, B. L. (2015). DREADDs (designer receptors exclusively activated by designer drugs): chemogenetic tools with therapeutic utility. *Annu Rev Pharmacol Toxicol, 55*, 399-417. doi: 10.1146/annurev-pharmtox-010814-124803

von Stein, A., Chiang, C., & Konig, P. (2000). Top-down processing mediated by interareal synchronization. *Proc Natl Acad Sci U S A, 97*(26), 14748-14753. doi: 10.1073/pnas.97.26.14748

von Stein, A., & Sarnthein, J. (2000). Different frequencies for different scales of cortical integration: from local gamma to long range alpha/theta synchronization. *Int J Psychophysiol, 38*(3), 301-313.

CHAPTER 2: TRANSCRANIAL DIRECT CURRENT STIMULATION (tDCS) OF FRONTAL CORTEX DECREASES PERFORMANCE ON THE WAIS-IV INTELLIGENCE TEST[1]

INTRODUCTION

The importance of frontal brain regions has been demonstrated for numerous cognitive processes contributing to intelligence. Dorsolateral prefrontal cortex (DLPFC), a functional area in frontal cortex, is recruited during tests of general intelligence (Duncan & Owen, 2000; Duncan et al., 2000; Esposito, Kirkby, Van Horn, Ellmore, & Berman, 1999; Prabhakaran, Smith, Desmond, Glover, & Gabrieli, 1997). The middle frontal gyrus (the anatomical location of DLPFC) has been implicated in abstracting and integrating logical relationships (Liu et al., 2012), the ability to resolve interference efficiently (Bunge, Ochsner, Desmond, Glover, & Gabrieli, 2001), and visuospatial reasoning (Krawczyk, Michelle McClelland, & Donovan, 2011). Medial of the middle frontal gyrus lies the superior frontal gyrus; the lateral part of the superior frontal gyrus has been implicated in aspects of fluid intelligence (Hampson, Driesen, Skudlarski, Gore, & Constable, 2006; Nagahama et al., 1999), while the medial portion contributes to the default mode network and exhibits deactivation and reduced blood flow during cognitive processing (Raichle et al., 2001; Shulman et al., 1997). Patients with lesions to left superior frontal gyrus demonstrate deficits in working memory compared to controls, particularly in the spatial domain (du Boisgueheneuc et al., 2006). The most anterior portion of the frontal cortex, prefrontal cortex (PFC), is activated in a performance-dependent way during reasoning and novel problem-solving tests of fluid intelligence (Gray, Chabris, & Braver, 2003). Spatial and verbal tasks requiring high general intelligence differentially increased activation of lateral PFC in comparison to control tasks (Duncan et al., 2000).

[1] This chapter previously appeared as an article in Behavioural Brain Research; doi: 10.1016/j.bbr.2015.04.031 (http://www.sciencedirect.com/science/article/pii/S0166432815002739). The original citation is as follows: **Kristin K. Sellers**, Juliann M. Mellin, Caroline M. Lustenberger, Michael R. Boyle, Won Hee Lee, Angel V. Peterchev, Flavio Frohlich (2015). Transcranial direct current stimulation (tDCS) of frontal cortex decreases performance on the WAIS-IV intelligence test. Behavioural Brain Research, 290: 32-44.

Given the widespread involvement of frontal brain areas in higher-order cognitive processing, they represent an attractive target for modulating cognitive function. The ability to both improve cognitive performance in healthy individuals and to alleviate deficits in patients with neuropsychiatric illnesses is the goal of substantial research efforts. A growing body of work has been conducted using transcranial direct current stimulation (tDCS), a form of non-invasive brain stimulation, in an attempt to modulate cognitive abilities (Cohen Kadosh, 2015; Horvath, Forte, & O, 2015; Tremblay et al., 2014). Anodal tDCS increases neural activity by depolarizing cortical neurons, whereas cathodal tDCS reduces neural activity by hyperpolarizing neurons (Nitsche & Paulus, 2000; Purpura & McMurtry, 1965). Large neuronal networks are sensitive to such weak perturbations of neuronal membrane voltage caused by these electric fields (Ali, Sellers, & Frohlich, 2013; Dayan, Censor, Buch, Sandrini, & Cohen, 2013; Frohlich & McCormick, 2010; Ozen et al., 2010; Reato, Rahman, Bikson, & Parra, 2010). Changes in neuronal excitability induced by tDCS outlast the duration of the stimulation (Nitsche & Paulus, 2000), likely through the recruitment of BDNF-dependent plasticity (Antal et al., 2010; Chaieb, Antal, Ambrus, & Paulus, 2014; Fritsch et al., 2010).

The reported effects of tDCS on cognitive abilities are diverse, with seemingly conflicting reports of increased and decreased performance. The majority of studies conducted to date only used one behavioral assay to test a specific facet of cognitive processing. To our knowledge, no one study has conducted a comprehensive battery of cognitive testing with the same study population in order to assess the effects of tDCS on performance. Thus, we here asked if tDCS affects performance on a comprehensive assay of overall cognition, a standardized Intelligence Quotient (IQ) test. One of the most widely utilized IQ tests is the Wechsler Adult Intelligence Scale, Fourth Edition (WAIS-IV). Use of the WAIS-IV test is advantageous because separate index scores can be calculated to provide insight into more fine-grained components of intelligence. Previous work has suggested that the different aspects of intelligence probed by the WAIS-IV indices and subtests do not share a single common neuronal substrate (Glascher et al., 2009).

Because of the broad activation of frontal areas, we first tested if bilateral tDCS over DLPFC changed performance on the WAIS-IV. We hypothesized that by targeting frontal areas with tDCS, we would induce improved performance. Interestingly, the effects of stimulation were detrimental to IQ,

specifically in tasks of perceptual reasoning. We then conducted a second study to test the effects of unilateral right or left tDCS on performance on the WAIS-IV; similar performance decreases were found with additional evidence for more pronounced decreases for right tDCS.

METHODS

Participants

In total, 44 healthy adults were recruited for this study (21 males, 23 females, mean age = 22.1 years, SD = 4.72 years) from the University of North Carolina at Chapel Hill community. The study was divided into two consecutive substudies for which participants were recruited separately. For Substudy 1, 22 participants participated in Session 1 of IQ testing, and 21 of these participants returned for Session 2 and received either bilateral tDCS or sham tDCS with subsequent repeat IQ testing. One participant could not be contacted for Session 2 and was therefore excluded from the study. For Substudy 2, 22 participants completed Session 1 of IQ testing, and 20 of these participants returned for Session 2 and received either right tDCS (anodal electrode on right hemisphere) or left tDCS (anodal electrode on left hemisphere) with subsequent repeat IQ testing. Analysis was conducted on the 20 participants who completed both sessions. No participants took part in both Substudy 1 and Substudy 2. By self-report, participants did not have a history of neurologic or psychiatric illness, were not currently using medication for a neurologic or psychiatric illness, were not currently undergoing counseling or psychotherapy treatment, did not have a first degree relative with a neurologic or psychiatric condition, had never undergone brain surgery, had no brain devices/implants, did not have any cardiovascular diseases, and were not pregnant. All participants signed written consent prior to participation. This study was approved by the UNC – Chapel Hill IRB.

Experimental Design

Both Substudy 1 and Substudy 2 followed a double-blind, between-subjects design with repeated-measure testing of IQ. In both substudies, participants completed the full WAIS-IV (Pearson Education, Inc., San Antonio, TX), as detailed below during the initial study visit (Session 1, baseline). Participants returned at least one week later (Session 2, mean time between sessions = 23.6 days, SD =

19.7) and received either sham or bilateral tDCS (Substudy 1, Figure 2.3A) or right or left tDCS (Substudy 2, Figure 2.3B) and immediately afterwards completed the same WAIS-IV test. At the conclusion of the Session 2, participants completed a questionnaire asking if they believed they received stimulation.

Wechsler Adult Intelligence Scale, Fourth Edition (WAIS-IV)

The WAIS-IV is a comprehensive clinical instrument for assessing intelligence of adults between the ages of 16-90 years. There has been substantial demonstration of the test's validity and reliability. The test is composed of 15 core and supplemental subtests which contribute to a composite score that represents general intellectual ability (full scale IQ, FSIQ) and scores in indices of specific cognitive areas. While the FSIQ is considered the best measure of overall cognitive ability, the test issuer recommends to further report the index scales that all contribute to the FSIQ: Verbal Comprehension Index (VCI), Perceptual Reasoning Index (PRI), Working Memory Index (WMI), and Processing Speed Index (PSI). The VCI measures verbal reasoning, verbal concept formation, and knowledge acquired from the environment (Kaufman & Lichtenberger, 2005). Strategies to solve the problems presented in this index may also utilize nonverbal factors such as forming mental pictures. The PRI measures perceptual and fluid reasoning, spatial processing, and visual-motor integration (Wechsler, 2008b). The WMI measures working memory, the ability to temporarily hold information in memory, manipulate or perform a mental operation on this information, and produce a response (Wechsler, 2008b); these processes require attention, concentration, mental control, and reasoning, and have been shown to be an essential component of higher order cognitive processes (Salthouse & Pink, 2008; Takeuchi, Taki, & Kawashima, 2010; Unsworth & Engle, 2007). The PSI provides a metric of the participant's ability to quickly and correctly scan, sequence, or discriminate simple visual information (Wechsler, 2008b); this measures incorporates short-term visual memory, attention, and visual-motor coordination (Groth-Marnat, 2003; Sattler, 2008a, 2008b). Important to note, the PSI includes cognitive decision-making or learning components, and is not simply measuring reaction time or visual discrimination.

These index scales are further composed of core and supplemental subtests as described in Table 2.1 (Sattler & Ryan, 2009; Wechsler, 2008b). The raw scores from these subtests are scaled to a metric with a mean of 10 and a standard deviation of 3, based on the given age group. Different scales

contribute to standard composite scores (i.e. VCI, PRI, WMI, PSI, and FSIQ), metrics with mean of 100 and standard deviation of 15. For our application, these metrics may be useful in isolating which facet(s) of intelligence are modulated by tDCS. All general testing, administration, and scoring guidelines were followed as prescribed by Pearson Education, Inc (Wechsler, 2008a).

Transcranial Direct Current Stimulation

For all participants, two stimulation electrodes (5x7cm, placed in saline soaked sponge sleeves) were positioned bilaterally over the middle frontal gyri, at positions F4 and F3 of the International 10-20 System. An additional single electrode located over Cz served as the cathode for both stimulation sites (Figure 2.1A). For bilateral stimulation (Substudy 1), two simultaneously triggered single channel stimulators were used to administer anodal tDCS to the frontal electrodes (NeuroConn DC-STIMULATOR PLUS, NeuroConn Ltd., Ilmenau, Germany). Both the participant and the experimenter administering stimulation and the WAIS-IV were blind to the stimulation condition until completion of the study. Bilateral stimulation consisted of 20 minutes of 2mA direct current applied to each of the frontal electrodes (Figure 2.1B, anodal current density at F3 and F4 = 0.057mA/cm^2, cathodal current density at Cz = 0.114mA/cm^2). Sham stimulation consisted of 40 seconds stimulation at 2mA in the same electrode configuration as for the bilateral stimulation, to mimic the skin sensation of bilateral stimulation (Figure 2.1C). Stimulation occurred while participants were resting but awake, sitting comfortably with eyes open. In Substudy 2, right tDCS or left tDCS was only delivered to either F4 or F3 (current density at F4, F3, and Cz = 0.057mA/cm^2), with the same duration and amplitude as used for Substudy 1. Sham stimulation (40 seconds) was delivered to the non-targeted hemisphere (Figures 2.1D-E). The current density and duration used in this study are well within currently accepted safety guidelines for tDCS (Bikson, Datta, & Elwassif, 2009). We adopted a study design that avoided stimulation during test performance since WAIS-IV test duration exceeds the maximal stimulation duration permitted by recent tDCS safety guidelines (Poreisz, Boros, Antal, & Paulus, 2007).

TDCS Electric Field Modeling

To determine which cortical structures were targeted by our stimulation paradigm, we simulated the electric field generated by the tDCS electrode configuration using a previously developed realistic finite element model of a human head incorporating heterogeneous and anisotropic tissue conductivity (Lee et al., 2012; Lee, Lisanby, Laine, & Peterchev, 2014). The head model is of a single subject (34 year old male) who did not participate in the study. Nevertheless, the simulated electric field distribution is informative of the general properties of the tDCS electrode configuration and current strength used in this study. The modeling procedure is briefly summarized below.

The model was derived from structural T1-weighted MRI images (1×1×1 mm^3 voxel). Image preprocessing included AC-PC spatial alignment, bias field correction, anisotropic diffusion filtering, and skull stripping (Lee et al., 2012). Individual tissue probability maps corresponding to gray matter, white matter, and cerebrospinal fluid (CSF) were automatically created using the segmentation tool FAST in FSL (FMRIB Analysis Group, Oxford, UK) (Zhang, Brady, & Smith, 2001). The non-brain regions were manually segmented into 11 tissue compartments including skin, muscle, skull compacta, skull spongiosa, vertebrae, spinal cord, lens, eyeball, sclera, optic nerve, and sinus, using a combination of segmentation editing tools from ITK-SNAP (Yushkevich et al., 2006) and an in-house segmentation algorithm based on thresholding and mathematical morphological operations. We modeled the tDCS sponge electrodes as rectangular cuboids with 5 cm × 7 cm surface intersecting the head (Figure 2.2). The complete 3D head model incorporating the tDCS electrodes was adaptively tessellated to produce the finite element model using the restricted Delaunay triangulation algorithm (Pons et al., 2007). The electrical conductivity of the head tissues was assigned as in (Lee et al., 2014). The electrodes were assumed to have the conductivity of saline (1.4 S/m). Constant electric current was applied to the electrode surfaces away from the head. For substudy 1, 2 mA were applied to each of the frontal electrodes and -4 mA to the posterior cathode. For substudy 2, 2 mA were applied to the frontal electrode (right and left tDCS modeled separately), -2 mA to the posterior cathode, and 0 mA to the frontal electrode contralateral to the stimulated side. Finally, the electric field was computed by solving the Laplace equation using the preconditioned conjugate solver within ANSYS (ANSYS Inc., Canonsburg, PA, USA) (Lee et al., 2012).

Data Analysis

For each administration of the WAIS-IV, raw scores were calculated for each of the 15 subtests. Age-normalized scaled scores were then determined from these raw scores in accordance with scoring guidelines provided by Pearson Testing, Inc. The scaled scores were tallied to provide sums of the scaled scores, and converted to composite scores: FSIQ, VCI, PRI, WMI, and PSI.

Statistical Analysis

Custom-written scripts in MATLAB (Mathworks, Natick, MA) and R (R Foundation for Statistical Computing, Vienna, Austria) (Team, 2014) were used for analysis. Libraries used in R included lme4 (Bates, Maechler, Bolker, & Walker, 2014) and pbkrtest (Halekoh & Hojsgaard, 2013). Wilcoxon rank-sum test was used to determine if continuous variables (age, time of day for Session 1, and time of day for Session 2) differed by stimulation condition (sham, right, left, or bilateral tDCS); chi-squared test was used to determine if categorical variables (gender) differed between stimulation conditions, and whether perception of stimulation differed between stimulation conditions.

We performed a linear mixed model analysis of the relationship between scores on the WAIS-IV and stimulation condition. We entered stimulation condition (sham, right, left, or bilateral tDCS) and session (baseline or post stimulation [post-stim]) as fixed effects, and subjects as a random effect into the model. Visual inspection of the residual plots did not reveal any obvious deviations from normality or homoscedasticity. We used the Kenward-Roger approximation to perform *F*-tests and to estimate p-values for each factor and their interaction in the mixed model (Halekoh & Hojsgaard). In the case of significant or trend level interactions, we conducted post-hoc Welch's t-tests in order to determine the source of significance. Specifically, we compared scores between stimulation conditions within each session, and then calculated the difference in scores across sessions for each stimulation condition. Significance was determined by $p<0.05$, and trend by $p<0.1$. We present both raw p-values and p-values corrected for multiple comparisons using False Discovery Rate (FDR) calculations. Unless otherwise stated, bar graphs depict the mean change in score ± sem. For each participant, the change in score was calculated between sessions (session 2 – session 1); these values were then averaged across participants.

Spearman's rank-order correlation was used to assess if the effect of stimulation was related to subtest administration order; group means of the change in score from Session 1 to Session 2 for each subtest were tested for significant correlation with subtest order (1 to 15). Spearman's rank-order correlation was also used to assess for age-dependent effects of stimulation; change in score between Session 1 and Session 2 on each WAIS-IV metric of interest for each stimulation condition was tested for significant correlation with participant age.

RESULTS

The results of both substudies are detailed below. In substudy 1, we tested the hypothesis that bilateral tDCS applied over frontal regions would improve performance on the WAIS-IV IQ test compared to sham stimulation. To our surprise, we found that bilateral tDCS had a negative effect on test performance compared to sham stimulation. Therefore, we conducted a second substudy in order to test whether the effects of right or left tDCS differed from bilateral stimulation. In agreement with our findings from substudy 1, we found that both right and left tDCS induced similar reductions in practice gains on the WAIS-IV. We present the data combined across these two substudies for a number of reasons. The WAIS-IV has been specifically designed and validated to produce reliable scores across different test administrators. In our study, there were no significant differences in baseline score between the different stimulation groups for FSIQ or any of the index scores. In addition, the similar finding of both studies (that tDCS decreased practice gains) indicates that this effect is robust. Therefore, presenting the results of the two substudies combined provides a more comprehensive view of the effects of unilateral and bilateral tDCS on a standardized assessment of IQ.

Demographic and Individual Characteristics

Participants in the stimulation groups did not differ significantly in age (sham mean = 25.7 years, sham SD = 8.41 years, right mean = 20.6 years, right SD = 2.12 years; left mean = 21.5 years, left SD = 2.27 years; bilateral mean = 20.5 years, bilateral SD = 2.02 years, Wilcoxon rank-sum test, all $p > 0.1$), time of day for Session 1 (Wilcoxon rank-sum test, all $p > 0.1$), time of day for Session 2 (Wilcoxon rank-sum test, all $p > 0.1$), or gender (sham = 5 males, 5 females; right = 4 males, 6 females; left = 6 males, 4

females; bilateral = 5 males, 6 females, $\chi^2(3, n=41) = 0.867$, $p = 0.833$). In substudy 1, 57% of participants correctly guessed whether they received brain stimulation, with chance level at 50% (possible responses were 'Yes' and 'No')(chi-square test assessing for association between stimulation condition and perception of stimulation , $\chi^2(1,N=21) = 3.82$, $p = 0.051$). In substudy 2, only 30% of participants correct guessed their stimulation condition, with change level at 25% (possible responses were 'Right side of head', 'Left side of head', 'Both sides of head', 'No stimulation')(chi-square test assessing for association between stimulation condition and perception of stimulation $\chi^2(1,N=20) = 0$, $p > 0.05$). In substudy 2, 55% of participants thought stimulation influenced their performance on the IQ test ('Do you think your performance on the IQ test was affected by the transcranial current stimulation').

Effects of Unilateral and Bilateral tDCS on WAIS-IV Scores

In the finite element simulation, our electrode montage predominantly induced electric fields in the middle and superior frontal gyri of frontal cortex (Figure 2.2). In the case of bilateral stimulation, electric fields were nearly symmetrical in both hemispheres (Figure 2.2A-D). For left tDCS, the electric field predominantly affected the left hemisphere, with limited spread into the right hemisphere (Figure 2.2E - G). Similarly, right tDCS targeted right middle and superior frontal gyri with only minimal applied electric field in the left hemisphere (Figure 2.2H - J). In order to test the effects of tDCS on intelligence, we assessed change in performance on the indices and subtests of the WAIS-IV as a function of stimulation condition. See Table 2.2 for the group means of scaled composite scores. The FSIQ is a global estimate of an individual's current level of cognitive ability, and is the most reliable and valid estimate of an individual's intellectual ability (Sattler & Ryan, 2009). In the linear mixed model assessing the effect of stimulation on FSIQ, the factor session was significant ($F(1,40) = 100$, $p < 0.001$), the factor stimulation condition was non-significant ($F(3,37) = 0.813$, $p > 0.1$), but the interaction between session and stimulation condition was significant ($F(3,37) = 4.38$, $p = 0.00979$). Post-hoc t-tests revealed that FSIQ did not differ significantly between groups at baseline (all $p > 0.1$) or after stimulation (all $p > 0.1$). However, the difference between FSIQ during post-stim and baseline was significantly different between sham and unilateral/bilateral stimulation (sham vs right tDCS: $t(17.3) = 3.63$, uncorrected $p = 0.00204$, corrected $p = 0.0079$; sham vs left tDCS: $t(17.6) = 2.28$, uncorrected $p = 0.0352$, corrected $p = 0.0790$; sham vs

bilateral tDCS: t(18.8) = 2.76, uncorrected p = 0.0127, corrected p = 0.0348). Right tDCS, left tDCS, and bilateral tDCS led to reduced practice gains compared to the sham condition (Figure 2.4: change in scores between session was calculated for each participant, and then averaged across participants, to provide mean difference in FSIQ ± SEM, sham tDCS = 9.80 ± 0.998, right tDCS = 4.10 ± 1.22; left tDCS = 6.30 ± 1.16; bilateral tDCS = 5.55 ± 1.18). Thus, unilateral and bilateral tDCS significantly reduced the practice gains in FSIQ between testing sessions compared to sham stimulation.

The WAIS also provides index scores to assess specific cognitive areas. To examine which index scale(s) contribute to the tDCS-induced effects on the FSIQ, we further performed linear mixed model analyses for each of the four index scales. The results are summarized in Table 2.3 and Figure 2.5. The factor session was significant in all indices except VCI, indicating that performance differed from Session 1 to Session 2 for the PRI, WMI, and PSI. Only VCI revealed a significant effect of the factor stimulation condition. Interestingly, only the PRI showed a significant interaction between session and stimulation condition. Post-hoc testing demonstrated that compared to sham stimulation (mean difference in PRI ± SEM = 12.1 ± 2.73), practice gains in the PRI were significantly lower following right tDCS (mean difference in PRI ± SEM = 1.90 ± 20.5, t(16.7) = 2.99, uncorrected p = 0.00837, corrected p =0.022), lower at trend level following left tDCS (mean difference in PRI ± SEM = 5.90 ± 1.82, t(15.7) = 1.89, uncorrected p = 0.0773, corrected p = 0.135), and lower at trend level following bilateral tDCS (mean difference in PRI ± SEM = 4.64 ± 2.44, t(18.51) = 2.04, uncorrected p = 0.0562, corrected p = 0.077) (Figure 2.6B). This effect was not driven by differences in baseline PRI between the groups (all p > 0.1).

Given the significant and trend-level interactions between session and stimulation condition on the PRI, we next analyzed the three subtests that comprise the PRI (Block Design, Matrix Reasoning, and Visual Puzzles). These subtests were performed consistently in the order prescribed by the WAIS-IV (Block Design: 1st, Matrix Reasoning: 4th, and Visual Puzzles: 8th subtests). Results of the linear mixed model on these subtests are summarized in Table 2.4 and Figure 2.6. Block Design and Visual Puzzles provide a significant session effect, while Matrix Reasoning had a trend level effect of session. Visual Puzzles exhibited a significant effect of stimulation condition. For Matrix Reasoning and Visual Puzzles, the interaction between session and stimulation condition was significant or significant at trend level.

Post-hoc t-tests revealed that Matrix Reasoning did not differ significantly between groups at baseline (all p>0.1). However, practice gains were dependent on the stimulation condition (Figure 2.6, mean difference in Matrix Reasoning ± SEM: sham tDCS = 1.80 ± 0.854, right tDCS = -0.200 ± 0.663, left tDCS = 1.70 ± 0.761, bilateral tDCS = -0.273 ± 0.469). Specifically, right tDCS decreased the practice gain at trend level compared to the sham condition ($t(17.0) = 1.850$, uncorrected $p = 0.0818$, corrected $p = 0.094$); bilateral tDCS also decreased practice gains at the trend level compared to sham tDCS ($t(14.1) = 2.128$, uncorrected $p = 0.0515$, corrected $p = 0.094$); practice gains were smaller following right tDCS compared to left tDCS at the trend level ($t(17.7) = -1.882$, uncorrected $p = 0.0764$, corrected $p = 0.094$); and bilateral tDCS resulted in reduced practice gains compared to left tDCS ($t(15.2) = 2.21$, uncorrected $p = 0.0431$, corrected $p = 0.094$) (Figure 2.6B).

In the case of Visual Puzzles, post-hoc t-tests indicated that right and left tDCS significantly decreased practice gains compared to the sham condition (Figure 2.6C, mean difference in Visual Puzzles ± SEM: sham tDCS = 2.60 ± 0.733, right tDCS = 0.200 ± 0.327, left tDCS = 0.400 ± 0.980, bilateral tDCS = 1.82 ± 0.807. Sham tDCS vs right tDCS: $t(12.4) = 2.99$, uncorrected $p = 0.0109$, corrected $p = 0.15$; sham tDCS vs left tDCS: $t(16.7) = 1.80$, uncorrected $p = 0.090$, corrected $p = 0.15$). No baseline differences were significant, but left vs bilateral tDCS exhibited trend-level differences at baseline ($t(16.9) = 2.05$, $p = 0.0568$).

WAIS-IV Subtest Order and Participant Age do not Explain Effects of tDCS

TDCS has been shown to induce outlasting effects on the excitability of motor cortex for multiple hours, assessed by measuring motor evoked potentials induced by transcranial magnetic stimulation pulses (Batsikadze, Moliadze, Paulus, Kuo, & Nitsche, 2013). However, no comparable physiological measurement exists to assess outlasting changes in excitability in frontal cortex. In theory, elapsed time since the end of stimulation could affect which subtests showed significant modulation based on stimulation condition. To test for this possibility, we calculated the correlation between group mean of change in score between sessions and subtest administration order. We found no significant correlation between the order of subtests and change in performance between the testing sessions for substudy 1 (Figure 2.7A: Mean of change in subtest scores, in order of subtest administration. Spearman's

correlation of change in score and subtest order was non-significant, sham tDCS: rho = -0.170, p = 0.544; bilateral tDCS: rho = -0.186, p = 0.506) or substudy 2 (Figure 2.7B, right tDCS: rho = 0.245, p = 0.379; left tDCS: rho = 0.218, p = 0.434).

Lastly, the plasticity recruited by tDCS is likely age-dependent (Fathi et al., 2010). Therefore, effects of stimulation could be masked by the age of participants. To test for this, we calculated correlations between change in scores in each stimulation group and participant age. Correlations were non-significant for all indices of the WAIS-IV and all subtests of the PRI, except for Figure Weights in the left tDCS condition (all p-values > 0.1, except Figure Weights: left, rho = 0.755, p = 0.011).

DISCUSSION

In the last decade, numerous studies have investigated whether tDCS can be used to improve cognitive abilities or alleviate deficits associated with neuropsychiatric diseases. The resulting literature is diverse, with reports of improved and/or decreased cognitive performance with stimulation in the domains of working memory, executive functioning, verbal and semantic processing, cognitive control during emotion regulation, verbal tasks, visuospatial memory, word fluency, verbal memory, categorization learning, memory performance and learning, language comprehension, and attention control (Horvath et al., 2015; Tremblay et al., 2014). In each of these studies, tDCS was targeted to DLPFC, through electrodes positioned over F4 and F3. Here, we sought to test if unilateral or bilateral tDCS over DLPFC altered performance on a standardized IQ test, a multi-faceted and comprehensive assessment of cognitive abilities. Specifically, the purpose of substudy 1 was to investigate if bilateral tDCS (anodes over both F4 and F3, cathode over Cz) modulates performance on a standard IQ test. Based on our finite element modeling, stimulation in this study primarily targeted the middle and superior frontal gyri. Other studies which applied stimulation through anodes positioned at F4 or F3 attributed stimulation effects to DLPFC, a functional region which lies on the middle frontal gyrus.

The application of bilateral stimulation was chosen because IQ tests assess multiple cognitive functions, which utilize broad frontal areas; previous investigations of the effects of brain stimulation on cognitive function have used similar approaches (Snowball et al., 2013). As a note, previous reports of ‘bilateral’ tDCS primarily positioned the anode on one side of the head (often M1) and the cathode over

the same region on the contralateral side of the head. This is markedly different from our bilateral stimulation, in which both sides of the head received anodal stimulation, and a common cathode was positioned at Cz. In a follow-up study, we tested whether the effects of right or left tDCS differed from bilateral stimulation. We found that all forms of tDCS (right, left, and bilateral) impaired performance on the FSIQ, compared to sham stimulation. More detailed analysis revealed that stimulation induced selective impairment of the PRI (significant for right tDCS, trending significant for left and bilateral tDCS). Of the three subtests which contribute to the PRI, performance on two exhibited selective impairment based on tDCS. Specifically, right tDCS decreased performance on Matrix Reasoning at the trend level compared to both sham and left tDCS, while the effects of left tDCS for this subtest were indistinguishable from sham stimulation. For Visual Puzzles, both right and left tDCS reduced practice gains compared to sham stimulation. There were no differences in baseline scores between the stimulation groups, thus this cannot explain the stimulation-induced reduction in practice gains on the FSIQ or PRI. Furthermore, our results from two independent substudies support each other. Data collected during the first substudy demonstrated that bilateral stimulation was detrimental to performance compared to sham stimulation. The results from our second substudy, performed following the completion of substudy 1, further support this finding and demonstrate that both right and left tDCS reduce practice gains in both the FSIQ and PRI. These results suggest that unilateral and bilateral tDCS over DLPFC impair performance on specific perceptual reasoning tasks, but may not affect verbal comprehension, working memory, or processing speed abilities.

Potential Mechanisms of tDCS

The mechanisms underlying the effects of tDCS are still under investigation. An important first consideration is that the physiological underpinnings of tDCS-induced changes differ during stimulation compared to after stimulation. Our discussion will focus on changes following stimulation, according to the experimental paradigm implemented in our study. Neurophysiological, imaging, and pharmacological investigations have demonstrated a number of physiological changes following tDCS (Nord, Lally, & Charpentier, 2013; Stagg & Nitsche, 2011), which are believed to depend upon changes in synaptic strength mediated by NMDA receptors and both GABAergic and glutamatergic synapses (Liebetanz,

Nitsche, Tergau, & Paulus, 2002; Nitsche et al., 2003). Early work with tDCS conducted in motor cortex demonstrated that anodal stimulation increased excitability while cathodal stimulation inhibited activity (Nitsche & Paulus, 2000). However, a meta-analysis looking at cognitive studies indicates that in non-motor areas, anodal stimulation may indeed still increase excitability but cathodal stimulation does not induce inhibitory effects (Jacobson, Koslowsky, & Lavidor, 2012); the authors posited that this may be due to higher brain activation states during cognitive tasks, and the greater range of behavioral measures used in cognitive tasks compared to TMS-induced motor evoked potentials, which are used to measure motor cortex excitability.

Using whole-brain arterial spin labeling, anodal tDCS in left DLPFC has been shown to increase perfusion to brain regions structurally connected with left DLPFC, increase functional coupling between bilateral DLPFC, but decrease functional coupling between left DLPFC and bilateral thalami; immediately following tDCS, perfusion decreased in the frontal lobes bilaterally, in an anatomical distribution similar to that of the default mode network (Stagg et al., 2013). Contrastingly, fMRI has demonstrated that immediately following anodal tDCS over left DLPFC, the default mode network and bilateral fronto-parietal networks exhibited greater co-activation and connectivity (Keeser, Meindl, et al., 2011). If perfusion indeed decreases immediately following tDCS, this may mediate the deficits in performance on the IQ test we observed in the present study. Future work will be needed to determine if the brain regions mediating perceptual reasoning abilities may be particularly affected by reduced perfusion, as could be hypothesized based on our finding of selective impairment in the PRI following unilateral and bilateral tDCS.

tDCS Effects on Perceptual Reasoning

We found that both unilateral and bilateral tDCS induced selective impairments in the PRI of the WAIS-IV. The PRI measures fluid reasoning, with tasks that assess nonverbal concept formation, visual perception and organization, visual-motor coordination, learning, and the ability to separate figure and ground in visual stimuli. Previous reports have found that anodal tDCS over frontal cortex improves perceptual sensitivity (Falcone, Coffman, Clark, & Parasuraman, 2012), learning to identify concealed objects in naturalistic surroundings (Clark et al., 2012), and perceptual learning (Sehm et al., 2013). Other

work has applied anodal tDCS to visual areas and improved perceptual learning (Pirulli, Fertonani, & Miniussi, 2013), while parietal tDCS has improved reaction time on contralateral search tasks (Reinhart & Woodman, 2015). However, another body of research has found that both right anodal and cathodal tDCS on DLPFC impair the efficiency of managing stimulus-response feature bindings, which taxes perceptual abilities; this study proposed that tDCS could create reversible 'frontal lesions', for at least specific cognitive tasks (Zmigrod, 2014; Zmigrod, Colzato, & Hommel, 2014). Another study found that anodal and cathodal tDCS over medial-frontal cortex did not change perceptual processing, but only subsequent error- and feedback-related negativities (Reinhart & Woodman, 2014). Furthermore, anodal tDCS of V1 was shown to block overnight consolidation of visual learning (Peters, Thompson, Merabet, Wu, & Shams, 2013). Thus, our work and previous studies indicate that at least some forms of frontal tDCS may produce a 'frontal lesion' effect, in which stimulation impairs performance on facets of perceptual reasoning. Future work will be needed to elucidate if these specific effects results from the location of applied stimulation, the specific tasks being tested, or a combination of these factors.

Previous Studies on tDCS and Working Memory

Our finding that tDCS does not affect working memory performance joins a diverse set of studies investigating the modulation of working memory ability by tDCS. A number of studies have found that anodal tDCS to left DLPFC improves performance on verbal and non-verbal working memory tasks (Keeser, Padberg, et al., 2011; Ohn et al., 2008), with some qualifiers such as improvement measured only in males (Meiron & Lavidor, 2013), or that stimulation was beneficial but selectively in older adults with more education (Berryhill & Jones, 2012). Other reports found no effects of tDCS on working memory accuracy (Lally, Nord, Walsh, & Roiser, 2013; Mylius et al., 2012; Zaehle, Sandmann, Thorne, Jancke, & Herrmann, 2011), but improvement in only reaction time (Hoy et al., 2013; Mulquiney, Hoy, Daskalakis, & Fitzgerald, 2011; Teo, Hoy, Daskalakis, & Fitzgerald, 2011). Conversely, one study found that accuracy, but not reaction time, was improved by anodal tDCS applied to DLPFC compared to sham and cathodal stimulation (Fregni et al., 2005). Additional evidence suggests that left tDCS improves verbal working memory while right tDCS improves visuospatial working memory (Jeon & Han, 2012). There is weak evidence that concurrently administered anodal tDCS to left DLPFC during a working memory task may

improve subsequent testing on another working memory test, compared to just tDCS or administration of the first working memory task alone (Andrews, Hoy, Enticott, Daskalakis, & Fitzgerald, 2011).

While the conceptualization of working memory is helpful for discussion and study, this remains a broad construct which incorporates multiple cognitive functions (including but not limited to rehearsal, maintenance, updating, and executive function) (Unsworth & Engle, 2007). Work conducted to disentangle which contributions to working memory may be modulated by tDCS has provided some insight that anodal tDCS over left DLPFC may not improve the ability to overcome bias (Gladwin, den Uyl, & Wiers, 2012) but may be mediated by specific effects on selective attention because of the presence of interference (Gladwin, den Uyl, Fregni, & Wiers, 2012). Overall, it is still unclear if and how tDCS modulates working memory. A meta-analysis on the effects of tDCS applied to DLPFC on n-back working memory tests (studies published through February 2013) indicates that only reaction time, but not accuracy, is improved by stimulation (Brunoni & Vanderhasselt, 2014). Of critical importance for comparison of studies, reaction time is not measured in the WAIS-IV working memory subtest, and thus our results are not directly comparable to tests of working memory which assessed reaction times. We did not conduct MRI scans to accommodate anatomical differences across participants; however, there is evidence that modulation of performance on working memory may result from differing current densities at DLPFC, despite consistent electrode placement according to the 10-20 system across participants (Kim et al., 2014). Importantly, our electrode montage differed in the location of the cathode compared to many previous studies. Thus, our induced current is not directly comparable to previous studies which administered anodal tDCS to DPFC.

Investigations of tACS and Intelligence

Other studies assessing the role of brain stimulation on forms of intelligence have utilized transcranial alternating current stimulation (tACS) that employs alternating current waveforms. tACS targets the temporal organization of network activity through frequency-specific enhancement of cortical oscillations and coherence (Ali et al., 2013; Frohlich & Schmidt, 2013; Herrmann, Rach, Neuling, & Struber, 2013). Such temporal structure plays an important role in mediating cognitive abilities such as attention (Miller & Buschman, 2013), working memory (Duzel, Penny, & Burgess, 2010; Siegel, Warden,

& Miller, 2009), and encoding and retrieval of memory (Uhlhaas, Haenschel, Nikolic, & Singer, 2008; Ward, 2003). One study found that gamma frequency tACS administered over left middle frontal gyrus reduced the amount of time required to solve the Raven's matrices (Santarnecchi et al., 2013). However, there was no difference between tACS and sham groups in accuracy. Another study found that theta frequency tACS over parietal cortex improved performance on a modified version of Raven's progressive matrices, mainly through participants correctly solving more difficult task items (Pahor & Jausovec, 2014). Interestingly, the Raven's matrices in these studies are similar to the Matrix Reasoning subtest of the PRI in the WAIS-IV. The Matrix Reasoning subtest has previously been used as a measure of fluid intelligence (Barbey, Colom, Paul, & Grafman, 2014), and scores on the test are speed-dependent. Thus, tDCS and tACS may have opposite effects on performance on assays of fluid intelligence. This difference likely relates to the mechanistic difference between tDCS (inducing changes in excitability) and tACS (modulating temporal patterning of activity). Future work will be required to more fully understand the role of each of these stimulation modalities on fluid intelligence, as well as other aspects of cognitive processing.

Neurobiological Substrate of Intelligence

The neurobiological substrate of intelligence is still unknown. Historically, it has been posited that the diverse functional roles of DLPFC provide a unified neural architecture for Spearman's classic general (*g*) factor model of intelligence (Duncan & Owen, 2000; Duncan et al., 2000). In this theory of intelligence, the *g* factor posits that an individual's mental performance across a broad range of cognitive tests is often comparable (Spearman, 1904). However, recent work utilizing lesion mapping has demonstrated that performance on metrics used to measure the *g* factor of intelligence depend upon fronto-parietal networks, in accordance with the Parieto-Frontal Integration Theory (P-FIT) of intelligence (Barbey et al., 2012; Glascher et al., 2010)(however, results from (Glascher et al., 2010) also demonstrate that regions of frontopolar cortex may play a unique role in *g*). In the P-FIT conceptualization of intelligence, different cognitive functions are mediated by a broadly distributed network of functionally specialized brain regions, including prefrontal, parietal, occipital, and temporal association cortices (Barbey, Colom, & Grafman, 2013; Colom et al., 2009; Glascher et al., 2009; Jung & Haier, 2007). Four stages of information

processing are supported by critical information flow between multiple brain regions, in particular frontal and parietal regions (Sternberg & Kaufman, 2011). In agreement of this model, the neurobiological substrate of intelligence has been hypothesized to correspond to genetically determined brain structure and connectivity (Choi et al., 2008; Colom, Jung, & Haier, 2006; Haier, Jung, Yeo, Head, & Alkire, 2004; Hulshoff Pol et al., 2006; Shaw et al., 2006; Thompson et al., 2001), and individuals with more efficient whole brain network organization have a higher overall level of intelligence (Cole, Yarkoni, Repovs, Anticevic, & Braver, 2012; Duncan, 2013; van den Heuvel, Stam, Kahn, & Hulshoff Pol, 2009). Thus, while our study was not a direct assay of the neurobiological substrate of intelligence, our results may provide insight on this question. The differential effects of tDCS on WAIS-IV index and subtest performance is in agreement with P-FIT; because of the spatial distribution of brain structures implicated in the variety of cognitive processes included in the WAIS-IV, the stimulation would differentially affect these networks.

Implications for Society: DIY Stimulation

The complexity of the neurobiological substrates of intelligence is particularly relevant given the growing interest of the lay public in brain stimulation. In a simplified form, many people believe that increased excitability induced by brain stimulation can be performance-enhancing (motivated by communication of findings that cognitive training enhances brain activity measured by fMRI in prefrontal and parietal area, including the middle frontal gyrus (Olesen, Westerberg, & Klingberg, 2004)). The relative low cost, technical ease, and attractive hypothetic benefits of brain stimulation have sparked the development of commercially available do-it-yourself (DIY) brain stimulation devices. However, DIY devices are not validated and may not be safe (Bikson, Bestmann, & Edwards, 2013). Furthermore, our study casts doubt on the hype surrounding the simplified idea that applying brain stimulation will lead to better cognitive performance ("Brain blast," 2013). In fact, the opposite effect was demonstrated in our study. This finding together with the very real safety risks of DIY brain stimulation will hopefully discourage the wider, uncontrolled use of tDCS outside the research laboratory.

LIMITATIONS AND CONCLUSIONS

There are certain limitations to this study which are important to consider. Because we wanted to administer the full version of the WAIS-IV in accordance to standard testing protocols, the same test was administered to each participant twice. It was clear that participants exhibited a practice effect as a result of the retesting (Estevis, Basso, & Combs, 2012). However, as all participants in all stimulation groups underwent this same procedure, we do not anticipate the reported effects to depend upon differences induced by this retesting. However, we cannot fully exclude the possibility that unilateral or bilateral tDCS induced a difference in recall from Session 1, rather than a true alteration to the neural substrates underlying cognitive processing. However, in such a case we would expect performance modulation that is less task-specific than what we found, since not only the perceptual reasoning index showed a learning effect for the sham group. Another limitation to keep in mind is that tDCS was administered before participants completed the WAIS-IV during Session 2. Thus, elapsed time since the end of stimulation might affect which subtests showed significant modulation. However, our correlational analysis showed that time of test was not associated with tDCS-induced performance changes and could therefore not explain the specific stimulation effect on Matrix Reasoning or Visual Puzzles. Lastly, there is growing recognition of important considerations when using tDCS in cognitive research, such as participant motivation (Berryhill, Peterson, Jones, & Stephens, 2014); our study may have suffered from one of these problems.

In conclusion, we found that unilateral and bilateral tDCS over DLPFC reduced practice gains in a comprehensive test of intelligence, with selective impairment in perceptual reasoning. The impairment found here suggests that tDCS indeed targeted selective neuronal network dynamics that enable cognition. Our study highlights that increasing neuronal activity in some frontal areas may not be beneficial to cognitive processing, with additional evidence that the timing of tDCS relative to task performance is an important consideration in the future development of brain stimulation for therapeutic applications.

FIGURES AND TABLES

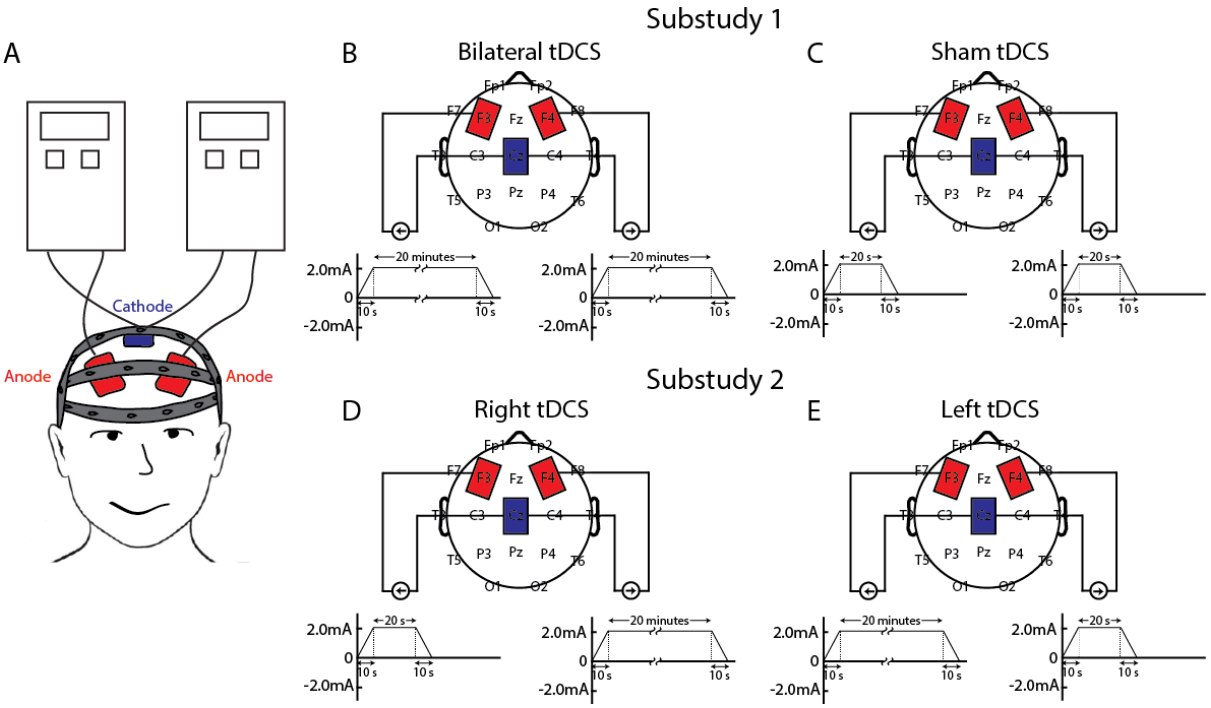

Figure 2.1. tDCS administered over DLPFC

(A) Two stimulators were used to deliver double-blinded unilateral or bilateral tDCS over DLPFC. In all stimulation conditions, three electrodes were placed, one each at F3, F4 (anodes, red electrodes), and Cz (cathode/return, blue electrode).

(B) For bilateral tDCS, both stimulators delivered 20 minutes of 2mA stimulation with a ramp up and ramp down of current.

(C) For sham tDCS, both stimulators administered 20 seconds of stimulation with a ramp up and ramp down of current, in order to mimic the sensations of stimulation.

(D) For right tDCS, 20 minutes of stimulation was delivered through the stimulator attached to electrodes F4 and Cz, while only the 20 seconds of sham stimulation were delivered through the stimulator attached to F3 and Cz.

(E) For left tDCS, 20 minutes of stimulation was delivered through the stimulator attached to F3 and Cz, while the stimulator attached to F4 and Cz administered 20 seconds of stimulation.

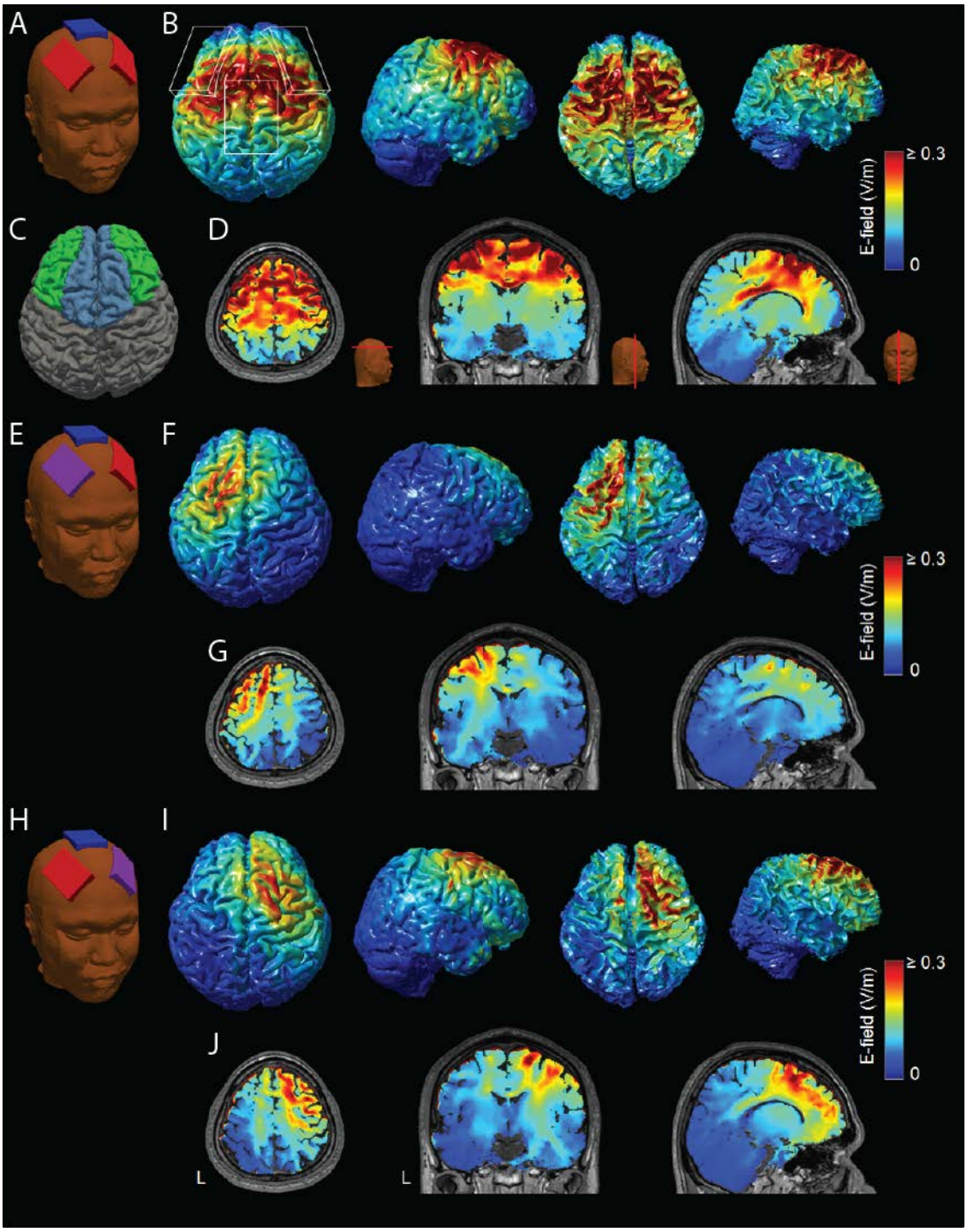

Figure 2.2. Electric field modeling of tDCS

(A) Anodal tDCS administered bilaterally over frontal cortex. Red electrodes represent anodes, blue electrodes represent cathodes.

(B) For bilateral stimulation, the greatest magnitude of the electric field was mostly localized to areas underneath and between the electrodes. Left panels: gray matter; right panels: white matter.

(C) The middle frontal gyri (green) and superior frontal gyri (blue) were the areas of frontal cortex with the highest amplitude electric field.

(D) Axial, coronal, and sagittal sections showing electric field induced by tDCS

(E) – (G) Anodal tDCS administered unilaterally on the left. Purple electrodes represent stimulation electrodes which were attached, but only received sham stimulation

(H) – (J) Anodal tDCS administered unilaterally on the right.

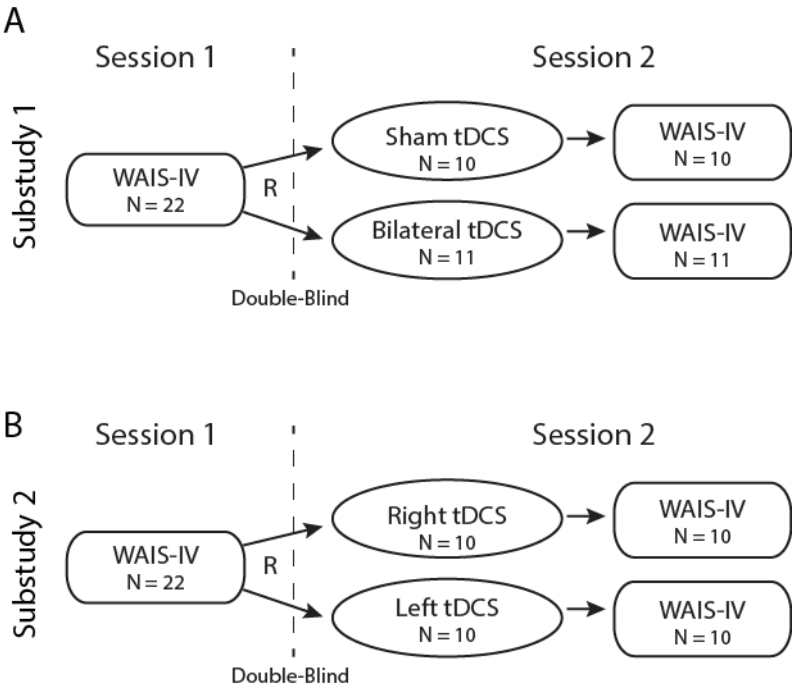

Figure 2.3. Double-blind, randomized, placebo-controlled study design with a repeated-measure of IQ.

(A) During Session 1, each participant was administered the Wechsler Adult Intelligence Scale, Fourth Edition (WAIS-IV). During Session 2 of substudy 1, each participant received either sham stimulation or bilateral tDCS. The WAIS-IV was immediately administered following stimulation in order to assess stimulation-induced modulation in performance.

(B) During Session 1, each participant was administered the Wechsler Adult Intelligence Scale, Fourth Edition (WAIS-IV). During Session 2 of substudy 2, each participant received either right or left tDCS. The WAIS-IV was immediately administered following stimulation in order to assess stimulation-induced modulation in performance.

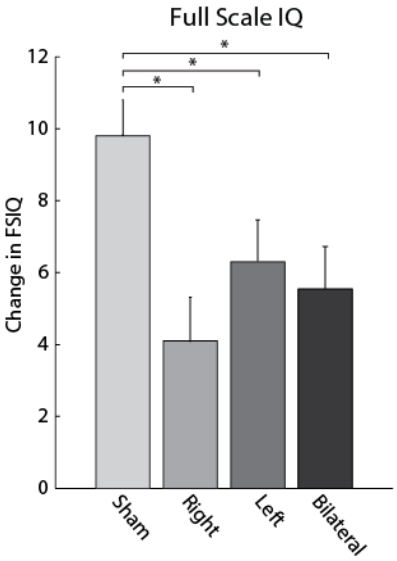

Figure 2.4. Unilateral and bilateral tDCS significantly decreased practice gains in the Full Scale IQ (FSIQ) compared to sham stimulation.

The difference in FSIQ between sessions (Session 2 – Session 1) was calculated for each participant, and then averaged across participants. Group means of individual differences are plotted. Error bars show 1 SEM. * indicates significant at $p < 0.05$.

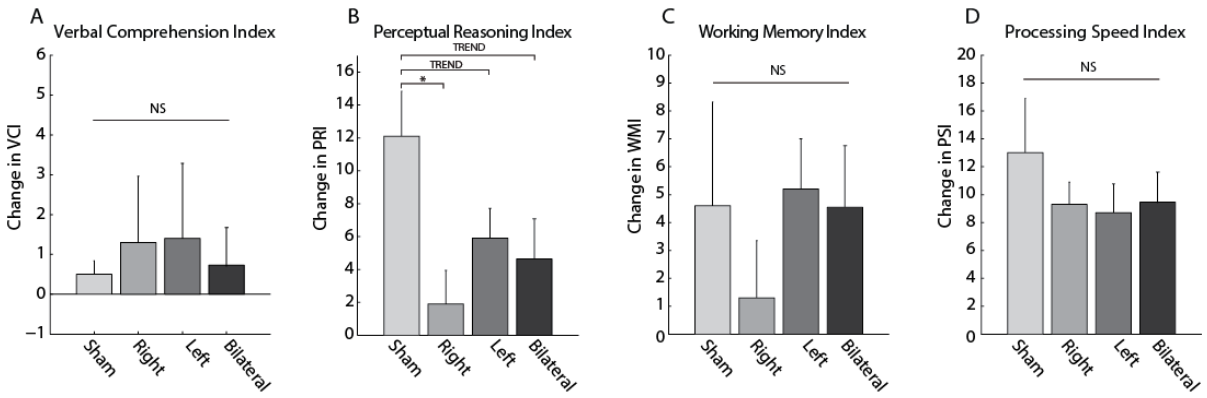

Figure 2.5. The WAIS-IV provides four index scores which represent the major components of intelligence.

Bars represent the group means of the individual differences of scores between Session 1 and Session 2. Error bars show 1 SEM. * indicates significant at $p < 0.05$.

(A) Verbal Comprehension Index (VCI).

(B) Perceptual Reasoning Index (PRI). Right tDCS significantly decreased practice gains on the PRI of the WAIS-IV, while left tDCS and bilateral tDCS decreased practice gains on the PRI at trend level.

(C) Working Memory Index (WMI).

(D) Processing Speed Index (PSI).

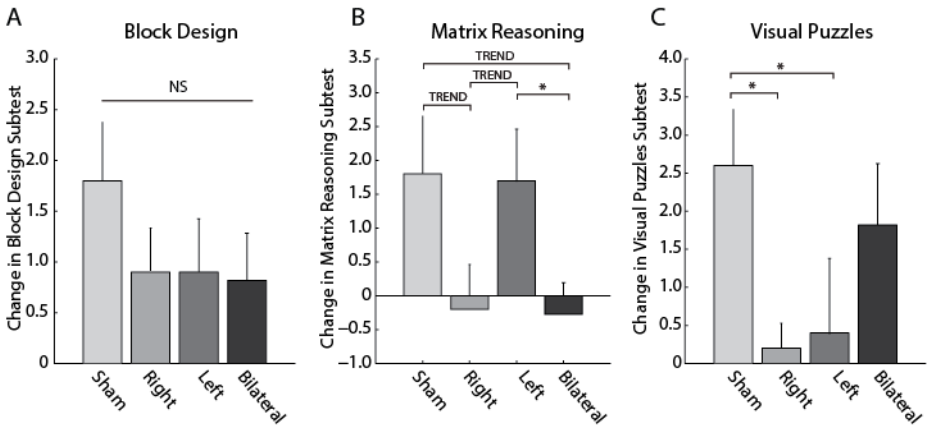

Figure 2.6. Perceptual reasoning abilities are assessed by 3 subtests. Differences between stimulation conditions were found in Matrix Reasoning, Visual Puzzles.

Bars represent the group means of the differences (by participant) of scores between Session 1 and Session 2. Error bars show 1 SEM. * indicates significant at $p < 0.05$.

(A) Block Design: No significant difference between stimulation conditions.

(B) Matrix Reasoning: Right and bilateral tDCS decreased practice gains, at trend level, compared to sham stimulation. Interestingly, practice gains in Matrix Reasoning were unchanged by left tDCS compared to sham stimulation.

(C) Visual Puzzles: Right and left stimulation tDCS significantly reduced practice gains compared to sham stimulation.

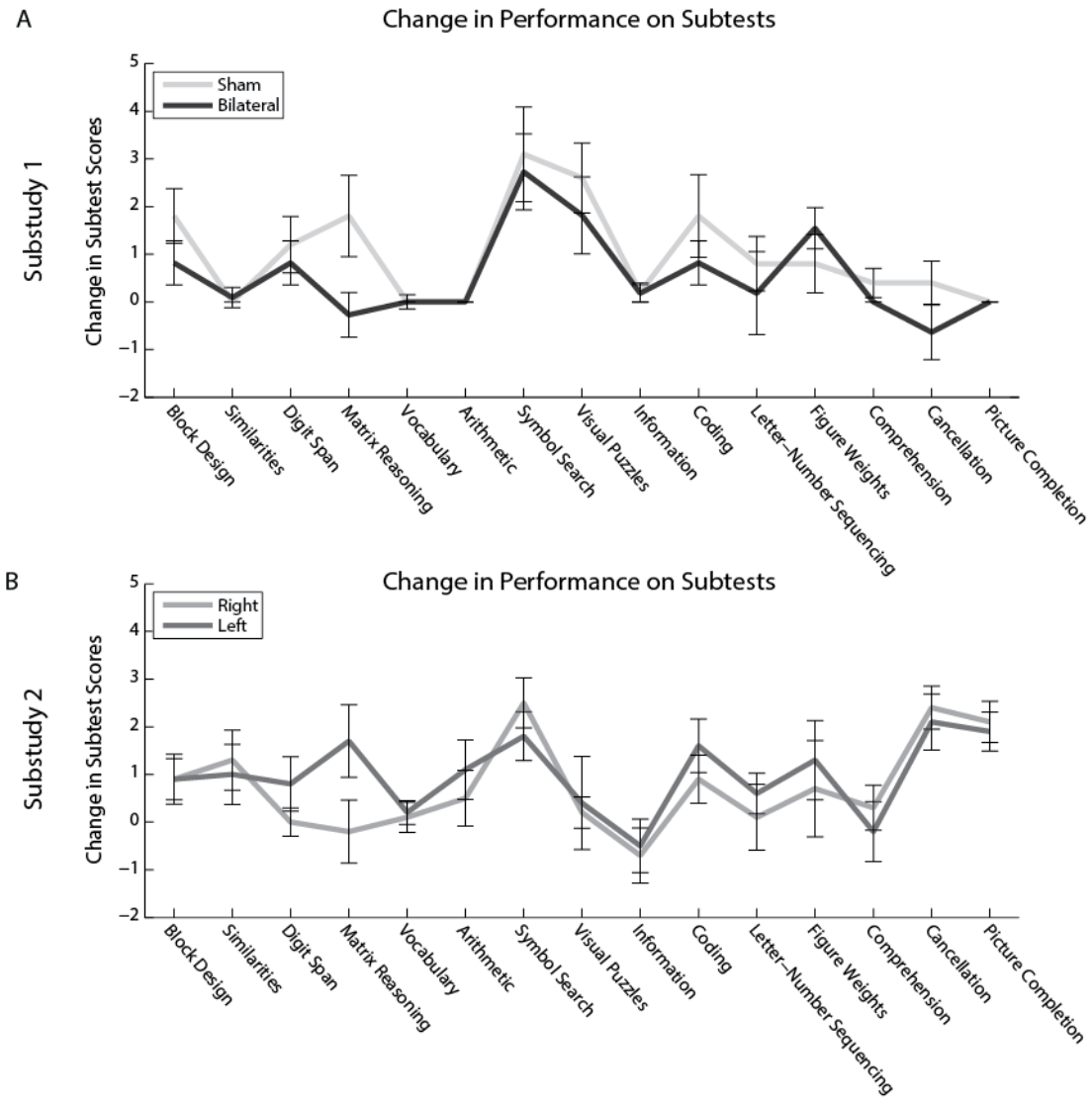

Figure 2.7. Changes in performance on the subtests were not influenced by test order.

Group means of the individual differences of each subtest score between Session 1 and Session 2 are plotted in order of test administration. Error bars show 1 SEM.

(A) Substudy 1: Sham or bilateral tDCS.

(B) Substudy 2: Right or left tDCS.

	Ability measured by each subtest:
Verbal Comprehension Index subtests	
Similarities	Verbal concept formation and reasoning
Vocabulary	Work knowledge and verbal concept formation
Information	Ability to acquire, retain, and retrieve general factual knowledge
Comprehension	Verbal reasoning and conceptualization, verbal comprehension and expression, ability to evaluate and use past experience, ability to demonstrate practical knowledge and judgment
Perceptual Reasoning Index subtests	
Block Design	Ability to analyze and synthesize abstract visual stimuli
Matrix Reasoning	Fluid intelligence, broad visual intelligence, analogic perceptual reasoning ability, classification and spatial ability, knowledge of part-whole relationships, simultaneous processing, and perceptual organization
Visual Puzzles	Visual perception and organization, nonverbal reasoning, spatial visualization and manipulation, the ability to anticipate relationships among parts, and the ability to analyze and synthesize abstract visual stimuli
Figure Weights	Quantitative and analogic reasoning, involves inductive and deductive logic
Picture Completion	Visual perception and organization, concentration, visual recognition of essential details of objects
Working Memory Index subtests	
Digit Span	Learning and memory, attention, auditory processing, mental manipulation, and working memory
Arithmetic	Mental manipulation, concentration, attention, short and long-term memory, numerical reasoning, and mental alertness
Letter-Number Sequencing	Spatial processing, mental manipulation, attention, concentration, memory span, and short-term auditory memory
Processing Speed Index subtests	
Symbol Search	Processing speed, short-term visual memory, visual motor coordination, visual discrimination, psychomotor speed, speed of mental operation, attention, and concentration
Coding	Processing speed, short-term visual memory, psychomotor speed, visual perception, visual-motor coordination, visual scanning ability, attention, and concentration
Cancellation	Processing speed, visual selective attention, vigilance, perceptual speed, visual-motor ability
Supplemental subtests in italics	

Table 2.1. WAIS-IV Indices and Subtests (according to test manual, Pearson Education, Inc.)

				Baseline		Post-Stim
Full-Scale IQ			Sham	117.5 ± 3.692		127.3 ± 3.636
			Right	117.1 ± 2.442		121.2 ± 2.361
			Left	113.8 ± 2.573		120.1 ± 2.722
			Bilateral	121.5 ± 4.959		127.1 ± 5.270
Verbal Comprehension Index			Sham	120.4 ± 3.263		120.9 ± 3.424
			Right	110.9 ± 2.822		112.2 ± 2.832
			Left	113.0 ± 2.940		114.4 ± 3.888
			Bilateral	126.5 ± 4.650		127.3 ± 4.667
Perceptual Reasoning Index			Sham	113.3 ± 4.230		125.4 ± 2.937
			Right	115.8 ± 2.670		117.7 ± 2.797
			Left	108.3 ± 4.224		114.2 ± 3.620
			Bilateral	117.5 ± 4.122		122.1 ± 4.808
Working Memory Index			Sham	112.7 ± 3.187		117.3 ± 5.190
			Right	115.0 ± 3.795		116.3 ± 4.500
			Left	108.8 ± 3.172		114.0 ± 2.295
			Bilateral	115.5 ± 5.206		120.1 ± 5.573
Processing Speed Index			Sham	107.7 ± 3.924		120.7 ± 3.783
			Right	114.1 ± 4.841		123.4 ± 4.655
			Left	114.6 ± 3.439		123.3 ± 2.725
			Bilateral	105.9 ± 4.785		115.4 ± 4.407
(Mean ± sem)						

Table 2.2. WAIS-IV scores by group and session

	Linear mixed models fixed factors					
	Session		Condition		Session x Condition	
Full-Scale IQ (FSIQ) Index Scales						
VCI	F(1,40) = 2.29	p > 0.1	F(3,37) = 3.78	p = 0.0184**	F(3,37) = 0.106	p > 0.1
PRI	F(1,40) = 23.8	p < 0.001**	F(3,37) = 1.17	p > 0.1	F(3,37) = 3.45	p = 0.0261**
WMI	F(1,40) = 9.90	p = 0.00312**	F(3,37) = 0.420	p > 0.1	F(3,37) = 0.471	p > 0.1
PSI	F(1,40) = 63.9	p < 0.001**	F(3,37) = 1.04	p > 0.1	F(3,37) = 0.565	p > 0.1
** significant effects (p < 0.05), *trend-level effects (p < 0.1)						

Table 2.3. Linear mixed model results for Full-Scale IQ (FSIQ) Index scales

		Linear mixed models fixed factors					
		Session		Condition		Session x Condition	
Perceptual Reasoning Index (PRI) Subtests							
Block Design		F(1,40) = 19.4	p < 0.001**	F(3,37) = 0.648	p > 0.1	F(3,37) = 0.853	p > 0.1
Matrix Reasoning		F(1,40) = 3.95	p = 0.0536*	F(3,37) = 0.750	p > 0.1	F(3,37) = 2.76	p = 0.0560*
Visual Puzzles		F(1,40) = 10.3	p = 0.00262**	F(3,37) = 3.41	p = 0.0274**	F(3,37) = 2.28	p = 0.0949*
** significant effects (p < 0.05), *trend-level effects (p < 0.1)							

Table 2.4. Linear mixed model results for Perceptual Reasoning Index (PRI) subtests

REFERENCES

Ali, M. M., Sellers, K. K., & Frohlich, F. (2013). Transcranial alternating current stimulation modulates large-scale cortical network activity by network resonance. *J Neurosci, 33*(27), 11262-11275. doi: 10.1523/JNEUROSCI.5867-12.2013

Andrews, S. C., Hoy, K. E., Enticott, P. G., Daskalakis, Z. J., & Fitzgerald, P. B. (2011). Improving working memory: the effect of combining cognitive activity and anodal transcranial direct current stimulation to the left dorsolateral prefrontal cortex. *Brain Stimul, 4*(2), 84-89. doi: 10.1016/j.brs.2010.06.004

Antal, A., Chaieb, L., Moliadze, V., Monte-Silva, K., Poreisz, C., Thirugnanasambandam, N., . . . Paulus, W. (2010). Brain-derived neurotrophic factor (BDNF) gene polymorphisms shape cortical plasticity in humans. *Brain Stimul, 3*(4), 230-237. doi: 10.1016/j.brs.2009.12.003

Barbey, A. K., Colom, R., & Grafman, J. (2013). Dorsolateral prefrontal contributions to human intelligence. *Neuropsychologia, 51*(7), 1361-1369. doi: 10.1016/j.neuropsychologia.2012.05.017

Barbey, A. K., Colom, R., Paul, E. J., & Grafman, J. (2014). Architecture of fluid intelligence and working memory revealed by lesion mapping. *Brain Struct Funct, 219*(2), 485-494. doi: 10.1007/s00429-013-0512-z

Barbey, A. K., Colom, R., Solomon, J., Krueger, F., Forbes, C., & Grafman, J. (2012). An integrative architecture for general intelligence and executive function revealed by lesion mapping. *Brain, 135*(Pt 4), 1154-1164. doi: 10.1093/brain/aws021

Bates, D., Maechler, M., Bolker, B., & Walker, S. (2014). lme4: Linear mixed-effects models using Eigen and S4. R package version 1.1-6. Retrieved from http://CRAN.R-project.org/package=lme4

Batsikadze, G., Moliadze, V., Paulus, W., Kuo, M. F., & Nitsche, M. A. (2013). Partially non-linear stimulation intensity-dependent effects of direct current stimulation on motor cortex excitability in humans. *J Physiol, 591*(Pt 7), 1987-2000. doi: 10.1113/jphysiol.2012.249730

Berryhill, M. E., & Jones, K. T. (2012). tDCS selectively improves working memory in older adults with more education. *Neurosci Lett, 521*(2), 148-151. doi: 10.1016/j.neulet.2012.05.074

Berryhill, M. E., Peterson, D. J., Jones, K. T., & Stephens, J. A. (2014). Hits and misses: leveraging tDCS to advance cognitive research. *Front Psychol, 5*, 800. doi: 10.3389/fpsyg.2014.00800

Bikson, M., Bestmann, S., & Edwards, D. (2013). Neuroscience: transcranial devices are not playthings. *Nature, 501*(7466), 167. doi: 10.1038/501167b

Bikson, M., Datta, A., & Elwassif, M. (2009). Establishing safety limits for transcranial direct current stimulation. *Clin Neurophysiol, 120*(6), 1033-1034. doi: 10.1016/j.clinph.2009.03.018

Brain blast. (2013). *Nature, 498*(7454), 271-272.

Brunoni, A. R., & Vanderhasselt, M. A. (2014). Working memory improvement with non-invasive brain stimulation of the dorsolateral prefrontal cortex: A systematic review and meta-analysis. *Brain Cogn, 86C*, 1-9. doi: 10.1016/j.bandc.2014.01.008

Bunge, S. A., Ochsner, K. N., Desmond, J. E., Glover, G. H., & Gabrieli, J. D. (2001). Prefrontal regions involved in keeping information in and out of mind. *Brain, 124*(Pt 10), 2074-2086.

Chaieb, L., Antal, A., Ambrus, G. G., & Paulus, W. (2014). Brain-derived neurotrophic factor: its impact upon neuroplasticity and neuroplasticity inducing transcranial brain stimulation protocols. *Neurogenetics, 15*(1), 1-11. doi: 10.1007/s10048-014-0393-1

Choi, Y. Y., Shamosh, N. A., Cho, S. H., DeYoung, C. G., Lee, M. J., Lee, J. M., . . . Lee, K. H. (2008). Multiple bases of human intelligence revealed by cortical thickness and neural activation. *J Neurosci, 28*(41), 10323-10329. doi: 10.1523/JNEUROSCI.3259-08.2008

Clark, V. P., Coffman, B. A., Mayer, A. R., Weisend, M. P., Lane, T. D., Calhoun, V. D., . . . Wassermann, E. M. (2012). TDCS guided using fMRI significantly accelerates learning to identify concealed objects. *Neuroimage, 59*(1), 117-128. doi: 10.1016/j.neuroimage.2010.11.036

Cohen Kadosh, R. (2015). Modulating and enhancing cognition using brain stimulation: Science and fiction. *Journal of Cognitive Psychology, 27*(2), 141-163. doi: 10.1080/20445911.2014.996569

Cole, M. W., Yarkoni, T., Repovs, G., Anticevic, A., & Braver, T. S. (2012). Global connectivity of prefrontal cortex predicts cognitive control and intelligence. *J Neurosci, 32*(26), 8988-8999. doi: 10.1523/JNEUROSCI.0536-12.2012

Colom, R., Haier, R. J., Head, K., Alvarez-Linera, J., Quiroga, M. A., Shih, P. C., & Jung, R. E. (2009). Gray matter correlates of fluid, crystallized, and spatial intelligence: Testing the P-FIT model. *Intelligence, 37*(2), 124-135. doi: DOI 10.1016/j.intell.2008.07.007

Colom, R., Jung, R. E., & Haier, R. J. (2006). Distributed brain sites for the g-factor of intelligence. *Neuroimage, 31*(3), 1359-1365. doi: 10.1016/j.neuroimage.2006.01.006

Dayan, E., Censor, N., Buch, E. R., Sandrini, M., & Cohen, L. G. (2013). Noninvasive brain stimulation: from physiology to network dynamics and back. *Nat Neurosci, 16*(7), 838-844. doi: 10.1038/nn.3422

du Boisgueheneuc, F., Levy, R., Volle, E., Seassau, M., Duffau, H., Kinkingnehun, S., . . . Dubois, B. (2006). Functions of the left superior frontal gyrus in humans: a lesion study. *Brain, 129*(Pt 12), 3315-3328. doi: 10.1093/brain/awl244

Duncan, J. (2013). The structure of cognition: attentional episodes in mind and brain. *Neuron, 80*(1), 35-50. doi: 10.1016/j.neuron.2013.09.015

Duncan, J., & Owen, A. M. (2000). Common regions of the human frontal lobe recruited by diverse cognitive demands. *Trends Neurosci, 23*(10), 475-483.

Duncan, J., Seitz, R. J., Kolodny, J., Bor, D., Herzog, H., Ahmed, A., . . . Emslie, H. (2000). A neural basis for general intelligence. *Science, 289*(5478), 457-460.

Duzel, E., Penny, W. D., & Burgess, N. (2010). Brain oscillations and memory. *Curr Opin Neurobiol, 20*(2), 143-149. doi: 10.1016/j.conb.2010.01.004

Esposito, G., Kirkby, B. S., Van Horn, J. D., Ellmore, T. M., & Berman, K. F. (1999). Context-dependent, neural system-specific neurophysiological concomitants of ageing: mapping PET correlates during cognitive activation. *Brain, 122 (Pt 5)*, 963-979.

Estevis, E., Basso, M. R., & Combs, D. (2012). Effects of practice on the Wechsler Adult Intelligence Scale-IV across 3- and 6-month intervals. *Clin Neuropsychol, 26*(2), 239-254. doi: 10.1080/13854046.2012.659219

Falcone, B., Coffman, B. A., Clark, V. P., & Parasuraman, R. (2012). Transcranial direct current stimulation augments perceptual sensitivity and 24-hour retention in a complex threat detection task. *PLoS One, 7*(4), e34993. doi: 10.1371/journal.pone.0034993

Fathi, D., Ueki, Y., Mima, T., Koganemaru, S., Nagamine, T., Tawfik, A., & Fukuyama, H. (2010). Effects of aging on the human motor cortical plasticity studied by paired associative stimulation. *Clin Neurophysiol, 121*(1), 90-93. doi: 10.1016/j.clinph.2009.07.048

Fregni, F., Boggio, P. S., Nitsche, M., Bermpohl, F., Antal, A., Feredoes, E., . . . Pascual-Leone, A. (2005). Anodal transcranial direct current stimulation of prefrontal cortex enhances working memory. *Exp Brain Res, 166*(1), 23-30. doi: 10.1007/s00221-005-2334-6

Fritsch, B., Reis, J., Martinowich, K., Schambra, H. M., Ji, Y., Cohen, L. G., & Lu, B. (2010). Direct current stimulation promotes BDNF-dependent synaptic plasticity: potential implications for motor learning. *Neuron, 66*(2), 198-204. doi: 10.1016/j.neuron.2010.03.035

Frohlich, F., & McCormick, D. A. (2010). Endogenous electric fields may guide neocortical network activity. *Neuron, 67*(1), 129-143. doi: 10.1016/j.neuron.2010.06.005

Frohlich, F., & Schmidt, S. L. (2013). Rational design of transcranial current stimulation (TCS) through mechanistic insights into cortical network dynamics. *Front Hum Neurosci, 7*, 804. doi: 10.3389/fnhum.2013.00804

Gladwin, T. E., den Uyl, T. E., Fregni, F. F., & Wiers, R. W. (2012). Enhancement of selective attention by tDCS: interaction with interference in a Sternberg task. *Neurosci Lett, 512*(1), 33-37. doi: 10.1016/j.neulet.2012.01.056

Gladwin, T. E., den Uyl, T. E., & Wiers, R. W. (2012). Anodal tDCS of dorsolateral prefontal cortex during an Implicit Association Test. *Neurosci Lett, 517*(2), 82-86. doi: 10.1016/j.neulet.2012.04.025

Glascher, J., Rudrauf, D., Colom, R., Paul, L. K., Tranel, D., Damasio, H., & Adolphs, R. (2010). Distributed neural system for general intelligence revealed by lesion mapping. *Proc Natl Acad Sci U S A, 107*(10), 4705-4709. doi: 10.1073/pnas.0910397107

Glascher, J., Tranel, D., Paul, L. K., Rudrauf, D., Rorden, C., Hornaday, A., . . . Adolphs, R. (2009). Lesion mapping of cognitive abilities linked to intelligence. *Neuron, 61*(5), 681-691. doi: 10.1016/j.neuron.2009.01.026

Gray, J. R., Chabris, C. F., & Braver, T. S. (2003). Neural mechanisms of general fluid intelligence. *Nat Neurosci, 6*(3), 316-322. doi: 10.1038/nn1014

Groth-Marnat, G. (2003). *Handbook of Psychological Assessment* (4th ed.). Hoboken, NJ: John Wiley & Sons.

Haier, R. J., Jung, R. E., Yeo, R. A., Head, K., & Alkire, M. T. (2004). Structural brain variation and general intelligence. *Neuroimage, 23*(1), 425-433. doi: 10.1016/j.neuroimage.2004.04.025

Halekoh, U., & Hojsgaard, S. A Kenward-Roger Approximation and Parametric Bootstrap Methods for Tests in Linear Mixed Models – the R Package pbkrtest. *Journal of Statistical Software, Submitted*.

Halekoh, U., & Hojsgaard, S. (2013). pbkrtest: Parametric bootstrap and Kenward Roger based methods for mixed model comparison. R package version 0.3-8.

Hampson, M., Driesen, N. R., Skudlarski, P., Gore, J. C., & Constable, R. T. (2006). Brain connectivity related to working memory performance. *J Neurosci, 26*(51), 13338-13343. doi: 10.1523/JNEUROSCI.3408-06.2006

Herrmann, C. S., Rach, S., Neuling, T., & Struber, D. (2013). Transcranial alternating current stimulation: a review of the underlying mechanisms and modulation of cognitive processes. *Front Hum Neurosci, 7*, 279. doi: 10.3389/fnhum.2013.00279

Horvath, J., Forte, C., & O, C. (2015). Quantitative Review Finds No Evidence of Cognitive Effects in Healthy Populations From Single-session Transcranial Direct Current Stimulation (tDCS). *Brain Stimul*. doi: 10.1016/j.brs.2015.01.400

Hoy, K. E., Emonson, M. R., Arnold, S. L., Thomson, R. H., Daskalakis, Z. J., & Fitzgerald, P. B. (2013). Testing the limits: Investigating the effect of tDCS dose on working memory enhancement in healthy controls. *Neuropsychologia, 51*(9), 1777-1784. doi: 10.1016/j.neuropsychologia.2013.05.018

Hulshoff Pol, H. E., Schnack, H. G., Posthuma, D., Mandl, R. C., Baare, W. F., van Oel, C., . . . Kahn, R. S. (2006). Genetic contributions to human brain morphology and intelligence. *J Neurosci, 26*(40), 10235-10242. doi: 10.1523/JNEUROSCI.1312-06.2006

Jacobson, L., Koslowsky, M., & Lavidor, M. (2012). tDCS polarity effects in motor and cognitive domains: a meta-analytical review. *Exp Brain Res, 216*(1), 1-10. doi: 10.1007/s00221-011-2891-9

Jeon, S. Y., & Han, S. J. (2012). Improvement of the working memory and naming by transcranial direct current stimulation. *Ann Rehabil Med, 36*(5), 585-595. doi: 10.5535/arm.2012.36.5.585

Jung, R. E., & Haier, R. J. (2007). The Parieto-Frontal Integration Theory (P-FIT) of intelligence: converging neuroimaging evidence. *Behavioral and Brain Sciences, 30*(2), 135-154; discussion 154-187. doi: 10.1017/S0140525X07001185

Kaufman, A., & Lichtenberger, E. (2005). *Assessing Adolescent and Adult Intelligence* (3rd ed.). Hoboken, NJ: Wiley.

Keeser, D., Meindl, T., Bor, J., Palm, U., Pogarell, O., Mulert, C., . . . Padberg, F. (2011). Prefrontal transcranial direct current stimulation changes connectivity of resting-state networks during fMRI. *J Neurosci, 31*(43), 15284-15293. doi: 10.1523/JNEUROSCI.0542-11.2011

Keeser, D., Padberg, F., Reisinger, E., Pogarell, O., Kirsch, V., Palm, U., . . . Mulert, C. (2011). Prefrontal direct current stimulation modulates resting EEG and event-related potentials in healthy subjects: a standardized low resolution tomography (sLORETA) study. *Neuroimage, 55*(2), 644-657. doi: 10.1016/j.neuroimage.2010.12.004

Kim, J. H., Kim, D. W., Chang, W. H., Kim, Y. H., Kim, K., & Im, C. H. (2014). Inconsistent outcomes of transcranial direct current stimulation may originate from anatomical differences among individuals: electric field simulation using individual MRI data. *Neurosci Lett, 564*, 6-10. doi: 10.1016/j.neulet.2014.01.054

Krawczyk, D. C., Michelle McClelland, M., & Donovan, C. M. (2011). A hierarchy for relational reasoning in the prefrontal cortex. *Cortex, 47*(5), 588-597. doi: 10.1016/j.cortex.2010.04.008

Lally, N., Nord, C. L., Walsh, V., & Roiser, J. P. (2013). Does excitatory fronto-extracerebral tDCS lead to improved working memory performance? *F1000Res, 2*, 219. doi: 10.12688/f1000research.2-219.v2

Lee, W. H., Deng, Z. D., Kim, T. S., Laine, A. F., Lisanby, S. H., & Peterchev, A. V. (2012). Regional electric field induced by electroconvulsive therapy in a realistic finite element head model: influence of white matter anisotropic conductivity. *Neuroimage, 59*(3), 2110-2123. doi: 10.1016/j.neuroimage.2011.10.029

Lee, W. H., Lisanby, S. H., Laine, A. F., & Peterchev, A. V. (2014). Stimulation strength and focality of electroconvulsive therapy and magnetic seizure therapy in a realistic head model. *IEEE Eng Med Biol Conf 2014, In press*.

Liebetanz, D., Nitsche, M. A., Tergau, F., & Paulus, W. (2002). Pharmacological approach to the mechanisms of transcranial DC-stimulation-induced after-effects of human motor cortex excitability. *Brain, 125*(Pt 10), 2238-2247.

Liu, J., Zhang, M., Jou, J., Wu, X., Li, W., & Qiu, J. (2012). Neural bases of falsification in conditional proposition testing: evidence from an fMRI study. *Int J Psychophysiol, 85*(2), 249-256. doi: 10.1016/j.ijpsycho.2012.02.011

Meiron, O., & Lavidor, M. (2013). Unilateral prefrontal direct current stimulation effects are modulated by working memory load and gender. *Brain Stimul, 6*(3), 440-447. doi: 10.1016/j.brs.2012.05.014

Miller, E. K., & Buschman, T. J. (2013). Cortical circuits for the control of attention. *Curr Opin Neurobiol, 23*(2), 216-222. doi: 10.1016/j.conb.2012.11.011

Mulquiney, P. G., Hoy, K. E., Daskalakis, Z. J., & Fitzgerald, P. B. (2011). Improving working memory: exploring the effect of transcranial random noise stimulation and transcranial direct current stimulation on the dorsolateral prefrontal cortex. *Clin Neurophysiol, 122*(12), 2384-2389. doi: 10.1016/j.clinph.2011.05.009

Mylius, V., Jung, M., Menzler, K., Haag, A., Khader, P. H., Oertel, W. H., . . . Lefaucheur, J. P. (2012). Effects of transcranial direct current stimulation on pain perception and working memory. *Eur J Pain, 16*(7), 974-982. doi: 10.1002/j.1532-2149.2011.00105.x

Nagahama, Y., Okada, T., Katsumi, Y., Hayashi, T., Yamauchi, H., Sawamoto, N., . . . Shibasaki, H. (1999). Transient neural activity in the medial superior frontal gyrus and precuneus time locked with attention shift between object features. *Neuroimage, 10*(2), 193-199. doi: 10.1006/nimg.1999.0451

Nitsche, M. A., Fricke, K., Henschke, U., Schlitterlau, A., Liebetanz, D., Lang, N., . . . Paulus, W. (2003). Pharmacological modulation of cortical excitability shifts induced by transcranial direct current stimulation in humans. *J Physiol, 553*(Pt 1), 293-301. doi: 10.1113/jphysiol.2003.049916

Nitsche, M. A., & Paulus, W. (2000). Excitability changes induced in the human motor cortex by weak transcranial direct current stimulation. *J Physiol, 527 Pt 3*, 633-639.

Nord, C. L., Lally, N., & Charpentier, C. J. (2013). Harnessing electric potential: DLPFC tDCS induces widespread brain perfusion changes. *Front Syst Neurosci, 7*, 99. doi: 10.3389/fnsys.2013.00099

Ohn, S. H., Park, C. I., Yoo, W. K., Ko, M. H., Choi, K. P., Kim, G. M., . . . Kim, Y. H. (2008). Time-dependent effect of transcranial direct current stimulation on the enhancement of working memory. *Neuroreport, 19*(1), 43-47. doi: 10.1097/WNR.0b013e3282f2adfd

Olesen, P. J., Westerberg, H., & Klingberg, T. (2004). Increased prefrontal and parietal activity after training of working memory. *Nat Neurosci, 7*(1), 75-79. doi: 10.1038/nn1165

Ozen, S., Sirota, A., Belluscio, M. A., Anastassiou, C. A., Stark, E., Koch, C., & Buzsaki, G. (2010). Transcranial electric stimulation entrains cortical neuronal populations in rats. *J Neurosci, 30*(34), 11476-11485. doi: 10.1523/JNEUROSCI.5252-09.2010

Pahor, A., & Jausovec, N. (2014). The effects of theta transcranial alternating current stimulation (tACS) on fluid intelligence. *Int J Psychophysiol, 93*(3), 322-331. doi: 10.1016/j.ijpsycho.2014.06.015

Peters, M. A., Thompson, B., Merabet, L. B., Wu, A. D., & Shams, L. (2013). Anodal tDCS to V1 blocks visual perceptual learning consolidation. *Neuropsychologia, 51*(7), 1234-1239. doi: 10.1016/j.neuropsychologia.2013.03.013

Pirulli, C., Fertonani, A., & Miniussi, C. (2013). The role of timing in the induction of neuromodulation in perceptual learning by transcranial electric stimulation. *Brain Stimul, 6*(4), 683-689. doi: 10.1016/j.brs.2012.12.005

Pons, J. P., Segonne, E., Boissonnat, J. D., Rineau, L., Yvinec, M., & Keriven, R. (2007). High-quality consistent meshing of multi-label datasets. *Inf Process Med Imaging, 20*, 198-210.

Poreisz, C., Boros, K., Antal, A., & Paulus, W. (2007). Safety aspects of transcranial direct current stimulation concerning healthy subjects and patients. *Brain Res Bull, 72*(4-6), 208-214. doi: 10.1016/j.brainresbull.2007.01.004

Prabhakaran, V., Smith, J. A., Desmond, J. E., Glover, G. H., & Gabrieli, J. D. (1997). Neural substrates of fluid reasoning: an fMRI study of neocortical activation during performance of the Raven's Progressive Matrices Test. *Cogn Psychol, 33*(1), 43-63. doi: 10.1006/cogp.1997.0659

Purpura, D. P., & McMurtry, J. G. (1965). Intracellular Activities and Evoked Potential Changes during Polarization of Motor Cortex. *J Neurophysiol, 28*, 166-185.

Raichle, M. E., MacLeod, A. M., Snyder, A. Z., Powers, W. J., Gusnard, D. A., & Shulman, G. L. (2001). A default mode of brain function. *Proc Natl Acad Sci U S A, 98*(2), 676-682. doi: 10.1073/pnas.98.2.676

Reato, D., Rahman, A., Bikson, M., & Parra, L. C. (2010). Low-intensity electrical stimulation affects network dynamics by modulating population rate and spike timing. *J Neurosci, 30*(45), 15067-15079. doi: 10.1523/JNEUROSCI.2059-10.2010

Reinhart, R. M., & Woodman, G. F. (2014). Causal control of medial-frontal cortex governs electrophysiological and behavioral indices of performance monitoring and learning. *J Neurosci, 34*(12), 4214-4227. doi: 10.1523/JNEUROSCI.5421-13.2014

Reinhart, R. M., & Woodman, G. F. (2015). Enhancing long-term memory with stimulation tunes visual attention in one trial. *Proc Natl Acad Sci U S A, 112*(2), 625-630. doi: 10.1073/pnas.1417259112

Salthouse, T. A., & Pink, J. E. (2008). Why is working memory related to fluid intelligence? *Psychon Bull Rev, 15*(2), 364-371.

Santarnecchi, E., Polizzotto, N. R., Godone, M., Giovannelli, F., Feurra, M., Matzen, L., . . . Rossi, S. (2013). Frequency-dependent enhancement of fluid intelligence induced by transcranial oscillatory potentials. *Curr Biol, 23*(15), 1449-1453. doi: 10.1016/j.cub.2013.06.022

Sattler, J. (2008a). *Assessment of Children: Cognitive Foundations* (5th ed.): Jerome M. Sattler, Publisher.

Sattler, J. (2008b). *Resource Guide to Accompany Assessment of Children: Cognitive Foundations* (5th ed.): Jerome M. Sattler Publisher.

Sattler, J., & Ryan, J. (2009). *Assessment with the WAIS-IV*. La Mesa, CA: Jerone M Sattler Publisher.

Sehm, B., Schnitzler, T., Obleser, J., Groba, A., Ragert, P., Villringer, A., & Obrig, H. (2013). Facilitation of inferior frontal cortex by transcranial direct current stimulation induces perceptual learning of severely degraded speech. *J Neurosci, 33*(40), 15868-15878. doi: 10.1523/JNEUROSCI.5466-12.2013

Shaw, P., Greenstein, D., Lerch, J., Clasen, L., Lenroot, R., Gogtay, N., . . . Giedd, J. (2006). Intellectual ability and cortical development in children and adolescents. *Nature, 440*(7084), 676-679. doi: 10.1038/nature04513

Shulman, G. L., Fiez, J. A., Corbetta, M., Buckner, R. L., Miezin, F. M., Raichle, M. E., & Petersen, S. E. (1997). Common Blood Flow Changes across Visual Tasks: II. Decreases in Cerebral Cortex. *J Cogn Neurosci, 9*(5), 648-663. doi: 10.1162/jocn.1997.9.5.648

Siegel, M., Warden, M. R., & Miller, E. K. (2009). Phase-dependent neuronal coding of objects in short-term memory. *Proc Natl Acad Sci U S A, 106*(50), 21341-21346. doi: 10.1073/pnas.0908193106

Snowball, A., Tachtsidis, I., Popescu, T., Thompson, J., Delazer, M., Zamarian, L., . . . Cohen Kadosh, R. (2013). Long-term enhancement of brain function and cognition using cognitive training and brain stimulation. *Curr Biol, 23*(11), 987-992. doi: 10.1016/j.cub.2013.04.045

Spearman, C. (1904). "General intelligence " objectively determined and measured. *American Journal of Psychology, 15*, 201-292. doi: Doi 10.2307/1412107

Stagg, C. J., Lin, R. L., Mezue, M., Segerdahl, A., Kong, Y., Xie, J., & Tracey, I. (2013). Widespread modulation of cerebral perfusion induced during and after transcranial direct current stimulation applied to the left dorsolateral prefrontal cortex. *J Neurosci, 33*(28), 11425-11431. doi: 10.1523/JNEUROSCI.3887-12.2013

Stagg, C. J., & Nitsche, M. A. (2011). Physiological basis of transcranial direct current stimulation. *Neuroscientist, 17*(1), 37-53. doi: 10.1177/1073858410386614

Sternberg, R. J., & Kaufman, S. B. (2011). *The Cambridge Handbook of Intelligence*. Cambridge ; New York: Cambridge University Press.

Takeuchi, H., Taki, Y., & Kawashima, R. (2010). Effects of working memory training on cognitive functions and neural systems. *Rev Neurosci, 21*(6), 427-449.

Team, R. C. (2014). R: A language and environment for statistical computing. . Vienna, Austria: R Foundation for Statistical Computing. Retrieved from http://www.R-project.org/

Teo, F., Hoy, K. E., Daskalakis, Z. J., & Fitzgerald, P. B. (2011). Investigating the Role of Current Strength in tDCS Modulation of Working Memory Performance in Healthy Controls. *Front Psychiatry, 2*, 45. doi: 10.3389/fpsyt.2011.00045

Thompson, P. M., Cannon, T. D., Narr, K. L., van Erp, T., Poutanen, V. P., Huttunen, M., . . . Toga, A. W. (2001). Genetic influences on brain structure. *Nat Neurosci, 4*(12), 1253-1258. doi: 10.1038/nn758

Tremblay, S., Lepage, J. F., Latulipe-Loiselle, A., Fregni, F., Pascual-Leone, A., & Theoret, H. (2014). The uncertain outcome of prefrontal tDCS. *Brain Stimul, 7*(6), 773-783. doi: 10.1016/j.brs.2014.10.003

Uhlhaas, P. J., Haenschel, C., Nikolic, D., & Singer, W. (2008). The role of oscillations and synchrony in cortical networks and their putative relevance for the pathophysiology of schizophrenia. *Schizophr Bull, 34*(5), 927-943. doi: 10.1093/schbul/sbn062

Unsworth, N., & Engle, R. W. (2007). On the division of short-term and working memory: an examination of simple and complex span and their relation to higher order abilities. *Psychol Bull, 133*(6), 1038-1066. doi: 10.1037/0033-2909.133.6.1038

van den Heuvel, M. P., Stam, C. J., Kahn, R. S., & Hulshoff Pol, H. E. (2009). Efficiency of functional brain networks and intellectual performance. *J Neurosci, 29*(23), 7619-7624. doi: 10.1523/JNEUROSCI.1443-09.2009

Ward, L. M. (2003). Synchronous neural oscillations and cognitive processes. *Trends Cogn Sci, 7*(12), 553-559.

Wechsler, D. (2008a). *Wechsler Adult Intelligence Scale - Fourth Edition: Administration and Scoring Manual*. San Antonio, TX: Pearson Education, Inc.

Wechsler, D. (2008b). *Wechsler Adult Intellignece Scale: Technical and Interpretive Manual* (4th ed.). San Antonio, TX, USA: Pearson Education, Inc.

Yushkevich, P. A., Piven, J., Hazlett, H. C., Smith, R. G., Ho, S., Gee, J. C., & Gerig, G. (2006). User-guided 3D active contour segmentation of anatomical structures: significantly improved efficiency and reliability. *Neuroimage, 31*(3), 1116-1128. doi: 10.1016/j.neuroimage.2006.01.015

Zaehle, T., Sandmann, P., Thorne, J. D., Jancke, L., & Herrmann, C. S. (2011). Transcranial direct current stimulation of the prefrontal cortex modulates working memory performance: combined behavioural and electrophysiological evidence. *BMC Neurosci, 12*, 2. doi: 10.1186/1471-2202-12-2

Zhang, Y., Brady, M., & Smith, S. (2001). Segmentation of brain MR images through a hidden Markov random field model and the expectation-maximization algorithm. *IEEE Trans Med Imaging, 20*(1), 45-57. doi: 10.1109/42.906424

Zmigrod, S. (2014). The role of the parietal cortex in multisensory and response integration: evidence from transcranial direct current stimulation (tDCS). *Multisens Res, 27*(2), 161-172.

Zmigrod, S., Colzato, L. S., & Hommel, B. (2014). Evidence for a role of the right dorsolateral prefrontal cortex in controlling stimulus-response integration: a transcranial direct current stimulation (tDCS) study. *Brain Stimul, 7*(4), 516-520. doi: 10.1016/j.brs.2014.03.004

CHAPTER 3: TARGETING THE NEUROPHYSIOLOGY OF COGNITIVE SYSTEMS WITH TRANSCRANIAL ALTERNATING CURRENT STIMULATION[2]

INTRODUCTION

Behavior arises from the dynamic interplay of sensory input and internal states such as motivation and expectation. Neural activity patterns in large-scale, distributed networks provide the substrate that mediates behavior. Over the last few years, there have been a rapidly rising number of reports that non-invasive brain stimulation with weak electric fields (transcranial current stimulation) can alter brain network dynamics and behavior. Most studies have employed transcranial direct current stimulation (tDCS), which modulates neuronal activity level and excitability in a polarity-specific way (Nitsche & Paulus, 2000). However, tDCS cannot be tailored to directly modulate specific activity patterns of brain networks. In contrast, transcranial alternating current stimulation (tACS) employs a sine-wave electric field that appears to preferentially enhance network oscillations at frequencies close to the stimulation frequency. The effect of tACS results from electric polarization of neurons which are aligned with the applied field (Radman, Ramos, Brumberg, & Bikson, 2009); in the case of tACS, the periodic nature of the sine-wave results in a temporally structured change in membrane voltages across the network thus influencing overall network activity (Deans, Powell, & Jefferys, 2007; Frohlich & McCormick, 2010). See (Herrmann, Rach, Neuling, & Struber, 2013) for a review on the physiological mechanisms of tACS. Thus, at least theoretically, tACS can be used to probe for the causal role of specific cortical activity patterns in cognition and to then remediate deficits in activity patterns in patient populations with cognitive impairment. For example, tACS at 40 Hz could be used to demonstrate the causal role of gamma

[2] This chapter previously appeared as an article in Expert Review of Neurotherapeutics; doi: 10.1586/14737175.2015.992782 (http://www.tandfonline.com/doi/abs/10.1586/14737175.2015.992782?journalCode=iern20). The original citation is as follows: Frohlich F, **Sellers KK**, Cordle AL. (2015). Targeting the neurophysiology of cognitive systems with transcranial alternating current stimulation. Expert Review of Neurotherapeutics, 15(2):145-67.

oscillations (>30 Hz) in a specific cognitive capability and then such stimulation could be used in patients with impaired gamma oscillations that cause the corresponding cognitive impairment. Clearly, this is an oversimplification that rests on several untested assumptions, yet the underlying conceptual framework at least provides guidance for a discovery process aimed at (1) elucidating the neural basis of cognition and (2) rational design of brain stimulation treatments for cognitive impairment.

Despite tACS being far from ready to implement in such applications of cognitive enhancement, we here discuss existing studies that utilize tACS. Specifically, this review follows the framework developed by the National Institute of Mental Health (NIMH) in the Research Domain Criteria project (RDoC) to provide a comprehensive update on the status of tACS research as related to the cognitive systems domain. The RDoC initiative was developed to aid psychiatry research by using a classification scheme based on neurobiological measures and observable behavior. The studies reviewed here were primarily conducted in healthy adult populations, and provide crucial insight into the effects of brain stimulation on cognitive processes. In turn, this work can inform future studies which more directly develop tACS as a treatment for neuropsychiatric disorders. The cognitive and behavior abnormalities observed in these patients may be related to the altered oscillatory activity in cortex (Buzsaki & Watson, 2012; Uhlhaas & Singer, 2010). Thus, future tACS paradigms may one day serve as an effective treatment modality towards alleviating cognitive and behavioral abnormalities associated with neuropsychiatric diseases.

To date, tDCS has been much more extensively studied that tACS (Nitsche et al., 2008; Nitsche & Paulus, 2011). Both basic science and clinical studies with tDCS have been extensively discussed and reviewed elsewhere (Berlim, Van den Eynde, & Daskalakis, 2013; Brunoni, Fregni, & Pagano, 2011; Kalu, Sexton, Loo, & Ebmeier, 2012; Monti et al., 2013). Studies have demonstrated that tDCS can induce (1) modulation of neurophysiological measures (e.g. motor-evoked potentials, MEPs) (Nitsche & Paulus, 2000), (2) changes in motor performance, (e.g. (Reis & Fritsch, 2011)), (3) alteration in brain activity as measured by EEG (Antal, Kincses, Nitsche, Bartfai, & Paulus, 2004), and (4) state-dependent stimulation effects (Antal, Terney, Poreisz, & Paulus, 2007). The use of tDCS for the treatment of tinnitus (Song, Vanneste, Van de Heyning, & De Ridder, 2012), major depression (Nitsche, Boggio, Fregni, & Pascual-Leone, 2009), Parkinson's disease (Benninger et al., 2010; Fregni et al., 2006) and especially in

stroke rehabilitation (Schlaug, Renga, & Nair, 2008) appear to be particularly effective, likely through correction of pathological hypo- or hyperexcitability.

However, a wide range of cognitive capabilities are mediated by the dynamic modulation of rhythmic oscillatory activity within and between different brain regions, rather than solely broad increases or decreases in excitability. For example, beta and gamma oscillations mediate interactions between sensory cortices and prefrontal cortex to direct attention (Benchenane, Tiesinga, & Battaglia, 2011), synchrony between frontal and parietal cortices in the delta frequency band appears to underlie decision making (Nacher, Ledberg, Deco, & Romo, 2013), and slow oscillatory activity aids the consolidation of declarative memories (Molle & Born, 2011). Similarly, cognitive deficits in neuropsychiatric disorders are associated with alterations in the structure of rhythmic oscillatory activity, rather than strict hypo- or hyper-excitability. A reduction in gamma band oscillations has consistently been demonstrated in patients with schizophrenia during working memory, executive control, and perceptual processing (Uhlhaas & Singer, 2012). Interestingly, patients with schizophrenia also exhibit elevated baseline gamma power (Kikuchi et al., 2014; Spencer, 2011). Individuals with autism spectrum disorder exhibit fronto-posterior networks with atypical modulation of gamma activity (Sun et al., 2012) and decreased frontoparietal theta coherence, which correlated with clinical disease severity (Kikuchi et al., 2014).

In light of the physiological and pathological relevance of rhythmic brain activity, the brain stimulation community has recently witnessed a surge of interest in the non-invasive application of weak electric current using sine-wave waveforms (tACS) in order to target brain oscillations at specific frequencies (Figure 3.1, A: In vitro studies have demonstrated that sine-waves applied with different periods (T) entrain action potential firing. B: Illustration of sine-wave current used in tACS studies). In terms of changes to neurophysiological activity, tACS can induce modulation of MEPs in a frequency-specific manner (Feurra, Bianco, et al., 2011; Wach et al., 2013b; Zaghi et al., 2010), increase oscillatory power matched to the frequency of stimulation (Pogosyan, Gaynor, Eusebio, & Brown, 2009; Voss et al., 2014; Zaehle, Rach, & Herrmann, 2010), and exhibit state-dependent effects (Feurra et al., 2013; Neuling, Rach, & Herrmann, 2013). Stimulation is typically delivered at frequencies within the range of the classic EEG frequency bands, which span the range of most commonly observed physiological oscillation frequencies of cortical network activity: delta (0.5-4Hz), theta (4-8Hz), alpha (8-12Hz), beta (12-30Hz),

and gamma (30-80Hz) (Wach et al., 2013a). Importantly, the effects of tACS are dependent on the frequency of the applied alternating current stimulation (Schutter & Hortensius, 2011; Wach et al., 2013a).

Coinciding with the emergence of tACS and other neurostimulation techniques for investigating brain dynamics, new initiatives to encourage more mechanism-driven scientific investigations into neuropsychiatric pathology have gained traction. In 2009, the NIMH launched the Research Domain Criteria project (RDoC) to classify psychopathology "based on dimensions of observable behavior and neurobiological measures" (Insel et al., 2010). In alignment with the fundamental premises of non-invasive brain stimulation, the framework postulates: "psychiatric conditions are disorders of brain circuits, tools of clinical neuroscience can characterize or identify brain circuit dysfunction, and biomarkers or biosignatures identified via neuroscience investigation can inform clinical management" (Insel et al., 2010). Although RDoC stresses "circuits" as a primary or central unit of analysis within cognitive domains and other domains of behavioral function, the framework also includes subjective reports and other units of analysis associated with psychological investigation. Environmental and developmental factors are suggested as orthogonal dimensions that span many levels of analysis (Morris & Cuthbert, 2012). Importantly, the authors of RDoC recognize the reliability of DSM diagnoses, which are largely based on clusters of clinical symptoms, but aim to provide a novel conceptual framework to guide and accelerate the study of fundamental brain pathologies (e.g. changes in the circuitry that mediates cognition) that often span many DSM diagnoses. They assert that the neurobiological mechanisms of psychiatric symptoms and syndromes do not map well onto DSM categories; in some cases there appears to be considerable heterogeneity of mechanisms within categories while in other instances there exists considerable mechanistic overlap between supposedly discrete categories or diagnoses.

We here make the argument that brain stimulation research should be driven by rational design such that stimulation paradigms are developed to target specific brain networks to alter and enhance brain function. Thus, we propose that the RDoC framework offers a unique opportunity to provide important structure and guidance to the rapidly growing tACS field and to accelerate targeted development of novel treatments based on tACS (Cuthbert & Insel, 2013). Therefore, in this review, tACS studies will be discussed though the lens of the RDoC domain of cognitive systems. We first review tACS studies which target or modulate the circuits and networks associated with the major cognitive domain

constructs of RDoC: attention, perception, working memory, declarative memory, language, and cognitive control (Figure 3.2). The purpose, stimulation parameters, and findings of each study discussed here are summarized in Table 3.1. Each construct is introduced according to its RDoC definition and implicated neurobiological systems or circuits. Reflecting the purpose of RDoC, these constructs cut across multiple established diagnostic categories. The construct of perception, for instance, involves numerous brain systems and circuits related to each of the sensory modalities as well as higher order processing. Deficits in these circuits could become the subject of investigation of perceptual disturbances in any of the various DSM clinical categories of pathology, including schizophrenia, dementia, bipolar disorder, alcoholic hallucinosis, numerous substance withdrawal or intoxication syndromes, and delirium. Most of the other constructs in the cognitive domain span a comparable spectrum of existing clinical diagnostic categories.

We conclude this article with a five year perspective on extending the field of tACS from basic science research conducted in healthy human participants to the testing and development of treatments for clinical populations suffering from neuropsychiatric illnesses. In using this approach, we seek to illustrate how the RDoC approach can facilitate translation of tACS research into the development of clinically meaningful interventions.

EXPERT COMMENTARY

Attention

According to RDoC, attention refers to “a range of processes that regulate access to capacity-limited systems, such as awareness, higher perceptual processes, and motor action. The concepts of capacity limitation and competition are inherent to the concepts of selective and divided attention” ("Workshop Proceedings of the NIMH Research Domain Criteria (RDoC) Project: Cognitive Systems, Rockville," 2010). Attention is conceptualized as including attention control and attention implementation. With regard to attention control functions, the workshop proceedings cite dorsal and ventral networks distributed through frontal and parietal cortices and subcortical structures. Regarding implementation of attention, local circuit interactions and feed-forward transmission of information through sensory systems are cited, and overlaps with the cognitive control construct are recognized ("Workshop Proceedings of the NIMH Research Domain Criteria (RDoC) Project: Cognitive Systems, Rockville," 2010). Attention capacity

is notably reduced in disorders such as attention-deficit-hyperactivity-disorder (ADHD) but also many other DSM-based diagnoses. Interestingly, EEG recordings conducted during the resting state in healthy control subjects and individuals with diagnosed ADHD have demonstrated that this clinical population exhibits increased oscillatory power in the low frequency bands and reduced power in higher frequencies (alpha and beta) (Woltering, Jung, Liu, & Tannock, 2012). Therefore, distinct patterns of oscillatory activity during rest (Woltering et al., 2012) and during attention-demanding tasks (Mazaheri et al., 2013) may be evident in psychiatric illnesses with deficits in attention.

To date, Laczo et al (Laczo, Antal, Niebergall, Treue, & Paulus, 2012) is the only study which has directly tested the effect of tACS on attention. The authors assessed spatial visual attention, a process which enables selective and covert (i.e. without gaze shifts) direction of limited processing capacity to specific locations in the visual field. Changes in contrast sensitivity were used to study the effect of attention on visual information processing. Based on previous work demonstrating the importance of gamma frequency oscillations in spatial visual attention, the authors hypothesized that gamma frequency tACS applied to the primary visual cortex would alter neural synchronization and change the effect of attention on contrast perception. Utilizing the longest duration of stimulation published to date (45 minutes ± 10 minutes), the authors demonstrated that 60Hz tACS improved contrast detection in healthy adults. However, the authors did not find a change in spatial attention. The reported lack of stimulation effect when applied over V1 may ensue from non-optimal placement of stimulation electrodes to target attentional circuits, since attention modulates primary visual cortex and sensory perception but frontal and parietal areas have been implicated as the circuitry controlling attentional processing (Buschman & Miller, 2007; Peers et al., 2005).

While much of the early work in tACS was conducted in the motor system, these studies mostly looked at alterations in excitability rather than capacity-limited allocation to the motor system. A notable exception, the study by Joundi and colleagues (Joundi, Jenkinson, Brittain, Aziz, & Brown, 2012) used tACS to directly probe the role of oscillatory activity in determining motor behavior. The authors administered tACS over motor cortex at both beta and gamma frequencies to healthy adults during a go/no-go paradigm which cued either motor action or motor inhibition. In contrast to altering the excitability of motor cortex, this task required attention for the regulation of motor action (or inaction). The

authors' findings support the general framework that beta oscillatory activity in motor cortex is antikinetic, while gamma oscillations in motor cortex are prokinetic. While the purpose of this study was not to directly assess the effect of tACS on the circuitry involved in attentional processing or modulation on performance, the involvement of attention in the behavioral task is important to note. Because the effect of tACS on attentional processing is unknown, it is difficult to disentangle the effects of stimulation on motor performance from potential modulation of attention which influenced performance on the motor task.

Understanding the effect of tACS on attention is still in its infancy. Future work should directly modulate frontal and parietal cortices, the putative control centers of attentional processing, and assess performance changes on attentional tasks. This work will need to assess if increased neuronal synchrony between cortical areas, enhancement of specific rhythmic activity within a given area, or yet another mechanism is required for improvement in attention. Subsequently or concurrently, individuals with deficits in attention can be tested for stimulation-induced improvements in attentional performance.

Perception

The perception construct is defined as "process(es) that perform computations on sensory data to construct and transform representations of the external environment, acquire information from, and make predictions about, the external world, and guide action" ("Workshop Proceedings of the NIMH Research Domain Criteria (RDoC) Project: Cognitive Systems, Rockville," 2010). Sub-constructs include (1) visual, (2) auditory, and (3) olfactory, somatosensory, and multimodal perception. Changes in gamma and alpha frequency oscillations are frequently observed with cognitive and perceptual tasks (Jensen & Mazaheri, 2010; Martinovic & Busch, 2011; Palva & Palva, 2007). Substantial evidence suggests that individuals diagnosed with schizophrenia exhibit abnormal gamma band oscillations (Uhlhaas, Haenschel, Nikolic, & Singer, 2008). Saliently, schizophrenia is associated with impairments in perception, commonly manifested as auditory hallucinations (Basar & Guntekin, 2008). During an auditory oddball task, individuals with schizophrenia exhibited abnormal gamma activation patterns compared to age- and gender- matched controls (Haig et al., 2000). Together, this body of work suggests that altered oscillatory activity in the gamma frequency band may underlie changes in perception seen in schizophrenia. It

remains to be studied if similar network pathologies may drive perceptual impairment in other psychiatric illnesses.

tACS studies on the visual modality of perception have built on the observation that switches in conscious perception of an ambiguous stimulus are correlated with alterations in synchronized activity in the gamma band (Engel, Fries, & Singer, 2001). Struber et al (Struber, Rach, Trautmann-Lengsfeld, Engel, & Herrmann, 2014) sought to test a causal role of gamma activity in conscious perception by administering bilateral 40Hz tACS over occipito-parietal areas while subjects were presented bistable apparent motion stimuli; stimulation was administered with a 180° phase difference between hemispheres. Switches between horizontal and vertical apparent motion are believed to indicate changes in interhemispheric functional coupling. The authors report that interhemispheric gamma band coherence increased while the proportion of perceived horizontal motion decreased. There were no changes in interhemispheric coherence or perceived motion induced by control 6Hz tACS administered with 0° or 180° phase difference. The authors suggest that these counterintuitive results (one might expect increased interhemispheric gamma coherence to correlate with increased horizontal perception) may have resulted from the phase offset of stimulation between the two hemispheres, which may have led to functional decoupling and thereby impaired perceived horizontal motion. The authors tested 0° phase difference 40Hz tACS, but did not find a significant effect on coherence or motion perception. Another study applied tACS over primary visual cortex at different gamma frequencies while subjects performed a four-alternative forced-choice detection task (Laczo et al., 2012). 60Hz tACS decreased contrast-discrimination thresholds, indicating an improvement in visual contrast perception. However, 40Hz and 80Hz tACS did not induce similar improvement on perception. Future studies may choose to look at the frequency of endogenous gamma oscillatory activity and incorporate theories of resonance when selecting a stimulation frequency for optimal modulation of activity.

While gamma oscillations have been implicated in switches in conscious perception, posterior alpha power is believed to regulate perception. Posterior alpha rhythms are influenced by visual spatial attention, and likely provide functional inhibition of non-relevant stimuli and locations. Specifically, studies have demonstrated that alpha activity in the posterior cortex decreases the quality of visual perception in the contralateral hemi-field (Ergenoglu et al., 2004; Romei, Gross, & Thut, 2010), while alpha power

increases have been measured in the occipital cortex hemisphere receiving visual information from the non-attended hemi-field (Kelly, Lalor, Reilly, & Foxe, 2006; Worden, Foxe, Wang, & Simpson, 2000). Brignani et al (Brignani, Ruzzoli, Mauri, & Miniussi, 2013) tested the role of alpha frequency activity on perception by delivering tACS at 10Hz over the left or right occipito-posterior area while healthy adults performed a visual detection and discrimination task. Individuals receiving alpha stimulation showed decreased visual perception compared to individuals who received sham tACS; however, individuals who received 6Hz tACS also exhibited poorer performance on the perception task. The authors were cautious about claiming tACS-induced modulation of visual perception because of only partially-confirmed frequency specificity and lack of retinotopic specificity. Lack of neurophysiological measurements in this study precludes conclusive statements about how the applied frequencies of tACS modulated posterior alpha rhythms. To address this question, Helfrich et al (Helfrich et al., 2014) developed a novel artifact rejection technique which permitted analysis of EEG data acquired during the application of tACS. The authors found that 10Hz alpha frequency tACS applied over the parieto-occipital cortex increased alpha activity in this area and induced synchronization of oscillatory activity with the phase of the applied stimulation. In further support of the role of alpha rhythms in gating perception, the authors found that alpha frequency tACS enhanced target detection performance in a phase-dependent manner through augmented cortical alpha synchronization.

In other studies of visual perception, tACS administered over occipital cortex was sufficient to induce visual phosphenes; beta frequency stimulation was most effective at inducing the perception of phosphenes in an illuminated room, whereas alpha frequency stimulation was more effective at inducing this visual experience in a dark room (Kanai, Paulus, & Walsh, 2010). Furthermore, 20Hz tACS over the occipital region has been found to decrease the threshold for inducing visual phosphenes elicited by transcranial magnetic stimulation (TMS) pulses (Kanai et al., 2010). However, there is debate as to whether tACS-induced phosphenes originate in the visual cortex or because of retinal stimulation (Schutter & Hortensius, 2010; Schwiedrzik, 2009).

In the auditory sensory modality, alpha frequency tACS with a direct current offset modulated the detection of auditory stimuli embedded in continuous band-limited white noise (Neuling, Rach, Wagner, Wolters, & Herrmann, 2012). Importantly, the authors found that detection threshold was dependent on

the phase of the oscillation that was entrained by application of tACS. Such phase-dependent modulation of excitability has been previously shown in observational studies that employed EEG and MEG (Hanslmayr et al., 2007; Mathewson et al., 2011; Palva & Palva, 2007; Rajagovindan & Ding, 2011). Effects of tACS on perception in the somatosensory system have also been tested. tACS was applied to right somatosensory cortex (exact stimulation location was localized with transcranial magnetic stimulation), corresponding to sensation in the contralateral hand (Feurra, Paulus, Walsh, & Kanai, 2011). Stimulation was applied systematically from 2-70Hz, in steps of 2Hz, and individuals were asked to subjectively rate the perception of tactile sensations in their hand. The authors found that alpha, beta, and high gamma frequency tACS produced tactile sensation in the contralateral hand in absence of physical stimulation. This report demonstrates frequency-specific effects of tACS on somatosensory perception.

Perception through the use of visual, auditory, olfactory, somatosensory, and multimodal modalities allows for internal representations of the external world. Oscillatory power and coherence between different brain areas and across the hemispheres mediates this processing. Continued work using tACS to selectively modulate these activity patterns can help to further elucidate the network activity patterns responsible for perception.

Working Memory

The construct of working memory (WM) is defined in RDoC as: “the active maintenance and flexible updating of goal/task relevant information (items, goals, strategies, etc.) in a form that has limited capacity and resists interference. These representations: may involve flexible binding of representations; may be characterized by the absence of external support for the internally maintained representation; and are frequently temporary, though this may be due to ongoing interference” ("Workshop Proceedings of the NIMH Research Domain Criteria (RDoC) Project: Working Memory, Rockville," 2010). Sub-constructs include (1) active maintenance, (2) flexible updating, (3) limited capacity, and (4) interference control. The RDoC workshop (2010) cites representative examples of circuits as including “extensive loops from the PFC through the basal ganglia that may be important for driving the flexible updating of PFC representations, and in learning new tasks. There are connections between the PFC and medial temporal lobe that may support encoding of the contents of WM into long term memory and retrieval of stored

memories that can be reactivated in WM" ("Workshop Proceedings of the NIMH Research Domain Criteria (RDoC) Project: Working Memory, Rockville," 2010). WM is critical in everyday life for communication, learning, and successful task completion.

Models of WM suggest that frontal areas are responsible for the executive function and processing aspects of WM, while posterior parietal cortex is linked to the limited capacity storage component of WM (Curtis & D'Esposito, 2003; Smith & Jonides, 1999; Todd & Marois, 2004). In electrophysiological investigations, activation of the frontoparietal network has been associated with WM tasks (Kawasaki, Kitajo, & Yamaguchi, 2010). Theta frequency power and phase synchronization between frontal and parietal regions have been implicated in integrating WM associations into coherent representations (Mizuhara & Yamaguchi, 2007; Wu, Chen, Li, Han, & Zhang, 2007). However, evidence that PFC can maintain the memory of a sample trace in the presence of distractors, unlike posterior parietal cortex, suggests that dorsolateral prefrontal cortex (DLPFC) supports both the storage and processing functions of WM (Miller & Cohen, 2001). For example, patients diagnosed with Alzheimer's disease exhibit deficits in WM. This clinical population often exhibits decreased evoked coherence in the left frontoparietal region in the theta frequency band and lower evoked coherence in the right frontoparietal region in the delta frequency band (Guntekin, Saatci, & Yener, 2008), indicating that altered frontoparietal connections may underlie WM deficits seen in Alzheimer's disease.

Polania and colleagues (Polania, Nitsche, Korman, Batsikadze, & Paulus, 2012) directly tested the effect of exogenously synchronizing (in-phase) and desynchronizing (anti-phase) left dorsolateral prefrontal cortex (DLPFC) and posterior parietal cortex (PPC) on WM performance. The authors first conducted EEG while subjects performed a delayed recall task. Increase in theta phase synchronization between DLPFC and PPC during WM retrieval was correlated with improved reaction times on the working memory task. Based on these findings, the authors hypothesized that exogenously increasing frontoparietal theta coupling (by applying stimulation with 0° phase difference) would improve WM reaction times, whereas exogenously reducing theta coupling (by applying stimulation with 180° phase difference) would deteriorate task performance. Indeed, they found that 0° relative phase tACS in the theta frequency administered between frontal and parietal areas decreased reaction time, while 180° relative phase tACS increased reaction time in healthy subjects; there was no significant effect for control

stimulation at 35Hz applied with either 0° phase difference or 180° phase difference. This study provides early causal evidence that theta phase-coupling of frontal and parietal areas improves cognitive performance as measured in a WM task. Meiron & Lavidor (Meiron & Lavidor, 2014) tested the effect of bilateral theta frequency tACS applied over DLPFC on a verbal working memory task. In healthy adults, tACS was effective at improving accuracy in a WM task compared to sham stimulation. Retrospective judgments were also assessed in this study, and the authors found that confidence scores improved in conditions of verum stimulation (the condition in which WM also improved).

Jausovec et al (Jausovec, Jausovec, & Pahor, 2013) administered theta tACS over left frontal cortex, left parietal cortex, or right parietal cortex in heathy adults who subsequently conducted tasks to assess spatial and verbal WM capacity. The authors found that tACS administered to either the right of left parietal cortex, but not frontal or sham stimulation, had a positive effect on subsequent WM storage capacity. The authors additionally found that left parietal tACS had a more pronounced effect on both spatial and verbal WM capacity in backward recall rather than forward recall. The findings of this study are consistent with the theory that the left parietal area is more important for WM storage capacity than DLPFC. In support of the aforementioned study, Jausovec & Jausovec (Jausovec & Jausovec, 2013) also applied theta tACS over either left parietal or left frontal cortex in healthy adults and assessed changes in WM storage capacity related to these two brain areas. They found that theta tACS over parietal areas, but not frontal or sham stimulation, improved performance on a visual-array comparison task. Furthermore, the authors report that exclusively parietal tACS induced a decrease in P300 latency in left parietal brain areas. The latency of this ERP component is an index of classification speed, thus the authors posit that theta tACS may have increased participant's capability to allocate resources to solve the working memory task more rapidly. Together, these studies do not fully elucidate the roles of frontal and parietal areas in working memory, but they provide appealing evidence that specific oscillatory activity in these areas contributes to cognitive performance.

Declarative Memory

Declarative memory is defined as "the acquisition or encoding, storage and consolidation, and retrieval of representation of facts and events. Declarative memory provides the critical substrate for

relational representations – i.e. for spatial, temporal, and other contextual relations among items, contributing to representations of events (episodic memory) and the integration and organization of factual knowledge (semantic memory). These representations facilitate the inferential and flexible extraction of new information from these relationships" ("Workshop Proceedings of the NIMH Research Domain Criteria (RDoC) Project: Cognitive Systems, Rockville," 2010). The consolidation of declarative memories is believed to depend on slow oscillations (<1Hz) prominent during non-rapid-eye-movement (non-REM) sleep (Molle & Born, 2011; Stickgold, 2005; Walker & Stickgold, 2004). These slow oscillations originate in the neocortex and then organize activity in the neocortex, thalamus, and hippocampus (Molle & Born, 2011).

Patients with schizophrenia often exhibit poor declarative memory, which has been linked to reduced hippocampal activation during conscious recollection but robust activation of the DLPFC during the effort to retrieve poorly encoded material (Heckers et al., 1998). Of particular interest, patients with schizophrenia also exhibit abnormal non-REM sleep, with a significant reduction in slow-wave sleep and sleep spindle activity (Lu & Goder, 2012). It has been suggested that this altered neural activity during sleep may mediate deficits in declarative memory consolidation observed in patients with schizophrenia (Wamsley et al., 2012).

Marshall et al (Marshall, Helgadottir, Molle, & Born, 2006) tested changes in memory consolidation induced by brain stimulation applied during sleep. The stimulation parameters used in this study differ from traditional tACS; specifically, 0.75Hz oscillating current was applied with a DC offset (with current amplitude between 0 and 260 μA). Subjects performed a paired-associate learning task, and memory retention was assessed before and after sleep. The authors demonstrated that stimulation applied at 0.75Hz with DC offset (the authors call their stimulation paradigm slow-oscillating transcranial direct current stimulation, so-tDCS) during non-REM sleep enhanced the retention of hippocampus-dependent declarative memories in healthy humans. so-tDCS administered bilaterally in frontolateral locations increased slow oscillatory activity and slow spindle activity in frontal cortex, and improved memory recall to a greater degree than sham stimulation. These effects were specific to stimulation frequency and declarative memory; so-tDCS at 5Hz decreased slow oscillations and did not change declarative memory consolidation, and there were no effects of stimulation on procedural memory. In a follow-up study, the

same group found that application of theta frequency so-tDCS with current amplitude between 0 and 260μA during non-REM sleep impaired declarative memory consolidation (Marshall, Kirov, Brade, Molle, & Born, 2011). These studies were conducted in healthy young adults; a similar study conducted in elderly subjects found no enhancement of memory consolidation following so-tDCS with 0.75Hz with current amplitude between 0 and 260μA (Eggert et al., 2013), indicating potential changes in offline memory consolidation with aging.

In the first application of TCS incorporating a periodic structure to a patient population, so-TDCS was applied during non-REM sleep to children with attention-deficit/hyperactivity disorder (ADHD) (Prehn-Kristensen et al., 2014). So-tDCS with 0.75Hz and current amplitude between 0 and 250μA, applied bilaterally to frontolateral locations, increased slow oscillatory power during sleep and improved declarative memory performance in children with ADHD to a level comparable to that of the unstimulated healthy control group. This study represents an important first milestone towards the study of tACS paradigms in patient populations.

The above work by Marshall and colleagues focused on changes in declarative memory consolidation. Additional studies have used so-tDCS to assess the role of slow-oscillatory activity during non-REM sleep and wakefulness on the encoding, rather than consolidation, of declarative memories. Application of bilateral frontolateral 0.75Hz so-tDCS (with current amplitude between 0 and 250 μA) during non-REM sleep periods during an afternoon nap was shown to improve subsequent encoding of declarative memory, with no effect on procedural learning (Antonenko, Diekelmann, Olsen, Born, & Molle, 2013). Even when applied during wakefulness, bilateral 0.75Hz so-tDCS (with current amplitude between 0 and 260 μA) at frontolateral locations appeared to improve the encoding of hippocampus-dependent memories when applied during learning (Kirov, Weiss, Siebner, Born, & Marshall, 2009). Together, this body of work demonstrates that slow oscillations play a causal role in consolidation of hippocampal-dependent memories during sleep and enable subsequent encoding of declarative memories. However, it remains an open question if the DC-offset of the applied current is responsible for inducing improvements in consolidation and encoding of declarative memory. Work conducted in the motor cortex has demonstrated that so-tDCS can induce bidirectional shifts in motor excitability similar to constant tDCS (Groppa et al., 2010). Demonstration that tACS with no offset is capable of inducing these behavioral

modifications will be required. Also, modeling the path and intensity of current flow will be beneficial for understanding how cortical areas contribute to hippocampus-dependent memory. Future work will be required to demonstrate if low frequency tACS or so-tDCS applied during sleep to patients with schizophrenia can increase slow-wave sleep and improve declarative memory consolidation.

Language

Language is defined as “a system of shared symbolic representations of the world, the self and abstract concepts that supports thought and communication” ("Workshop Proceedings of the NIMH Research Domain Criteria (RDoC) Project: Cognitive Systems, Rockville," 2010). There are no sub-constructs in RDoC. While it is clear that language is of critical importance for normal functioning, to date there have been no studies using tACS to enhance, modify, or probe language. However, previous research has established the importance of oscillatory activity in language processing and function. Neural synchronization achieved by the modulation of gamma frequency oscillations through cross-frequency coupling with theta oscillations is important for integration of activity across brain regions supporting language production and transmission (Doesburg, Vinette, Cheung, & Pang, 2012). Horton et al. (Horton, D'Zmura, & Srinivasan, 2013) demonstrated that both attended and unattended speech streams exhibit phase-locking to EEG activity in the posterior temporal cortices; these results support a model in which syllables in the attended stream arrive during periods of high neuronal excitability, while syllables in the competing speech stream arrive during periods of low neuronal excitability. Of particular interest is the function of theta oscillatory activity in the context of language. The phase of theta oscillations recorded from human auditory cortex reliably tracks and discriminates spoken sentences, potentially providing a mechanism for cortical speech analysis (Luo & Poeppel, 2007). Other work has shown that theta oscillatory amplitude is decreased in associative cortex during language production, and could reflect an inhibitory function similar to alpha rhythms in visual cortex and beta rhythms in motor cortex (Hermes et al., 2014).

Non-invasive brain stimulation modalities such as tDCS have been shown to influence language performance in healthy individuals and serve as a treatment for post-stroke aphasia (Demirtas-Tatlidede, Vahabzadeh-Hagh, & Pascual-Leone, 2013; Monti et al., 2013). The parameters and findings in these

studies may serve to inform the design of future tACS studies assessing language function. In healthy adults, anodal tDCS applied over the left PFC has been shown to improve performance on a letter cue-word generation task, improve naming performance, and decrease verbal reaction times, whereas cathodal tDCS decreased verbal fluency or had no effect (Fertonani, Rosini, Cotelli, Rossini, & Miniussi, 2010; Iyer et al., 2005). Anodal tDCS of the left posterior perisylvian area (which includes Wernicke's area) improved speed in a visual picture naming task without decrement in performance (Sparing, Dafotakis, Meister, Thirugnanasambandam, & Fink, 2008). The first study which assessed the effect of tDCS on patients with aphasia found that cathodal stimulation over the left frontotemporal area improved naming abilities by 33.6% (Monti et al., 2008). Additional studies with patients with aphasia which administered tDCS over frontal or temporal areas alone or in combination with speech therapy also found improvements in language (Monti et al., 2013).

While brain stimulation therapies have demonstrated promise for the treatment of aphasia and other language disorders, it remains to be demonstrated if the improvement in language is ecologically relevant for patients and if language improvement continues over time or if 'maintenance' stimulation is required to sustain function.

Cognitive Control

Cognitive control is "a system that modulates the operation of other cognitive and emotional systems, in the service of goal-directed behavior, when prepotent modes of responding are not adequate to meet the demands of the current context. Additionally, control processes are engaged in the case of novel contexts, where appropriate responses need to be selected from among competing alternatives" ("Workshop Proceedings of the NIMH Research Domain Criteria (RDoC) Project: Cognitive Systems, Rockville," 2010). Sub-constructs include (1) goal selection, (2) updating, (3) response election, inhibition or suppression, and (4) performance monitoring. As stated by the definition, the construct of cognitive control effectively organizes the other cognitive domain constructs. Conceptually, cognitive control is utilized in novel situations in order to perform a goal-directed behavior, whereas the construct of attention applies to directing limited-capacity systems. Of interest, a number of psychiatric illnesses exhibit both deficits in cognitive control and abnormal oscillatory activity. For example, individuals with bipolar disorder

show cognitive deficits and disorganized behavior, which are thought to reflect a disturbance in neural synchronization (Basar & Guntekin, 2008). Indeed, measures of neural synchronization evoked by auditory stimuli were reduced in patients with bipolar disorder compared to control subjects during both manic and mixed phases of the illness (O'Donnell et al., 2004). Another study demonstrated that the cortical brain activity of patients with bipolar disorder could be characterized by deficits in bilateral gamma band oscillatory power and exhibited synchronization to the stimulus across hemispheres during auditory click stimulation, both during periods of mild depression and euthymia (Oda et al., 2012). Children and adolescents with autism spectrum disorder (ASD) exhibited deficits in cognitive control compared to age-, IQ-, and gender-matched controls(Solomon, Ozonoff, Cummings, & Carter, 2008), as well as decreased levels of functional connectivity between frontal, parietal, and occipital regions (Solomon et al., 2009). Current theories concerning ASD suggest that dysfunctional integrative mechanisms may result from reduced neural synchronization (Uhlhaas & Singer, 2006).

A small number of studies have directly assessed the effect of tACS in cognitive control. Santarnecchi and colleagues (Santarnecchi et al., 2013) assessed the effect of tACS on fluid intelligence. Fluid intelligence refers to the ability to efficiently encode and manipulate new information, in essence a recapitulation of the RDoC construct of cognitive control. tACS was applied over left medial frontal gyrus in healthy adults. This cortical area has been implicated in abstract reasoning in a modality-independent manner, particularly in tasks involving logical conditional arguments rather than simple perceptual relations. The authors found a 15% improvement in the time required to solve a neuropsychological instrument indexing fluid reasoning, with a clear frequency-specific effect. 40Hz tACS improved the speed of task performance without loss of accuracy, while 5Hz, 10Hz, and 20Hz stimulation did not improve performance. Gamma frequency stimulation was effective only for trials in which conditional reasoning was required, indicating a specific effect on tasks requiring higher order cognitive control. Important for assessment of cognitive control, the authors included control experiments to assess waning attention and fatigue over the course of the session. The authors found no evidence of these confounding factors. No measures of neurophysiology were conducted in this study, so future work will be needed to demonstrate whether the improvement in fluid intelligence stems from positive modulation of mechanisms aiding performance, or negative modulation of processes detrimental to performance. Pahor & Jausovec (Pahor

& Jausovec, 2014) conducted an extension on this work by administering theta frequency tACS over either left frontal or parietal cortex in healthy adults, and then measuring EEG and assessing performance tests of fluid intelligence. The authors found that tACS improved performance on a modified version of Raven's progressive matrices and the Paper Folding and Cutting subtest of the Stanford-Binet IQ test; these improvements were more pronounced in cases of parietal stimulation. Parietal tACS decreased alpha power near the site of stimulation and increased theta power during rest, and frontal stimulation induced a task-dependent decrease in theta power in frontal areas.

Another aspect of cognitive control is the process of evaluating risks and benefits. Lateral prefrontal cortex has been implicated in adjusting decision making strategies according to dynamic contexts and demands (Lee & Seo, 2007; McClure, Laibson, Loewenstein, & Cohen, 2004). The DLPFC is believed to play a critical role in decision making under situations of risk. In particular, theta oscillations are believed to coordinate lateral PFC and sensory-motor networks in order to facilitate adaptive changes in performance. The relative balance of theta oscillations between the right and left hemispheres appears to be particularly important for decision making involving risk. In order to directly test the hypothesis that there is a causal link between lateralized oscillatory activity and risky decision making behavior, Sela et al (Sela, Kilim, & Lavidor, 2012) applied tACS to DLPFC in the right or left hemisphere of healthy adults. They found that theta frequency tACS over left DLPFC induced riskier decision making, while subjects receiving tACS over right DLPFC exhibited decision making no different than during sham stimulation. This study supports the framework that lateralization of theta activity in DLPFC is critical for adaptive decision-making in situations involving risk. Together, these studies provide evidence that tACS can improve multiple facets of cognitive control through targeted application in prefrontal regions.

DISCUSSION

Brain stimulation represents a promising approach for treating aberrant neuronal activity that mediates the symptoms of central nervous system disorders. Indeed, invasive brain stimulation in the form of deep brain stimulation for the treatment of Parkinson's disease has turned into a clinical success over the last two decades (Kalia, Sankar, & Lozano, 2013; Li, Qian, Arbuthnott, Ke, & Yung, 2014). Here, we propose that non-invasive brain stimulation can be employed to treat cognitive symptoms by targeting

the underlying, more subtle and distributed aberrations in brain network activity. In particular, we argue that the shift in psychiatry towards neurobiological mechanisms (manifested most prominently in the RDoC effort) provides a helpful conceptual framework for the targeted development and validation of tACS, a novel form of non-invasive brain stimulation that targets cortical oscillations, as a future treatment modality. We have highlighted recent studies that evaluated the effects of tACS on cognition. Interestingly and (maybe) surprisingly given their non-invasive nature and weak perturbation strength in comparison to TMS, most of these studies succeeded in providing some level of evidence for the causal (functional) role of cortical oscillations in mediating cognitive abilities. Since the field of tACS research is still in its infancy, it remains unclear to what extent these results from early pilot studies will withstand more rigorous large-scale, double-blinded studies. Nevertheless, we found that these early applications span most of the constructs in the cognitive systems domain (according to the RDoC framework) and therefore provide an attractive starting point for the development and evaluation of tACS-based treatment approaches for (psychiatric) illnesses that cause impairment of cognitive systems.

Indeed, the opportunity to potentially induce frequency–specific modulation of cortical network activity emphasizes the importance of identifying and validating network-level biomarkers of pathological functional activity in CNS disorders. Likely, this pathological activity (ideally detected with EEG) will be subtle and identification will require more sophisticated signal processing than the typical EEG markers currently used in routine neurological care. Yet, identification of such pathological EEG signatures that correspond to the individual constructs of the cognitive systems domain will not only provide novel biomarkers but also precipitate targeted, frequency-specific tACS paradigms. Therefore, tACS is well positioned to induce a shift from observational work to targeted, neurobiology-driven interventions. In essence, we here advocate for the rational design of tACS treatment approaches by bringing together the neurophysiology and the psychiatry scientific communities. Below we outline a non-exhaustive list of promising approaches to achieve this goal within the next five years.

State-Dependent Effects of Stimulation

Individualized targeting of tACS can be achieved by a multitude of different approaches. tACS interacts with endogenous network dynamics that are quite complex. Therefore the response to

stimulation may be hard to predict and mechanistically explain. Despite the emerging overall picture that resonance-like phenomena enable enhancement of endogenous oscillations (Ali, Sellers, & Frohlich, 2013; Frohlich & Schmidt, 2013; Reato, Rahman, Bikson, & Parra, 2010), many fundamental aspects such as the possible context-dependence of stimulation effects remain mostly unclear (Reato et al., 2010). A major premise of tACS is that the applied or exogenous oscillation is targeting an endogenous oscillation. However, the necessary and sufficient conditions for such synergistic interaction between endogenous and exogenous rhythmic signals remain to be elucidated.

Feedback Stimulation

Motivated by the state-dependence of responses to brain stimulation and the often transient nature of impaired brain function in CNS disorders, targeted stimulation that is administered based on specific patterns of neuronal activity could be a promising avenue of research. Indeed, the most advanced "adaptive" or "feedback" brain stimulation systems that only apply stimulation when triggering network level activity patterns are detected have been developed for epileptic seizures, both in animal models (Berenyi, Belluscio, Mao, & Buzsaki, 2012; Krook-Magnuson, Armstrong, Oijala, & Soltesz, 2013) and in humans (Heck et al., 2014). Ideally, stimulation waveforms are adapted in real-time based on measurements of ongoing brain activity. One challenge for this approach is the requirement to record over several cycles of oscillations in order to capture the essential properties of the oscillatory activity. Additionally, the development of such closed-loop tACS systems is hampered by the technical challenge of simultaneously recording EEG signals and applying tACS. Recent work has suggested several workarounds, such as using other signals as surrogates for rhythmic brain activity (e.g. tremor signal measured with accelerometer in (Brittain, Probert-Smith, Aziz, & Brown, 2013)) or leveraging intrinsic coupling of different cortical oscillation frequencies. In this latter approach, stimulation at a given frequency modulates a cortical oscillation at a different frequency and therefore the periodic stimulation artifact can be removed by bandpass filtering (Boyle & Frohlich, 2013).

Spatial Targeting

Recent progress in methods of focusing the applied electric field by using small electrodes and

more than two stimulation electrodes has enabled a significantly improved level of spatial specificity in tACS. Conventional stimulation paradigms utilize two 5x7cm electrodes. By using one smaller active electrode (typically a circle electrode with outer radius = 12mm and inner radium = 6mm) and four return electrodes each placed equidistant at 3.5cm from the stimulation electrode, electrode montages such as high-definition tDCS (HD-tDCS) (Datta, Truong, Minhas, Parra, & Bikson, 2012; Minhas et al., 2010) can focus current distribution onto a targeted cortical area. Finite element modeling is the standard approach to model the electric field applied to the brain by TCS. The electric field induced by conventional stimulation montages extends into cortical areas outside those directly under the stimulation electrodes; in contrast, electric fields applied to the brain using HD-tDCS montages were more restricted to the area under the region demarked by the return electrodes (Kuo et al., 2013). A realistic head model found that conventional stimulation with the anode over motor cortex and the cathode on the forehead induced modulation over the entire cortical surface, whereas HD-tDCS applied over the same location only induced electric fields in motor cortex, with no cortical modulation in frontal regions, the contralateral motor region, or the occipital lobe (Datta et al., 2009). With more localized application of current, the likelihood for off-target effects is decreased. Likely, such increased spatial specificity can be employed not only for tDCS but also for tACS. However, the key strength of tACS may be the enhancement of coherence between brain areas, in which broad spatial targeting could indeed be crucial for frequency-specific synchronization of several cortical areas.

Limitations and Barriers to Successful Clinical Applications of tACS

Despite the promise of tACS to modulate oscillatory activity in cortex, there are a number of important unresolved questions that remain. Further work will be required to elaborate on these topics prior to the successful development of tACS as a neurotherapeutic. First, it remains an open question to what extent tACS can induce oscillatory activity at a chosen frequency. In vitro application of sine-wave electric field has demonstrated that weak electric fields are capable of enhancing endogenous oscillations when matched in frequency, but fail to induce a frequency shift if the stimulation frequency does not match the endogenous oscillatory frequency (Schmidt, Iyengar, Foulser, Boyle, & Frohlich, 2014). Application of 25Hz and 40Hz tACS during lucid dreaming, a period of elevated low-gamma power,

further increases gamma oscillatory activity while other frequencies of tACS had no effect on oscillatory structure (Voss et al., 2014). Thus, future work will be required to ascertain the extent to which tACS is capable of inducing oscillatory structure in addition to increasing the strength of endogenous oscillations.

Second, the magnitude and duration of sustained aftereffects of tACS remain an open question. One study found enhanced oscillatory power matched to the stimulation frequency for 30 minutes following stimulation, but only when tACS was administered under conditions of low oscillatory power in the matched frequency (Neuling et al., 2013). Alpha frequency tACS administered to parieto-occipital cortex has been shown to induce enhanced alpha-band oscillations outlasting the duration of the stimulation (Helfrich et al., 2014). Computer simulations of tACS have demonstrated that in the case of multistable states, stimulation can induce outlasting changes in the form of switching to another network activity state (Kutchko & Frohlich, 2013). Outlasting effects of tDCS on the excitability of motor cortex have been reported to last multiple hours after stimulation (Batsikadze, Moliadze, Paulus, Kuo, & Nitsche, 2013). It is unclear if the same mechanisms mediate outlast effects in tDCS and tACS. Finally, the effects of tACS must be studied in patient populations. Abnormal neuronal architecture, found in some neuropsychiatric diseases, may alter the way in which tACS modulates oscillatory activity.

CONCLUSION

The future application of tACS in the clinic for the treatment of cognitive impairment critically depends on interdisciplinary work that fuses basic science and clinical approaches to characterize the pathological changes in brain circuits that mediate cognitive symptoms and the ability of tACS to remediate these deficits. Creating a systematic way of approaching pathology in neuropsychiatric conditions, as done with RDoC, will assist in translating discoveries of basic neurophysiology to characterizing biomarkers or circuits that can be targeted with neuromodulation techniques such as tACS.

We recognize and stress that to our knowledge no published tACS study has targeted impairment of the cognitive domain in patients with psychiatric illness. Although it appears reasonable to assume that tACS interventions that enhance cognition in the healthy research participant will also enhance and therefore restore cognitive abilities in patients with cognitive impairment, no direct evidence for such extrapolation exists to date. However, tDCS has recently been used to improve deficits in cognitive

control in patients with major depressive disorder (Wolkenstein & Plewnia, 2013). Since cortical oscillations represent the fundamental mediator of cognition (Wang, 2010), we here make the argument that tACS, which directly targets these network activity patterns, may bring more specific and more effective treatment of cognitive dysfunction. Nevertheless, bridging the gap between the well-known, yet hard to treat, cognitive deficits in psychiatric illnesses and the exciting yet early studies on the effectiveness of tACS on modulating cognition represents the most fundamental challenge for tACS to become a candidate neurotherapeutic for the treatment of psychiatric disorders.

FIGURES AND TABLES

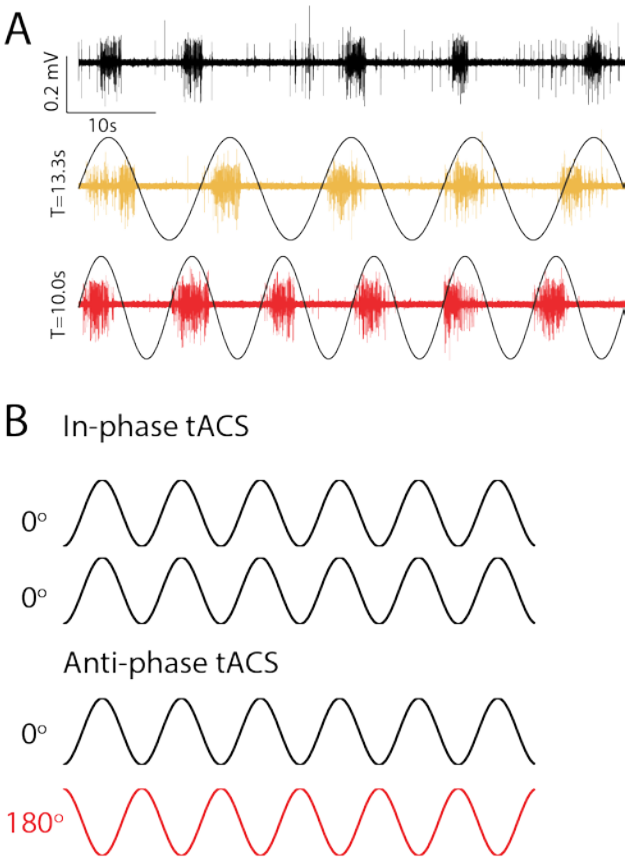

Figure 3.1 Transcranial alternating current stimulation (tACS) applies a weak sine-wave electric field to the scalp.

(A) As demonstrated in vitro, weak sine-waves with different periods (T) entrain action potential firing. Top: no EF applied, middle: T = 13.3 seconds, bottom: T = 10.0 seconds. Adapted from (Frohlich & McCormick, 2010), reprinted with permission.

(B) TACS delivers sine-wave electrical current of differing frequencies and phase-alignment (phase denoted on the far left).

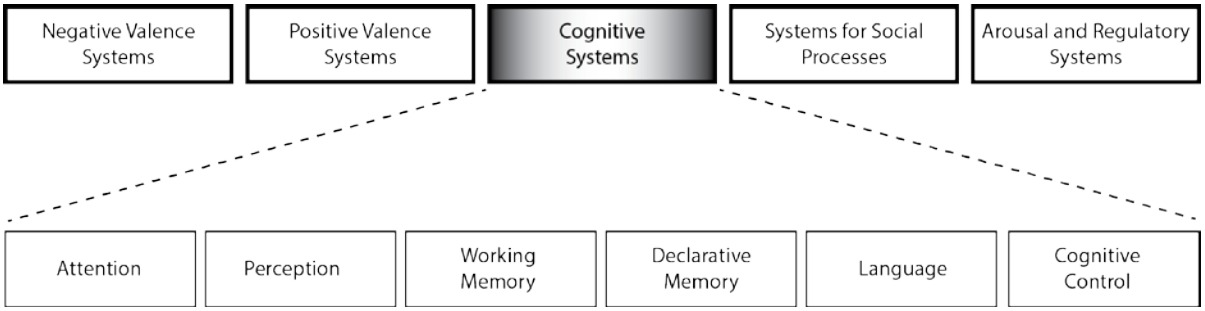

Figure 3.2. The Research Domain Criteria project (RDoC) is an initiative by the NIMH to classify psychopathology based on dimensions of observable behavior and neurobiological measures. The project includes five domains, each of which contains constructs. In this review, we focus on the six constructs of the Cognitive Systems domain (Insel et al., 2010).

ATTENTION							
Author(s)	**Journal**	**Reason for study and behavioral task used**	**Stimulation location**	**Verum stimulation parameters**	**Sham stimulation parameters**	**Participant population**	**Main Finding(s)**
Joundi et al (2012)	Current Biology	Sought to demonstrate that oscillatory cortical activity can modify motor behavior. Subjects performed a task assessing motor performance in a go/no-go paradigm.	5x7cm electrodes over the hand area of left motor cortex and the ipsilateral shoulder.	Trials of 5 seconds of 20 or 70Hz sine-wave current. Amplitude selected per individual to be 50μA below phosphene/scalp sensation threshold.	None (stimulation delivered for half of the behavior trials)	18 healthy adults	In a task requiring attention for the regulation of motor (in)action, gamma frequency tACS was prokinetic and beta frequency tACS was antikinetic.
Laczo et al (2012)	Brain Stimulation	Sought to investigate if cortical oscillations in the gamma frequency range are the neuronal mechanism underlying the enhancement of information processing during spatial visual attention.	4x4cm electrode placed over Oz and 4x7cm reference electrode placed over Cz.	45±10 minutes of 40, 60, or 80Hz sine-wave current delivered at 1.5mA. Follow-up experiment, designed to avoid possible after effects of tACS, used 15±5 minutes of stimulation.	20 seconds of tACS	20 healthy male and female adults	60Hz tACS over primary visual cortex improved contrast detection during stimulation.

PERCEPTION							
Author(s)	**Journal**	**Reason for study and behavioral task used**	**Stimulation location**	**Verum stimulation parameters**	**Sham stimulation parameters**	**Participant population**	**Main Finding(s)**
Helfrich et al (2014)	Current Biology	Studied neuronal entrainment by measuring EEG during tACS and implementing advanced artifact	5x7cm electrodes over Cz and Oz	20 minutes of 10Hz sine-wave current applied at 1mA	10Hz tACS ramped up for 10 seconds, and then	14 healthy right-handed male and female	EEG recordings conducted simultaneously with tACS revealed that 10Hz tACS over

		rejection. Participants performed a visual oddball paradigm; the visual stimulus was presented at four difference phase angles of tACS.			discontinued	adults	parieto-occipital cortex increased alpha activity and modulated target detection performance in a stimulation phase-dependent manner.
Struber et al (2014)	Brain Topography	Tested a causal role for gamma activity in conscious perception, as assessed by perceived horizontal or vertical movement in bistable apparent motion stimuli presented during tACS.	5x7cm electrodes over P7-PO7 and P8-PO8 for anti-phase stimulation. 5x7cm electrodes over C3, C4, O1, and O2 for in-phase stimulation	15 minutes of 6 or 40Hz sine-wave current applied either in-phase or anti-phase between hemispheres; intensity determined by individual phosphene threshold (<1.5mA)	Stimulation turned off after detection of sensory threshold	45 healthy male and female adults	40Hz tACS, but not 6Hz tACS, increased interhemispheric gamma band coherence and decreased the proportion of perceived horizontal motion. This was only effective when stimulation was applied with 180° phase difference.
Brignani et al (2013)	PLoS One	Sought to determine if tACS could affect cortical activity; tested participants with a Gabor patch detection and discrimination task.	$16cm^2$ electrode over PO7 or PO8, $35cm^2$ reference electrode positioned over Cz	3 blocks of 5 minutes of 6, 10, or 25Hz sine-wave current applied at 1mA	10Hz tACS for 10 seconds	96 healthy, right-handed male and female adults	Participants who received 6Hz and 10Hz tACS showed poorer performance in detecting targets in comparison to participants who received no stimulation. However, these results were not retinotopically specific.
Laczo et al (2012)	Brain Stimulation	Sought to externally modulate gamma oscillations, the hypothesized neuronal mechanism of spatial visual attention. The authors assessed modulation of gamma oscillations by probing	4x4cm electrode over Oz and 7x4cm reference electrode over Cz	15 minutes each of 40, 60, and 80Hz sine-wave stimulation applied at 1.5mA (± 10 minutes total stimulation time). A second set of	20 seconds of tACS	20 healthy male and female adults	Contrast-discrimination thresholds decreased significantly during 60Hz tACS, with no effect of 40Hz or 80Hz tACS.

		contrast sensitivity and contrast discrimination.		experiments applied 15 ± 5 minutes of 40, 60, or 80Hz sine-wave stimulation at 1.5mA with at least 2 days separating conditions			
Neuling et al (2012)	NeuroImage	Sought to address the long-standing question of whether perception is continuous or periodic (mediated by spontaneous oscillatory activity) by applying an external oscillation to entrain brain oscillations and demonstrate behavioral consequences. Participants performed an auditory detection task.	5x7cm electrodes positioned at T7 and T8	21 minutes of 1mA direct current (anode on right hemisphere) modulated by 10Hz sinusoidal current of 425 ± 81μA (sinusoidal current amplitude was individually adjusted based on participants' feedback for comfort)	None	16 healthy right-handed male and female adults	DC-offset tACS enhanced alpha power relative to the pre-stimulation period, and auditory detection thresholds were dependent on the phase of the oscillation entrained by the stimulation. Detection thresholds were higher when the stimuli were presented during the stimulation positive half-wave compared to thresholds for stimuli presented during the negative half-wave.
Feurra (2011)	Frontiers in Psychology	Sought to probe the role of oscillatory neural activity by assessing if tACS applied over somatosensory cortex could elicit tactile sensation in a frequency-dependent manner.	3x4cm electrode over right somatosensory cortex and 5x7cm reference electrode over P3	5 seconds per trial of sine-wave stimulation ranging from 2 to 70Hz, step-size 2Hz, (order randomized), applied at 1.5mA	None	14 healthy adults	Alpha and high gamma tACS applied over somatosensory cortex were effective at producing tactile sensation in the contralateral hand. Beta stimulation produced weaker tactile sensation in the contralateral hand.
Kanai et al (2010)	Clinical Neuro-	Investigated whether tACS can modulate the	3x3cm electrode over	5-8 minutes of 5, 10, 20, or 40Hz	None	16 healthy male and	20Hz tACS decreased TMS-phosphene

	physiology	excitability of visual cortex in a frequency-dependent manner, without involving potential retinal stimulation. Authors assessed if tACS modulated the intensity threshold for transcranial magnetic stimulation (TMS) pulses to induce visual phosphenes when delivered to visual cortex.	Oz and 5x7cm reference electrode over Cz; Control condition: 3x3cm electrode over Fz and 5x7cm reference electrode over Cz	sine-wave stimulation delivered at 750μA		female adults	threshold (increased the excitability of visual cortex); tACS at other frequencies did not affect visual cortex excitability.
Kanai et al (2008)	Current Biology	Tested if tACS can interact with ongoing rhythmic activity in visual cortex. Administered tACS with room lights on and off and assessed participant's perception of phosphenes.	3x4cm electrode 4cm above the inion (near the midpoint between O1 and O2), 6x9cm reference electrode placed over Cz	10 second trials of sine-wave stimulation delivered with room light on and then room lights off (4, 8, 10, 12, 14, 16, 18, 20, 22, 24, 30, and 40Hz, order randomized) delivered at 1mA. Current intensity was then iteratively reduced (750, 500, 250, 125μA) to determine phosphene threshold at each frequency.	None	16 healthy male and female adults	tACS in the beta frequency range induced phosphenes most effectively when administered in an illuminated room, while alpha frequency stimulation most effectively induced phosphenes in a dark room. Theta and gamma frequency stimulation did not produce visual phosphenes.
WORKING MEMORY							
Author(s)	**Journal**	**Reason for study and behavioral task used**	**Stimulation location**	**Verum stimulation parameters**	**Sham stimulation parameters**	**Participant population**	**Main Finding(s)**
Meiron & Lavidor	Clinical Neuro-	Sought to determine how theta tACS modulated	4x4cm electrodes	20 minutes of 4.5Hz sine-wave	20 seconds of 4.5Hz	24 healthy right-	Online working memory accuracy improved with

(2014)	physiology	associations between working memory accuracy and later retrospective self-evaluation scores. Participants completed a verbal working memory task.	placed over F3-AF3, F4-AF4	stimulation delivered at 1mA	sine-wave stimulation delivered at 1mA	handed female adults	bilateral tACS over DLPFC, compared to sham stimulation; improvement in working memory was accompanied by higher subjective retrospective success-confidence scores.
Jausovec, Jausovec & Pahor (2014)	Acta Psychologica	Sought to explore the relationship between working memory functions and brain activity in frontal and parietal areas by analyzing the influence of theta tACS on performance in tasks of working memory storage capacity and executive process.	5x7cm electrode over either F3, P3, or P4; 5x7cm return electrode over right eyebrow	15 minutes of theta stimulation (individual alpha frequency minus 5Hz) delivered at 250μA below individual thresholds for skin sensation (range = 1000μA to 2250μA).	30 seconds tACS	36 healthy right-handed male and female adults	tACS over right or left parietal areas improved working memory storage capacity, whereas there was no difference measured for frontal or sham stimulation.
Jausovec & Jausovec (2014)	Biological Psychology	Sought to investigate the influence of tACS on left parietal and frontal brain activity on working memory storage capacity.	5x7cm electrode over either F3 or P3; 5x7cm return electrode over right eyebrow	15 minutes of theta stimulation (individual alpha frequency minus 5Hz) delivered at 250μA below individual thresholds for skin sensation (range = 1000μA to 2000μA).	30 seconds tACS	24 healthy right-handed male and female adults	Left parietal tACS increased working memory storage capacity, whereas no difference was measured for either left frontal stimulation or sham stimulation. Increased working memory storage capacity was accompanied by ERP 300 latency decrease.
Polania et al (2012)	Current Biology	Sought to demonstrate a causal link between frontoparietal theta coupling and cognitive performance. Participants completed a delayed	5x5cm electrode placed over F3, P3, and return electrode over Cz	14 ±1.5 minutes of 6Hz sine-wave stimulation applied in-phase (0° phase difference) or	30 seconds of 6Hz sine-wave stimulation applied in-phase (0°	46 healthy right-handed male and female adults	6Hz tACS with 0° phase difference ('synchronizing' condition) improved visual memory-matching reaction times

		letter discrimination task.		anti-phase (180° phase difference) at 1mA. Control experiment: Same as above, with 35Hz tACS.	phase difference), then 20 second linear ramp-down		relative to sham stimulation. 6Hz tACS with 180° phase difference ('desynchronizing' condition) impaired performance relative to sham stimulation. 35Hz tACS did not induce changes in performance.

DECLARATIVE MEMORY							
Author(s)	**Journal**	**Reason for study and behavioral task used**	**Stimulation location**	**Verum stimulation parameters**	**Sham stimulation parameters**	**Participant population**	**Main Finding(s)**
Prehn-Kristensen et al (2014)	Brain Stimulation		10mm in diameter electrodes were positioned at F3 and F4 (anodes), and the reference electrodes (cathodes) were placed at both mastoids.	Five 5 minute epochs (each separated by 1 minute of no stimulation) of 0.75Hz sine-wave current was applied oscillating between 0 and 250μA.	Non-active sham.	12 children with ADHD and 12 healthy children; all males between the ages 9-14 years.	Stimulation enhanced slow oscillation power during sleep in children with ADHD and improved declarative memory performance to a level equal to that of healthy children who did not receive stimulation. Children with ADHD who received sham stimulation showed no improvement.
Antonenko et al (2013)	European Journal of Neuro-science	Sought to demonstrate a causal role for slow wave activity during sleep in enhancing the capacity for encoding of information during subsequent wakefulness.	10mm in diameter electrodes were positioned at F3 and F4, and the reference	Six to eight 4 minute stimulation epochs during non-REM sleep. 0.75Hz sine-wave current was	Non-active sham.	15 healthy, right-handed male and female adults	Stimulation enhanced slow wave activity during sleep and significantly improved subsequent encoding on declarative tasks (picture recognition,

		Participants completed a word pair learning task, the Verbal Learning and Memory Test, and a finger sequence tapping task.	electrodes were placed at both mastoids.	applied oscillating between 0 and 250μA.			cured recall of word pairs, and free recall of word lists); stimulation had no effect on procedural finger sequence tapping skill.
Eggert et al (2013)	Brain Stimulation	Investigated whether sleep-dependent memory consolidation could be improved by application of brain stimulation in a population of older adult participants (as has previously been shown for healthy young volunteers). Participants performed declarative (common word-pair association task) and procedural (sequential finger tapping task) memory tasks.	10mm in diameter electrodes were positioned at F3 and F4 (anodes), and the reference electrodes (cathodes) were placed at both mastoids.	Five epochs of 316 seconds of 0.75Hz sine-wave current was applied oscillating between 0 and 260μA.	Non-active sham	26 healthy, male and female adults between the ages of 60-90 years	Stimulation applied in this population of healthy older adults failed to demonstrate a beneficial effect on either declarative or procedural memory consolidation.
Marshall et al (2011)	PLoS One	Sought to investigate the role of theta oscillations during REM and non-REM sleep for memory formation. Participants completed declarative (word paired-associates task) and procedural (finger sequence tapping, mirror-tracing tasks) memory tasks.	8mm in diameter electrodes were positioned at F3 and F4 (anodes), and the reference electrodes were placed at both mastoids (cathodes).	Five 5 minute epochs (each separated by 1 minute of no stimulation) of 5Hz sine-wave current was applied oscillating between 0 and 260μA.	Non-active sham	41 healthy male and female adults	5Hz DC-offset tACS during non-REM sleep reduced frontal slow oscillatory activity, reduced frontal slow spindle power, and induced a decrement in consolidation of declarative memory. Stimulation during REM sleep increased global gamma activity.
Kirov et al (2009)	PNAS	Sought to determine whether increases in slow oscillatory activity by DC-offset tACS improved memory consolidation	8mm in diameter electrodes were positioned at	Five 5 minute epochs (each separated by 1 minute of no stimulation) of	Non-active sham	28 healthy male and female adults	0.75Hz DC-offset tACS applied during wakefulness increased EEG slow oscillatory activity locally and theta

		specific to slow wave sleep, or whether this induced slow oscillatory activity could improve memory during wakefulness. Participants completed declarative (verbal and non-verbal paired-associate learning) and procedural (finger sequence tapping and mirror tracing) memory tasks.	F3 and F4 (anodes), and the reference electrodes were placed at both mastoids (cathodes).	0.75Hz sine-wave current was applied oscillating between 0 and 260μA.			activity globally. Stimulation improved encoding of hippocampus-dependent memories when applied during learning, but did not aid in consolidation of memories when applied after learning.
Marshall et al (2006)	Nature	Sought to investigate if brain potentials have a physiological meaning in memory function. Participants completed declarative (paired-associate learning) and procedural (finger sequence tapping and mirror tracing tasks) memory tasks.	8mm in diameter electrodes were positioned at F3 and F4 (anodes), and the reference electrodes were placed at both mastoids (cathodes).	Five 5 minute epochs (each separated by 1 minute of no stimulation) of 0.75Hz sine-wave current was applied oscillating between 0 and 260μA. Control stimulation: same as above, 5Hz sine-wave.	Non-active sham	13 healthy right-handed male and female adults	0.75Hz DC-offset tACS enhanced slow cortical oscillations and slow spindle activity during early non-REM sleep. Retention of hippocampus-dependent declarative memories was enhanced, while there was no effect on procedural memory; 5Hz stimulation decreased slow oscillations and did not change declarative memory.

COGNITIVE CONTROL							
Author(s)	**Journal**	**Reason for study and behavioral task used**	**Stimulation location**	**Verum stimulation parameters**	**Sham stimulation parameters**	**Participant population**	**Main Finding(s)**
Pahor & Jausovec	International Journal	Sought to examine whether theta tACS can	5x7cm electrode over	15 minutes of theta stimulation	1 minute of tACS	28 healthy right-	Theta tACS improved subsequent

(2014)	of Psychophysiology	affect subsequent performance on tasks of fluid intelligence, and if theta tACS changed power in theta and alpha frequency bands.	either F3 or P3, 7x10cm return electrode over Fp2	(individual alpha frequency minus 5Hz) delivered at 250μA below individual thresholds for skin sensation (range = 1000μA to 2250μA).		handed male and female adults	performance on tests of fluid intelligence; this effect was more pronounced in individuals who received left parietal stimulation rather than left frontal stimulation. Theta tACS decreased alpha power in areas near the stimulation site.
Santarnecchi et al (2013)	Current Biology	Sought to demonstrate a causal role for gamma synchronization in fluid intelligence. Participants completed visuospatial abstract reasoning tasks (Raven's matrices).	5x7cm electrodes placed over left middle frontal gyrus and Cz	5H, 10, 20, or 40Hz sine-wave current delivered at 750μA. Stimulation delivered for duration of task performance.	20 seconds of stimulation applied at the frequency from the previous block	20 healthy right-handed male and female adults	Gamma frequency tACS improved completion time by 15% on a visuospatial abstract reasoning task for complex trials involving conditional/logical reasoning.
Sela et al (2012)	Frontiers in Neuro-science	Sought to investigate the hypothesis that the balance of theta frequency oscillatory activity between right and left frontal regions, with a dominant role for the right hemisphere, is crucial for regulatory control during risky decision-making. Participants completed the Balloon Analog Risk Task.	Left hemisphere: 5x5cm electrodes placed over F3 and CP5; right hemisphere: 5x5cm electrodes placed over F4 and CP6	15 minutes of 6.5Hz sine-wave current delivered at 1mA.	30 seconds of tACS	27 healthy right-handed male and female adults	Participants receiving theta frequency tACS in the left hemisphere exhibited riskier decision-making style compared to participants receiving right hemisphere or sham stimulation.

Table 3.1.Summary of the purpose, stimulation parameters, and findings of each tACS study discussed in this review

REFERENCES

Ali, M. M., Sellers, K. K., & Frohlich, F. (2013). Transcranial alternating current stimulation modulates large-scale cortical network activity by network resonance. *J Neurosci, 33*(27), 11262-11275. doi: 10.1523/JNEUROSCI.5867-12.2013

Antal, A., Kincses, T. Z., Nitsche, M. A., Bartfai, O., & Paulus, W. (2004). Excitability changes induced in the human primary visual cortex by transcranial direct current stimulation: direct electrophysiological evidence. *Invest Ophthalmol Vis Sci, 45*(2), 702-707.

Antal, A., Terney, D., Poreisz, C., & Paulus, W. (2007). Towards unravelling task-related modulations of neuroplastic changes induced in the human motor cortex. *Eur J Neurosci, 26*(9), 2687-2691. doi: 10.1111/j.1460-9568.2007.05896.x

Antonenko, D., Diekelmann, S., Olsen, C., Born, J., & Molle, M. (2013). Napping to renew learning capacity: enhanced encoding after stimulation of sleep slow oscillations. *Eur J Neurosci, 37*(7), 1142-1151. doi: 10.1111/ejn.12118

Basar, E., & Guntekin, B. (2008). A review of brain oscillations in cognitive disorders and the role of neurotransmitters. *Brain Res, 1235*, 172-193. doi: 10.1016/j.brainres.2008.06.103

Batsikadze, G., Moliadze, V., Paulus, W., Kuo, M. F., & Nitsche, M. A. (2013). Partially non-linear stimulation intensity-dependent effects of direct current stimulation on motor cortex excitability in humans. *J Physiol, 591*(Pt 7), 1987-2000. doi: 10.1113/jphysiol.2012.249730

Benchenane, K., Tiesinga, P. H., & Battaglia, F. P. (2011). Oscillations in the prefrontal cortex: a gateway to memory and attention. *Curr Opin Neurobiol, 21*(3), 475-485. doi: 10.1016/j.conb.2011.01.004

Benninger, D. H., Lomarev, M., Lopez, G., Wassermann, E. M., Li, X., Considine, E., & Hallett, M. (2010). Transcranial direct current stimulation for the treatment of Parkinson's disease. *J Neurol Neurosurg Psychiatry, 81*(10), 1105-1111. doi: 10.1136/jnnp.2009.202556

Berenyi, A., Belluscio, M., Mao, D., & Buzsaki, G. (2012). Closed-loop control of epilepsy by transcranial electrical stimulation. *Science, 337*(6095), 735-737. doi: 10.1126/science.1223154

Berlim, M. T., Van den Eynde, F., & Daskalakis, Z. J. (2013). Clinical utility of transcranial direct current stimulation (tDCS) for treating major depression: a systematic review and meta-analysis of randomized, double-blind and sham-controlled trials. *J Psychiatr Res, 47*(1), 1-7. doi: 10.1016/j.jpsychires.2012.09.025

Boyle, M., & Frohlich, F. (2013). EEG Feedback-Controlled Transcranial Alternating Current Stimulation. *6th Annual International IEEE EMBS Conference on Neural Engineering*, 140-143. doi: 10.1109/NER.2013.6695891

Brignani, D., Ruzzoli, M., Mauri, P., & Miniussi, C. (2013). Is transcranial alternating current stimulation effective in modulating brain oscillations? *PLoS One, 8*(2), e56589. doi: 10.1371/journal.pone.0056589

Brittain, J. S., Probert-Smith, P., Aziz, T. Z., & Brown, P. (2013). Tremor suppression by rhythmic transcranial current stimulation. *Curr Biol, 23*(5), 436-440. doi: 10.1016/j.cub.2013.01.068

Brunoni, A. R., Fregni, F., & Pagano, R. L. (2011). Translational research in transcranial direct current stimulation (tDCS): a systematic review of studies in animals. *Rev Neurosci, 22*(4), 471-481. doi: 10.1515/RNS.2011.042

Buschman, T. J., & Miller, E. K. (2007). Top-down versus bottom-up control of attention in the prefrontal and posterior parietal cortices. *Science, 315*(5820), 1860-1862. doi: 10.1126/science.1138071

Buzsaki, G., & Watson, B. O. (2012). Brain rhythms and neural syntax: implications for efficient coding of cognitive content and neuropsychiatric disease. *Dialogues Clin Neurosci, 14*(4), 345-367.

Curtis, C. E., & D'Esposito, M. (2003). Persistent activity in the prefrontal cortex during working memory. *Trends Cogn Sci, 7*(9), 415-423.

Cuthbert, B. N., & Insel, T. R. (2013). Toward the future of psychiatric diagnosis: the seven pillars of RDoC. *BMC Med, 11*, 126. doi: 10.1186/1741-7015-11-126

Datta, A., Bansal, V., Diaz, J., Patel, J., Reato, D., & Bikson, M. (2009). Gyri-precise head model of transcranial direct current stimulation: improved spatial focality using a ring electrode versus conventional rectangular pad. *Brain Stimul, 2*(4), 201-207, 207 e201. doi: 10.1016/j.brs.2009.03.005

Datta, A., Truong, D., Minhas, P., Parra, L. C., & Bikson, M. (2012). Inter-Individual Variation during Transcranial Direct Current Stimulation and Normalization of Dose Using MRI-Derived Computational Models. *Front Psychiatry, 3*, 91. doi: 10.3389/fpsyt.2012.00091

Deans, J. K., Powell, A. D., & Jefferys, J. G. R. (2007). Sensitivity of coherent oscillations in rat hippocampus to AC electric fields. *Journal of Physiology-London, 583*(2), 555-565. doi: DOI 10.1113/jphysiol.2007.137711

Demirtas-Tatlidede, A., Vahabzadeh-Hagh, A. M., & Pascual-Leone, A. (2013). Can noninvasive brain stimulation enhance cognition in neuropsychiatric disorders? *Neuropharmacology, 64*, 566-578. doi: 10.1016/j.neuropharm.2012.06.020

Doesburg, S. M., Vinette, S. A., Cheung, M. J., & Pang, E. W. (2012). Theta-modulated gamma-band synchronization among activated regions during a verb generation task. *Front Psychol, 3*, 195. doi: 10.3389/fpsyg.2012.00195

Eggert, T., Dorn, H., Sauter, C., Nitsche, M. A., Bajbouj, M., & Danker-Hopfe, H. (2013). No Effects of Slow Oscillatory Transcranial Direct Current Stimulation (tDCS) on Sleep-Dependent Memory Consolidation in Healthy Elderly Subjects. *Brain Stimul, 6*(6), 938-945. doi: DOI 10.1016/j.brs.2013.05.006

Engel, A. K., Fries, P., & Singer, W. (2001). Dynamic predictions: oscillations and synchrony in top-down processing. *Nat Rev Neurosci, 2*(10), 704-716. doi: 10.1038/35094565

Ergenoglu, T., Demiralp, T., Bayraktaroglu, Z., Ergen, M., Beydagi, H., & Uresin, Y. (2004). Alpha rhythm of the EEG modulates visual detection performance in humans. *Brain Res Cogn Brain Res, 20*(3), 376-383. doi: 10.1016/j.cogbrainres.2004.03.009

Fertonani, A., Rosini, S., Cotelli, M., Rossini, P. M., & Miniussi, C. (2010). Naming facilitation induced by transcranial direct current stimulation. *Behav Brain Res, 208*(2), 311-318. doi: 10.1016/j.bbr.2009.10.030

Feurra, M., Bianco, G., Santarnecchi, E., Del Testa, M., Rossi, A., & Rossi, S. (2011). Frequency-dependent tuning of the human motor system induced by transcranial oscillatory potentials. *J Neurosci, 31*(34), 12165-12170. doi: 10.1523/JNEUROSCI.0978-11.2011

Feurra, M., Pasqualetti, P., Bianco, G., Santarnecchi, E., Rossi, A., & Rossi, S. (2013). State-dependent effects of transcranial oscillatory currents on the motor system: what you think matters. *J Neurosci, 33*(44), 17483-17489. doi: 10.1523/JNEUROSCI.1414-13.2013

Feurra, M., Paulus, W., Walsh, V., & Kanai, R. (2011). Frequency specific modulation of human somatosensory cortex. *Front Psychol, 2*, 13. doi: 10.3389/fpsyg.2011.00013

Fregni, F., Boggio, P. S., Santos, M. C., Lima, M., Vieira, A. L., Rigonatti, S. P., . . . Pascual-Leone, A. (2006). Noninvasive cortical stimulation with transcranial direct current stimulation in Parkinson's disease. *Mov Disord, 21*(10), 1693-1702. doi: 10.1002/mds.21012

Frohlich, F., & McCormick, D. A. (2010). Endogenous electric fields may guide neocortical network activity. *Neuron, 67*(1), 129-143. doi: 10.1016/j.neuron.2010.06.005

Frohlich, F., & Schmidt, S. L. (2013). Rational design of transcranial current stimulation (TCS) through mechanistic insights into cortical network dynamics. *Front Hum Neurosci, 7*, 804. doi: 10.3389/fnhum.2013.00804

Groppa, S., Bergmann, T. O., Siems, C., Molle, M., Marshall, L., & Siebner, H. R. (2010). Slow-oscillatory transcranial direct current stimulation can induce bidirectional shifts in motor cortical excitability in awake humans. *Neuroscience, 166*(4), 1219-1225. doi: 10.1016/j.neuroscience.2010.01.019

Guntekin, B., Saatci, E., & Yener, G. (2008). Decrease of evoked delta, theta and alpha coherences in Alzheimer patients during a visual oddball paradigm. *Brain Res, 1235*, 109-116. doi: 10.1016/j.brainres.2008.06.028

Haig, A. R., Gordon, E., De Pascalis, V., Meares, R. A., Bahramali, H., & Harris, A. (2000). Gamma activity in schizophrenia: evidence of impaired network binding? *Clin Neurophysiol, 111*(8), 1461-1468.

Hanslmayr, S., Aslan, A., Staudigl, T., Klimesch, W., Herrmann, C. S., & Bauml, K. H. (2007). Prestimulus oscillations predict visual perception performance between and within subjects. *Neuroimage, 37*(4), 1465-1473. doi: 10.1016/j.neuroimage.2007.07.011

Heck, C. N., King-Stephens, D., Massey, A. D., Nair, D. R., Jobst, B. C., Barkley, G. L., . . . Morrell, M. J. (2014). Two-year seizure reduction in adults with medically intractable partial onset epilepsy treated with responsive neurostimulation: Final results of the RNS System Pivotal trial. *Epilepsia, 55*(3), 432-441. doi: 10.1111/epi.12534

Heckers, S., Rauch, S. L., Goff, D., Savage, C. R., Schacter, D. L., Fischman, A. J., & Alpert, N. M. (1998). Impaired recruitment of the hippocampus during conscious recollection in schizophrenia. *Nat Neurosci, 1*(4), 318-323. doi: 10.1038/1137

Helfrich, R. F., Schneider, T. R., Rach, S., Trautmann-Lengsfeld, S. A., Engel, A. K., & Herrmann, C. S. (2014). Entrainment of brain oscillations by transcranial alternating current stimulation. *Curr Biol, 24*(3), 333-339. doi: 10.1016/j.cub.2013.12.041

Hermes, D., Miller, K. J., Vansteensel, M. J., Edwards, E., Ferrier, C. H., Bleichner, M. G., . . . Ramsey, N. F. (2014). Cortical theta wanes for language. *Neuroimage, 85 Pt 2*, 738-748. doi: 10.1016/j.neuroimage.2013.07.029

Herrmann, C. S., Rach, S., Neuling, T., & Struber, D. (2013). Transcranial alternating current stimulation: a review of the underlying mechanisms and modulation of cognitive processes. *Front Hum Neurosci, 7*, 279. doi: 10.3389/fnhum.2013.00279

Horton, C., D'Zmura, M., & Srinivasan, R. (2013). Suppression of competing speech through entrainment of cortical oscillations. *J Neurophysiol, 109*(12), 3082-3093. doi: 10.1152/jn.01026.2012

Insel, T., Cuthbert, B., Garvey, M., Heinssen, R., Pine, D. S., Quinn, K., . . . Wang, P. (2010). Research domain criteria (RDoC): toward a new classification framework for research on mental disorders. *Am J Psychiatry, 167*(7), 748-751. doi: 10.1176/appi.ajp.2010.09091379

Iyer, M. B., Mattu, U., Grafman, J., Lomarev, M., Sato, S., & Wassermann, E. M. (2005). Safety and cognitive effect of frontal DC brain polarization in healthy individuals. *Neurology, 64*(5), 872-875. doi: 10.1212/01.WNL.0000152986.07469.E9

Jausovec, N., & Jausovec, K. (2013). Increasing working memory capacity with theta transcranial alternating current stimulation (tACS). *Biol Psychol, 96C*, 42-47. doi: 10.1016/j.biopsycho.2013.11.006

Jausovec, N., Jausovec, K., & Pahor, A. (2013). The influence of theta transcranial alternating current stimulation (tACS) on working memory storage and processing functions. *Acta Psychol (Amst), 146C*, 1-6. doi: 10.1016/j.actpsy.2013.11.011

Jensen, O., & Mazaheri, A. (2010). Shaping functional architecture by oscillatory alpha activity: gating by inhibition. *Front Hum Neurosci, 4*, 186. doi: 10.3389/fnhum.2010.00186

Joundi, R. A., Jenkinson, N., Brittain, J. S., Aziz, T. Z., & Brown, P. (2012). Driving oscillatory activity in the human cortex enhances motor performance. *Curr Biol, 22*(5), 403-407. doi: 10.1016/j.cub.2012.01.024

Kalia, S. K., Sankar, T., & Lozano, A. M. (2013). Deep brain stimulation for Parkinson's disease and other movement disorders. *Curr Opin Neurol, 26*(4), 374-380. doi: 10.1097/WCO.0b013e3283632d08

Kalu, U. G., Sexton, C. E., Loo, C. K., & Ebmeier, K. P. (2012). Transcranial direct current stimulation in the treatment of major depression: a meta-analysis. *Psychol Med, 42*(9), 1791-1800. doi: 10.1017/S0033291711003059

Kanai, R., Paulus, W., & Walsh, V. (2010). Transcranial alternating current stimulation (tACS) modulates cortical excitability as assessed by TMS-induced phosphene thresholds. *Clin Neurophysiol, 121*(9), 1551-1554. doi: 10.1016/j.clinph.2010.03.022

Kawasaki, M., Kitajo, K., & Yamaguchi, Y. (2010). Dynamic links between theta executive functions and alpha storage buffers in auditory and visual working memory. *Eur J Neurosci, 31*(9), 1683-1689. doi: 10.1111/j.1460-9568.2010.07217.x

Kelly, S. P., Lalor, E. C., Reilly, R. B., & Foxe, J. J. (2006). Increases in alpha oscillatory power reflect an active retinotopic mechanism for distracter suppression during sustained visuospatial attention. *J Neurophysiol, 95*(6), 3844-3851. doi: 10.1152/jn.01234.2005

Kikuchi, M., Yoshimura, Y., Hiraishi, H., Munesue, T., Hashimoto, T., Tsubokawa, T., . . . Minabe, Y. (2014). Reduced long-range functional connectivity in young children with autism spectrum disorder. *Soc Cogn Affect Neurosci*. doi: 10.1093/scan/nsu049

Kirov, R., Weiss, C., Siebner, H. R., Born, J., & Marshall, L. (2009). Slow oscillation electrical brain stimulation during waking promotes EEG theta activity and memory encoding. *Proc Natl Acad Sci U S A, 106*(36), 15460-15465. doi: 10.1073/pnas.0904438106

Krook-Magnuson, E., Armstrong, C., Oijala, M., & Soltesz, I. (2013). On-demand optogenetic control of spontaneous seizures in temporal lobe epilepsy. *Nat Commun, 4*, 1376. doi: 10.1038/ncomms2376

Kuo, H. I., Bikson, M., Datta, A., Minhas, P., Paulus, W., Kuo, M. F., & Nitsche, M. A. (2013). Comparing cortical plasticity induced by conventional and high-definition 4 x 1 ring tDCS: a neurophysiological study. *Brain Stimul, 6*(4), 644-648. doi: 10.1016/j.brs.2012.09.010

Kutchko, K. M., & Frohlich, F. (2013). Emergence of metastable state dynamics in interconnected cortical networks with propagation delays. *PLoS Comput Biol, 9*(10), e1003304. doi: 10.1371/journal.pcbi.1003304

Laczo, B., Antal, A., Niebergall, R., Treue, S., & Paulus, W. (2012). Transcranial alternating stimulation in a high gamma frequency range applied over V1 improves contrast perception but does not modulate spatial attention. *Brain Stimul, 5*(4), 484-491. doi: 10.1016/j.brs.2011.08.008

Lee, D., & Seo, H. (2007). Mechanisms of reinforcement learning and decision making in the primate dorsolateral prefrontal cortex. *Ann N Y Acad Sci, 1104*, 108-122. doi: 10.1196/annals.1390.007

Li, Q., Qian, Z. M., Arbuthnott, G. W., Ke, Y., & Yung, W. H. (2014). Cortical effects of deep brain stimulation: implications for pathogenesis and treatment of Parkinson disease. *JAMA Neurol, 71*(1), 100-103. doi: 10.1001/jamaneurol.2013.4221

Lu, W., & Goder, R. (2012). Does abnormal non-rapid eye movement sleep impair declarative memory consolidation?: Disturbed thalamic functions in sleep and memory processing. *Sleep Med Rev, 16*(4), 389-394. doi: 10.1016/j.smrv.2011.08.001

Luo, H., & Poeppel, D. (2007). Phase patterns of neuronal responses reliably discriminate speech in human auditory cortex. *Neuron, 54*(6), 1001-1010. doi: 10.1016/j.neuron.2007.06.004

Marshall, L., Helgadottir, H., Molle, M., & Born, J. (2006). Boosting slow oscillations during sleep potentiates memory. *Nature, 444*(7119), 610-613. doi: 10.1038/nature05278

Marshall, L., Kirov, R., Brade, J., Molle, M., & Born, J. (2011). Transcranial electrical currents to probe EEG brain rhythms and memory consolidation during sleep in humans. *PLoS One, 6*(2), e16905. doi: 10.1371/journal.pone.0016905

Martinovic, J., & Busch, N. A. (2011). High frequency oscillations as a correlate of visual perception. *Int J Psychophysiol, 79*(1), 32-38. doi: 10.1016/j.ijpsycho.2010.07.004

Mathewson, K. E., Lleras, A., Beck, D. M., Fabiani, M., Ro, T., & Gratton, G. (2011). Pulsed out of awareness: EEG alpha oscillations represent a pulsed-inhibition of ongoing cortical processing. *Front Psychol, 2*, 99. doi: 10.3389/fpsyg.2011.00099

Mazaheri, A., Fassbender, C., Coffey-Corina, S., Hartanto, T. A., Schweitzer, J. B., & Mangun, G. R. (2013). Differential Oscillatory Electroencephalogram Between Attention-Deficit/Hyperactivity Disorder Subtypes and Typically Developing Adolescents. *Biol Psychiatry*. doi: 10.1016/j.biopsych.2013.08.023

McClure, S. M., Laibson, D. I., Loewenstein, G., & Cohen, J. D. (2004). Separate neural systems value immediate and delayed monetary rewards. *Science, 306*(5695), 503-507. doi: 10.1126/science.1100907

Meiron, O., & Lavidor, M. (2014). Prefrontal oscillatory stimulation modulates access to cognitive control references in retrospective metacognitive commentary. *Clin Neurophysiol, 125*(1), 77-82. doi: 10.1016/j.clinph.2013.06.013

Miller, E. K., & Cohen, J. D. (2001). An integrative theory of prefrontal cortex function. *Annu Rev Neurosci, 24*, 167-202. doi: 10.1146/annurev.neuro.24.1.167

Minhas, P., Bansal, V., Patel, J., Ho, J. S., Diaz, J., Datta, A., & Bikson, M. (2010). Electrodes for high-definition transcutaneous DC stimulation for applications in drug delivery and electrotherapy, including tDCS. *J Neurosci Methods, 190*(2), 188-197. doi: 10.1016/j.jneumeth.2010.05.007

Mizuhara, H., & Yamaguchi, Y. (2007). Human cortical circuits for central executive function emerge by theta phase synchronization. *Neuroimage, 36*(1), 232-244. doi: 10.1016/j.neuroimage.2007.02.026

Molle, M., & Born, J. (2011). Slow oscillations orchestrating fast oscillations and memory consolidation. *Prog Brain Res, 193*, 93-110. doi: 10.1016/B978-0-444-53839-0.00007-7

Monti, A., Cogiamanian, F., Marceglia, S., Ferrucci, R., Mameli, F., Mrakic-Sposta, S., . . . Priori, A. (2008). Improved naming after transcranial direct current stimulation in aphasia. *J Neurol Neurosurg Psychiatry, 79*(4), 451-453. doi: 10.1136/jnnp.2007.135277

Monti, A., Ferrucci, R., Fumagalli, M., Mameli, F., Cogiamanian, F., Ardolino, G., & Priori, A. (2013). Transcranial direct current stimulation (tDCS) and language. *J Neurol Neurosurg Psychiatry, 84*(8), 832-842. doi: 10.1136/jnnp-2012-302825

Morris, S. E., & Cuthbert, B. N. (2012). Research Domain Criteria: cognitive systems, neural circuits, and dimensions of behavior. *Dialogues Clin Neurosci, 14*(1), 29-37.

Nacher, V., Ledberg, A., Deco, G., & Romo, R. (2013). Coherent delta-band oscillations between cortical areas correlate with decision making. *Proc Natl Acad Sci U S A, 110*(37), 15085-15090. doi: 10.1073/pnas.1314681110

Neuling, T., Rach, S., & Herrmann, C. S. (2013). Orchestrating neuronal networks: sustained after-effects of transcranial alternating current stimulation depend upon brain states. *Front Hum Neurosci, 7*, 161. doi: 10.3389/fnhum.2013.00161

Neuling, T., Rach, S., Wagner, S., Wolters, C. H., & Herrmann, C. S. (2012). Good vibrations: oscillatory phase shapes perception. *Neuroimage, 63*(2), 771-778. doi: 10.1016/j.neuroimage.2012.07.024

Nitsche, M. A., Boggio, P. S., Fregni, F., & Pascual-Leone, A. (2009). Treatment of depression with transcranial direct current stimulation (tDCS): a review. *Exp Neurol, 219*(1), 14-19. doi: 10.1016/j.expneurol.2009.03.038

Nitsche, M. A., Cohen, L. G., Wassermann, E. M., Priori, A., Lang, N., Antal, A., . . . Pascual-Leone, A. (2008). Transcranial direct current stimulation: State of the art 2008. *Brain Stimul, 1*(3), 206-223. doi: 10.1016/j.brs.2008.06.004

Nitsche, M. A., & Paulus, W. (2000). Excitability changes induced in the human motor cortex by weak transcranial direct current stimulation. *J Physiol, 527 Pt 3*, 633-639.

Nitsche, M. A., & Paulus, W. (2011). Transcranial direct current stimulation--update 2011. *Restor Neurol Neurosci, 29*(6), 463-492. doi: 10.3233/RNN-2011-0618

O'Donnell, B. F., Hetrick, W. P., Vohs, J. L., Krishnan, G. P., Carroll, C. A., & Shekhar, A. (2004). Neural synchronization deficits to auditory stimulation in bipolar disorder. *Neuroreport, 15*(8), 1369-1372.

Oda, Y., Onitsuka, T., Tsuchimoto, R., Hirano, S., Oribe, N., Ueno, T., . . . Kanba, S. (2012). Gamma band neural synchronization deficits for auditory steady state responses in bipolar disorder patients. *PLoS One, 7*(7), e39955. doi: 10.1371/journal.pone.0039955

Pahor, A., & Jausovec, N. (2014). The effects of theta transcranial alternating current stimulation (tACS) on fluid intelligence. *Int J Psychophysiol, 93*(3), 322-331. doi: 10.1016/j.ijpsycho.2014.06.015

Palva, S., & Palva, J. M. (2007). New vistas for alpha-frequency band oscillations. *Trends Neurosci, 30*(4), 150-158. doi: 10.1016/j.tins.2007.02.001

Peers, P. V., Ludwig, C. J., Rorden, C., Cusack, R., Bonfiglioli, C., Bundesen, C., . . . Duncan, J. (2005). Attentional functions of parietal and frontal cortex. *Cereb Cortex, 15*(10), 1469-1484. doi: 10.1093/cercor/bhi029

Pogosyan, A., Gaynor, L. D., Eusebio, A., & Brown, P. (2009). Boosting cortical activity at Beta-band frequencies slows movement in humans. *Curr Biol, 19*(19), 1637-1641. doi: 10.1016/j.cub.2009.07.074

Polania, R., Nitsche, M. A., Korman, C., Batsikadze, G., & Paulus, W. (2012). The importance of timing in segregated theta phase-coupling for cognitive performance. *Curr Biol, 22*(14), 1314-1318. doi: 10.1016/j.cub.2012.05.021

Prehn-Kristensen, A., Munz, M., Goder, R., Wilhelm, I., Korr, K., Vahl, W., . . . L, B. (2014). Transcranial Oscillatory Direct Current Stimulation During Sleep Improves Declarative Memory Consolidation in Children with Attention-deficit/hyperactivity Disorder to a Level Comparable to Healthy Controls. *Brain Stimul, In Press*.

Radman, T., Ramos, R. L., Brumberg, J. C., & Bikson, M. (2009). Role of cortical cell type and morphology in subthreshold and suprathreshold uniform electric field stimulation in vitro. *Brain Stimul, 2*(4), 215-228. doi: DOI 10.1016/j.brs.2009.03.007

Rajagovindan, R., & Ding, M. (2011). From prestimulus alpha oscillation to visual-evoked response: an inverted-U function and its attentional modulation. *J Cogn Neurosci, 23*(6), 1379-1394. doi: 10.1162/jocn.2010.21478

Reato, D., Rahman, A., Bikson, M., & Parra, L. C. (2010). Low-intensity electrical stimulation affects network dynamics by modulating population rate and spike timing. *J Neurosci, 30*(45), 15067-15079. doi: 10.1523/JNEUROSCI.2059-10.2010

Reis, J., & Fritsch, B. (2011). Modulation of motor performance and motor learning by transcranial direct current stimulation. *Curr Opin Neurol, 24*(6), 590-596. doi: 10.1097/WCO.0b013e32834c3db0

Romei, V., Gross, J., & Thut, G. (2010). On the role of prestimulus alpha rhythms over occipito-parietal areas in visual input regulation: correlation or causation? *J Neurosci, 30*(25), 8692-8697. doi: 10.1523/JNEUROSCI.0160-10.2010

Santarnecchi, E., Polizzotto, N. R., Godone, M., Giovannelli, F., Feurra, M., Matzen, L., . . . Rossi, S. (2013). Frequency-dependent enhancement of fluid intelligence induced by transcranial oscillatory potentials. *Curr Biol, 23*(15), 1449-1453. doi: 10.1016/j.cub.2013.06.022

Schlaug, G., Renga, V., & Nair, D. (2008). Transcranial direct current stimulation in stroke recovery. *Arch Neurol, 65*(12), 1571-1576. doi: 10.1001/archneur.65.12.1571

Schmidt, S., Iyengar, A., Foulser, A., Boyle, M., & Frohlich, F. (2014). Endogenous Cortical Oscillations Constrain Neuromodulation by Weak Electric Fields *Brain Stimul, In Press*. doi: 10.1016/j.brs.2014.07.033

Schutter, D. J., & Hortensius, R. (2010). Retinal origin of phosphenes to transcranial alternating current stimulation. *Clin Neurophysiol, 121*(7), 1080-1084. doi: 10.1016/j.clinph.2009.10.038

Schutter, D. J., & Hortensius, R. (2011). Brain oscillations and frequency-dependent modulation of cortical excitability. *Brain Stimul, 4*(2), 97-103. doi: 10.1016/j.brs.2010.07.002

Schwiedrzik, C. M. (2009). Retina or visual cortex? The site of phosphene induction by transcranial alternating current stimulation. *Front Integr Neurosci, 3*, 6. doi: 10.3389/neuro.07.006.2009

Sela, T., Kilim, A., & Lavidor, M. (2012). Transcranial alternating current stimulation increases risk-taking behavior in the balloon analog risk task. *Front Neurosci, 6*, 22. doi: 10.3389/fnins.2012.00022

Smith, E. E., & Jonides, J. (1999). Storage and executive processes in the frontal lobes. *Science, 283*(5408), 1657-1661.

Solomon, M., Ozonoff, S. J., Cummings, N., & Carter, C. S. (2008). Cognitive control in autism spectrum disorders. *Int J Dev Neurosci, 26*(2), 239-247. doi: 10.1016/j.ijdevneu.2007.11.001

Solomon, M., Ozonoff, S. J., Ursu, S., Ravizza, S., Cummings, N., Ly, S., & Carter, C. S. (2009). The neural substrates of cognitive control deficits in autism spectrum disorders. *Neuropsychologia, 47*(12), 2515-2526. doi: 10.1016/j.neuropsychologia.2009.04.019

Song, J. J., Vanneste, S., Van de Heyning, P., & De Ridder, D. (2012). Transcranial direct current stimulation in tinnitus patients: a systemic review and meta-analysis. *ScientificWorldJournal, 2012*, 427941. doi: 10.1100/2012/427941

Sparing, R., Dafotakis, M., Meister, I. G., Thirugnanasambandam, N., & Fink, G. R. (2008). Enhancing language performance with non-invasive brain stimulation--a transcranial direct current stimulation study in healthy humans. *Neuropsychologia, 46*(1), 261-268. doi: 10.1016/j.neuropsychologia.2007.07.009

Spencer, K. M. (2011). Baseline gamma power during auditory steady-state stimulation in schizophrenia. *Front Hum Neurosci, 5*, 190. doi: 10.3389/fnhum.2011.00190

Stickgold, R. (2005). Sleep-dependent memory consolidation. *Nature, 437*(7063), 1272-1278. doi: 10.1038/nature04286

Struber, D., Rach, S., Trautmann-Lengsfeld, S. A., Engel, A. K., & Herrmann, C. S. (2014). Antiphasic 40 hz oscillatory current stimulation affects bistable motion perception. *Brain Topogr, 27*(1), 158-171. doi: 10.1007/s10548-013-0294-x

Sun, L., Grutzner, C., Bolte, S., Wibral, M., Tozman, T., Schlitt, S., . . . Uhlhaas, P. J. (2012). Impaired gamma-band activity during perceptual organization in adults with autism spectrum disorders: evidence for dysfunctional network activity in frontal-posterior cortices. *J Neurosci, 32*(28), 9563-9573. doi: 10.1523/JNEUROSCI.1073-12.2012

Todd, J. J., & Marois, R. (2004). Capacity limit of visual short-term memory in human posterior parietal cortex. *Nature, 428*(6984), 751-754. doi: 10.1038/nature02466

Uhlhaas, P. J., Haenschel, C., Nikolic, D., & Singer, W. (2008). The role of oscillations and synchrony in cortical networks and their putative relevance for the pathophysiology of schizophrenia. *Schizophr Bull, 34*(5), 927-943. doi: 10.1093/schbul/sbn062

Uhlhaas, P. J., & Singer, W. (2006). Neural synchrony in brain disorders: relevance for cognitive dysfunctions and pathophysiology. *Neuron, 52*(1), 155-168. doi: 10.1016/j.neuron.2006.09.020

Uhlhaas, P. J., & Singer, W. (2010). Abnormal neural oscillations and synchrony in schizophrenia. *Nat Rev Neurosci, 11*(2), 100-113. doi: 10.1038/nrn2774

Uhlhaas, P. J., & Singer, W. (2012). Neuronal dynamics and neuropsychiatric disorders: toward a translational paradigm for dysfunctional large-scale networks. *Neuron, 75*(6), 963-980. doi: 10.1016/j.neuron.2012.09.004

Voss, U., Holzmann, R., Hobson, A., Paulus, W., Koppehele-Gossel, J., Klimke, A., & Nitsche, M. A. (2014). Induction of self awareness in dreams through frontal low current stimulation of gamma activity. *Nat Neurosci, 17*(6), 810-812. doi: 10.1038/nn.3719

Wach, C., Krause, V., Moliadze, V., Paulus, W., Schnitzler, A., & Pollok, B. (2013a). The effect of 10 Hz transcranial alternating current stimulation (tACS) on corticomuscular coherence. *Front Hum Neurosci, 7*, 511. doi: 10.3389/fnhum.2013.00511

Wach, C., Krause, V., Moliadze, V., Paulus, W., Schnitzler, A., & Pollok, B. (2013b). Effects of 10 Hz and 20 Hz transcranial alternating current stimulation (tACS) on motor functions and motor cortical excitability. *Behav Brain Res, 241*, 1-6. doi: 10.1016/j.bbr.2012.11.038

Walker, M. P., & Stickgold, R. (2004). Sleep-dependent learning and memory consolidation. *Neuron, 44*(1), 121-133. doi: 10.1016/j.neuron.2004.08.031

Wamsley, E. J., Tucker, M. A., Shinn, A. K., Ono, K. E., McKinley, S. K., Ely, A. V., . . . Manoach, D. S. (2012). Reduced sleep spindles and spindle coherence in schizophrenia: mechanisms of impaired memory consolidation? *Biol Psychiatry, 71*(2), 154-161. doi: 10.1016/j.biopsych.2011.08.008

Wang, X. J. (2010). Neurophysiological and computational principles of cortical rhythms in cognition. *Physiol Rev, 90*(3), 1195-1268. doi: 10.1152/physrev.00035.2008

Wolkenstein, L., & Plewnia, C. (2013). Amelioration of cognitive control in depression by transcranial direct current stimulation. *Biol Psychiatry, 73*(7), 646-651. doi: 10.1016/j.biopsych.2012.10.010

Woltering, S., Jung, J., Liu, Z., & Tannock, R. (2012). Resting state EEG oscillatory power differences in ADHD college students and their peers. *Behav Brain Funct, 8*, 60. doi: 10.1186/1744-9081-8-60

Worden, M. S., Foxe, J. J., Wang, N., & Simpson, G. V. (2000). Anticipatory biasing of visuospatial attention indexed by retinotopically specific alpha-band electroencephalography increases over occipital cortex. *J Neurosci, 20*(6), RC63.

Workshop Proceedings of the NIMH Research Domain Criteria (RDoC) Project: Cognitive Systems, Rockville. (2010).

Workshop Proceedings of the NIMH Research Domain Criteria (RDoC) Project: Working Memory, Rockville. (2010).

Wu, X., Chen, X., Li, Z., Han, S., & Zhang, D. (2007). Binding of verbal and spatial information in human working memory involves large-scale neural synchronization at theta frequency. *Neuroimage, 35*(4), 1654-1662. doi: 10.1016/j.neuroimage.2007.02.011

Zaehle, T., Rach, S., & Herrmann, C. S. (2010). Transcranial alternating current stimulation enhances individual alpha activity in human EEG. *PLoS One, 5*(11), e13766. doi: 10.1371/journal.pone.0013766

Zaghi, S., de Freitas Rezende, L., de Oliveira, L. M., El-Nazer, R., Menning, S., Tadini, L., & Fregni, F. (2010). Inhibition of motor cortex excitability with 15Hz transcranial alternating current stimulation (tACS). *Neurosci Lett, 479*(3), 211-214. doi: 10.1016/j.neulet.2010.05.060

CHAPTER 4: ANESTHESIA DIFFERENTIALLY MODULATES SPONTANEOUS NETWORK DYNAMICS BY CORTICAL AREA AND LAYER[3]

INTRODUCTION

Anesthesia is routinely used in both human patients for invasive procedures and systems neuroscience for electrophysiological and imaging studies of brain activity. Yet, there is a gap in knowledge between the well-characterized molecular targets of anesthetic agents throughout the central nervous system (Alkire, Hudetz, & Tononi, 2008) and the effects on overall behavioral state such as loss of consciousness (E. N. Brown, Purdon, & Van Dort, 2011). Specifically, little is known about how anesthesia modulates brain activity at the network level to achieve profound alterations in arousal and cognition. Bridging this gap by elucidating the network-level effects of anesthesia will (1) aid in the development of more refined anesthesia monitoring techniques to reduce the number of anesthesia-related adverse side effects, (2) instigate the reinterpretation of decades of work on systems neuroscience conducted in anesthetized animals, and (3) provide fundamental insight into cortical network dynamics across cortical layers and areas.

Traditionally, anesthesia has been assumed to suppress brain activity (Friedman et al., 2010; Steyn-Ross, Steyn-Ross, & Sleigh, 2004), yet recent studies have revealed that anesthetic agents may rather modulate the dynamics of large-scale neuronal networks (Cimenser et al., 2011; Lewis et al., 2012; McCarthy, Ching, Whittington, & Kopell, 2012). At the macroscopic level, anesthesia alters electroencephalogram (EEG) by shifting oscillatory activity from high-frequency, low-amplitude patterns to low-frequency, high-amplitude activity (Voss & Sleigh, 2007). Recent analysis strategies to quantify the

[3] This chapter previously appeared as an article in the Journal of Neurophysiology; doi: 10.1152/jn.00404.2013 (http://jn.physiology.org/content/110/12/2739.long). The original citation is as follows: **Kristin K. Sellers**, Davis V. Bennett, Axel Hutt, and Flavio Frohlich (2013). Anesthesia differentially modulates spontaneous network dynamics by cortical area and layer. Journal of Neurophysiology, 110(12):2739-2751.

modulation of network dynamics have revealed that anesthesia may disrupt integration of information across brain regions through decreasing long-range coherence (O. A. Imas, Ropella, Ward, Wood, & Hudetz, 2005; Olga A. Imas, Ropella, Wood, & Hudetz, 2006; John & Prichep, 2005), and reduce cortical information capacity by shrinking the repertoire of distinct activity patterns (Alkire et al., 2008).

In support of such sophisticated modulation of network dynamics by anesthesia, studies using functional magnetic resonance imaging (fMRI) in awake and anesthetized primates have found profoundly altered stimulus-evoked responses and functional connectivity induced by anesthesia (J. V. Liu et al., 2013). Despite only indirect coupling between blood oxygenation dynamics measured by fMRI and electrical brain activity (Logothetis & Wandell, 2004; Magri, Schridde, Murayama, Panzeri, & Logothetis, 2012), fMRI has provided important indications of the complexity of the network-level effects of anesthesia. Resting-state fMRI (rs-fMRI) in humans has demonstrated reduced functional connectivity during anesthesia compared to the awake state, which scaled with depth of anesthesia (Peltier et al., 2005). Also, a growing body of evidence suggests that anesthesia does not affect all cortical areas similarly (Bonhomme, Boveroux, Brichant, Laureys, & Boly, 2012; Heinke & Koelsch, 2005; Heinke & Schwarzbauer, 2001). In particular, rs-fMRI findings indicate that propofol-induced loss of consciousness correlates with decreased corticocortical and thalamocortical connectivity in frontoparietal networks, while connectivity is preserved in sensory cortices (Boveroux et al., 2010). Positron emission tomography data (White & Alkire, 2003) in humans has also demonstrated that anesthesia-induced loss of consciousness by isoflurane or halothane is accompanied by decreased corticocortical and thalamocortical connectivity. However, this remains an area of debate, as computational models investigating propofol anesthesia suggest that there is increased functional coupling between the thalamus and cortex (Ching, Cimenser, Purdon, Brown, & Kopell, 2010).

Yet, the changes in mesoscopic and microscopic network dynamics caused by anesthesia as a function of cortical area, cortical layer, and anesthetic depth remain poorly understood. To address this gap in knowledge, we here examined how anesthesia modulates spontaneous network activity in a primarya sensory area (primary visual cortex, V1) and a higher-order association area (prefrontal cortex, PFC) by electrophysiological recordings of local field potential (LFP, mesoscopic network activity) and multiunit spiking activity (MU, microscopic network activity) in awake and anesthetized ferrets. We used

isoflurane at three concentrations (0.5%, 0.75%, and 1.0%, each with continuous and equal xylazine administration for maintaining adequate sedation) because isoflurane is a commonly employed anesthetic in neuroscience. We hypothesized that a primary sensory cortical area (V1) and an association cortical area (PFC) would exhibit differential modulation of network dynamics in response to anesthesia due to their different functional roles. Indeed, we found that the effects of anesthesia on these two cortical areas were vastly different. In V1, modulation induced by anesthesia in input layer IV (granular layer) differed from modulation of activity in supragranular and infragranular layers. In contrast, in PFC, anesthesia altered network dynamics and induced highly rhythmic activity patterns with fewer differences across cortical layers. To our knowledge, this is the first study that comprehensively examines the dose-dependent effects of an anesthetic on two different cortical areas across layers with such high temporal resolution.

METHODS

Surgery

Adolescent female ferrets (*Mustela putoris furo*, 15-20 weeks old) were used in this study. All experiments were conducted in animals that had not reached sexual maturity to avoid possible estrous-dependent changes in physiology. This intermediate model species was chosen due to key similarities with primates; in particular, ferrets have a gyrencephalic cortex, a highly developed visual system, and cortical association areas such as prefrontal cortex. Aseptic surgical procedures were used to prepare animals for multichannel electrophysiological recordings in V1 and PFC. Animals received an initial intramuscular injection of ketamine (30 mg/kg) and xylazine (1-2 mg/kg). The method of anesthesia maintenance used during surgery depended on the specific experimental preparation (see below). Animal physiology (electrocardiogram, pulse oxygen level, endtidal CO_2 for a subset of animals, and rectal body temperature) was continuously measured. Endtidal CO_2 was between 30 and 50mmHg (Kohn, 1997). Animals were warmed with a water heating blanket to maintain rectal temperature of 38.0-39.0° C. The animal's eyes were protected with paralube for the duration of surgery.

Surgical procedures consisted of an initial midline incision of the scalp, retraction of the soft tissue, and a circular craniotomy located over V1 (approximately 3mm anterior to lambda and 9mm lateral

to midline) and/or PFC (approximately 5mm anterior to bregma and 2mm lateral to the midline). The potential for brain swelling was reduced with a preventative injection of furosemide (1mg/kg, IM). Dura was removed and the brain was covered with warm, sterile 4% agar. Probe location in V1 was verified by eliciting visually evoked potentials and mapping receptive fields, while insertion location in PFC was confirmed by histology to be in the anterior sigmoid gyrus (Duque & McCormick, 2010) (recording probe dipped in DiI prior to insertion, Invitrogen, Grand Island, NY). A stainless steel head post was implanted with bone screws and dental cement. All procedures were approved by the UNC – Chapel Hill IACUC and exceed guidelines set forth by the NIH and USDA.

Experiments in Anesthetized Animals

Most recordings in anesthetized animals ("anesthetized recordings", female ferrets) were conducted immediately following surgery. For these experiments, animals were intubated and artificially respirated (10-11cc, 50bpm, 100% medical-grade oxygen), and isoflurane was used to maintain deep anesthesia during surgery. These animals were continuously administered an IV via the cephalic vein (4.25mL/hr 5% dextrose lactated ringer's, 0.015mL/hr xylazine during surgery with the addition of 0.079mL/hr vecuronium bromide during recordings). Paralysis by vecuronium bromide was used to enhance the stability of electrophysiological recordings. Surgical procedures are outlined above.

Anesthetized recordings were conducted during resting-state (dark room, no stimuli) under varying concentrations of isoflurane anesthesia (iso, 0.5%, 0.75%, 1.0%). Continuous administration of xylazine via IV guaranteed the complete absence of withdrawal response to toe pinch for all concentrations of isoflurane used in this study. The use of xylazine as an additional anesthetic was mandated by UNC-CH IACUC requirements. Unless otherwise stated, 'anesthesia' subsequently refers to this paradigm of isoflurane and xylazine administration. The temporal order of anesthetic concentration was randomized across animals. 20 minute elapsed after changing anesthetic concentration prior to starting a new recording, exceeding the approximately 4-7 minutes required to reach new baseline neural activity for our experimental setup. The animal's eyes were moistened with saline prior to each recording and animal vital signs were monitored throughout the recordings.

Two linear 16-channel silicon probes (100µm contact site spacing along the z-axis, Neuronexus, Ann Arbor, MI) were used in cases of dual craniotomies. Animals were headfixed during these recordings. A silver chloride wire tucked between the skull and soft tissue and held in place with 4% agar in saline was used as the reference for both linear probes. Each probe was slowly advanced into cortex with a micromanipulator (Narishige, Tokyo, Japan); correct depth was determined by small deflections of the LFP at superficial electrode recording sites and larger deflections of the LFP at deeper electrode recording sites. Unfiltered signals were first amplified with MPA8I head-stages with gain 10 (Multichannel Systems, Reutlingen, Germany), then further amplified with gain 500 (Model 3500, A-M Systems, Carlsborg, WA), digitized at 20kHz (Power 1401, Cambridge Electronic Design, Cambridge, UK), and digitally stored using Spike2 software (Cambridge Electronic Design). In this study, all three concentrations of isoflurane anesthesia corresponded to lack of behavioral responses. Burst suppression was not present in any recording; rather, we found rhythmic occurrence of UP (active phase) and DOWN states (quiet phase); the DOWN states were relatively short, typically at most 1-1.5 sec long, and therefore did not last the 10s of seconds typically seen during the suppression period of burst suppression patterns. Infrared videography (Handycam HDR-cx560v, Sony, Tokyo, Japan) of the animal was conducted.

Experiments in Awake Animals

Prior to surgery in animals which were recorded from while awake (“awake recordings”), animals were trained to be calmly restrained for up to 2 hours. Female ferrets were used for awake recordings because their growth had plateaued, and they were therefore more suited for chronic implants compared to males. All animals were spayed in case they were kept until the age of sexual maturity; all animals in this study were used prior to the age of sexual maturity. Deep anesthesia was maintained for the duration of the surgery with intramuscular injections of ketamine (30 mg/kg) and xylazine (1-2 mg/kg) approximately every 40 minutes. Surgical procedures are outlined above. Additionally, the base of a custom-fabricated cylindrical chamber with a removable cap (material: Ultem 1000) was secured to the skull with bone screws and dental cement in order to allow subsequent access to the craniotomy for recordings. Upon completion of these surgical procedures, the incision was closed with sutures and

treated with antibiotic cream. Yohimbine (0.25 – 0.5mg/kg, IM) was then administered to reverse anesthesia. The animal was kept warm with a heating blanket and observed during recovery from anesthesia. Meloxicam (0.2 mg/kg, IM) and enrofloxacin (0.5 mg/kg, IM) were administered to prevent infection and to minimize post-surgical discomfort.

Awake recordings during resting-state (dark room, no stimuli) began after animals had fully recovered from surgery (at least 5 days). Each recording session was brief (typically < 2 hours), during which the animal was restrained and headfixed. Multichannel electrophysiological data were recorded with acutely inserted, linear 32-channel silicon probes (50µm contact site spacing along the z-axis, Neuronexus, Ann Arbor, MI). In these electrodes, the reference was located on the same shank (0.5 mm above the top recording site) and was positioned in the 4% agar in saline above the brain. Infrared videography was used to monitor whisking and minor movements that, together with the fact that the animal's eyes remained open, established the absence of sleep during these recording sessions. A subset of animals which had been used for awake recordings (both V1 and PFC craniotomy locations) was also used for anesthetized recordings to minimize the number of animals used in this study. At the conclusion of the study, all animals were humanely killed with an overdose of sodium pentobarbital and immediately perfused with 4% formaldehyde in 0.1M phosphate buffered saline for subsequent histological verification of recording locations.

Data Analysis and Statistical Methods

Recorded broadband signals were processed offline with custom-written scripts in MATLAB (Mathworks, Natick, MA). Continuous recordings were segmented into non-overlapping 5 second trials. A subset of these trials was manually excluded due to motion artifacts in the LFP signal (defined as extreme values in the raw trace). If not stated otherwise, figures represent medians across recordings sessions, recording sites, and trials (62 recording sessions; total trials in V1: awake = 3612, 0.5% iso = 729, 0.75% iso = 2557, 1.0% iso = 2860; total trials in PFC: awake = 6327, 0.5% iso = 2298, 0.75% iso = 2722, 1.0% iso = 3394). If not stated otherwise, values are presented as median ± sem. Time-dependent frequency content was determined by convolution of raw extracellular voltage signals with a family of Morlet wavelets (0.5Hz – 40Hz, step-width 0.5Hz) with normalized amplitude, providing an optimal trade-off

between time and frequency uncertainty (Goupillaud, Grossmann, & Morlet, 1984). Total power in each frequency band (delta = 0.5-4Hz, theta = 4-8Hz, alpha = 8-12Hz, beta = 12-20Hz, gamma = 20-40Hz) was calculated by taking the median value across all trials. When comparing results presented here to prior studies, it is important to consider that there is no consensus about the frequency range used for each frequency band, particularly in differentiating the beta and gamma frequency bands. For readability, we did not divide beta into 'beta 1' and 'beta 2', but attributed frequencies often assigned to 'beta 2' (23-30Hz) to the gamma band. Early seminal work looking at fast oscillations which increased during alertness and during sensory processing examined frequency ranges from 20-40Hz (Steriade, Dossi, Pare, & Oakson, 1991) in cats, another carnivore intermediate model species. Spectra are first presented averaged across all recording electrodes, and subsequently shown by cortical layer; all spectra are shown on a logarithmic scale. Bootstrapping with 100 iterations of resampling, a distribution-independent method, was used to calculate standard errors when parametric models were a poor fit for the data. Cross-correlation was determined as peaks of the cross-correlogram computed with the MATLAB xcorr function; the trial-shuffled control correlation was subtracted to exclude changes in correlation peak due to changes in signal amplitude across awake and anesthetized recordings. High-pass filtered data (4^{th} order butterworth filter, 300Hz cutoff) were subjected to a threshold of -3*std for detection of action potentials (multiunit activity). In order to quantify the correspondence between mesoscopic LFP oscillatory structure and microscopic MU activity, spike-field coherence (SFC) was calculated. Spike-triggered averages from 1 second segments of LFP around each spike were obtained. Multitaper spectral estimates were used to determine spectra of the spike-triggered averages (MATLAB pmtm function with time-bandwidth product of 3.5). SFC values are the ratio of spike-triggered average spectra to the average of spectra calculated from each LFP segment (Fries, 2009). The choice of frequency analysis for SFC was motivated by existing literature to enable comparisons with the findings presented here. 10 second non-overlapping trials were used to determine spike-field coherence to provide longer data windows (V1: awake = 1715, 0.5% iso = 360, 0.75% iso = 1115, 1.0% iso = 1423; PFC: awake = 2288, 0.5% iso = 1137, 0.75% iso = 1187, 1.0% iso = 1628). The non-parametric Kruskall-Wallis test was implemented using the MATLAB function kruskalwallis to determine if samples from awake animals and animals administered different concentrations of anesthesia came from the same distribution. 1-way

ANOVA with Tukey's honestly significant difference criterion was used to correct for multiple comparisons.

In order to verify electrode location in V1, receptive fields were determined by presenting the animal with a series of gray screens with one square of a 19-10 grid colored white or black for 40ms. Each square was shown for 30 repeats (order randomized) with 160ms between each stimulus. Evoked MU spiking for each grid location was determined by calculating the number of spikes elicited between 60 – 140ms after presentation of each stimulus, and subtracting the number of spikes which occurred in the 80ms preceding presentation of the stimulus. Histology procedures consisted of cutting 100µm coronal sections of fixed tissue using a vibratome. Cresyl violet was used for Nissl staining. Stained sections and sections with DiI tracks from the recording electrodes were imaged using an Olympus BX51 microscope.

RESULTS

In order to elucidate the effects of anesthesia on mesoscopic and microscopic cortical network dynamics, we performed electrophysiological recordings of spontaneous activity in absence of sensory stimulation. We studied network dynamics in awake (n = 6) and anesthetized (n = 5) ferrets. In both conditions, the eyes of the animals were open (Figure 4.1A: infrared image of right eye of an awake and anesthetized ferret). To test our hypothesis that anesthesia differentially modulates dynamics in different cortical areas, we compared the effects of isoflurane anesthesia in a sensory cortical area, primary visual cortex (Figure 4.1B, V1, central vision, lateral gyrus), and a higher-order association cortical area, prefrontal cortex (Figure 4.1B, PFC, anterior sigmoid gyrus). We used linear depth probes to simultaneously record LFP and MU activity from all cortical layers (Figure 4.1C) to determine if different elements of the cortical microcircuit were equally sensitive to modulation by anesthesia. Three concentrations of isoflurane anesthetic (0.5%, 0.75%, and 1.0%) were used to assess differences in network activity between the awake and the anesthetized states (62 recording sessions total). In agreement with our hypothesis, we found that anesthesia had fundamentally different effects on V1 and PFC.

Anesthesia Increased Spectral Power in PFC but Altered Distribution of Power in V1

We found that anesthesia had differential effects on the oscillation structure of network activity in V1 and PFC. Relative to activity in the awake animal, the LFP in V1 exhibited changes in rhythmic structure with increased depth of anesthesia (Figure 4.1D, left). The LFP measured in PFC in the awake animal exhibited only minimal rhythmic structure but showed prominent slow rhythms during anesthesia (Figure 4.1D, right). Furthermore, V1 exhibited frequency-specific modulation of global power with varying depths of anesthesia (Figure 4.2A, left, dotted lines indicate ± 2 std). In awake animals, the LFP in V1 exhibited a spectral peak at ~18Hz (Figure 4.2A: left, trace insert). With 0.5% and 0.75% isoflurane, the V1 LFP spectral peak occurred at a lower frequency. This spectral peak in V1 of animals anesthetized with 0.5% and 0.75% isoflurane was similar to the spindle frequency peak which appeared in anesthetized recordings in PFC (discussed below). With 1.0% isoflurane anesthesia, there was no longer a pronounced peak in V1 spectral power. In contrast, PFC in the awake animal did not exhibit a clear spectral peak. With anesthesia, the entire spectrum shifted to higher power (Figure 4.2A, right, dotted lines indicate ± 2 std) and a peak in the spindle frequency at ~10Hz emerged (Figure 4.2A: right, trace insert). To further probe these marked differences in frequency structure, we calculated total power in each frequency band traditionally associated with distinct cognitive and behavioral functions (X. J. Wang, 2010) (delta = 0.5-4Hz, theta = 4-8Hz, alpha = 8-12Hz, beta = 12-20Hz, gamma = 20-40Hz). Relative to awake animals, anesthesia modestly modulated total power in V1 for each frequency band (Figure 4.2B, left, ** indicates Kruskal-Wallis test significant to $p<0.001$, * indicates Kruskal-Wallis test significant to $p<0.05$. See Table 4.1 for all values). The most pronounced change was the suppression of power in the beta band with anesthesia (beta power: awake = 8.05 ± 0.14, 0.5% iso = 5.66 ± 0.07, 0.75% iso = 5.22 ± 0.04, 1.0% iso = 4.90 ± 0.04, Kruskal-Wallis test between all anesthesia concentrations significant to $p<0.001$), which corresponds to the loss of the 18Hz peak in the spectrum (Figure 4.2A, left). In contrast, in PFC, anesthesia dramatically increased power in all frequency bands, most profoundly in the delta range (Figure 4.2B, right, delta power: awake = 4.94 ± 0.23, 0.5% iso = 26.19 ± 0.66, 0.75% iso = 31.01 ± 0.63, 1.0% iso = 52.19 ± 0.32, ** indicates Kruskal-Wallis test significant to $p<0.001$, * indicates Kruskal-Wallis test significant to $p<0.05$. See Table 4.2 for all values). This increase in slow rhythmic power

reflects the increase in cortical slow oscillations commonly associated with anesthesia (Steriade, Nunez, & Amzica, 1993).

Given the two different modulation profiles for V1 and PFC, we next examined how anesthesia affected the relative contributions of the different frequency bands to the overall LFP signal. We computed the power in each frequency band as a percent of total power and again found two very different effect profiles of anesthesia. In V1, the distribution of power in the different frequency bands was mostly resilient to anesthesia. The limited changes to the power distribution included both increases and decreases in relative contribution when comparing awake animals to animals anesthetized with different isoflurane concentrations (Figure 4.3A). Again, in clear contrast to V1, the relative distribution of power in PFC shifted from the gamma to the delta band. We found an almost doubled contribution of delta oscillations to the overall spectrum when comparing awake to deeply anesthetized (1.0% isoflurane) animals (Figure 4.3B: Delta = black, awake = 22%, 0.5% iso = 31%, 0.75% = 32%, 1.0% iso = 43%). Concomitantly, the relative contribution of the gamma band shrank to less than half (Figure 4.3B: Gamma = yellow, awake = 30%, 0.5% iso = 19%, 0.75% = 19%, 1.0% iso = 14%). Interestingly, the intermediate frequency bands (theta, alpha, and beta) failed to show such a pronounced redistribution of relative power with anesthesia. In summary, these analyses demonstrate that, in agreement with our hypothesis, network dynamics in V1 were quite resilient to anesthesia whereas PFC exhibited profound alterations in rhythmic structure in presence of anesthetics.

Laminar Effects of Anesthesia

Given the distinct functional roles of different cortical layers, we next examined if the changes in spectral power with anesthesia were uniform across cortical depth. We found that the prominent peak at ~18Hz in V1 of the awake animal was almost exclusively localized to deep (infragranular) layers (Figure 4.4A, left, red box). The spectral peaks seen at slightly lower frequencies with intermediate concentrations of anesthesia (Figure 4.2A, 0.5% and 0.75% isoflurane) were also predominantly in infragranular layers (Figures 4.4B and C, left, red box). The highest concentration of anesthesia (1.0% isoflurane) abolished this intermediate frequency peak in the deep layers (Figure 4.4D, left). In contrast, compared to spectral power in awake animals in PFC (Figure 4.4A, right), spectral power in PFC was

greatly increased across all cortical layers with 0.5% (Figure 4.4B, right), 0.75% (Figure 4.4C, right), and 1.0% isoflurane (Figure 4.4D, right). A local peak around 10Hz is evident in layer IV and infragranular layers of PFC in anesthetized animals, corresponding to the peak in spindle frequencies (Figure 4.2A, right). Cortical layers likely mediate sophisticated information processing, in which individual layers play different roles in the overall functioning of cortical microcircuits. We therefore examined if anesthesia impaired these distinct processing roles by increasing the correlation between the activity in different layers. To this end, we calculated the average of exhaustive pairwise cross-correlations of electrodes (shuffle controlled). Overall, LFP signals in V1 exhibited lower cross-correlation than those in PFC (Figure 4.4E, note different scales). In further agreement with our hypothesis that modulation by anesthesia varies by cortical areas, correlation increased in PFC but decreased in V1 in anesthetized animals compared to awake animals (cross correlation V1: awake = 0.0012 ± <.0001, 0.5% iso = 0.0005 ± 0.0002, 0.75% iso = 0.0008 ± 0001, 1.0% iso = 0.0011 ± 0001, Kruskal-Wallis test between all anesthesia concentrations significant to $p<0.05$, except awake and 0.5% is non-significant. Cross correlation PFC: awake = 0.0004 ± 0.0003, 0.5% iso = 0.0121 ± 0.0012, 0.75% iso = 0.0149 ± 0.0015, 1.0% iso = 0.0316 ± 0.0009, Kruskal-Wallis test between all anesthesia concentrations significant to $p<0.001$). Thus, we also found a selective increase in correlated processing across layers with anesthesia in PFC.

Cortical Area- and Layer-Specific Alterations to Microscopic Network Dynamics with Anesthesia

Thus far, we have presented key differences in the mesoscopic network structure of V1 and PFC induced by anesthesia based on LFP recordings. We next asked if microscopic dynamics in these cortical circuits, mediated by action potential firing, were similarly modulated. In looking at simultaneous LFP and MU traces, increased coordination is evident between mesoscopic and microscopic processes with anesthesia, particularly in PFC. Both V1 and PFC in the awake animal exhibited MU firing that was not time-locked to any gross structures of the LFP (Figure 4.5A, top: V1. Figure 4.5B, top: PFC). With anesthesia, MU activity in V1 and PFC became more rhythmic (Figure 4.5A, bottom: V1. Figure 4.5B, bottom: PFC). The slow rhythm in both LFP and MU activity was generated by alternating epochs of MU firing and quiescence; this activity structure corresponds to the slow oscillation (UP and DOWN states) that represents a hallmark of anesthesia (red shaded boxes in Figure 4.5 highlight DOWN states). Taking

into account cortical depth, we quantified these changes to the mesoscopic and microscopic network activity by probing for region-specific effects of anesthesia on MU firing rates and on the temporal relationship between LFP and MU (spike-field coherence).

In agreement with our hypothesis that V1 and PFC would also exhibit differential modulation of microscopic dynamics, we found area-specific changes in MU firing rate. Averaged across cortical layers, anesthesia did not significantly modulate firing rate in V1 or PFC (Figure 4.6A, V1 median firing rate: awake = 24.6 ± 2.87, 0.5% iso = 24 ± 6.40, 0.75% = 23.6 ± 0.65, 1.0% iso = 23.9 ± 0.49, Kruskal-Wallis test between all anesthesia concentrations non-significant at p=0.05. PFC median firing rate: awake = 23.9 ± 0.68, 0.5% iso = 24.8 ± 1.54, 0.75% = 25.7 ± 1.08, 1.0% iso = 24.2 ± 0.37, Kruskal-Wallis test between all anesthesia concentrations non-significant at p=0.05). Given these non-significant changes in MU firing rates when averaged across cortical depth, we next examined if modulation of MU activity depended on cortical depth since the firing of neurons in different layers likely perform distinct tasks. Indeed, we found depth-dependent response profiles in V1 and in PFC. In V1, moderate concentrations of anesthesia (0.5% and 0.75% isoflurane) increased MU firing specifically in input layer IV with a concomitant reduction of firing in the other layers (Figure 4.6B, left). In PFC, MU spiking decreased exclusively in supragranular layers for intermediate concentrations of anesthesia (0.5% and 0.75% isoflurane) (Figure 4.6B, right). Together, these data show that specifically layer IV was susceptible to changes in firing rate induced by anesthesia in V1 but not PFC. This unique, differential alteration to the activity of the input layer in a primary sensory cortex points towards modulation by anesthesia based on the functional role of specific cortical layers.

Anesthesia Induced Targeted Increases in Spike-Field Coherence

Having established that anesthesia had area- and layer-specific effects on both mesoscopic and microscopic network dynamics independently, we next asked how anesthesia altered the relationship between mesoscopic LFP network dynamics and microscopic MU firing. Spike-field coherence (SFC) was used to measure preferential firing of action potentials as a function of LFP phase. For a given frequency, higher values indicate that MU firing was more tightly coupled to the LFP phase. In awake animals, both V1 and PFC exhibited low SFC across cortical layers (Figure 4.7A). With all concentrations of anesthesia,

spiking in V1 was more tightly coupled to the phase of the LFP at all frequencies in supragranular and infragranular layers (Figures 4.7B, C, and D, left). The strongest increase in coupling was found in the slowest and fastest frequencies. Notably, increase in SFC exhibited layer-dependence and remained minimal in input layer IV for all concentrations of anesthesia. Anesthesia in PFC resulted in increased SFC in superficial layers at higher frequencies, and across layers at low frequencies (Figures 4.7B, C, D, right). In PFC, the strength of SFC increased with deepening anesthesia from 0.5% isoflurane to 1.0% isoflurane. In summary, MU spiking was mostly independent of LFP phase in the awake animal. In the anesthetized animal, MU spiking was modulated by LFP phase in a cortical area and layer-specific manner. These results further confirm that understanding the effects of anesthesia on cortex requires not only recordings across cortical layers but also analysis strategies that bridge the micro- and mesoscopic scale.

DISCUSSION

While the molecular targets of anesthetics have been well characterized, changes in mesoscopic and microscopic network dynamics caused by anesthesia are not well understood. Here, we utilized *in vivo* electrophysiological recordings to investigate these alterations as a function of cortical area, cortical layer, and anesthetic depth. We developed this anesthesia model in ferrets, which have a gyrencephalic cortex similar to humans, to increase the translational relevance of this study. In agreement with our hypothesis, we found that anesthesia induced profoundly different modulation of both mesoscopic and microscopic network activity in a primary sensory cortical area (V1) and an association cortical area (PFC). The present study provides a dramatic improvement in spatial resolution of network dynamics compared to previous work using EEG. The use of laminar probes allowed for measurement of modulation by anesthesia with layer specificity. We found that layer IV in V1 was mostly resistant to spectral changes induced by anesthesia, whereas infragranular layers exhibited pronounced modulation of these mesoscopic dynamics. Contrastingly, PFC demonstrated dramatically increased LFP power with anesthesia across cortical layers. Modulation of microscopic dynamics by anesthesia also exhibited specificity by cortical area and layer. MU spiking was preferentially increased in V1 in input layer IV, while spiking in PFC decreased at the most superficial electrodes at lower concentrations of anesthesia. We

also found that layer IV in V1 was spared from increases in SFC induced by anesthesia; in PFC, superficial layers and slow frequencies exhibited increased SFC with deepening anesthesia.

Modulation of Spectral Power

Activity in different frequency bands has been correlated with a broad range of cognitive and behavioral states (X. J. Wang, 2010). The targeted modulation of specific frequency bands by anesthesia likely reflects changes in underlying network dynamics, which may lead to the dramatic behavioral effects caused by anesthesia in animals and humans. We found that the distribution of power across frequency bands in V1 in the awake animal exhibited little change when compared to the data from anesthetized animals. V1 exhibited alterations in spectral power in specific frequency bands. The beta frequency peak in V1 of awake animals, which localized to deeper layers, is in agreement with reports of sub-gamma power in deeper layers of V1 in awake macaque monkeys (Maier, Adams, Aura, & Leopold, 2010). Our results demonstrate that isoflurane anesthesia abolished this beta peak. Given that the beta range has been implicated as a carrier for visual attention (Wrobel, 2000), changes to this rhythm may underlie changes in visual processing as well as altered integration with other brain regions. In contrast, the modulation profile in PFC was characterized by broad increases in power and two-fold changes in the relative presence of different cortical oscillations. A comparison of mesoscopic and microscopic network dynamics in our animal model with previous findings in humans revealed some similar modulatory effects of anesthesia. A frontal shift of EEG power during anesthesia, anteriorization, is commonly observed in animals (Tinker, Sharbrough, & Michenfelder, 1977) and humans (Feshchenko, Veselis, & Reinsel, 2004; Gugino et al., 2001). Previous reports in humans found increases in delta, theta, and alpha power in frontal areas with deepening administration of propofol and sevoflurane (gamma frequencies were not investigated) (Feshchenko et al., 2004; Gugino et al., 2001). Our PFC recordings in anesthetized animals exhibited dramatic increases in power across all frequency bands. Our anesthetized recordings also exhibited a PFC spectral peak in the alpha range as seen in anesthetized humans (Purdon et al., 2013). Additionally, both V1 and PFC showed a shift in power towards lower frequencies with deep anesthesia, in accordance with a long history of human studies (Faulconer, 1952; Gibbs, Gibbs, & Lennox, 1937). Use of high-density EEG in humans anesthetized with propofol has demonstrated increased delta and

alpha activity in frontal electrodes sites (Cimenser et al., 2011). In agreement, our results demonstrate increased total power as well as increased relative power for both of these frequency bands in PFC. Cimenser et al. (2011) also reported decreased alpha and increased delta activity at occipital sites. In our study, we found the same modulation pattern, but only for the deepest anesthesia concentration of 1% isoflurane. More prominently, our data showed a strong suppression of oscillations in the beta band in V1 for all concentrations of anesthesia. Visual attention has been associated with beta band activity; therefore the reduction in beta band power may be correlated with the suppression of attentional processing during anesthesia. The differences in both overall and relative spectral power modulation in V1 and PFC indicate differential effects of anesthesia in these two cortical areas. Moreover, we found that the prominent modulation of the beta band in V1 was mostly localized to deeper cortical layers. This suggests that examination at the spatial resolution of individual layers is necessary to fully understand modulation of network activity.

Modulation According to Distinct Functional Roles across Laminar Structure and Cortical Area

By organizing with respect to laminae, neuronal networks exhibit differential patterns of spontaneous and evoked firing by layer (de Kock, Bruno, Spors, & Sakmann, 2007; Sakata & Harris, 2009; Wallace & Palmer, 2008). It has been unknown if and how anesthesia differentially modulates network activity in V1 and PFC based on laminar structure. Because of the complex feedforward and feedback projections across laminae (Douglas & Martin, 2004), differential modulation of activity across cortical layers by anesthesia could significantly alter processing of sensory information. Intriguingly, our results show that the effects of anesthesia are not consistent across cortical layers. In supragranular layers, SFC increased across frequencies in anesthetized V1. Layer IV in V1 exhibited different modulation compared to supragranular and infragranular layers, with minimal SFC in layer IV during anesthesia. In infragranular layers of V1, SFC increased with anesthesia across all frequencies, with the most prominent effect in the delta frequency range and at fast frequencies. Interestingly, the modulation of SFC by anesthesia in V1 exhibited a different laminar profile compared to the increase in oscillatory power with deepening cortical depth. This indicates that increased SFC was not driven by stronger oscillatory power. The beta spectral peak seen in V1 of awake animals localized to infragranular layers.

With 0.5% and 0.75% isoflurane in V1, the beta peak was not present but a spectral peak in the alpha frequency range appeared in infragranular layers. With 1.0% isoflurane in V1, no mid-frequency spectral peak was evident. In PFC, spectral power increased across all cortical layers with 0.5%, 0.75%, and 1.0% isoflurane. Supragranular layers in PFC exhibited increased SFC at faster frequencies. In layer IV and infragranular layers of PFC in anesthetized animals, a local peak around 10Hz developed (corresponding to the spindle frequencies) and SFC increased at slow frequencies. In PFC, both spectral power and SFC increased in layer IV and infragranular layers at low frequencies. However, increased SFC across frequencies in supragranular layers did not correspond with change in the spectral power.

The primary input to V1 layer IV comes from the lateral geniculate nucleus (LGN) (Hubel & Wiesel, 1972). Anesthesia has been shown to decrease levels of spontaneous activity in the LGN and decrease the firing rates of LGN neurons responding to visual stimuli (Alitto, Moore, Rathbun, & Usrey, 2011). While overall spiking rates in V1 were not significantly altered by anesthesia, layer IV exhibited increased firing with a concomitant decrease in firing rate in other layers during 0.5% and 0.75% isoflurane. This seemingly paradoxical increase of activity with anesthesia has been previously examined by modeling propofol anesthesia, and might be caused by antisynchrony of interneuron activity mediated by the M-current (McCarthy, Brown, & Kopell, 2008). Alterations in the balance of excitatory and inhibitory drive between awake and anesthetized animals (Haider, Hausser, & Carandini, 2012) could underlie the differences observed in cortical network dynamics.

Our results also demonstrate that the laminar effects of anesthesia are specific to cortical area; modulation of firing rate was similar across layers in PFC, with alterations only in the most superficial layers. Activity across electrodes was highly correlated during anesthesia in PFC. Therefore, it appears that modulation of network dynamics varies based on not only cortical layer, but also cortical area. A possible explanation for this specificity stems from differences in the structural and functional architecture of these cortical areas. Layer IV in ferret V1 is highly granulated, whereas granulation of layer IV in PFC is rather poor (Duque & McCormick, 2010), indicating there are variations in the cellular composition. PFC is involved in mediating higher cognitive functions (Fuster, 2008; Jacobsen, 1936), and is critical for top-down feedback to optimize processing of behaviorally relevant sensory information (Buschman & Miller, 2007; Fritz, David, Radtke-Schuller, Yin, & Shamma, 2010; Gregoriou, Gotts, Zhou, & Desimone, 2009).

Necessary for these functions, layer IV in ferret PFC receives many afferents from the mediodorsal nuclei of the thalamus (Duque & McCormick, 2010). Various anesthetics have been shown to decrease thalamic activity (Andrada, Livingston, Lee, & Antognini, 2012) and thalamocortical connectivity (Hudetz, 2012). At first glance, reduced thalamic activity is seemingly at odds with increased MU firing in layer IV of V1. However, layer IV in V1 receives not only feedforward excitation from the thalamus, but also feedforward inhibition (from layer IV inhibitory interneurons driven by the thalamus) (Miller, 2003). Therefore, decreased thalamic activity may reduce feedforward inhibition, resulting in similar MU spiking rates between awake and anesthetized animals. Elucidating whether anesthetics act directly on cortical areas or if alterations in activity are mediated by thalamocortical connectivity is an area of active research (Boly et al., 2012; Kim, Hwang, Kang, Kim, & Choi, 2012). Furthermore, the propagation of cortical activity across layers may differ between sensory processing and spontaneous activity (Sakata & Harris, 2009). Taken together, these results demonstrate that the effects of anesthesia vary by cortical area and cortical layer. Interestingly, the laminar profiles of these effects vary for microscopic spiking activity, mesoscopic spectral power changes, and SFC looking at the coherence between these levels of network activity.

Improvements in Spatial and Temporal Resolution

Work conducted using EEG and functional magnetic resonance imaging (fMRI) has provided valuable insight into macroscopic activity changes induced by anesthesia. However, these recording modalities have inherent limitations in spatial and temporal resolution (Babiloni, Pizzella, Gratta, Ferretti, & Romani, 2009). Furthermore, fMRI is not a direct measure of neural activity, but rather depends on fluctuations in the blood oxygenation level dependent (BOLD) signal (G. G. Brown, Perthen, Liu, & Buxton, 2007) which change with neuronal energy demands. This neurovascular coupling is directly dependent on blood flow and blood volume (Kannurpatti, Biswal, Kim, & Rosen, 2008). Particularly relevant for the current study, anesthesia has been shown to alter blood flow to the brain, thereby disrupting normal neurovascular coupling. Isoflurane is known to induce vasodilation of cerebral arteries in a dose-dependent manner (Flynn, Buljubasic, Bosnjak, & Kampine, 1992) and increase relative blood flow to subcortical regions (Hansen, Warner, Todd, Vust, & Trawick, 1988; Reinstrup et al., 1995). Studies in animals (Disbrow, Slutsky, Roberts, & Krubitzer, 2000) and humans (Antognini, Buonocore, Disbrow, &

Carstens, 1997) have reported decreased BOLD activation with increasing concentrations of anesthetics, including isoflurane. However, these results are difficult to interpret given the unknown contributions of alterations in neurovascular coupling versus true modulation of neural activity. Additionally, evidence suggests that the fMRI activity-electrophysiology relationship varies across cortical areas because of differences in neurovascular coupling, particularly in sensory cortices compared to association cortical areas (Ojemann, Ojemann, & Ramsey, 2013). Even with improvements in neuroimaging acquisition and analysis strategies (Alkire, 2008; He, Yang, Wilke, & Yuan, 2011), these techniques are still indirect measures of neural activity, with limited spatial and temporal resolution. Our electrophysiological recordings provide direct measures of neural activity with excellent spatial and temporal resolution in comparison. Furthermore, our approach does not suffer from potential confounds due to alterations in blood supply to cortical areas.

Comparison of Different Anesthetic Agents

There are a large number of different anesthetic agents, which act through a variety of molecular mechanisms. Isoflurane is an inhalant anesthetic which potentiates GABA acting on $GABA_A$ receptors, exerting effects in cortical and subcortical areas (Harrison, Kugler, Jones, Greenblatt, & Pritchett, 1993). However, the potentiation achieved by isoflurane is typically half that caused by propofol (see below), indicating that isoflurane also acts at other molecular targets (Franks, 2006). These targets may include glycine receptors (Harrison et al., 1993) as well as two-pore-domain potassium channels (Patel et al., 1999). At the mesoscopic network level, the power of spontaneous gamma oscillations have been found to be unchanged by increasing concentrations of isoflurane anesthesia in rats (Hudetz, Vizuete, & Pillay, 2011). Similarly, we found only small total power changes in the gamma frequency band in V1, but more prominent alterations in the power of gamma frequencies relative to total power. At the microscopic network level, administration of isoflurane in rat somatosensory cortex has been shown to reduce spontaneous action potential firing (Hentschke, Schwarz, & Antkowiak, 2005). Xylazine, an agonist for alpha-2 adrenergic receptors which are found widely across cortical layers (Hedler, Stamm, Weitzell, & Starke, 1981; Nicholas, Pieribone, & Hokfelt, 1993), was also used in this study. Activation of alpha-2 adrenoreceptors has been shown to increase cortical activity in prefrontal cortex by acting on the H-

channels (M. Wang et al., 2007). Taken together, these studies may explain why we did not find differences in MU firing rate between awake and anesthetized animals in PFC. $GABA_A$ mediated decrease in firing rate could have been compensated for by increased cortical activity driven by alpha-2 adrenoreceptors in PFC. Previous studies testing the application of alpha-2 adrenergic agonists in rat visual cortex support the role for alpha-2 adrenoreceptors in the modulation of sensory inputs to the visual cortex through increasing single-to-noise ratio in visually-driven cells (when delivered in low concentrations) and decreasing firing rates of visually-driven and non-visually-driven cells (when administered at high concentrations) (Kolta, Diop, & Reader, 1987). It remains to be fully elucidated how the interaction of isoflurane and alpha-2 adrenoreceptors affect spontaneous MU spiking activity in visual cortex. In comparing our findings to other studies using isoflurane anesthesia, it is important to remember that xlyazine was continuously administered to all anesthetized animals. This contributed to an anesthetic drug-sparing effect, in which lower concentrations of isoflurane were required to maintain complete sedation (Doherty et al., 2007; Soares, Ascoli, Gremiao, Gomez de Segura, & Marsico Filho, 2004). Therefore, anesthesia at 0.5%, 0.75%, and 1.0% isoflurane in this study corresponded to lack of behavioral responses, induced UP and DOWN states, but did not lead to burst suppression. Burst suppression activity is characterized by periods of high-voltage activity which are interspersed quasi-periodically with long (10-20 second) periods of isoelectric activity; importantly, burst suppression activity is not rhythmic (Ching, Purdon, Vijayan, Kopell, & Brown, 2012). The anesthetic paradigm used in this study did not induce burst suppression because DOWN states remained relatively short (1-1.5 seconds at the longest) and alternated rhythmically with UP states. However, it should be noted that there is no firmly agreed upon delineation between UP and DOWN state activity and burst suppression.

Propofol is another commonly used anesthetic delivered intravenously which acts primarily at $GABA_A$ receptors to potentiate inhibitory current flow. The specific subunit composition of the $GABA_A$ receptor appears to modulate the effect of propofol (Franks, 2006). Cats anesthetized with propofol exhibit a spectral peak around 12Hz, and decreased spontaneous single-unit firing of occipital cortical neurons (Andrada et al., 2012). Loss of consciousness (LOC) induced by propofol in humans is marked by frontal alpha oscillations as measured by EEG (Purdon et al., 2013). Our results show a similar spectral peak in the alpha band in PFC, despite using different anesthetics.

Theories of Cortical Disintegration and Reduced Encoding Capacity

There are two related leading postulates of the mechanism underlying behavioral alternations during anesthesia. The first is characterized by disruption of cortical integration (Alkire et al., 2008; Hudetz, 2006). Anesthetics may disrupt cortical integration by acting on structures that facilitate long-range corticocortical interactions (Mashour, 2004). Sensory neuronal processing may still occur, either in a form identical to or altered from the awake state (Plourde et al., 2006), but conscious sensation is abolished because of impaired transmission or an inability of other brain regions to receive or interpret the information. The thalamus is likely involved in this information processing pathway; isoflurane has been shown to attenuate the output of somatosensory signals from an area of the rat thalamus, while its input is only marginally affected (Detsch, Vahle-Hinz, Kochs, Siemers, & Bromm, 1999). Comparison of connectivity as measured by fMRI in awake marmoset and during propofol anesthesia has shown that propofol decreases thalamocortical connectivity (Liu, Lauer, Ward, Li, & Hudetz, 2013). Humans anesthetized with sevoflurane show a dose-dependent reduction of synchronized neural activity during resting state (temporally correlated slow-fluctuations between functionally related areas) as determined by fMRI scans and connectivity maps calculated from seed regions in motor areas (Peltier et al., 2005). LOC induced by propofol anesthesia in humans has been associated with the functional isolation of cortical regions but the preservation of connectivity within local networks as measured by ECoG and implanted temporal cortex microelectrode arrays (Cimenser et al., 2011; Lewis et al., 2012; McCarthy et al., 2012). Although not the same as anesthesia, sleep exhibits many similar behavioral effects, namely the loss of consciousness. Indeed, lack of consciousness during sleep has been related to a breakdown in effective cortical connectivity, or the ability of a set of neuronal groups to causally affect the firing of other neuronal groups (Massimini, Boly, Casali, Rosanova, & Tononi, 2009; Massimini et al., 2005). Our results contribute to this postulated mechanism of anesthesia by providing evidence of profoundly different effects of anesthesia on a primary sensory area and an association cortical area. V1 exhibited minimal alterations in spectral power compared to PFC, which displayed massive differences in anesthetized spectra relative to the awake animal.

In the second proposed mechanism of anesthesia, a disruption in the repertoire of cortical activity patterns reduces the brain's ability to encode information (Alkire et al., 2008). Our correlation results

support this hypothesis. Correlation of activity across electrodes was much higher with anesthesia in PFC, but reduced in V1. The ability to maintain sensory responses during anesthesia may be linked with less correlated activity across cortical layers in this primary sensory area. In contrast, increased correlation across cortical layers in PFC may be related to the corresponding lack of consciousness or higher-order cognitive functions.

The focus of the present study was on elucidating the cortical area and layer-specific effects of anesthesia when comparing steady state brain dynamics in awake and anesthetized animals. We chose to look at spontaneous cortical dynamics because of the emerging functional role of spontaneous activity in cortex (Berkes, Orban, Lengyel, & Fiser, 2011; Fox & Raichle, 2007; Han, Caporale, & Dan, 2008). Together with recent studies on the loss of consciousness induced by anesthesia (Alkire, Haier, & Fallon, 2000; Massimini, Ferrarelli, Sarasso, & Tononi, 2012; Purdon et al., 2013), the insights into the effects of anesthesia on mesoscopic and microscopic network dynamics with high resolution provide an emerging picture of anesthesia as a complex and sophisticated modulator of cortical network activity. The results here provide a starting point for developing computational models to further understand the complex interaction between mesoscopic and microscopic network activity. The present work clearly demonstrates that such models should incorporate laminar profiles of activity and be tailored to specific cortical areas to accurately represent the functioning of cortical networks.

FIGURES AND TABLES

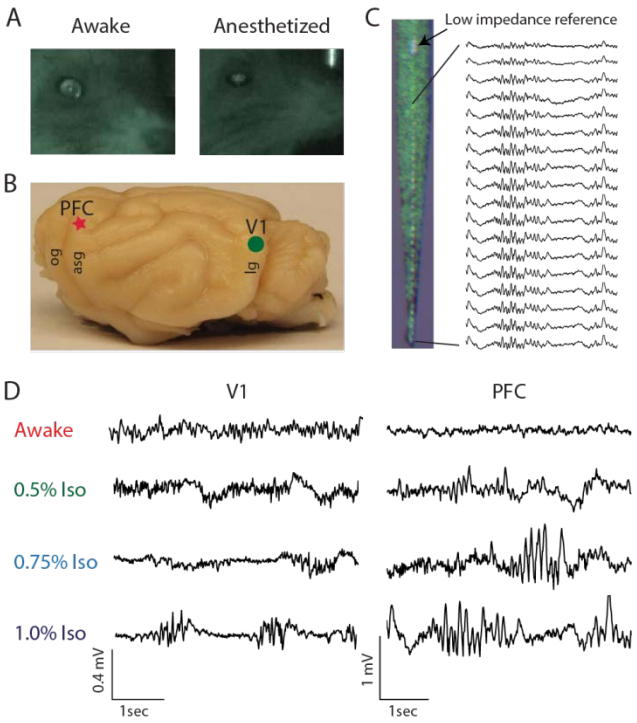

Figure 4.1. Extracellular local field potential (LFP) recordings were conducted in ferret primary visual cortex (V1) and prefrontal cortex (PFC) to study the effects of anesthesia on spontaneous network activity.

(A) Infrared images of an awake (left) and anesthetized (right) ferret show eyes were open in both cases during electrophysiological recordings.

(B) Recording probe locations in the left hemisphere of ferret cortex. PFC: anterior sigmoid gyrus (2mm from midline) posterior to presylvian sulcus. V1: lateral gyrus (9 mm from midline, central vision).

(C) Linear probes with 16- and 32-channels were used to simultaneously record from all cortical layers. In 32-channel probes (pictured here), the low-impedance reference was 0.5mm above the most superficial electrode site.

(D) LFP traces from V1 (left) and PFC (right) of awake and anesthetized (0.5%, 0.75%, and 1.0% isoflurane) animals. LFP structure in V1 was altered by anesthesia, and LFP amplitude and rhythmicity were strongly increased by anesthesia in PFC. Note different scales for V1 and PFC.

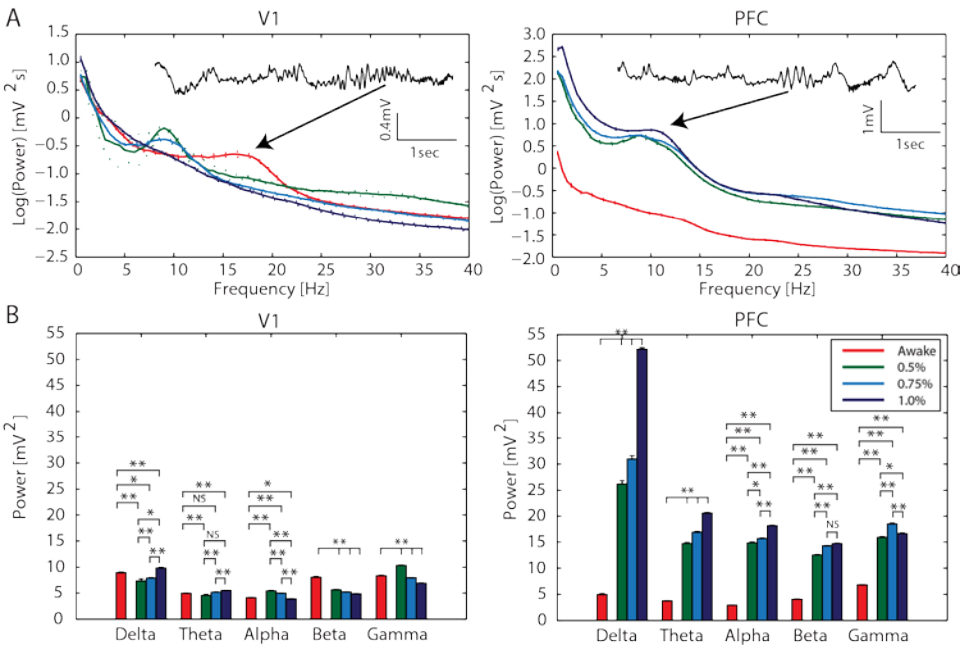

Figure 4.2. Anesthesia modulated LFP in a frequency-specific manner in V1 but induced broadband enhancement of LFP power in PFC.

(A) Left: Time-averaged LFP spectra (0.5 – 40Hz) in V1 demonstrate modulation of power as a function of anesthesia (LFP trace inset: ~18 Hz activity in the awake animal). The spectral peak was at lower frequencies for anesthesia concentrations of 0.5% and 0.75% isoflurane and was abolished by 1.0% isoflurane anesthesia. Right: Dramatic increase in LFP spectral power by anesthesia in PFC. Anesthesia induced a spectral peak in the spindle frequency, ~10Hz (LFP trace inset: 1.0% isoflurane). Dotted lines indicate ± 2 std calculated by bootstrap.

(B) Total power in each frequency band. Left: Anesthesia modulated power specific to each frequency band in V1. Right: In PFC, anesthesia mediated broadband power increase, with the most prominent effect in the delta range. Error bars indicate 1 SEM. ** indicates that power in frequency bands was significantly different across awake and anesthetized animals at $p<0.001$; * indicates that power in frequency bands was significantly different at $p<0.05$

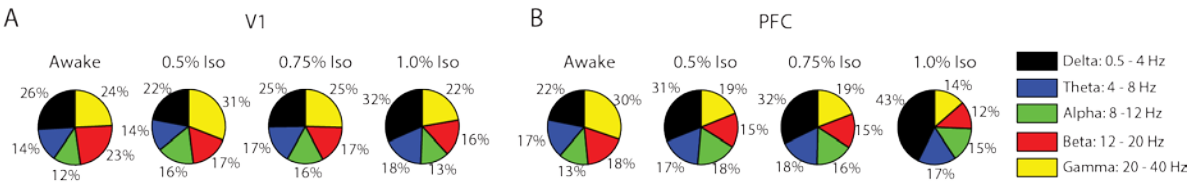

Figure 4.3. Distribution of oscillatory power across frequency bands was differentially affected by depth of anesthesia in V1 and PFC.

(A) Power in each frequency band as a percent of total power. Distribution of power across frequency bands in V1 was mostly resistant to change by anesthesia. The modest differences between awake and anesthetized animals varied by frequency band and exhibited no apparent monotonic relationship.

(B) In PFC, distribution of spectral power shifted from gamma (yellow) to delta (black) frequency bands with increasing depth of anesthesia.

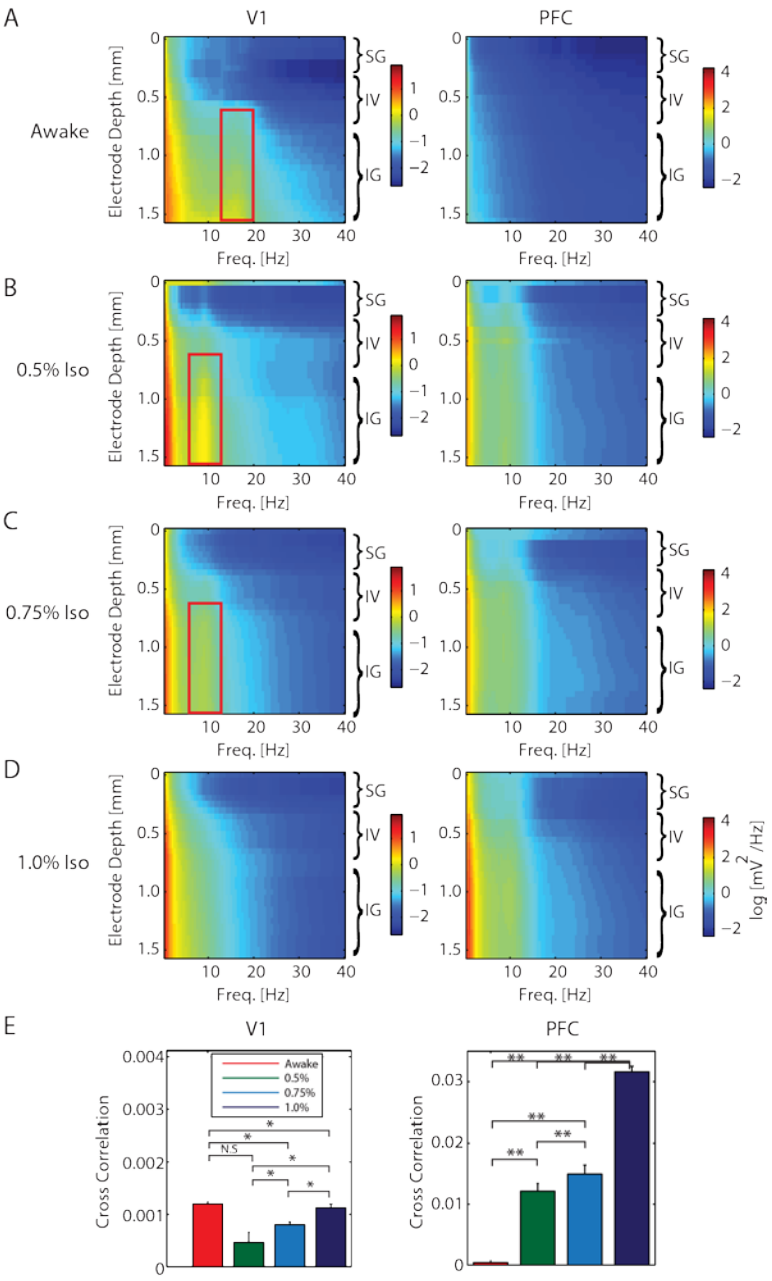

Figure 4.4. Activity across cortical layers maintained independence with anesthesia in V1 but became strongly correlated in PFC.

(A) Left: In V1 of awake animals, oscillatory power was stronger at deeper cortical layers. Red box highlights the infragranular localization of the ~18Hz oscillatory peak found exclusively in the awake animal. Right: Activity in PFC of the awake animal did not exhibit any intermediate frequency spectral peak. Note different color scales for V1 and PFC. SG = supragranular layers, IV = layer IV, IG = infragranular layers.

(B) Left: In V1 of animals anesthetized with 0.5% isoflurane, the intermediate frequency peak appeared at a lower frequency (~10Hz) as highlighted by the red box. This oscillation was localized in infragranular layers. Right: 0.5% isoflurane increased oscillatory power across layers in PFC relative to the awake animal.

(C) Left: In V1 of animals anesthetized with 0.75% isoflurane, the intermediate frequency peak (red box) appeared at ~10Hz. This oscillation was localized in infragranular layers. Right: Compared to awake animals, 0.75% isoflurane increased oscillatory power across layers in PFC.

(D) Left: 1.0% isoflurane abolished the intermediate frequency peak in V1. Right: In PFC, 1.0% isoflurane increased spectral power across cortical layers compared to power in awake animals. An increase in low frequency power is evident relative to corresponding power in animals anesthetized with 0.5% and 0.75% isoflurane.

(E) Correlation of activity across cortical layers was much higher in PFC. Left: In V1, anesthesia decreased the cross-correlation of LFP activity across cortical layers. Right: Increasing concentrations of anesthesia increased cross-correlation of LFP activity across cortical layers in PFC. Error bars indicate 1 SEM. ** indicates Kruskal-Wallis test between anesthesia concentrations significant at $p<0.001$. * indicates Kruskal-Wallis test between anesthesia concentrations significant at $p<0.05$. Note different scales for V1 and PFC.

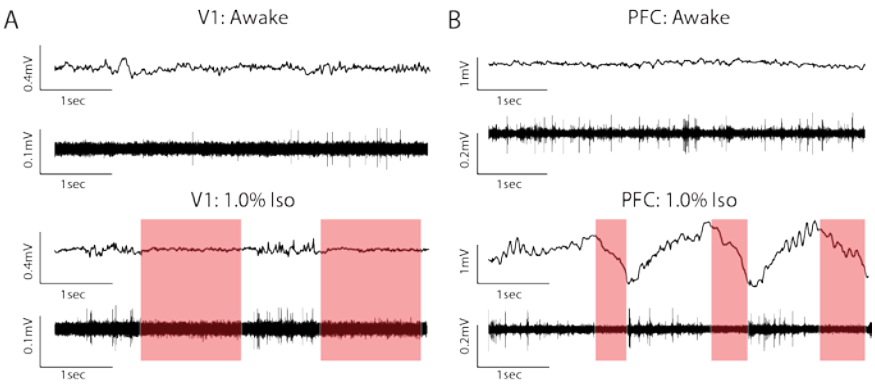

Figure 4.5. Paired LFP and MU spiking traces.

(A) Matching LFP and high-pass filtered traces of MU spiking activity from representative trials for V1. In the anesthetized animal (bottom), MU firing became more rhythmic and correlated with structure of the LFP. Red shaded boxes indicate DOWN states.

(B) Same representation as in (a) for PFC. Anesthesia strongly increased rhythmic structure of the LFP and coordinated MU firing. Red shaded boxes indicate DOWN states. Note different scales for V1 and PFC.

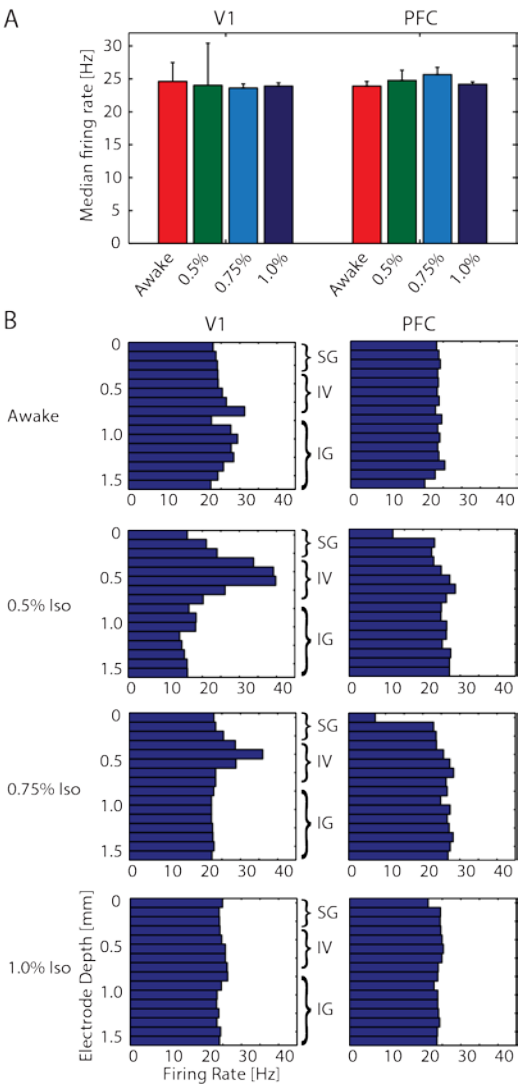

Figure 4.6. Anesthesia altered MU firing rate and spiking across cortical layers differently in V1 and PFC.

(A) Median spontaneous MU firing rates exhibited non-significant difference with anesthesia in V1 and PFC. Error bars indicate 1 SEM. Kruskal-Wallis tests between anesthesia concentrations within each cortical area were non-significant at p=0.05.

(B) MU firing as a function of cortical depth. Left: In V1, intermediate concentrations of anesthesia (0.5% and 0.75% isoflurane) increased MU firing specifically in layer IV with concomitant decreases in spiking rate in supragranular and infragranular layers. Right: MU firing rates

decreased with 0.5% and 0.75% isoflurane exclusively in supragranular layers. 1.0% isoflurane did not exhibit alteration to spiking across cortical layers in PFC. SG = supragranular layers, IV = layer IV, IG = infragranular layers.

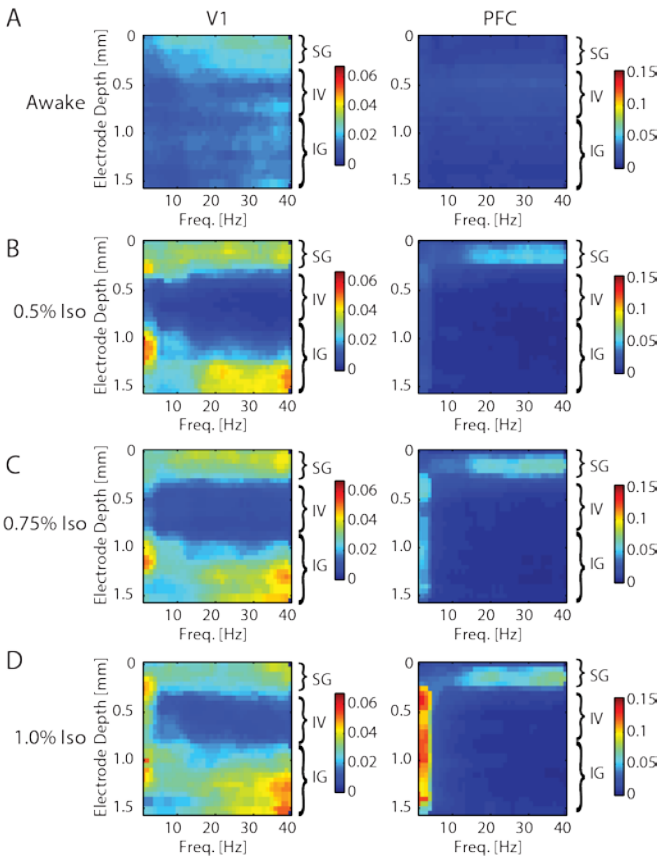

Figure 4.7. Anesthesia induced frequency-, layer-, and cortical area-specific increases in spike-field coherence (SFC).

(A) SFC was minimal in awake recordings in both V1 (left) and PFC (right). Note different color scales for V1 and PFC. SG = supragranular layers, IV = layer IV, IG = infragranular layers.

(B) SFC increased with 0.5% isoflurane. V1 (left) exhibited increased SFC in supragranular and infragranular layers. Input layer IV was resistant to increased SFC induced by anesthesia. PFC (right) exhibited increased SFC primarily in supragranular layers at faster frequencies.

(C) With 0.75% isoflurane, SFC increased in V1 (left) in supragranular and infragranular layers, while PFC (right) exhibited increased SFC at supragranular layers and across layers at slow frequencies.

(D) SFC was strongest with 1.0% isoflurane. SFC was strongest in V1 (left) with 1.0% isoflurane; layer IV remained resistant to increased SFC induced by anesthesia. In PFC (right), 1.0% isoflurane induced strong SFC at slow frequencies across layers and at supragranular layers.

	Delta	Theta	Alpha	Beta	Gamma
Awake	8.93 ± 0.127	4.99 ± 0.083	4.14 ± 0.061	8.06 ± 0.138	8.38 ± 0.082
0.5% Iso	7.35 ± 0.446	4.60 ± 0.164	5.44 ± 0.0801	5.66 ± 0.068	10.33 ± 0.080
0.75% Iso	7.89 ± 0.148	5.20 ± 0.063	5.00 ± 0.052	5.22 ± 0.039	7.97 ± 0.055
1.0% Iso	9.82 ± 0.149	5.52 ± 0.069	3.91 ± 0.055	4.90 ± 0.044	6.92 ± 0.076

Total power [mV^2] ± sem

Table 4.1. Total spectral power by frequency band in V1

	Delta	Theta	Alpha	Beta	Gamma
Awake	4.94 ± 0.235	3.77 ± 0.052	2.94 ± 0.027	4.08 ± 0.027	6.82 ± 0.033
0.5% Iso	26.19 ± 0.664	14.76 ± 0.197	14.91 ± 0.146	12.56 ± 0.123	15.95 ± 0.190
0.75% Iso	31.01 ± 0.629	16.93 ± 0.167	15.72 ± 0.120	14.31 ± 0.095	18.53 ± 0.167
1.0% Iso	52.19 ± 0.315	20.59 ± 0.123	18.19 ± 0.111	14.77 ± 0.084	16.68 ± 0.138

Total power [mV^2] ± sem

Table 4.2. Total spectral power by frequency band in PFC

REFERENCES

Alitto, H. J., Moore, B. D. t., Rathbun, D. L., & Usrey, W. M. (2011). A comparison of visual responses in the lateral geniculate nucleus of alert and anaesthetized macaque monkeys. *J Physiol, 589*(Pt 1), 87-99. doi: 10.1113/jphysiol.2010.190538

Alkire, M. T. (2008). Loss of effective connectivity during general anesthesia. *International anesthesiology clinics, 46*(3), 55-73. doi: 10.1097/AIA.0b013e3181755dc6

Alkire, M. T., Haier, R. J., & Fallon, J. H. (2000). Toward a unified theory of narcosis: brain imaging evidence for a thalamocortical switch as the neurophysiologic basis of anesthetic-induced unconsciousness. *Consciousness and Cognition, 9*(3), 370-386. doi: 10.1006/ccog.1999.0423

Alkire, M. T., Hudetz, A. G., & Tononi, G. (2008). Consciousness and anesthesia. *Science, 322*(5903), 876-880. doi: 10.1126/science.1149213

Andrada, J., Livingston, P., Lee, B. J., & Antognini, J. (2012). Propofol and etomidate depress cortical, thalamic, and reticular formation neurons during anesthetic-induced unconsciousness. *Anesth Analg, 114*(3), 661-669. doi: 10.1213/ANE.0b013e3182405228

Antognini, J. F., Buonocore, M. H., Disbrow, E. A., & Carstens, E. (1997). Isoflurane anesthesia blunts cerebral responses to noxious and innocuous stimuli: a fMRI study. *Life sciences, 61*(24), PL 349-354.

Babiloni, C., Pizzella, V., Gratta, C. D., Ferretti, A., & Romani, G. L. (2009). Fundamentals of electroencefalography, magnetoencefalography, and functional magnetic resonance imaging. *International review of neurobiology, 86*, 67-80. doi: 10.1016/S0074-7742(09)86005-4

Berkes, P., Orban, G., Lengyel, M., & Fiser, J. (2011). Spontaneous cortical activity reveals hallmarks of an optimal internal model of the environment. *Science, 331*(6013), 83-87. doi: 10.1126/science.1195870

Boly, M., Moran, R., Murphy, M., Boveroux, P., Bruno, M. A., Noirhomme, Q., . . . Friston, K. (2012). Connectivity changes underlying spectral EEG changes during propofol-induced loss of consciousness. *J Neurosci, 32*(20), 7082-7090. doi: 10.1523/JNEUROSCI.3769-11.2012

Bonhomme, V., Boveroux, P., Brichant, J. F., Laureys, S., & Boly, M. (2012). Neural correlates of consciousness during general anesthesia using functional magnetic resonance imaging (fMRI). *Archives italiennes de biologie, 150*(2-3), 155-163. doi: 10.4449/aib.v150i2.1242

Boveroux, P., Vanhaudenhuyse, A., Bruno, M. A., Noirhomme, Q., Lauwick, S., Luxen, A., . . . Boly, M. (2010). Breakdown of within- and between-network resting state functional magnetic resonance imaging connectivity during propofol-induced loss of consciousness. *Anesthesiology, 113*(5), 1038-1053. doi: 10.1097/ALN.0b013e3181f697f5

Brown, E. N., Purdon, P. L., & Van Dort, C. J. (2011). General anesthesia and altered states of arousal: a systems neuroscience analysis. *Annu Rev Neurosci, 34*, 601-628. doi: 10.1146/annurev-neuro-060909-153200

Brown, G. G., Perthen, J. E., Liu, T. T., & Buxton, R. B. (2007). A primer on functional magnetic resonance imaging. *Neuropsychology review, 17*(2), 107-125. doi: 10.1007/s11065-007-9028-8

Buschman, T. J., & Miller, E. K. (2007). Top-down versus bottom-up control of attention in the prefrontal and posterior parietal cortices. *Science, 315*(5820), 1860-1862. doi: 10.1126/science.1138071

Ching, S., Cimenser, A., Purdon, P. L., Brown, E. N., & Kopell, N. J. (2010). Thalamocortical model for a propofol-induced alpha-rhythm associated with loss of consciousness. *Proceedings of the National Academy of Sciences of the United States of America, 107*(52), 22665-22670. doi: 10.1073/pnas.1017069108

Ching, S., Purdon, P. L., Vijayan, S., Kopell, N. J., & Brown, E. N. (2012). A neurophysiological-metabolic model for burst suppression. *Proc Natl Acad Sci U S A, 109*(8), 3095-3100. doi: 10.1073/pnas.1121461109

Cimenser, A., Purdon, P. L., Pierce, E. T., Walsh, J. L., Salazar-Gomez, A. F., Harrell, P. G., . . . Brown, E. N. (2011). Tracking brain states under general anesthesia by using global coherence analysis. *Proc Natl Acad Sci U S A, 108*(21), 8832-8837. doi: 10.1073/pnas.1017041108

de Kock, C. P., Bruno, R. M., Spors, H., & Sakmann, B. (2007). Layer- and cell-type-specific suprathreshold stimulus representation in rat primary somatosensory cortex. *J Physiol, 581*(Pt 1), 139-154. doi: 10.1113/jphysiol.2006.124321

Detsch, O., Vahle-Hinz, C., Kochs, E., Siemers, M., & Bromm, B. (1999). Isoflurane induces dose-dependent changes of thalamic somatosensory information transfer. *Brain Res, 829*(1-2), 77-89.

Disbrow, E. A., Slutsky, D. A., Roberts, T. P., & Krubitzer, L. A. (2000). Functional MRI at 1.5 tesla: a comparison of the blood oxygenation level-dependent signal and electrophysiology. *Proc Natl Acad Sci U S A, 97*(17), 9718-9723. doi: 10.1073/pnas.170205497

Doherty, T., Redua, M. A., Queiroz-Castro, P., Egger, C., Cox, S. K., & Rohrbach, B. W. (2007). Effect of intravenous lidocaine and ketamine on the minimum alveolar concentration of isoflurane in goats. *Vet Anaesth Analg, 34*(2), 125-131. doi: 10.1111/j.1467-2995.2006.00301.x

Douglas, R. J., & Martin, K. A. (2004). Neuronal circuits of the neocortex. *Annu Rev Neurosci, 27*, 419-451. doi: 10.1146/annurev.neuro.27.070203.144152

Duque, A., & McCormick, D. A. (2010). Circuit-based localization of ferret prefrontal cortex. *Cereb Cortex, 20*(5), 1020-1036. doi: 10.1093/cercor/bhp164

Faulconer, A., Jr. (1952). Correlation of concentrations of ether in arterial blood with electro-encephalographic patterns occurring during ether-oxygen and during nitrous oxide, oxygen and ether anesthesia of human surgical patients. *Anesthesiology, 13*(4), 361-369.

Feshchenko, V. A., Veselis, R. A., & Reinsel, R. A. (2004). Propofol-induced alpha rhythm. *Neuropsychobiology, 50*(3), 257-266. doi: 10.1159/000079981

Flynn, N. M., Buljubasic, N., Bosnjak, Z. J., & Kampine, J. P. (1992). Isoflurane produces endothelium-independent relaxation in canine middle cerebral arteries. *Anesthesiology, 76*(3), 461-467.

Fox, M. D., & Raichle, M. E. (2007). Spontaneous fluctuations in brain activity observed with functional magnetic resonance imaging. *Nat Rev Neurosci, 8*(9), 700-711. doi: 10.1038/nrn2201

Franks, N. P. (2006). Molecular targets underlying general anaesthesia. *Br J Pharmacol, 147 Suppl 1*, S72-81. doi: 10.1038/sj.bjp.0706441

Friedman, E. B., Sun, Y., Moore, J. T., Hung, H. T., Meng, Q. C., Perera, P., . . . Kelz, M. B. (2010). A conserved behavioral state barrier impedes transitions between anesthetic-induced unconsciousness and wakefulness: evidence for neural inertia. *PLoS One, 5*(7), e11903. doi: 10.1371/journal.pone.0011903

Fries, P. (2009). Neuronal gamma-band synchronization as a fundamental process in cortical computation. *Annual review of neuroscience, 32*, 209-224. doi: 10.1146/annurev.neuro.051508.135603

Fritz, J. B., David, S. V., Radtke-Schuller, S., Yin, P., & Shamma, S. A. (2010). Adaptive, behaviorally gated, persistent encoding of task-relevant auditory information in ferret frontal cortex. *Nat Neurosci, 13*(8), 1011-1019. doi: 10.1038/nn.2598

Fuster, J. M. (2008). *The Prefrontal Cortex* (4th ed.). San Diego: Elsevier Ltd.

Gibbs, F. A., Gibbs, E. L., & Lennox, W. G. (1937). Effect on the electro-encephalogram of certain drugs which influence nervous activity. *Archives of Internal Medicine, 60*(1), 154-166.

Goupillaud, P., Grossmann, A., & Morlet, J. (1984). Cycle-Octave and Related Transforms in Seismic Signal Analysis. *Geoexploration, 23*(1), 85-102. doi: Doi 10.1016/0016-7142(84)90025-5

Gregoriou, G. G., Gotts, S. J., Zhou, H., & Desimone, R. (2009). High-frequency, long-range coupling between prefrontal and visual cortex during attention. *Science, 324*(5931), 1207-1210. doi: 10.1126/science.1171402

Gugino, L. D., Chabot, R. J., Prichep, L. S., John, E. R., Formanek, V., & Aglio, L. S. (2001). Quantitative EEG changes associated with loss and return of consciousness in healthy adult volunteers anaesthetized with propofol or sevoflurane. *British journal of anaesthesia, 87*(3), 421-428.

Haider, B., Hausser, M., & Carandini, M. (2012). Inhibition dominates sensory responses in the awake cortex. *Nature*. doi: 10.1038/nature11665

Han, F., Caporale, N., & Dan, Y. (2008). Reverberation of recent visual experience in spontaneous cortical waves. *Neuron, 60*(2), 321-327. doi: 10.1016/j.neuron.2008.08.026

Hansen, T. D., Warner, D. S., Todd, M. M., Vust, L. J., & Trawick, D. C. (1988). Distribution of cerebral blood flow during halothane versus isoflurane anesthesia in rats. *Anesthesiology, 69*(3), 332-337.

Harrison, N. L., Kugler, J. L., Jones, M. V., Greenblatt, E. P., & Pritchett, D. B. (1993). Positive modulation of human gamma-aminobutyric acid type A and glycine receptors by the inhalation anesthetic isoflurane. *Mol Pharmacol, 44*(3), 628-632.

He, B., Yang, L., Wilke, C., & Yuan, H. (2011). Electrophysiological imaging of brain activity and connectivity-challenges and opportunities. *IEEE transactions on bio-medical engineering, 58*(7), 1918-1931. doi: 10.1109/TBME.2011.2139210

Hedler, L., Stamm, G., Weitzell, R., & Starke, K. (1981). Functional characterization of central alpha-adrenoceptors by yohimbine diastereomers. *Eur J Pharmacol, 70*(1), 43-52.

Heinke, W., & Koelsch, S. (2005). The effects of anesthetics on brain activity and cognitive function. *Current opinion in anaesthesiology, 18*(6), 625-631. doi: 10.1097/01.aco.0000189879.67092.12

Heinke, W., & Schwarzbauer, C. (2001). Subanesthetic isoflurane affects task-induced brain activation in a highly specific manner: a functional magnetic resonance imaging study. *Anesthesiology, 94*(6), 973-981.

Hentschke, H., Schwarz, C., & Antkowiak, B. (2005). Neocortex is the major target of sedative concentrations of volatile anaesthetics: strong depression of firing rates and increase of GABAA receptor-mediated inhibition. *Eur J Neurosci, 21*(1), 93-102.

Hubel, D. H., & Wiesel, T. N. (1972). Laminar and columnar distribution of geniculo-cortical fibers in the macaque monkey. *The Journal of comparative neurology, 146*(4), 421-450. doi: 10.1002/cne.901460402

Hudetz, A. G. (2006). Suppressing consciousness: Mechanisms of general anesthesia. *Seminars in Anesthsia, Perioperative Medicine and Pain, 25*, 196-204.

Hudetz, A. G. (2012). General anesthesia and human brain connectivity. *Brain connectivity, 2*(6), 291-302. doi: 10.1089/brain.2012.0107

Hudetz, A. G., Vizuete, J. A., & Pillay, S. (2011). Differential effects of isoflurane on high-frequency and low-frequency gamma oscillations in the cerebral cortex and hippocampus in freely moving rats. *Anesthesiology, 114*(3), 588-595. doi: 10.1097/ALN.0b013e31820ad3f9

Imas, O. A., Ropella, K. M., Ward, B. D., Wood, J. D., & Hudetz, A. G. (2005). Volatile anesthetics disrupt frontal-posterior recurrent information transfer at gamma frequencies in rat. *Neuroscience letters, 387*(3), 145-150. doi: 10.1016/j.neulet.2005.06.018

Imas, O. A., Ropella, K. M., Wood, J. D., & Hudetz, A. G. (2006). Isoflurane disrupts anterio-posterior phase synchronization of flash-induced field potentials in the rat. *Neurosci Lett, 402*(3), 216-221.

Jacobsen, C. F. (1936). Studies of Cerebral Function in Primates: I. Functions of Frontal Association Area in Primates. *Comparative Psychology Monographs, 13*, 3-60.

John, E. R., & Prichep, L. S. (2005). The anesthetic cascade: a theory of how anesthesia suppresses consciousness. *Anesthesiology, 102*(2), 447-471.

Kannurpatti, S. S., Biswal, B. B., Kim, Y. R., & Rosen, B. R. (2008). Spatio-temporal characteristics of low-frequency BOLD signal fluctuations in isoflurane-anesthetized rat brain. *Neuroimage, 40*(4), 1738-1747. doi: 10.1016/j.neuroimage.2007.05.061

Kim, S. P., Hwang, E., Kang, J. H., Kim, S., & Choi, J. H. (2012). Changes in the thalamocortical connectivity during anesthesia-induced transitions in consciousness. *Neuroreport, 23*(5), 294-298. doi: 10.1097/WNR.0b013e3283509ba0

Kohn, D. F. (1997). *Anesthesia and analgesia in laboratory animals*. San Diego: Academic Press.

Kolta, A., Diop, L., & Reader, T. A. (1987). Noradrenergic effects on rat visual cortex: single-cell microiontophoretic studies of alpha-2 adrenergic receptors. *Life Sci, 41*(3), 281-289.

Lewis, L. D., Weiner, V. S., Mukamel, E. A., Donoghue, J. A., Eskandar, E. N., Madsen, J. R., . . . Purdon, P. L. (2012). Rapid fragmentation of neuronal networks at the onset of propofol-induced unconsciousness. *Proc Natl Acad Sci U S A, 109*(49), E3377-3386. doi: 10.1073/pnas.1210907109

Liu, J. V., Hirano, Y., Nascimento, G. C., Stefanovic, B., Leopold, D. A., & Silva, A. C. (2013). fMRI in the awake marmoset: Somatosensory-evoked responses, functional connectivity, and comparison with propofol anesthesia. *Neuroimage, 78C*, 186-195. doi: 10.1016/j.neuroimage.2013.03.038

Liu, X., Lauer, K. K., Ward, B. D., Li, S. J., & Hudetz, A. G. (2013). Differential effects of deep sedation with propofol on the specific and nonspecific thalamocortical systems: a functional magnetic resonance imaging study. *Anesthesiology, 118*(1), 59-69. doi: 10.1097/ALN.0b013e318277a801

Logothetis, N. K., & Wandell, B. A. (2004). Interpreting the BOLD signal. *Annual review of physiology, 66*, 735-769. doi: 10.1146/annurev.physiol.66.082602.092845

Magri, C., Schridde, U., Murayama, Y., Panzeri, S., & Logothetis, N. K. (2012). The amplitude and timing of the BOLD signal reflects the relationship between local field potential power at different frequencies. *J Neurosci, 32*(4), 1395-1407. doi: 10.1523/JNEUROSCI.3985-11.2012

Maier, A., Adams, G. K., Aura, C., & Leopold, D. A. (2010). Distinct superficial and deep laminar domains of activity in the visual cortex during rest and stimulation. *Front Syst Neurosci, 4*. doi: 10.3389/fnsys.2010.00031

Mashour, G. A. (2004). Consciousness unbound: toward a paradigm of general anesthesia. *Anesthesiology, 100*(2), 428-433.

Massimini, M., Boly, M., Casali, A., Rosanova, M., & Tononi, G. (2009). A perturbational approach for evaluating the brain's capacity for consciousness. *Prog Brain Res, 177*, 201-214. doi: 10.1016/S0079-6123(09)17714-2

Massimini, M., Ferrarelli, F., Huber, R., Esser, S. K., Singh, H., & Tononi, G. (2005). Breakdown of cortical effective connectivity during sleep. *Science, 309*(5744), 2228-2232. doi: 10.1126/science.1117256

Massimini, M., Ferrarelli, F., Sarasso, S., & Tononi, G. (2012). Cortical mechanisms of loss of consciousness: insight from TMS/EEG studies. *Archives italiennes de biologie, 150*(2-3), 44-55. doi: 10.4449/aib.v150i2.1361

McCarthy, M. M., Brown, E. N., & Kopell, N. (2008). Potential network mechanisms mediating electroencephalographic beta rhythm changes during propofol-induced paradoxical excitation. *J Neurosci, 28*(50), 13488-13504. doi: 10.1523/JNEUROSCI.3536-08.2008

McCarthy, M. M., Ching, S., Whittington, M. A., & Kopell, N. (2012). Dynamical changes in neurological diseases and anesthesia. *Curr Opin Neurobiol, 22*(4), 693-703. doi: 10.1016/j.conb.2012.02.009

Miller, K. D. (2003). Understanding layer 4 of the cortical circuit: a model based on cat V1. *Cereb Cortex, 13*(1), 73-82.

Nicholas, A. P., Pieribone, V., & Hokfelt, T. (1993). Distributions of mRNAs for alpha-2 adrenergic receptor subtypes in rat brain: an in situ hybridization study. *J Comp Neurol, 328*(4), 575-594. doi: 10.1002/cne.903280409

Ojemann, G. A., Ojemann, J., & Ramsey, N. F. (2013). Relation between functional magnetic resonance imaging (fMRI) and single neuron, local field potential (LFP) and electrocorticography (ECoG) activity in human cortex. *Front Hum Neurosci, 7*, 34. doi: 10.3389/fnhum.2013.00034

Patel, A. J., Honore, E., Lesage, F., Fink, M., Romey, G., & Lazdunski, M. (1999). Inhalational anesthetics activate two-pore-domain background K+ channels. *Nat Neurosci, 2*(5), 422-426. doi: 10.1038/8084

Peltier, S. J., Kerssens, C., Hamann, S. B., Sebel, P. S., Byas-Smith, M., & Hu, X. (2005). Functional connectivity changes with concentration of sevoflurane anesthesia. *Neuroreport, 16*(3), 285-288.

Plourde, G., Belin, P., Chartrand, D., Fiset, P., Backman, S. B., Xie, G., & Zatorre, R. J. (2006). Cortical processing of complex auditory stimuli during alterations of consciousness with the general anesthetic propofol. *Anesthesiology, 104*(3), 448-457.

Purdon, P. L., Pierce, E. T., Mukamel, E. A., Prerau, M. J., Walsh, J. L., Wong, K. F., . . . Brown, E. N. (2013). Electroencephalogram signatures of loss and recovery of consciousness from propofol. *Proc Natl Acad Sci U S A, 110*(12), E1142-1151. doi: 10.1073/pnas.1221180110

Reinstrup, P., Ryding, E., Algotsson, L., Messeter, K., Asgeirsson, B., & Uski, T. (1995). Distribution of cerebral blood flow during anesthesia with isoflurane or halothane in humans. *Anesthesiology, 82*(2), 359-366.

Sakata, S., & Harris, K. D. (2009). Laminar structure of spontaneous and sensory-evoked population activity in auditory cortex. *Neuron, 64*(3), 404-418. doi: 10.1016/j.neuron.2009.09.020

Soares, J. H., Ascoli, F. O., Gremiao, I. D., Gomez de Segura, I. A., & Marsico Filho, F. (2004). Isoflurane sparing action of epidurally administered xylazine hydrochloride in anesthetized dogs. *Am J Vet Res, 65*(6), 854-859.

Steriade, M., Dossi, R. C., Pare, D., & Oakson, G. (1991). Fast oscillations (20-40 Hz) in thalamocortical systems and their potentiation by mesopontine cholinergic nuclei in the cat. *Proc Natl Acad Sci U S A, 88*(10), 4396-4400.

Steriade, M., Nunez, A., & Amzica, F. (1993). A novel slow (< 1 Hz) oscillation of neocortical neurons in vivo: depolarizing and hyperpolarizing components. *J Neurosci, 13*(8), 3252-3265.

Steyn-Ross, M. L., Steyn-Ross, D. A., & Sleigh, J. W. (2004). Modelling general anaesthesia as a first-order phase transition in the cortex. *Progress in Biophysics & Molecular Biology, 85*(2-3), 369-385. doi: DOI 10.1016/j.pbiomolbio.2004.02.001

Tinker, J. H., Sharbrough, F. W., & Michenfelder, J. D. (1977). Anterior shift of the dominant EEG rhytham during anesthesia in the Java monkey: correlation with anesthetic potency. *Anesthesiology, 46*(4), 252-259.

Voss, L., & Sleigh, J. (2007). Monitoring consciousness: the current status of EEG-based depth of anaesthesia monitors. *Best practice & research. Clinical anaesthesiology, 21*(3), 313-325.

Wallace, M. N., & Palmer, A. R. (2008). Laminar differences in the response properties of cells in the primary auditory cortex. *Experimental brain research. Experimentelle Hirnforschung. Experimentation cerebrale, 184*(2), 179-191. doi: 10.1007/s00221-007-1092-z

Wang, M., Ramos, B. P., Paspalas, C. D., Shu, Y., Simen, A., Duque, A., . . . Arnsten, A. F. (2007). Alpha2A-adrenoceptors strengthen working memory networks by inhibiting cAMP-HCN channel signaling in prefrontal cortex. *Cell, 129*(2), 397-410. doi: 10.1016/j.cell.2007.03.015

Wang, X. J. (2010). Neurophysiological and computational principles of cortical rhythms in cognition. *Physiol Rev, 90*(3), 1195-1268. doi: 10.1152/physrev.00035.2008

White, N. S., & Alkire, M. T. (2003). Impaired thalamocortical connectivity in humans during general-anesthetic-induced unconsciousness. *Neuroimage, 19*(2 Pt 1), 402-411.

Wrobel, A. (2000). Beta activity: a carrier for visual attention. *Acta neurobiologiae experimentalis, 60*(2), 247-260.

CHAPTER 5: AWAKE VS. ANESTHETIZED: LAYER-SPECIFIC SENSORY PROCESSING IN VISUAL CORTEX AND FUNCTIONAL CONNECTIVITY BETWEEN CORTICAL AREAS[4]

INTRODUCTION

Most of what we understand about the processing of sensory signals in the brain rests on studies in anesthetized animals (Gilbert, 1977; Hubel & Wiesel, 1959). An implicit assumption, which has remained mostly unchallenged, is that circuits of basic sensory processing are comparatively spared from the effects of anesthetics in contrast to higher-order cortical areas. Yet, general anesthesia profoundly alters global brain function. In particular, anesthetics alter the temporal structure of brain activity (Lennox, 1949) and may thereby disrupt information processing that relies on precise timing of neuronal activity and functional interactions between brain areas. Impairment of dynamic interactions within and between neuronal circuits may represent a key mechanism by which anesthetics alter overall cognitive and behavioral states (Alkire, 2008; Heinke & Koelsch, 2005; Kreuzer et al., 2010; Lee et al., 2013; White & Alkire, 2003). Non-invasive imaging and EEG studies have provided support for impaired large-scale organization of spontaneous ("resting") activity across brain areas in humans (John et al., 2001; Moeller, Nallasamy, Tsao, & Freiwald, 2009) (but see (Vincent et al., 2007)). These findings have precipitated a new model of the network-level mechanism of action of anesthetics; in this model, information processing is impaired by alterations of large-scale network dynamics and functional connectivity during anesthesia (Alkire, Hudetz, & Tononi, 2008). Yet, the underlying alterations to micro- and mesoscale cortical circuit function, in particular during sensory processing, remain little studied.

[4] This chapter previously appeared as an article in the Journal of Neurophysiology; doi: 10.1152/jn.00923.2014 (http://jn.physiology.org/content/113/10/3798.long). The original citation is as follows: **Kristin K. Sellers**, Davis V. Bennett, Axel Hutt, James H. Williams, and Flavio Frohlich (2015). Awake vs. anesthetized: Layer-specific sensory processing in visual cortex and functional connectivity between cortical areas. Journal of Neurophysiology, 113(10):3798-3815.

To close this gap in knowledge, we asked if and how response dynamics and functional connectivity of sensory processing are altered during anesthesia. To answer this question, we measured mesoscopic (local field potential, LFP) and microscopic (multiunit activity, MUA) network dynamics simultaneously across cortical layers during presentation of visual stimuli in V1 and PFC of awake and anesthetized ferrets. Investigating both mesoscopic and microscopic network dynamics provided deeper insight into overall neuronal activity patterns, since mesoscopic LFP activity reflects synaptic currents which do not necessarily result in local suprathreshold activity, while microscopic MUA represents suprathreshold input to recorded neurons. Anesthetized recordings utilized three concentrations of isoflurane (each with a constant xylazine infusion). Our study first focused on primary visual cortex (V1), since V1 is well-suited for elucidating differential effects of anesthetics across cortical layers given the extensive body of work examining the distinct role of each cortical layer in sensory function (Binzegger, Douglas, & Martin, 2009; Hirsch & Martinez, 2006). To test large-scale interaction dynamics within cortico-cortical circuits, we then probed the response dynamics in PFC and subsequently directly measured functional connectivity between V1 and PFC by simultaneous recordings in both areas.

METHODS

Surgery

Adolescent female ferrets (*Mustela putoris furo*, 15-20 weeks old at study onset, 750-1000g) were used in this study (awake: n = 14 animals; anesthetized: n = 10 animals). Details of the animal model and recording methods were described previously (Sellers, Bennett, & Frohlich, 2015; Sellers, Bennett, Hutt, & Frohlich, 2013). All animals underwent aseptic surgery in preparation for subsequent electrophysiological recordings in V1 and PFC. All electrophysiology was conducted with acute insertions of recording electrodes. General anesthesia was induced with an initial intramuscular injection of ketamine (30 mg/kg) and xylazine (1-2 mg/kg). The method of anesthesia maintenance used during surgery depended upon the specific experimental preparation: ketamine/xylazine for implantation of recording chambers (awake group) and isoflurane/xylazine for acute recordings. The choice of drugs and doses was designed to achieve general anesthesia throughout surgery and the anesthetized recordings, with complete absence of withdrawal response to toe pinch as an assay of anesthetic depth (assessed

prior to administration of vecuronium bromide). This fulfilled requirements by the local IACUC. Physiologic monitors included electrocardiogram, peripheral capillary oxygen saturation, and rectal body temperature, with end-tidal CO_2 for a subset of animals. A water heating blanket was used to maintain animal temperature between 38.0-39.0°C, and when measured, end-tidal CO_2 was between 30 and 50 mmHg (Kohn, 1997). Paralube was used to protect the eyes for the duration of the surgery.

Surgical procedures consisted of an initial midline incision of the scalp, retraction of the soft tissue, and a circular craniotomy located over left V1 (approximately 3 mm anterior to lambda and 9 mm lateral to the midline) and/or left PFC (approximately 5 mm anterior to bregma and 2 mm lateral to the midline, rostral anterior sigmoid gyrus) (Duque & McCormick, 2010) (Figure 5.1B). The potential for brain swelling was reduced with a preventative injection of furosemide (1 mg/kg, IM). After removal of dura, the brain was covered with warm, sterile 4% agar. A stainless steel head post was implanted with bone screws and dental cement. All procedures were approved by the UNC – Chapel Hill IACUC and exceed the guidelines set forth by the NIH and USDA.

Procedures in Awake Animals

Prior to recordings in animals that were awake (“awake recordings”), there was an initial phase of habituation to restraint, followed by surgical implantation of the recording chamber to access the craniotomy, and finally a period for full recovery of at least 5 days. The animals were habituated to be calmly restrained for up to 2 hours in the recording apparatus. General anesthesia during surgery was maintained by intramuscular injections of ketamine (30 mg/kg) and xylazine (1-2 mg/kg) approximately every 40 minutes. The base of a custom-fabricated cylindrical chamber with a removable cap (material: Ultem 1000) was secured to the skull with bone screws and dental cement in order to allow subsequent access to the craniotomy for recordings. Upon completion of these surgical procedures, the incision was closed with sutures and treated with antibiotic cream. Yohimbine (0.25-0.5 mg/kg, IM) was administered for emergence; the animal was kept warm with a heating blanket and observed during recovery. Meloxicam (0.2 mg/kg, IM) and enrofloxacin (5 mg/kg, IM) were administered to prevent infection and to minimize post-surgical discomfort.

Procedures in Anesthetized Animals

Prior to recordings in anesthetized animals ("anesthetized recordings"), general anesthesia was induced with an intramuscular injection of ketamine (30 mg/kg) and xylazine (1-2 mg/kg) and the animals were intubated and mechanically ventilated (10-11 cc, 50 bpm, 100% medical grade oxygen). Eyes were kept lubricated with sterile saline (applied at the beginning of the wait period for anesthesia stabilization) and vital signs were monitored throughout recording. Any effect from ketamine administered during induction was minimal as multiple hours elapsed prior to the start of electrophysiological recordings and the elimination half-life of ketamine has been reported to be 45-60 minutes (Davidson & Plumb, 2003; W. B. Saunders Company).

General anesthesia was maintained with isoflurane (iso, 0.5%, 0.75%, 1.0%) and a constant infusion of xylazine. Intravenous access was established in the cephalic vein and fluids included 4.25 mL/hr 5% dextrose lactated ringer's with 1.5 mg/kg/hr xylazine. To optimize electrophysiological stability, 0.79 mg/kg/hr vecuronium bromide was added during some recordings. The temporal order of isoflurane concentrations was randomized across animals to control for changes related to continuous infusion of xylazine. At least 20 minutes elapsed after changing anesthetic concentration prior to starting a new recording, exceeding the amount of time required in our setup for the LFP to stabilize at the new anesthetic concentration.

We were interested in assessing differences in sensory-evoked activity over a range of anesthetic depths that each maintained general anesthesia. Informally in the course of pilot experiments, all dosing achieved loss of the righting reflex but systematic assessment during the recordings was technically not feasible. The dosing used did not induce long periods of isoelectric brain activity.

Visual and Auditory Stimulation and Multichannel Electrophysiology

We recorded LFP and MU spiking in response to visual and auditory stimulation. In a first set of experiments, multichannel electrophysiological data were recorded with acutely inserted, linear silicon depth probes that simultaneously recorded neuronal activity in all cortical layers (32 channels, 50μm contact site spacing along the z-axis for single craniotomies; two 16 channel probes, 100μm contact site spacing along the z-axis for dual craniotomies, one in V1 and one in PFC, Neuronexus, Ann Arbor, MI).

For 32-channel probes, the reference electrode was located on the same shank (0.5mm above the top recording site) and was positioned in 4% agar in saline above the brain. A silver chloride wire tucked between the skull and soft tissue and held in place with 4% agar in saline was used as the reference for both 16-channel probes used during anesthetized recordings. Probes were slowly advanced into cortex using a micromanipulator (Narishige, Tokyo, Japan), and correct depth was determined online by small deflections of the LFP at superficial electrode recording sites and larger deflections of the LFP at deeper electrode recording sites. Current source density (CSD) analysis was performed offline to verify electrode positioning across cortical layers (Figure 5.1C). CSD was determined by calculating the second spatial derivative of the low-pass filtered and smoothed LFP in response to full-field flashes presented at a rate of 1Hz (Ulbert, Halgren, Heit, & Karmos, 2001). The first sink-source pair in the CSD was used to determine putative layer IV. All electrode penetrations were within 1 mm of the same location in V1, corresponding to 5 degrees visual field in azimuth and 4.8 degrees visual field in elevation (given magnification factors in area 17 of 0.2 mm in cortex/degrees of visual space in the azimuth and 0.207 mm in cortex/degrees of visual space in elevation (Cantone, Xiao, McFarlane, & Levitt, 2005)). Unfiltered signals were first amplified with MPA8I head-stages with gain 10 (Multichannel Systems, Reutlingen, Germany), then further amplified with gain 500 (Model 3500, A-M Systems, Carlsborg, WA), digitized at 20kHz (Power 1401, Cambridge Electronic Design, Cambridge, UK), and digitally stored using Spike2 software (Cambridge Electronic Design).

Upon correct depth placement of the electrode(s), the animal was presented with visual or auditory stimuli. The same stimuli were presented to awake and anesthetized animals. Each awake recording session was brief (typically < 2 hours), during which the animal was head fixed. Visual stimuli were presented on a 52 x 29 cm monitor with 120Hz refresh rate and full high-definition resolution (1,920 x 1,080 pixels, GD235HZ, Acer Inc, New Taipei City, Taiwan) at 47 cm distance from the animal (Figure 5.1A, left). The same monitor and animal positions were used across sessions, for both awake and anesthetized animals. Visual stimuli filled 58 degrees of the visual field horizontally, 33 degrees of the visual field vertically, and were controlled by the Psychophysics toolbox (Brainard, 1997) for MATLAB (Mathworks, Natick, MA) and a GeForce580 GPU (NVIDIA, Santa Clara, CA). Correct timing of individual display frames was ascertained by a photodiode covering a small flashing square in the corner of the

monitor. The visual stimulus was 10 seconds long and consisted of 10 transitions between static checkerboard frozen noise stimuli (“1 Hz noise”, Figure 5.1A, bottom); each trial consisted of 10 seconds visual stimulus bracketed by 10 seconds of black or gray dark. This visual stimulus was part of a larger set of stimuli that was presented during each recording session in randomized order. The checkerboard visual stimulus enabled the study of responses to both abrupt transitions (i.e. “impulse responses”) and to sustained static visual input in between transitions (i.e. “step responses”). Receptive field mapping was conducted to functionally verify recording location in V1 (Figure 5.1D). Receptive fields were determined by presenting the animal with a series of gray screens with one square of a 19x10 grid colored white or black for 40ms. Each square was shown for 30 repeats of each color in a randomized presentation order. MUA evoked by each square was calculated by subtracting baseline MUA during the 50ms immediately prior to the stimulus onset from MUA 30-80ms after stimulus onset. Based on comparable receptive field maps across recordings, consistent craniotomy and electrode insertion locations, and unchanged animal and monitor position, we are confident of consistent visual stimulation across recording sessions. We validated our PFC recording locations by histological verification of probe location (recording probe dipped in DiI, Invitrogen, Grand Island, NY, before insertion) to ensure the electrode was properly inserted in the rostral portion of the anterior sigmoid gyrus (Duque & McCormick, 2010), 2 mm from the midline (Figure 5.1E).

Auditory stimulation consisted of open-field white noise played on two speakers (Dayton Audio B652, 8 ohm impedance, 70Hz-20kHz, Dayton Audio, Springboro, OH) through an amplifier (PylePro, 2x40 watt, Pyle, Brooklyn, NY) at 64.3 dB-SPL (System 824 sound level meter, Larson Davis, Depew, NY). Auditory stimulation trial structure was similar to visual stimulation (10.7s silence, 10.7s auditory stimulation, 10.7s silence). We used a microphone to record sound on a channel of our electrophysiology recording system during the entirety of auditory stimulation sessions. We applied a threshold to this auditory signal channel in order to detect the onset of stimulation and synchronize the presentation of auditory stimuli with neural recordings.

During awake recordings, continuous infrared video recording (Handycam, HDR-cx560v, Sony, Tokyo, Japan) was used to document that the animal was awake as evidenced by open eyes, whisking, and nose twitching. Two of the awake animals (one each: V1 and PFC recording locations) was

subsequently used for anesthetized recordings to minimize the total number of animals used in this study. Presented anesthetized data were combined across both sets of animals. At the conclusion of the study, animals were humanely killed with an overdose of sodium pentobarbital and immediately perfused with 4% formaldehyde in 0.1M phosphate buffered saline for subsequent histological verification of recording locations.

Experiments Assessing Interaction of V1 and PFC

In a second set of experiments, simultaneous recordings in V1 and PFC were conducted in both awake and isoflurane/xylazine anesthetized animals in order to assess the interaction of V1 and PFC. For experimental feasibility, single metal electrodes were used to acquire electrophysiological data instead of multichannel probes. Electrophysiological signals were recorded using single metal electrodes acutely inserted in putative layer IV, measured 0.3-0.6mm from the surface of cortex (tungsten microelectrode, 250µm shank diameter, 500 kOhms impedance, FHC Inc., Bowdoin, ME). A silver chloride wire tucked between the skull and soft tissue was used as the reference. Unfiltered signals were amplified with gain 1000 (Model 1800, A-M Systems, Carlsborg, WA), digitized at 20 kHz (Power 1401, Cambridge Electronic Design, Cambridge, UK), and digitally stored using Spike2 software (Cambridge Electronic Design). All other details of the surgical and experimental procedures were the same as described above.

Data Analysis and Statistical Analysis

Recorded broadband signals were processed offline with custom-written scripts in MATLAB (Mathworks, Natick, MA). For some depth probes, a few select channels had to be excluded because of known defects in Neuronexus B-stock probes; in these cases, we interpolated data from neighboring channels. This was only the case for approximately 30% of recordings conducted using 32-channel probes (and never for the 16-channel probes), in which either one or two channels were defective; there were never instances of consecutive defective channels, thus the spatial blurring was minimal (since there always was at least one usable electrode site for every 100µm of cortical depth). About 15% of the trials were manually excluded due to motion artifacts in the LFP signal (defined as extreme values in the raw traces). If not stated otherwise, the mean across recording sites and trials was calculated per

recording session, and figures represent means across recording sessions (number of recording sessions, visual stimulation: V1 awake = 39, V1 0.5% iso = 16, 0.75% iso = 17, 1.0% iso = 18, PFC awake = 27, PFC anesthetized = 51. Auditory stimulation: V1 awake = 5, V1 anesthetized = 5, PFC awake = 15, PFC anesthetized = 17). Laminar probes and CSD allowed for analysis of responses by layers: putative supragranular (LI-II/III), granular (LIV), and infragranular layers (LV-VI). Varying isoflurane levels were collapsed for the analysis of PFC and the response to auditory stimulation.

High-pass filtered data (4^{th} order butterworth filter, 300Hz cutoff) were subjected to a threshold of -3*std for detection of action potentials (MUA). The distribution of thresholds for awake recordings was within the range of thresholds obtained in anesthetized recordings. For response histograms, spiking rate was calculated based on 20ms bins. Time constants were calculated by fitting an exponential with offset to the MUA response for the time periods indicated: $a + b*e^{(-t/\tau)}$. MU response latency was calculated from histograms with 5ms bins for increased temporal resolution. Time-dependent frequency content was determined by convolution of the raw extracellular voltage signals with a family of Morlet wavelets (0.5Hz – 40Hz, step-width 0.5Hz) with normalized amplitude, providing an optimal trade-off between time and frequency uncertainty (Goupillaud, Grossmann, & Morlet, 1984). The same methods were applied to recordings from awake and anesthetized animals. All spectra are shown on a logarithmic scale. Power in each frequency band (delta = 0.5-4Hz, theta = 4-8Hz, alpha = 8-12Hz, beta = 12-30Hz, gamma = 30-40Hz) was calculated for each recording session. The power enhancement ratio was calculated as the ratio between spectral power during visual stimulation to spectral power during spontaneous activity before stimulation.

Spike-field coherence (SFC) was used to quantify the interaction between mesoscopic LFP frequency structure and microscopic MU activity. SFC measures phase synchronization between the LFP and spike times as a function of frequency. Spike-triggered averages from 1 second segments of LFP around each spike were obtained. Multi-taper spectral estimates were used to determine spectra of the spike-triggered averages (MATLAB pmtm function with time-bandwidth product of 3.5). Multi-taper spectral analysis was used because this approach is optimized for spectral analysis of short data segments (such as those obtained from data surrounding each spike time), and is well-suited for non-stationary signal with rapid fluctuations (van Vugt, Sederberg, & Kahana, 2007). SFC values were given

by the ratio of spike-triggered average spectra to the average of spectra calculated from each LFP segment (Fries, Reynolds, Rorie, & Desimone, 2001). Thus, SFC is normalized for spike rate and spectral power. The SFC ratio was defined as the ratio of the mean SFC for 0.5-30Hz to the mean SFC for 30-40Hz.

To assess phase synchrony, we calculated inter-trial phase coherence (ITPC) (Tallon-Baudry, Bertrand, Delpuech, & Pernier, 1996). ITPC within V1 and PFC, separately, was calculated by convolving the raw extracellular voltage signals with a family of Morlet wavelets (0.5Hz – 40Hz, step-width 0.5Hz) with normalized amplitude, and then calculating the mean length of the angle vector across trials. These values were calculated per channel, and statistics were conducted across sessions. Normalization was conducted by subtracting the average ITPC during full-field dark screen (visual stimulation) or silence (auditory stimulation). Recordings conducted under all doses of anesthetics were combined. We defined a region of interest of 0.5-10Hz for 500ms after stimulus onset to measure differences in phase coherence between awake and anesthetized animals. We normalized the average ITPC in our region of interest by subtracting averaged ITPC from 500ms during the preceding dark/silent period. While a commonly applied metric to assess phase-resetting, evidence suggests that ITPC may also reflect evoked responses. In order to test for this, we utilized the methods proposed by (Martinez-Montes et al., 2008). Specifically, we calculated the t-like statistic, which assesses if there is a significant difference between the sample mean of the wavelet coefficients for each time point and frequency and the average of these sample means for the pre-stimulus period. A local false discovery rate (FDR) of 0.2 was used to test for significance and correct for multiple comparisons in the time-frequency map.

In order to test the relationship of activity between V1 and PFC, in a second set of experiments, we recorded LFP and MUA simultaneously from V1 and PFC in two awake and two isoflurane/xylazine anesthetized ferrets using single metal electrodes inserted into putative layer IV (number of sessions: awake = 18, 0.5% iso = 10, 1.0% iso = 21). In order to gain insight into the functional connectivity between V1 and PFC, the time-dependent spectral coherence was estimated by first convolving the raw signal in V1 and PFC with a family of Morlet wavelets across frequencies [0.2 Hz – 40 Hz, step-width of 0.2 Hz for time-dependent analysis and step-width of 0.5 Hz for time-averaged analysis]. For each trial, the auto spectra in V1 and PFC and the cross spectrum were calculated. The auto spectra in V1, auto

spectra in PFC, and cross spectrum were averaged across trials, without smoothing within trials. The time-frequency spectral coherence was then calculated as the square of the averaged cross spectrum, normalized by the product of the averaged auto spectra from V1 and PFC (Zhan, Halliday, Jiang, Liu, & Feng, 2006). This method of calculating coherence does not assume a stationary signal. Spectral coherence was calculated per recording session, and means were calculated across sessions to provide group-averaged results. Time-averaged spectral coherence was obtained by averaging over time during presentation of the visual stimulus. This coherence measure assumes a linear dependence of activity between V1 and PFC and takes values from 0 (absent coherence) to 1 (perfect coherence).

Since the functional relationship of V1 and PFC activity is not well-understood and the assumption of linear dependency may not hold, we additionally calculated nonlinear phase-locking between V1 and PFC (Lachaux, Rodriguez, Martinerie, & Varela, 1999). The raw signal in V1 and PFC was convolved with a family of Morlet wavelets across frequencies (0.5 – 40Hz, step-width 0.5Hz) to obtain instantaneous phases of the signal from each brain area. The circular variance of the phase differences between V1 and PFC was computed over trials in each recording, and then averaged across recordings to provide the group-averaged phase-locking value (V1-PFC PLV). V1-PFC PLVs range from 0 to 1, reflecting absent to perfect phase-locking, respectively.

Statistical tests were performed using ANOVA, with post hoc testing if the main effect was significant at $p < 0.05$. Tukey's honestly significant difference criterion was used to correct for multiple comparisons. Unless otherwise stated, mean ± sem are reported.

RESULTS

In order to elucidate how micro- and mesoscale network dynamics of sensory processing differ between awake and anesthetized animals, we performed multichannel electrophysiology combined with sensory stimulation in head-fixed ferrets (Figure 5.1A, top). The visual stimulus (10s) consisted of 10 frozen-noise, static checkerboard patterns that were consecutively presented at a frequency of 1 Hz (Figure 5.1A, bottom). We recorded LFP and MUA from V1 (n = 13 animals) and PFC (n = 9 animals) to quantify MUA and LFP network dynamics (Figure 5.1B: recording locations of V1 and PFC shown on photograph of a ferret brain). These two cortical recording locations were chosen to capture responses in

and interactions between a primary sensory area and a higher-order cortical association area. We used multichannel depth probes for simultaneous electrophysiological recordings from all cortical layers (Figure 5.1C: current source density in V1, the top sink source pair was indicative of putative granular layer IV; layers were identified and grouped as supragranular (LI-LII/III), granular (LIV), or infragranular (LV-LVI)). Receptive field mapping demonstrated well-defined visual responses and therefore provided functional verification of recording location in V1 (Figure 5.1D); post-mortem histological processing was used to confirm recording location in PFC (Figure 5.1E). Infrared videography was used to verify that animals were awake for the entirety of the awake recordings as determined by the presence of whisking, minor movements, and blinking. Animals had not been trained in any task and were freely viewing during the recordings.

Disruption of Temporal Precision and Laminar Distribution of Visually Evoked MUA during Anesthesia

In one conceptual framework, anesthetics could selectively alter information flow between higher-order (cortical) areas and spare processing in primary sensory cortices, leaving sensory responses intact. Alternatively, anesthesia could indiscriminately suppress visual responses and therefore reduce overall representation of sensory input. Lastly, anesthetics could disrupt specific aspects of the spatio-temporal response dynamics in the cortical microcircuit. In order to disambiguate between these possibilities, we first asked if and how visual responses in V1 measured by multiunit activity (MUA) were altered during anesthesia. We found that MUA responses differed strikingly between recordings in the awake and anesthetized animal. Importantly, we did not find broad suppression of visual responses by anesthetics. Rather, we identified several pronounced differences in the temporal structure of MUA responses between awake and anesthetized animals. In the awake animal, MUA response dynamics exhibited two salient features. First, in response to the onset of the 10 sec visual stimulus, a strong MUA response occurred (Figure 5.2A, left, representative high-pass filtered trace from infragranular layers, taken from recording shown in Figure 5.2B left, blue line indicates spike-extraction threshold set at -3*std; Figure 5.2B, left, responses from a single recording; Figure 5.3A, left, averaged group-level responses; MUA rates were calculated based on 20 ms bins). MU responses markedly decreased with subsequent

transitions to the next checkerboard pattern within each trial of the 10s visual stimulus (Figures 5.2A & B, Figure 5.3A, left). Second, awake animals exhibited temporally precise, transient increases in MUA in response to each transition in the stimulus (Figure 5.3A, bottom left). In anesthetized animals, the amplitude of visually-evoked MUA was comparable for the stimulus onset and the subsequent noise-pattern transitions in the stimulus (Figures 5.2A, right, representative high-pass filtered trace from infragranular layers, taken from the recording shown in Figure 5.2B right, blue line indicates spike-extraction threshold; Figure 5.2B, right, responses from a single recording; Figure 5.3A, right, averaged group-level responses). Furthermore, there was a pronounced 'tail' of continued MUA response following the initial temporally precise response to transitions in the stimulus (Figure 5.3A, bottom right). Accordingly, the decay time constant for the MUA response was significantly longer in anesthetized animals compared to in awake animals (Figures 5.3A, bottom, time constant for MU activity during seconds 4-5 of visual stimulation: awake = 0.050s, 95% CI [0.037 0.066], 1.0% iso = 0.140s, 95% CI [0.119 0.160]).

We calculated MU firing rate using 5 ms bins to provide better temporal resolution at the onset of the visual stimulus but found no alteration in the response latency of MU firing (Figure 5.3B). The latency of MU spiking after onset of the visual stimulus exhibited a significant group factor of condition (awake, 0.5% iso, 0.75% iso, 1.0% iso, $F= 2.86$, $p = 0.041$), however no post host tests were significant (Figure 5.3C, mean response latency ± 1 sem, defined as exceeding a threshold of 2*stdev of baseline spiking activity, awake = 0.019s ± 0.0011s; 0.5% iso = 0.018s ± 0.00070s; 0.75% iso = 0.016s ± 0.00071s; 1% iso = 0.015s ± 0.00056s). Together, these results indicate that anesthetics altered V1 visually-evoked spiking by maintaining a large amplitude response to each subsequent transition in the stimulus and concomitantly inducing prolonged MUA responses to transients in the visual input.

Previous work has demonstrated that anesthetics selectively alter spontaneous activity as a function of cortical layer (Sellers et al., 2013). We here sought to investigate if MUA responses to visual input also differed across cortical layers during anesthesia. Understanding the impact of anesthetics on dynamics across layers in the cortical microcircuit is particularly tractable in V1 because of the well-established pathway of information flow between cortical layers in visual processing (Binzegger et al., 2009). 32-channel depth probes allowed for simultaneous acquisition of electrophysiological activity

across all cortical layers (Figure 5.4A, group-averaged MU spiking rate during visual stimulation across cortical layers for awake animals and animals anesthetized with 0.5%, 0.75%, & 1.0% isoflurane all with xylazine). In awake animals, there was a trend level difference in visually-evoked spiking rates across cortical layers (Figure 5.4B, far left, mean firing rate averaged across 10 seconds of visual stimulation ± 1 sem: supragranular = 34.11Hz ± 1.918, granular = 40.01Hz ± 2.302, infragranular = 40.68 Hz ± 2.138, $F = 2.67$, $p = 0.07$). For the three levels of anesthetic, there were significant and trend level effects of cortical layer on increased visually-evoked spiking, particularly with differences in the granular layer (Figure 5.4B, right, mean firing rate averaged across 10 seconds of visual stimulation ± 1 sem: 0.5% iso, supragranular = 33.39Hz ± 4.267, granular = 49.25Hz ± 7.181, infragranular = 36.70Hz ± 4.194, $F = 2.37$, $p = 0.1$; 0.75% iso, supragranular = 40.24Hz ± 4.339, granular = 53.85Hz ± 5.824, infragranular = 37.66Hz ± 2.629, $F = 3.81$, $p = 0.03$; 1.0% iso, supragranular = 39.72Hz ± 4.676, granular = 48.29Hz ± 5.604, infragranular = 34.25Hz ± 2.247, $F = 2.58$, $p = 0.09$).

Given this trending increase in MUA response in the granular layer during anesthesia, we next asked if anesthetics altered adaptation dynamics to the 1 Hz temporal structure of the stimulus as a function of cortical depth. In awake animals, we observed adaptation of supragranular, granular, and infragranular layers to repeated presentations of the stimulus (Figure 5.4C, left: impulse-like response to each of the ten screen changes during the visual stimulus, calculated as the mean MU firing rate for 200ms after each screen change). During anesthesia, this adaptation of MUA responses was slowed; supragranular, granular, and infragranular layers each exhibited inconsistent modulation in response across the ten transitions between checkerboard-noise patterns within the visual stimulus (Figure 5.4C, right). Decreased activity in the main output layer (layer V, infragranular layers) relative to activity in the input layer (layer IV, granular layers) suggests that the interaction between cortical areas may be impaired under anesthesia.

Amplified Visually-Evoked Frequency Structure during Anesthesia

Given these changes in the temporal activity structure of microscopic sensory responses measured by MUA, we next asked if mesoscopic activity patterns, in particular the frequency structure of the LFP, were also altered by anesthetics. During visual stimulation in awake animals, the LFP (Figure

5.5A, left, raw trace from infragranular layers, taken from recording shown in Figure 5.5B left) and spectral content (Figure 5.5B, left, single recording example; Figure 5.6A, left, group-averaged results) modestly reflected the temporal (1 Hz) structure of the visual stimulus. In contrast, in anesthetized animals, spectral power was predominantly driven by the temporal patterning of the visual stimulus (Figures 5.5A right, raw trace from infragranular layers taken from recording shown in 5.5B right; 5.5B right, single recording example; Figure 5.6A, right, group-averaged results). To assess if this difference in spectral modulation was limited to certain cortical layers, we determined stimulation-induced modulation of spectral power by cortical layer (Figure 5.6B, ratio of spectral power during visual stimulation to power of spontaneous activity). Indeed, we found similar response profiles across layers; in addition, in both awake and anesthetized animals, spectral modulation at low frequencies was greater in granular and infragranular layers compared to supragranular layers. We next quantified the enhancement of power in each frequency band by the visual stimulus, by calculating the ratio of power during visual stimulation to power during spontaneous activity before stimulation. Visual stimulation enhanced power for frequency bands in both awake and anesthetized animals, with the greatest enhancement at the highest concentrations of isoflurane (Figure 5.6C, percent enhancement ± 1 sem, awake animal: delta = 26.42 ± 3.653% enhancement, theta = 12.40 ± 3.725% enhancement, alpha = 5.565 ± 3.091% enhancement, beta = 0.4129 ± 1.945% enhancement, gamma = 11.89 ± 1.503% enhancement. 1% iso: delta = 167.4 ± 22.87% enhancement, theta = 143.0 ± 17.42% enhancement, alpha = 112.8 ± 10.07% enhancement, beta = 75.57 ± 8.024% enhancement, gamma = 48.39 ± 6.889% enhancement). Enhancement in each frequency band for animals anesthetized with 0.5%, 0.75%, or 1.0% isoflurane all with xylazine was significantly greater than enhancement in the matching frequency band in awake animals (delta: $F = 26.69$, $p < 0.05$; theta: $F = 29.18$, $p < 0.05$; alpha: $F = 40.90$, $p < 0.05$; beta: $F = 57.67$, $p < 0.05$; gamma: $F = 15.71$, $p < 0.05$). In addition, post hoc tests demonstrated that delta, theta, alpha, and beta power enhancement were significantly different between 0.5% iso and 1.0% iso, and beta power enhancement was significantly different between 0.75% iso and 1.0% iso. Thus, increasing concentrations of isoflurane increased power across all frequency bands, but with the greatest enhancement in the lower frequency bands and in granular and infragranular layers.

Selective Enhancement of Spike-Field Coherence at Low-Frequencies during Anesthesia

Given the prolonged MUA responses to visual stimulation together with the broad-band increases in stimulus-driven frequency structure during anesthesia, we asked how the functional interaction between microscopic and mesoscopic network dynamics was modulated by anesthetics. Spike-field coherence (SFC) links mesoscopic LFP network dynamics to microscopic MUA by quantifying the interaction between network frequency structure and spiking activity. We found that SFC was minimal in awake animals, while anesthetics induced differential effects based on cortical layer (Figure 5.7A). In order to further quantify the frequency- and layer-specificity of changes in SFC during anesthesia, we developed a metric to indicate the relative enhancement of low frequency SFC (Figure 5.7B-D, SFC ratio = mean SFC from 0.5Hz to 30Hz / mean SFC from 30Hz to 40Hz). With anesthetic, the SFC ratio increased for supragranular (Figure 5.5B, SFC ratio ± 1 sem: awake = 0.991 ± 0.0714, 0.5% iso = 1.84 ± 0.283, 0.75% iso = 2.00 ± 0.311, 1.0% iso = 2.54 ± 0.458), granular (Figure 5.7C, awake = 1.17 ± 0.103, 0.5% iso = 2.22 ± 0.202, 0.75% iso = 2.38 ± 0.216, 1.0% iso = 2.86 ± 0.262), and infragranular layers (Figure 5.7D, awake = 1.05 ± 0.0588, 0.5% iso = 3.42 ± 0.403, 0.75% iso = 2.83 ± 0.409, 1.0% iso = 2.99 ± 0.496). For each cortical depth, anesthesia condition was a significant factor (supragranular, $F = 7.28$; granular $F = 20.8$; infragranular $F = 15.8$; all $p < 0.05$). These results demonstrate that during anesthesia there was increased synchronization of the LFP and spiking activity, preferentially at lower frequencies. Given the likely role of mesoscale dynamics measured by the LFP in enabling and timing the interaction between cortical areas, we next investigated the effects of anesthetics on functional cortical connectivity.

Altered Visual Representation in PFC by Anesthetics

Motivated by the evidence for prominent changes in the magnitude, duration, and adaptation of visually-evoked responses in V1 by anesthetics, we next asked if representation of the visual input in PFC was also altered by anesthetics. If anesthetic agents cause functional disconnectivity of cortico-cortical circuits, PFC responses to sensory stimulation present in the awake animal should be absent in the anesthetized animal. Indeed, the onset of visual stimulation induced modulation of the LFP and spectral power in PFC of the awake animal (Figure 5.8A, left: single trial example taken from recording session plotted in Figure 5.8B left; Figure 5.8B, left: responses from a single recording), whereas visual

stimulation did not evoke this activity in PFC of the anesthetized animal (Figure 5.8A, right: single trial example taken from recording session plotted in Figure 5.8B right; Figure 5.8B, right: responses from a single recording). To quantify this difference between the awake and anesthetized animals, we defined a region of interest (ROI) of 0.5-10 Hz for 500 ms after stimulus onset, normalized by the 500 ms prior to stimulus onset. Averaged across recordings, spectral modulation was different between awake and anesthetized animals (ROI analysis, induced spectral modulation ± 1 sem, awake: 0.186 ± 0.0389, $F = 22.91$, $p < 0.05$; anesthetized: 0.0651 ± 0.0186, $F = 12.24$, $p < 0.05$, significant difference between the two conditions, $F = 9.14$, $p < 0.05$).

We next asked if the representation of sensory input in PFC differed across cortical layers. Based on previous findings that layer II/III frontal cortex receives convergent synaptic inputs from sensory and motor systems (Opris, Hampson, Stanford, Gerhardt, & Deadwyler, 2011), we expected that the most prominent effects of anesthetics would be found in superficial layers. We calculated the enhancement of spectral power as the ratio of power during stimulation to spontaneous activity prior to stimulation. As expected, visual stimulation in awake animals induced the strongest spectral modulation in layer II/III, according to the temporal pattern of the visual stimulus (Figure 5.8C, left). In anesthetized animals, we found slight, non-specific spectral enhancement in the low frequencies (Figure 5.8C, right). Additionally, we examined MUA in PFC (Figure 5.8D, representative high-pass filtered traces from infragranular layers of awake and anesthetized animals). Awake animals exhibited modulation of PFC MUA by the visual stimulus, quantified as the difference in MUA between the 500 ms window before stimulus onset and the MUA in the initial 500 ms after stimulus onset (mean ± 1 sem, 2.47Hz ± 0.452, $F = 29.85$, $p < 0.05$), while PFC MUA was not modulated by the visual stimulus in anesthetized animals (1.05Hz ± 0.547, $F = 3.69$, $p=0.06$).

We next computed the ITPC of the LFP. This metric assumes values above zero (maximum value of 1) if sensory stimulation consistently altered the phase of the ongoing activity across trials. However, ITPC may be sensitive to evoked responses in addition to phase-resetting (Krieg et al., 2011; Martinez-Montes et al., 2008). Thus, for each ITPC result, we additionally calculated if there was a significant evoked response for each (see Figure 5.11). PFC of awake animals exhibited increased ITPC at the stimulus onset, in particular at low frequencies (Figure 5.8E, left, mean ROI phase-locking ± 1 sem:

awake = 0.0945 ± 0.0201, F = 22.03, $p < 0.05$, appearance of increased phase synchrony prior to the visual stimulus onset is an artifact of the wavelet analysis and does not indicate a response prior to stimulus onset). Critically, this engagement was minimal in PFC of the anesthetized animal (Figure 5.8E, right, mean ROI ITPC ± 1 sem: anesthetized = 0.0213 ± 0.00638, F = 11.14, $p < 0.05$, significantly different from the awake condition, F = 20.92, $p < 0.05$). This minimal response to the visual input in PFC during anesthesia supports altered functional interaction induced by anesthetics.

As a reference, we applied this ITPC metric to our V1 data as we expected to see a larger, stimulus-driven effect under anesthesia based on the above presented results. Indeed, phase-coherence at the onset of the visual stimulus was observed in the awake animal (Figure 5.8F, left: mean ITPC ± 1 sem = 0.150 ± 0.0225, F = 44.41, $p < 0.05$) but was stronger and remained elevated throughout the duration of visual stimulation in anesthetized animals (Figure 5.8F, right: mean ITPC ± 1 sem = 0.324 ± 0.0187, F = 299.66, $p < 0.05$, awake vs anesthetized significantly different, F = 30.76, $p < 0.05$). Therefore, in agreement with the MUA and frequency spectrum LFP results, visual input had a more pronounced effect on network dynamics in V1 of the anesthetized animal.

Altered Representation of Auditory Stimulus in V1 and PFC by Anesthetics

Given this reduced representation of visual stimuli in PFC under anesthesia, we next asked if anesthetics similarly modulate the functional connectivity that mediates cross-modal sensory signaling in the brain. To address this question, we used auditory stimuli to investigate if the response to such input differed in V1 and PFC between the awake and the anesthetized animal. In V1, presentation of the auditory stimulus induced modulation in both the LFP and the spectrogram (Figure 5.9A, left: single trial example taken from recording session shown in Figure 5.9B left; Figure 5.9B, left: responses from a single recording). These effects were absent in the anesthetized animal (Figure 5.9A, right: single trial example taken from recording session shown in Figure 5.9B right. Figure 5.9B, right: responses from a single recording). At the group level, we found a small modulation of spectral power, although not significant (ROI analysis, mean ± 1 sem, 0.146 ± 0.106, F = 1.91, p=0.20), but no significant spectral modulation in anesthetized animals (-0.0251 ± 0.0515, F = 0.24, p = 0.63). To investigate if there was differential spectral modulation by cortical layer, we calculated the enhancement of spectral power as the

ratio of power during stimulation to spontaneous activity prior to stimulation. In awake animals (Figure 5.9C, left), there was prominent low frequency modulation in V1 granular layers and alpha frequency modulation in infragranular layers, whereas anesthetized animals exhibited no prominent differences across cortical layers (Figure 5.9C, right). In looking at the MUA (Figure 5.9D, representative high-pass filtered traces from an awake and anesthetized animal), we found significant MUA response in V1 exclusively in awake animals (awake: mean ± 1 sem, 19.7Hz ± 7.04, $F = 7.71$, $p = 0.02$; anesthetized: 0.271 ± 0.914, $F = 0.09$, $p = 0.77$; difference between awake and anesthetized significantly different, $F = 10.57$, $p < 0.05$).

We again examined ITPC within V1 in response to the auditory, white-noise stimulus. Interestingly, we found that V1 exhibited increased phase synchrony in response to the auditory stimulus in the awake animal while there was no such response in the anesthetized animal (Figure 5.9E, left, mean ROI ITPC ± 1 sem in V1 awake = 0.207 ± 0.0163, $F = 161.82$, $p < 0.05$; Figure 5.9E, right, mean ROI ITPC ± 1 sem in V1 anesthetized = 0.00756 ± 0.0114, $F = 0.44$, $p = 0.52$; significantly different between the two conditions, $F = 72.30$, $p < 0.05$), consistent with intact functional connectivity between visual and auditory areas exclusively in awake animals. See Figure 5.11 for additional analysis testing for evoked responses.

We next extended this analysis to recordings conducted in PFC during presentation of the auditory stimulus. In PFC, auditory stimulation induced modulation at the onset of the stimulus, as evidenced in both the LFP and the spectrogram (Figure 5.10A, left: single trial example taken from the recording shown in Figure 5.10B left; Figure 5.10B, left: responses from a single recording). These effects were absent in the anesthetized animal (Figure 5.10A, right: single trial example taken from the recording shown in Figure 5.10B right. Figure 5.10B, right: responses from a single recording). At the group level, onset of the auditory stimulus also induced subtle modulation of spectral power in the awake animal only (ROI analysis, induced spectral modulation ± 1 sem, awake: 0.109 ± 0.0356, $F = 9.35$, $p < 0.05$, anesthetized: 0.0128 ± 0.0518, $F = 0.06$, $p = 0.81$; difference between awake and anesthetized significant at trend level, $F = 2.49$, $p = 0.12$).

We next calculated spectral modulation across cortical layers in PFC induced by the auditory stimulus. We found no pronounced differences between the awake and anesthetized change in spectral

power for the broadband auditory stimulus at the group level (Figure 5.10C). In looking at MUA (Figure 5.10D, representative high-pass filtered traces from an awake and anesthetized animal), we found that MUA was altered by auditory stimulation only in the awake animal (induced modulation mean ± 1 sem, awake: 1.84Hz ± 0.860, $F = 4.59$, $p = 0.04$, anesthetized: -0.948 ± 0.814, $F = 1.36$, $p = 0.25$, awake and anesthetized significantly different, $F = 5.55$, $p = 0.03$). Furthermore, PFC exhibited increased phase synchrony at the onset of the auditory stimulus in exclusively the awake animal (Figure 5.10E, left, mean ROI ITPC ± 1 sem in PFC awake = 0.0917 ± 0.0188, $F = 23.78$, $p < 0.05$; Figure 5.10E, right, mean ROI ITPC ± 1 sem in PFC anesthetized = 0.00828 ± 0.0107, $F = 0.60$, $p = 0.44$, significantly different between the two conditions, $F = 15.83$, $p < 0.05$), consistent with intact functional connectivity in only the awake animal.

As stated above, ITPC is likely driven by not only phase resetting but also evoked responses. We utilized the approach of (Martinez-Montes et al., 2008) to find the time points and frequencies at which there was a significant difference in sample mean of the wavelet coefficients compared to the baseline rest period (which the authors termed the T-mean statistic). Indeed, we found that visual stimulation in V1 induced an evoked response in both awake and anesthetized animals (Figure 5.11A, corresponding to ITPC results in Figure 5.8F), while visual stimulation only induced an evoked response in PFC of awake animals (Figure 5.11B, corresponding to Figure 5.8E). Auditory stimulation only induced an evoked response in V1 and PFC of awake animals (Figure 5.11C, auditory stimulation in V1, corresponding to ITPC results in Figure 5.9E; Figure 5.11D, auditory stimulation in PFC, corresponding to ITPC results in Figure 5.10E). Thus, this additional analysis identified a likely role of evoked responses as one of the main sources contributing to non-zero ITPC values.

Decreased Spectral Coherence and Phase Synchrony between V1 and PFC with Anesthesia

Motivated by evidence for altered sensory processing across cortical areas and sensory modalities under anesthesia, we next directly investigated mesoscale functional connectivity between V1 and PFC by recording LFP and MUA simultaneously with single electrodes in V1 and PFC of awake and anesthetized animals during visual stimulation. We first used spectral coherence between LFP in V1 and PFC to quantify functional connectivity between the two areas. Averaged over the duration of the visual

stimulus, awake animals exhibited greater spectral coherence between V1 and PFC compared to anesthetized animals (Figure 5.12A, group-averaged and time-averaged spectral coherence between V1 and PFC). Spectral coherence averaged within each frequency band during visual stimulation was significantly greater in awake animals compared to animals anesthetized with isoflurane/xylazine (Figure 5.12B, mean spectral coherence between V1 and PFC during stimulation in each frequency band ± 1 sem for awake animals and animals anesthetized with 0.5% and 1.0% iso, respectively: delta = 0.34 ± 0.037, 0.15 ± 0.012, 0.15 ± 0.010, theta = 0.30 ± 0.033, 0.13 ± 0.0043, 0.11 ± 0.0030, alpha = 0.27 ± 0.026, 0.14 ± 0.0065, 0.12 ± 0.0043, beta = 0.24 ± 0.016, 0.11 ± 0.0013, 0.11 ± 0.0022, gamma = 0.22 ± 0.013, 0.11 ± 0.0013, 0.11 ± 0.0020, all awake vs 0.5% iso and 1.0% iso for a given frequency band significantly different, $F = 19.88$, $p < 0.05$). These results demonstrate that administration of isoflurane/xylazine anesthetics significantly reduced spectral coherence and thus impaired functional connectivity between V1 and PFC during sensory stimulation. However, it is important to note that the V1 autospectrum appears in the denominator of this metric, and thus differences in spectral coherence between awake and anesthetized animals may result from the larger V1 LFP response in anesthetized animals. In addition, the interactions between V1 and PFC may deviate from linearity, leading to biased coherence results. Thus, we further confirmed this finding of impaired mesoscale functional connectivity by determining the effect of anesthetics on nonlinear phase synchrony between the two cortical areas. In agreement with the spectral coherence data, averaged over the duration of the visual stimulation, awake animals exhibited greater V1-PFC PLV than animals anesthetized with isoflurane/xylazine, (Figure 5.12C, group-averaged and time-averaged V1-PFC PLV). V1-PFC PLVs averaged within each frequency band during visual stimulation were significantly greater in awake animals compared to animals anesthetized with isoflurane/xylazine (Figure 5.12D, mean V1-PFC PLV during stimulation in each frequency band ± 1 sem for awake animals and animals anesthetized with 0.5% and 1.0% iso, respectively: delta = 0.91 ± 0.0035, 0.83 ± 0.0035, 0.82 ±0.0029, theta = 0.92 ± 0.0032, 0.81 ± 0.0022, 0.82 ± 0.0016, alpha = 0.91 ± 0.0025, 0.80 ± 0.0036, 0.81 ± 0.0025, beta = 0.91 ± 0.0016, 0.81 ± 0.0010, 0.81 ± 0.0012, gamma =0.91 ± 0.0014, 0.81 ± 0.0023, 0.81 ± 0.0018, all awake vs 0.5% iso and 1.0% iso for a given frequency band significantly different, $F = 389.73$, $p < 0.05$). Together, these results provide support for disruption of functional connectivity between V1 and PFC at the mesoscale by anesthetics.

DISCUSSION

Anesthetics profoundly alter brain activity and are widely used in both clinical practice and systems neuroscience research. During general anesthesia, spontaneous macroscopic network dynamics are fundamentally altered and have been thoroughly studied in humans using EEG (Brown, Lydic, & Schiff, 2010; Katoh, Suzuki, & Ikeda, 1998; Lennox, 1949; Rampil, 1998), ECoG (Laura D. Lewis et al., 2012), and recently with fMRI (Heinke & Schwarzbauer, 2002; Purdon et al., 2009). Also, the molecular targets of anesthetics have been well described and are comprised of relatively complex sets of intrinsic and synaptic ion channels for most anesthetic agents (Brown, Purdon, & Van Dort, 2011; Campagna, Miller, & Forman, 2003). The effects of anesthetics on intermediate, mesoscale network dynamics have been less well studied. A recent report has demonstrated layer-specific modulation of sensory-evoked activity in auditory cortex (Raz et al., 2014). A more complete understanding of the effects of anesthesia across lamina is crucial since the architecture of the cortical microcircuits that spans all cortical layers likely plays a fundamental role in cortical information processing (Binzegger et al., 2009). The importance of this question derives from the fact that a vast majority of systems neuroscience studies of sensory processing have been performed in the anesthetized preparation due to obvious advantages of experimental stability and data throughput in comparison to the awake preparation. We here asked how sensory processing is altered during anesthesia, in particular how micro- and mesoscale activity in primary visual cortex and prefrontal cortex and the functional connectivity between these areas are modulated.

Dynamics of Visual Responses

The main findings of the present study demonstrate that the anesthetics used did not simply suppress sensory responses but rather induced a set of specific changes to the temporal structure of both micro- and mesoscale response patterns. At the microscale of MUA, we found that the awake, freely-viewing animal exhibited temporally precise, brief responses in V1 that were most pronounced at the stimulus onset and substantially reduced for the subsequent transitions in the visual stimulus. Anesthetics caused temporally prolonged MUA activity, with similar large amplitude responses to each transition in the visual stimulus. At the mesoscale of the LFP, we found that anesthetics induced a more pronounced

representation of the temporal structure of the stimulus and accordingly a tighter interaction between LFP and MUA (especially for low frequencies). Together, these results demonstrate that anesthetics alter the overall network dynamics in V1 during visual processing.

Timing and Synaptic Inhibition

MUA in the awake animal exhibited precise timing and selective response to transitions in the visual input. Thus, V1 acted as a "change detector" or highpass filter. Precise timing of neuronal spiking has emerged as a hallmark of sensory processing in the visual (Tiesinga, Fellous, & Sejnowski, 2008), auditory (Kayser, Logothetis, & Panzeri, 2010; Lu, Liang, & Wang, 2001), and somatosensory (Petersen, Panzeri, & Diamond, 2001) systems (but see also (Oram, Wiener, Lestienne, & Richmond, 1999)). Precise timing of spiking responses likely emerges from the interaction of synaptic excitation and inhibition (Okun & Lampl, 2008; Wehr & Zador, 2003). For example, precise spike timing in layer IV of the somatosensory system is mediated by the feedforward recruitment of synaptic inhibition provided by fast-spiking inhibitory interneurons (Gabernet, Jadhav, Feldman, Carandini, & Scanziani, 2005; Higley & Contreras, 2006). Disruption of such precisely balanced synaptic excitation and inhibition could therefore represent a possible mechanism of action for the changes described here. Importantly, intracellular recordings in cortex of awake animals recently failed to provide evidence for the canonical regime of balanced excitation and inhibition (Haider, Hausser, & Carandini, 2013; M. Rudolph, Pospischil, Timofeev, & Destexhe, 2007); rather inhibition dominated in the awake animal and balanced excitation and inhibition was found in the anesthetized animal (Haider, Duque, Hasenstaub, & McCormick, 2006) and *in vitro* (Shu, Hasenstaub, & McCormick, 2003).

Layer-specific Modulation of Network Dynamics by Anesthetics

The observed layer-specific alterations of sensory processing during anesthesia likely stem from the interplay of several mechanisms at the molecular and cellular level. In particular, changes in neuromodulatory tone and synaptic inhibition as a function of layer are candidate mechanisms (Kimura et al., 2014). Xylazine, used in this study to achieve complete anesthesia for all concentrations of isoflurane (as required by local IACUC regulations), acts as an α2-adrenergic agonist on presynaptic and

postsynaptic receptors; isoflurane acts to potentiate $GABA_A$ receptors, glycine receptors, $5\text{-}HT_3$ receptors, kainate receptors, and two-pore-domain background K^+ channels, and inhibit nACh receptors, AMPA receptors, voltage-gated Na currents at nerve terminals, and at least some types of voltage-gated Ca channels (Eckle, Digruccio, Uebele, Renger, & Todorovic, 2012; Hemmings, 2009; Hemmings et al., 2005; Patel et al., 1999; U. Rudolph & Antkowiak, 2004). The specificity and efficacy of targeting at each of these binding sites, which can induce both complementary and competitive effects, could modulate sensory responses. In particular, bilateral norepinephrine projections to the visual cortex are robust, but exhibit different densities across supragranular, granular, and infragranular layers (Pinaud, Tremere, & De Weerd, 2006). In visual cortex of rats, microiontophoresis of norepinephrine enhanced visually-evoked responses, while serotonin suppressed stimulus-evoked excitation and inhibition (Waterhouse, Azizi, Burne, & Woodward, 1990). Therefore, differences in the laminar profile of sensory processing between awake and anesthetized animals may arise from action at these molecular targets which are expressed in varying densities across cortical layers. Furthermore, layer-specific differences in inhibitory feedforward and feedback circuits could also contribute to the differing effects of anesthetics across layers. In particular, feedforward inhibition is pathway- and layer- specific, capable of modulating network activity through stronger feedforward inhibition and relatively weaker feedback inhibition (Yang, Carrasquillo, Hooks, Nerbonne, & Burkhalter, 2013). A reduction in synaptic inhibition caused by anesthetics could therefore account for the increase in visually-evoked firing rates that we measured in layer IV of anesthetized animals.

In addition, projections from cholinergic nuclei to V1 (Pinaud et al., 2006) and PFC (Chandler, Lamperski, & Waterhouse, 2013) have been established. The release of acetylcholine in primary sensory cortices during sensory stimulation has been found to depend upon activity in PFC (Rasmusson, Smith, & Semba, 2007). Thus, disruption of cortico-cortical connectivity between V1 and PFC induced by anesthesia may contribute to altered visual responses in V1 via reduced acetylcholine release.

Relationship to Previous Studies of Sensory Processing in Awake and Anesthetized Animals

Previous work has investigated several aspects of alteration to electrophysiological sensory responses by anesthetics agents (Detsch, Vahle-Hinz, Kochs, Siemers, & Bromm, 1999; Schumacher,

Schneider, & Woolley, 2011; Villeneuve & Casanova, 2003), demonstrating altered contextual (figure-ground) modulation but maintained receptive field properties (Lamme, Zipser, & Spekreijse, 1998), impairment of motion integration (Pack, Berezovskii, & Born, 2001), increased correlation structure of activity (Greenberg, Houweling, & Kerr, 2008), and increased gamma oscillations in V1 induced by visual stimulation flashes (O. A. Imas, Ropella, Ward, Wood, & Hudetz, 2005) during anesthesia. We primarily utilized isoflurane and xylazine in combination because of their widespread and historic use in studying sensory processing in the visual, auditory, and olfactory systems of both animals and humans (Heinke & Schwarzbauer, 2001; Hudetz & Imas, 2007; Madler, Keller, Schwender, & Poppel, 1991; Rojas, Navas, Greene, & Rector, 2008; Sebel, Ingram, Flynn, Rutherfoord, & Rogers, 1986; Villeneuve & Casanova, 2003; Vincis, Gschwend, Bhaukaurally, Beroud, & Carleton, 2012). Our results demonstrated enhanced neural responses at the frequency of the presented stimulus, and we found that with isoflurane and xylazine anesthetics, visual responses were temporally prolonged compared to responses in awake animals. However, previous reports have demonstrated that anesthetics reduce the sustained portion of sensory responses. With pentobarbital/chloral hydrate anesthesia, only the phasic response to auditory stimuli were still present in recordings from rat primary auditory cortex (Gaese & Ostwald, 2001). In addition, desflurane anesthesia induced differential changes in early and late poststimulus unit responses in V1 elicited by visual flash stimulation, with preserved reactivity of cortical units within 100ms of stimulus presentation but reduced late component responses with deepening anesthesia (Hudetz, Vizuete, & Imas, 2009). The reason for the apparent contradiction with our current results is not entirely clear, but may stem from anesthetic-induced changes in the number of units which were visually-responsive, and thus different findings from analysis at the single unit vs multiunit level. Furthermore, given that the mechanism of action of anesthetic agents varies at the molecular level, it is likely that the differential effects of anesthetic agents extend to the systems level studied here.

Fundamental differences in sensory processing between awake and anesthetized animals are not unique to visual cortex. In agreement with our finding of temporally prolonged sensory-evoked responses during anesthesia, barrel cortex of rats anesthetized with urethane and chloral hydrate exhibited sustained sensory-evoked activity (Devonshire, Grandy, Dommett, & Greenfield, 2010). At anesthetic depths prior to burst suppression, responses to auditory stimulation measured in auditory cortex were

intact during isoflurane anesthesia, whereas visually-elicited modulation in auditory cortex was reduced (Raz et al., 2014). These results nicely complement our results that during anesthesia, sensory responses are maintained only in the primary sensory cortex for the matched modality of stimulation, but responses to sensory stimulation across cortical areas are silenced.

Disruption of Cortico-cortical Connectivity during Anesthesia

Primary sensory cortices do not operate in isolation, but rather send projections to and receive projections from higher cortical areas such as PFC that play a crucial role in defining overall state by mechanisms such as allocation of attention (Buschman & Miller, 2007; Gregoriou, Gotts, Zhou, & Desimone, 2009). Top-down feedback facilitates the processing of task-relevant information (Morishima et al., 2009) and modulates activity in sensory cortices (Anton-Erxleben, Stephan, & Treue, 2009; J. Fritz, Shamma, Elhilali, & Klein, 2003). Intriguingly, recent evidence suggests that impairment of such information flow between cortical areas represents a network mechanism of action for anesthetics (Alkire et al., 2008; Bonhomme, Boveroux, Brichant, Laureys, & Boly, 2012; Raz et al., 2014). Specifically, studies using EEG and fMRI have demonstrated that general anesthesia alters the functional connectivity and information transfer between anterior and posterior areas of the brain (Jordan et al., 2013; Lee et al., 2013). A study of healthy human subjects anesthetized with propofol suggested that cognitive binding, defined as the integration of low-order neural representations of sensory stimuli with high-order cortices, (Mashour, 2004) is disrupted by blocking the projection of the sensory information to high-order processing networks (Liu et al., 2012). Our results support this model and provide increased temporal and spatial resolution of these effects of anesthesia. We found that anesthetics reduced visual- and auditory-evoked phase-locking responses in PFC, and that anesthetics limited responses in V1 elicited by auditory stimulation. This agrees with imaging studies that demonstrated decreases in fronto-parietal functional connectivity and in cross-modal interactions between auditory and visual areas (Boveroux et al., 2010; Schrouff et al., 2011). Furthermore, we found that cortico-cortical interactions between V1 and PFC were disrupted by anesthetics, as assessed through both amplitude and phase measures. A study of event-related potentials in anesthetized rats similarly found reduced long-range antero-posterior coherence (Olga A. Imas, Ropella, Wood, & Hudetz, 2006). In seeming contrast to the disruption of cortical

connectivity during anesthesia, some studies have demonstrated cross-modal responses during isoflurane anesthesia (Land, Engler, Kral, & Engel, 2012; Takagaki, Zhang, Wu, & Lippert, 2008); however, these results were only obtained under conditions of burst suppression and were attributed to propagating waves of activity across cortical areas, which together suggest a different mechanism of action.

In awake animals, we found MUA responses in PFC elicited by visual and auditory stimulation. These results are particularly interesting in light of a previous study which did not find MUA responses in frontal cortex of ferrets in response to auditory stimuli presented during passive listening (J. B. Fritz, David, Radtke-Schuller, Yin, & Shamma, 2010). The stimuli used in our study were “broadband” stimuli (white auditory noise and visual checker board patterns) which may have recruited bottom-up attention, thus explaining this difference. Bottom-up attention is elicited by a salient stimulus and is believed to involve different neural pathways compared to other forms of attention (Miller & Buschman, 2012). Furthermore, the behavioral training status of the animals was different; the animals in the current study were completely untrained while (J. B. Fritz et al., 2010) studied animals which had been trained in an auditory discrimination task. Although the animals were not engaged in a behavioral task during the presentation of the auditory stimuli, the global brain state may have been different because of effortful inhibition of behavioral responses or monitoring for a switch to the active condition. Lastly, it needs to be emphasized that precise anatomical and functional demarcations of ferret frontal cortex are currently missing and it is therefore possible that slight differences in recording locations across studies lead to different findings. Together, these differences may explain the modest spiking responses we found in our study.

Our findings provide insight at the mesoscopic network-level of two cortical areas, which could account for previous reports of reduced functional connectivity as measured through blood oxygenation level dependent (BOLD) signals, and anesthetic-induced decreases in directional connectivity at the level of EEG in human subjects anesthetized with propofol, ketamine, or sevoflurane (Jordan et al., 2013; Lee et al., 2013; Mashour, 2013). Loss of consciousness induced by other pharmacological agents such as the benzodiazepine midazolam also induced a breakdown of cortical functional connectivity (Ferrarelli et al., 2010). Interruption of cortico-cortical signaling agrees with the framework that anesthetics disrupt

cortical functional connectivity and integration (Alkire et al., 2008; Mashour, 2004; Nallasamy & Tsao, 2011), and functionally isolate different neuronal networks (L. D. Lewis et al., 2012). Modeling work has demonstrated that reduced functional connectivity between cortical areas during slow wave sleep may be caused by a shift in the balance of synaptic excitation and inhibition (Esser, Hill, & Tononi, 2009), a mechanism which could also underlie anesthesia and aligns nicely with experiments demonstrating altered synaptic excitation and inhibition induced by anesthesia. Additionally, indirect cortico-thalamo-cortical loops are also impaired by anesthetics and may therefore also contribute to the functional disconnectivity found in our study (Alkire & Miller, 2005).

As with any study, there are limitations to the experiments discussed here. All doses of anesthetics administered corresponded to general anesthesia with the same behavioral state; animals had lost the righting reflex and were unresponsive to toe pinch. This may explain the limited dose-dependent differences. Other studies have more completely investigated differing depths of anesthesia, ranging from sedation to unconscious immobility (Hudetz et al., 2009). In addition, not all animals in the study were recorded from during both the awake and anesthetized conditions. Previous reports have found that spontaneous firing rates can be affected by anesthetics, thus the background MUA activity (sometimes referred to as noise level) could have been reduced in the case of anesthetized recordings. Specifically, work performed in cultured brain slices (Antkowiak & Helfrich-Forster, 1998) and *in vivo* (Hentschke, Schwarz, & Antkowiak, 2005) have demonstrated that volatile anesthetics, including isoflurane, administered at half the concentration used for general anesthesia and at concentrations inducing hypnosis in humans decreased spontaneous action potential firing in neocortical neurons. Somatosensory cortex of urethane anesthetized rats exhibited rhythmic bursts of synchronized action potential firing, which led to decreased overall spontaneous firing rate (Erchova, Lebedev, & Diamond, 2002). Direct pairwise comparisons between the awake and anesthetized condition in the same animal could reduce potential confounds of inter-animal differences in neural dynamics. Such a study design could have been achieved by recording from chronically implanted probes from each animal daily in both the awake and anesthetized conditions. Despite these limitations we believe this work provides a framework for interpreting sensory responses recorded in anesthetized animals and insight into fundamental mechanisms of action of anesthetic agents.

FIGURES

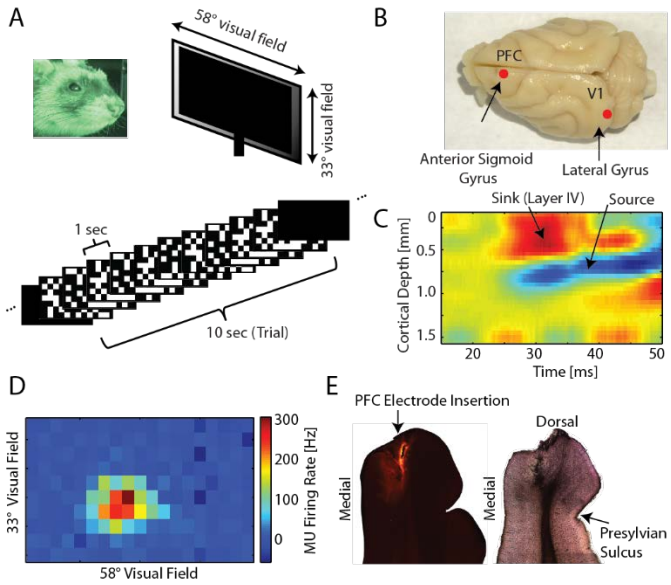

Figure 5.1. Multichannel electrophysiology in V1 and PFC of awake and anesthetized ferrets during presentation of visual stimuli.

(A) Top: Full-field visual stimuli were presented to awake and anesthetized head-fixed ferrets. Bottom: Each trial of visual stimulation consisted of 10 seconds dark (spontaneous activity), 10 seconds of checkerboard frozen noise with abrupt transitions to a new pattern every second, and 10 seconds dark again.

(B) LFP and MU activity were recorded in primary visual cortex (V1, lateral gyrus) and prefrontal cortex (PFC, rostral anterior sigmoid gyrus, 2mm from the midline) during presentation of sensory stimuli.

(C) The use of multichannel depth probes allowed for simultaneous recordings across all cortical layers. Current source density (CSD) analysis was used to determine the depth of putative supragranular, granular, and infragranular layers. The top sink/source pair was indicative of putative granular layer IV. The figure depicts a representative CSD for one recording location in an awake animal.

(D) Receptive field mapping was conducted to provide functional verification of electrode position in V1. Figure depicts a representative receptive field map for one recording electrode for an animal anesthetized with 1.0% isoflurane and xylazine. Map depicts visual field covered by computer

monitor that spanned classical receptive fields and a large amount of surrounding visual space (full-field visual stimulation).

(E) Histological examination to verify electrode location in PFC. Left: Electrode track location (electrode dipped in DiI prior to insertion) in representative coronal section of PFC. Right: Neighboring coronal section (Nissl stain).

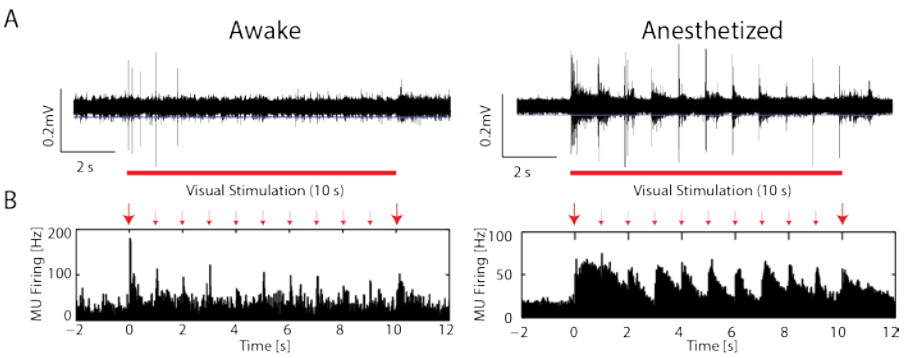

Figure 5.2. Representative MUA responses in awake and anesthetized animals

(A) Representative traces of high-pass filtered MU spiking activity from infragranular layers in an awake (left) and 1.0% isoflurane with xylazine anesthetized (right) animal during visual stimulation. Awake animals exhibited MUA primarily at stimulus onset and the first few transitions of noise patterns. In anesthetized animals, MUA was strongly driven by the stimulus transitions for the entire duration of the visual stimulation. Red bars indicate presentation times of the visual stimulus. Blue lines indicate threshold for extracting spikes; both large amplitude spikes and small amplitude spikes were extracted.

(B) MU spike-time histograms from a single recording session for an awake animal (left) and an animal anesthetized with 1.0% isoflurane with xylazine (right). Raw traces shown in (A) are from these recording sessions. Large red arrows indicate stimulus onset and offset; small red arrows indicate transitions between noise patterns in the stimulus.

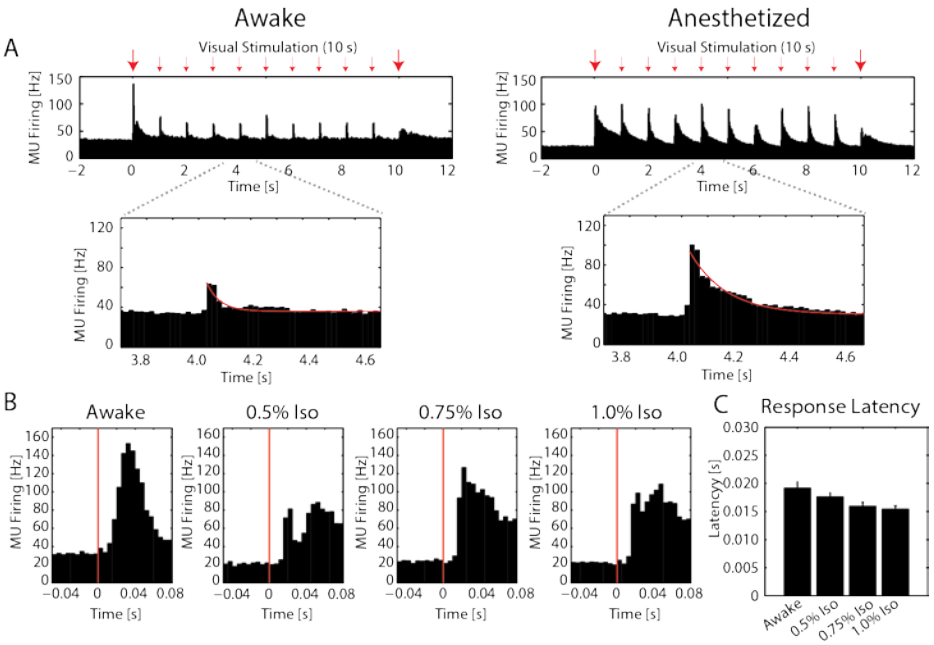

Figure 5.3. Differences in MUA response dynamics between awake and anesthetized animals.

(A) Group-averaged MU spike-time histograms. Top: In awake animals (left), MU firing was temporally precise and aligned to transitions in the visual stimulus. In 1.0% isoflurane with xylazine anesthetized animals (right), firing rate remained elevated following transitions to subsequent noise patterns during visual stimulation. Large red arrows indicate stimulus onset and offset; small red arrows indicate transitions between noise patterns in the stimulus. Bottom: MUA exhibited a shorter decay time-constant in awake animals compared to anesthetized animals. Red line: Exponential fit of decay time-course. All plots show averages across cortical layers.

(B) Group-averaged MU spiking response latency in awake and anesthetized animals. 5 ms binning was used for finer temporal resolution. All plots show averages across cortical layers. Red lines: Stimulus onset.

(C) Group-averaged mean MU response latency, defined as exceeding a threshold of 2*std of baseline spiking activity. Response latency was not significantly different between awake and anesthetized animals. All plots show averages across cortical layers. Error bars indicate 1 sem.

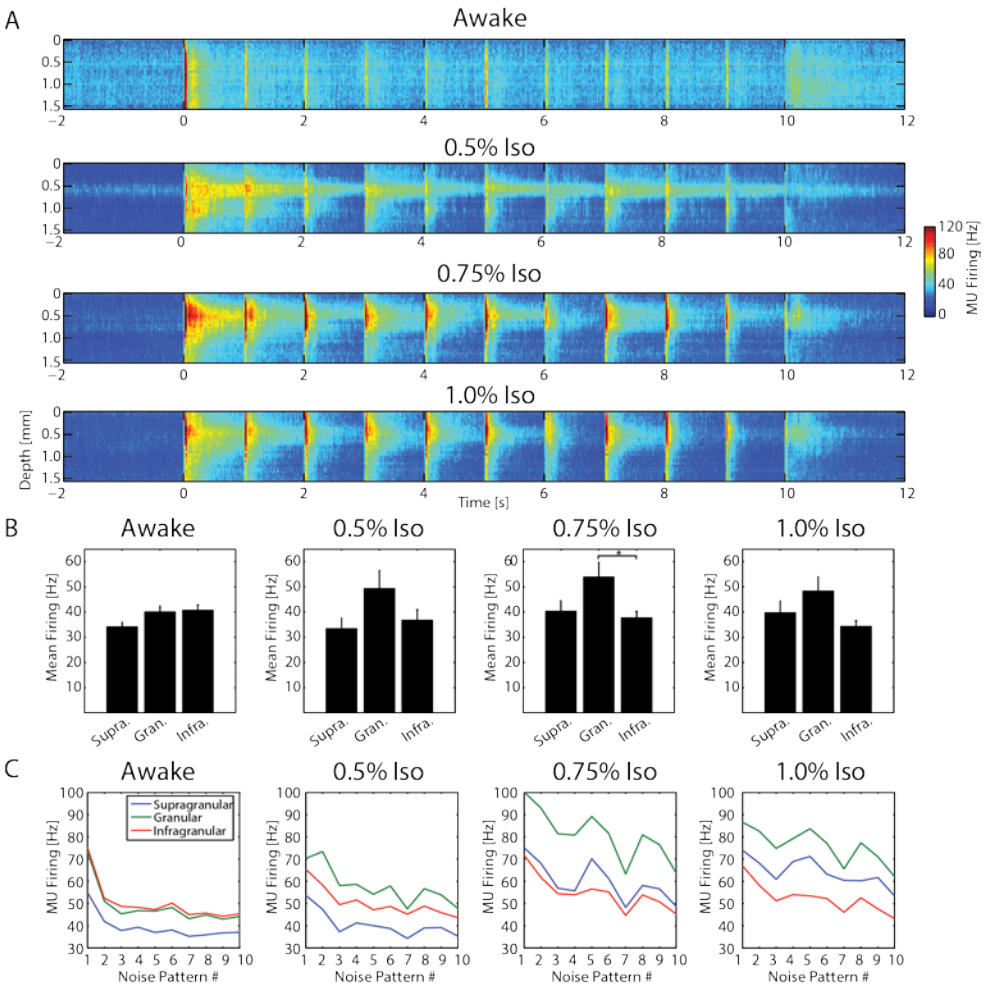

Figure 5.4. Disruption of the laminar distribution and adaptation of visually-evoked MUA responses.

(A) Group-averaged MU firing rate across cortical layers. Compared to awake animals (top), increasing concentrations of anesthetic (bottom, 0.5%, 0.75%, 1.0% isoflurane all with xylazine) altered the laminar distribution of MU firing, notably increasing relative strength of the response in putative layer IV (electrode depth 0.3mm – 0.6mm).

(B) Group-averaged mean firing rate across 10 seconds of visual stimulation for supragranular, granular, and infragranular layers. Awake animals exhibited slightly higher MU firing rate in granular and infragranular layers compared to supragranular layers. 0.5%, 0.75%, and 1.0% isoflurane all with xylazine increased firing rate in granular layers at the trend level relative to supragranular and infragranular layers. Error bars indicate 1 sem. * indicates significantly different at $p < 0.05$.

(C) Response to each of the ten transitions between subsequent noise patterns during the visual stimulus, calculated as the mean MU firing rate for 200ms after each screen change, for supragranular (blue), granular (green), and infragranular (red) layers. Awake animals exhibited pronounced spike rate adaptation for later noise patterns, while anesthetics slowed this adaptation of MUA.

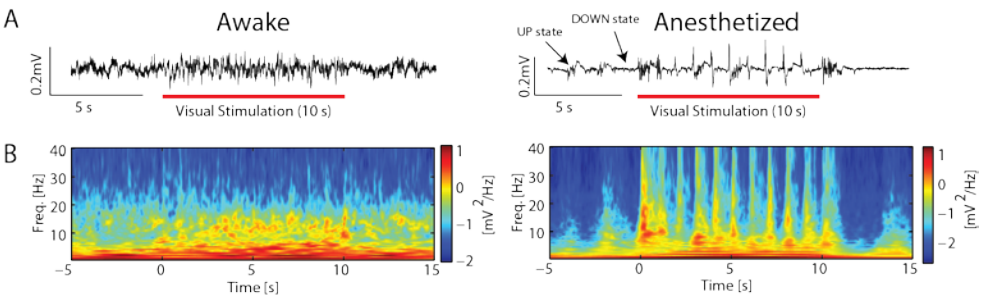

Figure 5.5. Representative LFP responses to visual input in V1

(A) Representative LFP traces from infragranular layers in V1 in an awake (left) and 1.0% isoflurane with xylazine anesthetized (right) animal during visual stimulation. Note UP and DOWN states in the LFP trace from the anesthetized animal. Red bars indicate presentation of visual stimulus.

(B) Spectrograms of single recordings from awake (left) and 1.0% isoflurane with xylazine anesthetized (right) animals. Raw traces shown in (A) are from these recording sessions. Plots show averages across cortical layers.

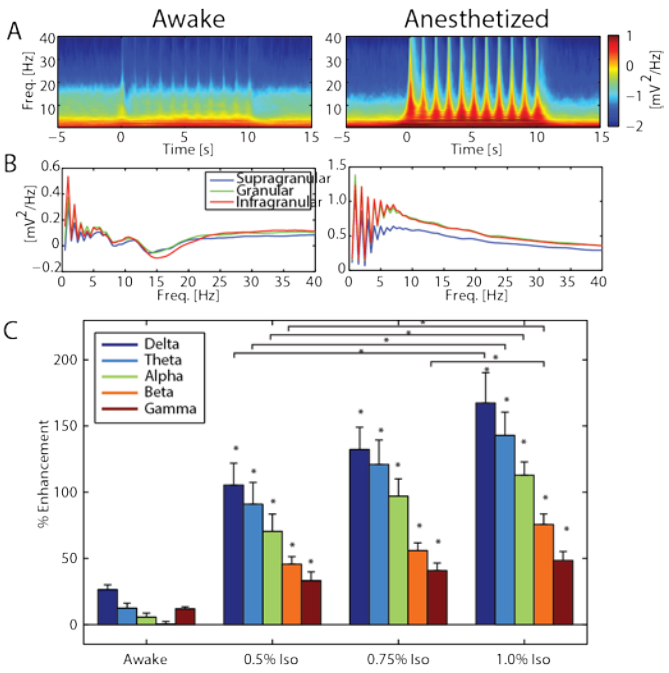

Figure 5.6. Differences in mesoscale LFP responses to visual input in V1

(A) Group-averaged spectrograms of awake (left) and 1.0% isoflurane with xylazine anesthetized (right) animals. Plots show averages across cortical layers.

(B) Group-averaged ratio of spectral power during visual stimulation to spectral power during spontaneous activity prior to visual stimulation by cortical layer. In both awake (left) and 1.0% isoflurane with xylazine anesthetized (right) animals, the 1Hz structure of the visual stimulus is apparent in the activity of all cortical layers.

(C) Enhancement ratio of spectral power during visual stimulation to spectral power during spontaneous activity prior to visual stimulation. Plots show averages across cortical layers. In both awake and anesthetized animals (0.5%, 0.75%, and 1.0% isoflurane all with xylazine), all frequency bands exhibited increased power. Greater enhancement in power was evident as isoflurane concentration increased. Error bars indicate 1 sem. * above bars indicates significantly different from values in awake animals, $p < 0.05$. Additional significant differences at $p < 0.05$ are indicated.

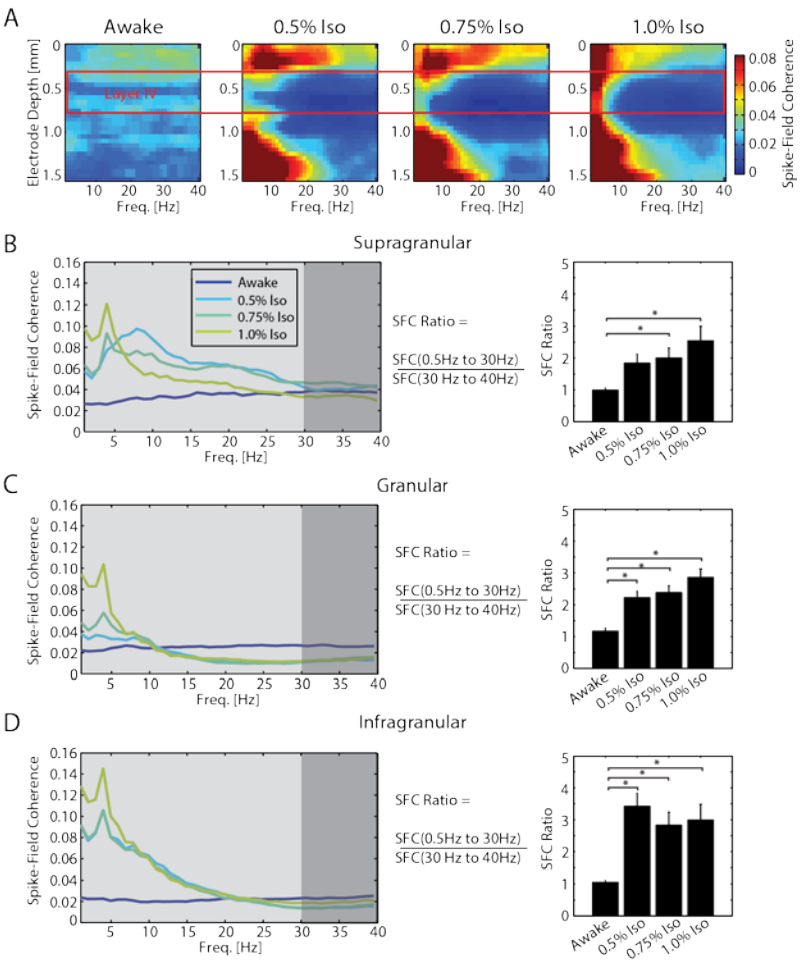

Figure 5.7. Anesthetics increased spike-field coherence (SFC) in V1 during visual stimulation, preferentially at low frequencies.

(A) SFC was used to quantify the interaction between mesoscopic LFP frequency structure and microscopic MUA during presentation of the visual stimulus. This figure shows group-averaged SFC by cortical depth during presentation of visual stimulation. SFC was low in awake animals across cortical layers (left). Anesthesia induced layer-specific changes to SFC (right, 0.5%, 0.75%, and 1.0% isoflurane all with xylazine). Specifically, compared to awake animals, anesthetized animals exhibited increased SFC in supragranular and infragranular layers, increased SFC at low frequencies in granular layers, and decreased SFC at higher frequencies in granular layers. Putative granular layer IV (electrode depth 0.3mm-0.6mm) indicated by red box.

(B) The SFC ratio (mean SFC from 0.5Hz to 30Hz / mean SFC from 30Hz to 40Hz) was used to indicate the relative enhancement of low frequency SFC. In supragranular layers, anesthetics

enhanced SFC broadly across frequencies compared to SFC in the awake animal. Error bars indicate 1 sem. * indicates significantly different at $p < 0.05$.

(C) In granular layers, anesthetics enhanced SFC in low frequencies in a dose-dependent manner and decreased SFC at higher frequencies compared to SFC in awake animals. Error bars indicate 1 sem. * indicates significantly different at $p < 0.05$.

(D) Anesthetics enhanced SFC in low frequencies most prominently in infragranular layers. Error bars indicate 1 sem. * indicates significantly different at $p < 0.05$.

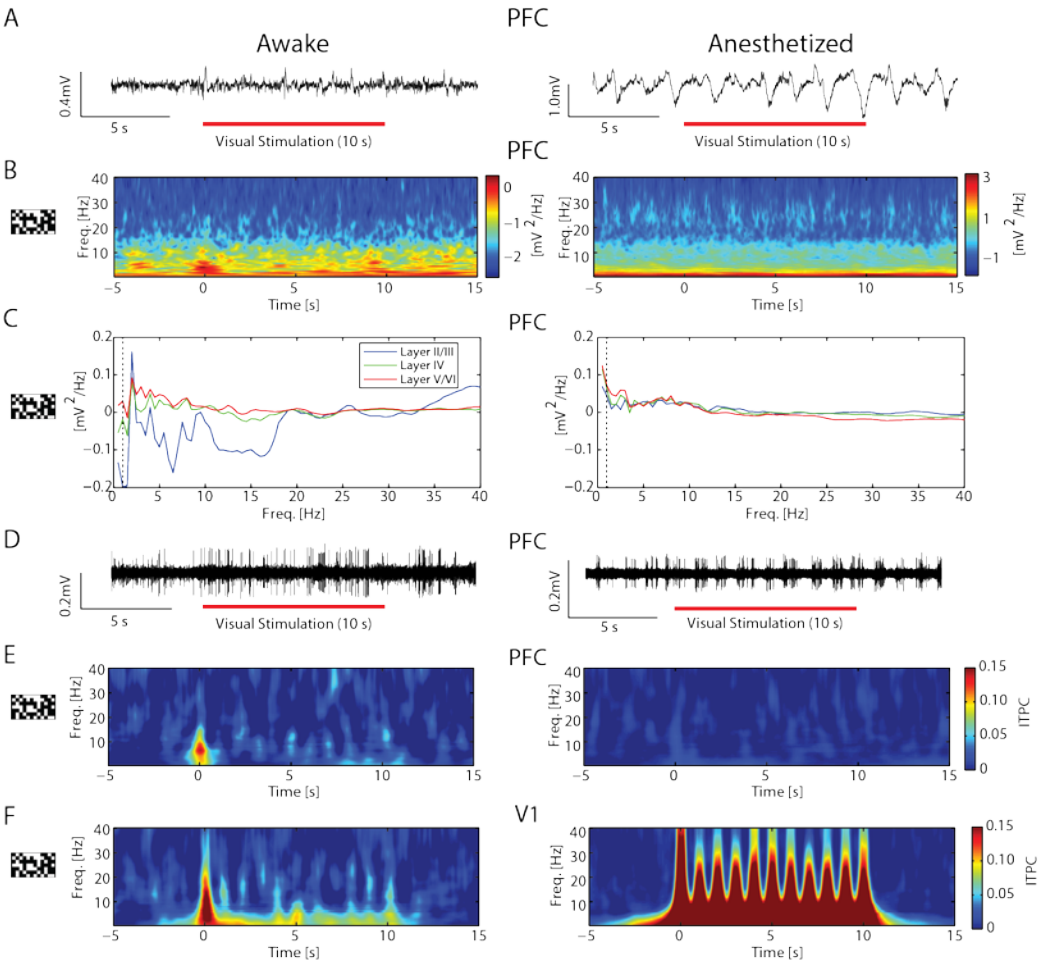

Figure 5.8. Visual stimulation induced spectral modulation and increased inter-trial phase coherence (ITPC) in PFC of awake animals, but not in PFC of anesthetized animals.

(A) Representative LFP traces from infragranular layers in PFC in an awake (left) and 1.0% isoflurane with xylazine anesthetized (right) animal during visual stimulation. Red bars indicate presentation of the visual stimulus.

(B) Spectrograms of single recordings from PFC in awake (left) and 1.0% isoflurane with xylazine anesthetized (right) animals. In awake animals, the onset of the visual stimulus at time = 0s induced spectral modulation, particularly in low frequencies. Plots show averages across cortical layers.

(C) Group-averaged ratio of PFC spectral power during visual stimulation to spectral power during spontaneous activity, by cortical layer. In awake animals (left), the visual stimulation induced spectral modulation in superficial layers according to the temporal pattern of the visual stimulus. In

anesthetized animals (right), superficial layers exhibited minimal spectral modulation by the visual stimulus. Dashed lines indicate 1Hz.

(D) Representative traces of high-pass filtered MU spiking activity from PFC infragranular layers in an awake (left) and 1.0% isoflurane with xylazine anesthetized (right) animal during visual stimulation. Awake animals exhibited increased MUA at stimulus onset. In anesthetized animals, MUA was highly rhythmic, likely driven by anesthesia.

(E) Phase-coherence was used to probe for responses to sensory stimuli. Group-averaged ITPC increased at the onset of visual stimulation in PFC of awake animals (left). In PFC of anesthetized animals, there was no increase of group-averaged phase-coherence induced by visual stimulation (right). Plots show averages across cortical layers.

(F) V1 in awake (left) and anesthetized (right) animals exhibited increased group-averaged phase-coherence during presentation of the visual stimulus. Plots show averages across cortical layers.

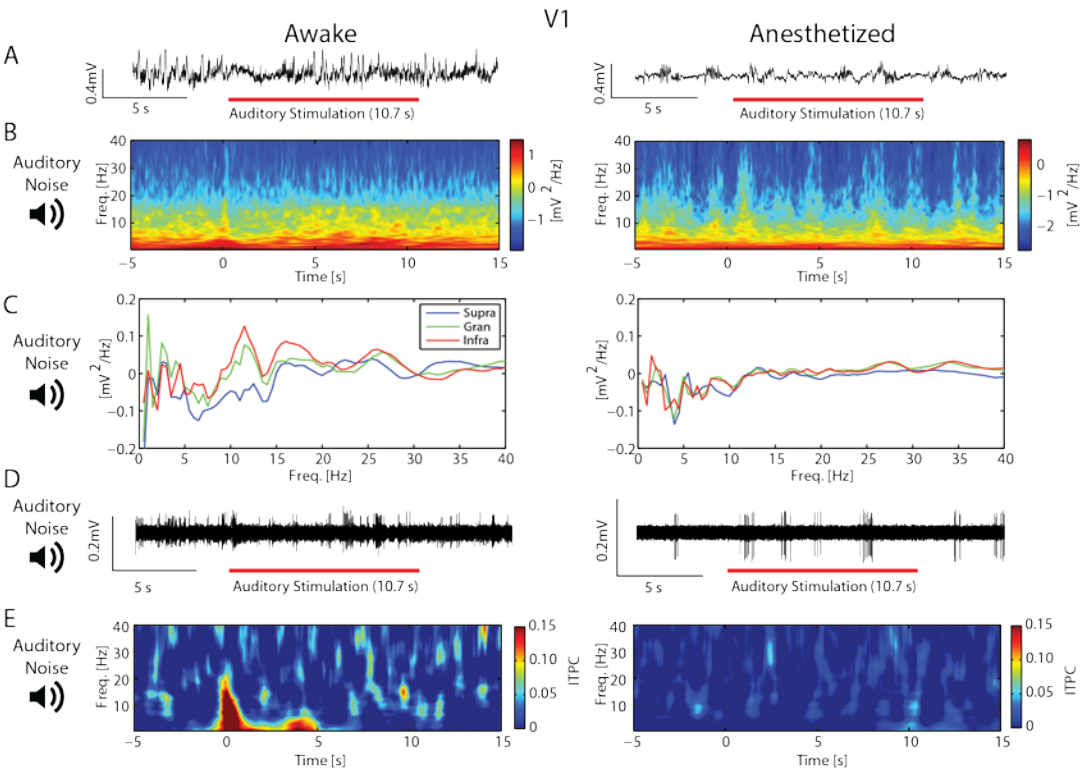

Figure 5.9. V1 spectral modulation and increase in ITPC by auditory stimulation were suppressed by anesthetics.

(A) Representative LFP traces from infragranular layers in V1 in an awake (left) and 1.0% isoflurane with xylazine anesthetized (right) animal during auditory stimulation. Red bars indicate presentation of the auditory stimulus.

(B) Spectrograms of single recordings from V1 in awake (left) and 1.0% isoflurane with xylazine anesthetized (right) animals. In awake animals, the onset of the auditory stimulus at time = 0s induced spectral modulation. Plots show averages across cortical layers.

(C) Group-averaged ratio of V1 spectral power during auditory stimulation to spectral power during spontaneous activity, by cortical layer. In awake animals (left), the strongest effect of auditory stimulation on spectral power was found at low frequencies in the granular layer and in the alpha band in infragranular layers. These dynamics were absent in anesthetized animals (right).

(D) Representative traces of high-pass filtered MU spiking activity from V1 infragranular layers in an awake (left) and 1.0% isoflurane with xylazine anesthetized (right) animal during auditory stimulation.

(E) Auditory stimulation elicited increased group-averaged phase-coherence in V1 of awake animals (left). In V1 of anesthetized animals, there was no detectable increase in group-averaged phase-coherence induced by auditory stimulation (right). Plots show averages across cortical layers.

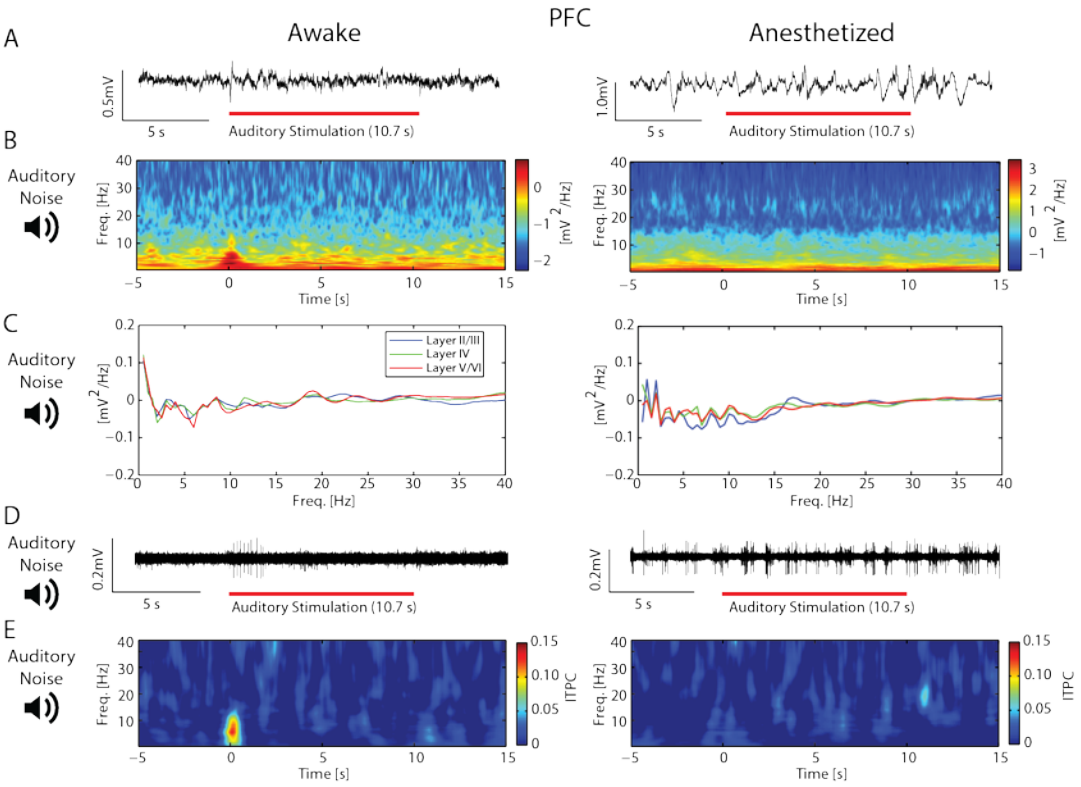

Figure 5.10. Auditory stimulation induced increase in spectral power and ITPC in PFC of awake animals.

(A) Representative LFP traces from infragranular layers in PFC in an awake (left) and 1.0% isoflurane with xylazine anesthetized (right) animal during auditory stimulation. Red bars indicate presentation of the auditory stimulus.

(B) Spectrograms of single recordings from PFC of awake (left) and 1.0% isoflurane with xylazine anesthetized (right) animals. In only the awake animal, the onset of the auditory stimulus at time = 0s induced spectral modulation. Plots show averages across cortical layers.

(C) Group-averaged ratio of PFC spectral power during auditory stimulation to spectral power during spontaneous activity, by cortical layer.

(D) Representative traces of high-pass filtered MU spiking activity from PFC infragranular layers in an awake (left) and 1.0% isoflurane with xylazine anesthetized (right) animal during auditory stimulation. Awake animals exhibited increased MUA at stimulus onset. In anesthetized animals, MUA was highly rhythmic, likely driven by anesthesia.

(E) PFC in awake animals (left) exhibited increased group-averaged ITPC at the onset of auditory noise stimulation. There was no detectable increase in group-averaged phase-coherence induced by auditory noise stimulation in PFC of anesthetized animals (right). Plots show averages across cortical layers.

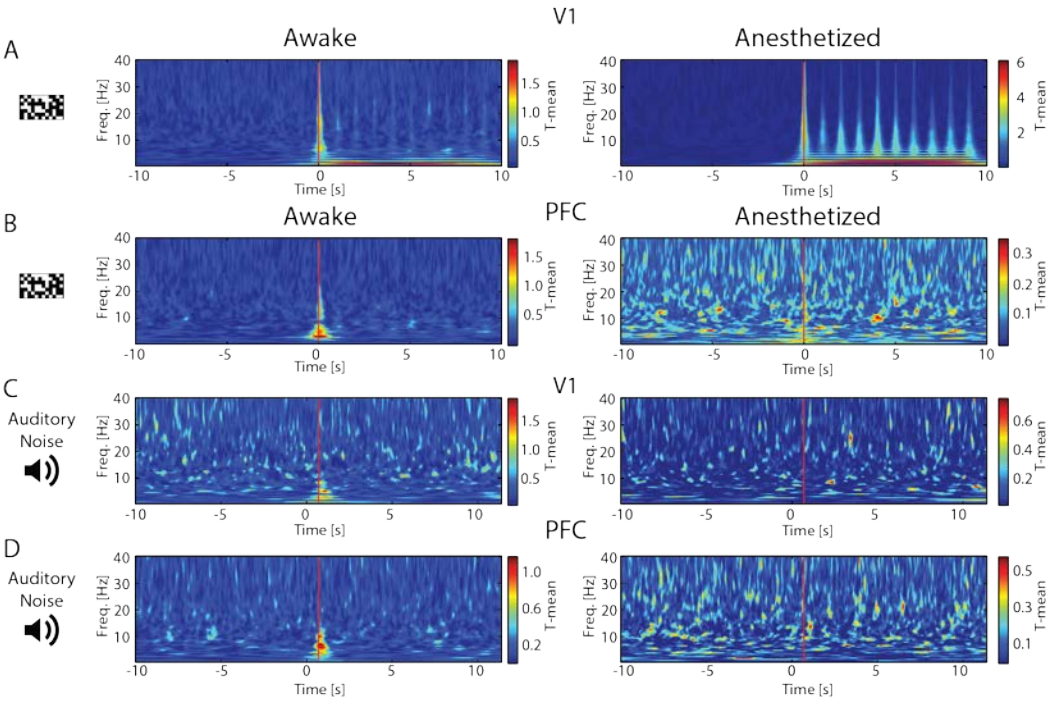

Figure 5.11. Inter-trial phase coherence is likely driven by not only phase resetting but also stimulation-induced evoked responses.

(A) We adopted the approach of (Martinez-Montes et al., 2008) to find the time points and frequencies at which there was a significant difference in sample mean of the wavelet coefficients compared to the baseline rest period (the T-mean). Group-averaged results demonstrate that in V1, visual stimulation induced an evoked response for both awake (left) and anesthetized (right) animals, according to the temporal patterning of the visual stimulus. This corresponds to ITPC results in Figure 5.8F. Plots show averages across cortical layers. Red line indicates stimulus onset.

(B) Group-averaged results demonstrate that in PFC, visual stimulation induced an evoked response at stimulus onset for awake animals (left) but this effect was absent in anesthetized animals (right). This corresponds to ITPC results in Figure 5.8E. Plots show averages across cortical layers. Red line indicates stimulus onset.

(C) In V1, auditory stimulation induced an evoked response at stimulus onset in awake (left) but not anesthetized (right) animals. This corresponds to ITPC results in Figure 5.9E. Plots show averages across cortical layers. Red line indicates stimulus onset.

(D) In PFC, auditory stimulation induced an evoked response at stimulus onset in awake (left) but not anesthetized (right) animals. This corresponds to ITPC results in Figure 5.10E. Plots show averages across cortical layers. Red line indicates stimulus onset.

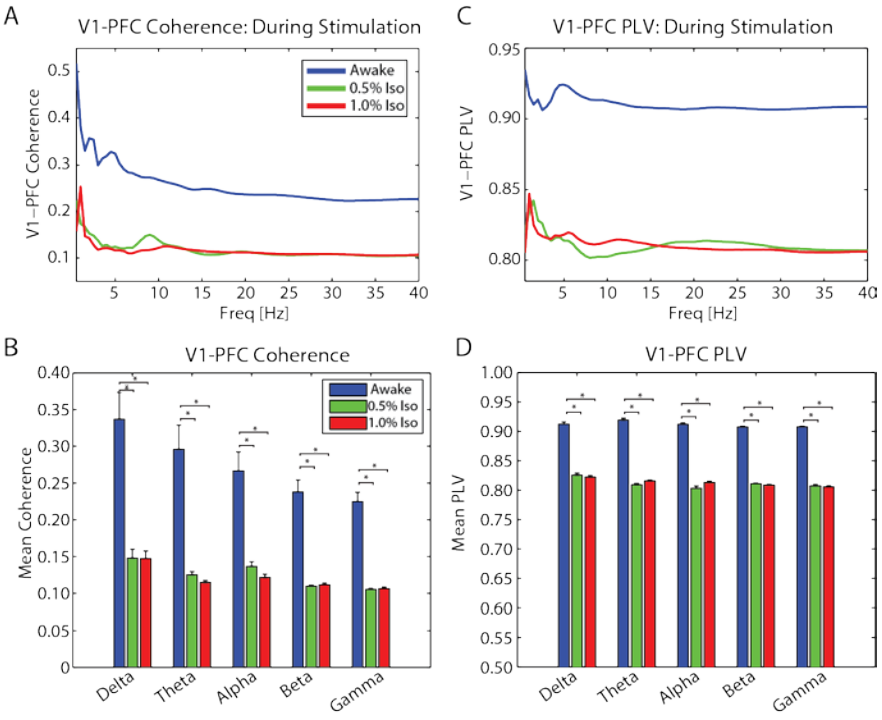

Figure 5.12. Functional connectivity: Spectral coherence and phase synchrony during visual stimulation between V1 and PFC were reduced with isoflurane/xylazine anesthetics.

(A) Single electrodes in V1 and PFC were used to assess functional connectivity between these cortical areas. Group-averaged and time-averaged spectral coherence between V1 and PFC during visual stimulation. Spectral coherence was highest in awake animals (blue line) across frequencies compared to animals anesthetized with 0.5% isoflurane with xlyazine (green line) or 1.0% isoflurane with xlyazine (red line).

(B) Mean spectral coherence between V1 and PFC during stimulation in each frequency band. Error bars indicate 1 sem. * indicates significantly different at $p < 0.05$.

(C) Group-averaged and time-averaged phase synchrony between V1 and PFC (V1-PFC PLV) was highest in awake animals (blue line) across frequencies compared to animals anesthetized with 0.5% isoflurane with xlyazine (green line) or 1.0% isoflurane with xlyazine (red line). Awake animals exhibited a local peak in V1-PFC PLV in the theta frequency band.

(D) Mean V1-PFC PLV during visual stimulation in each frequency band. Error bars indicate 1 sem. * indicates significantly different at $p < 0.05$.

REFERENCES

Alkire, M. T. (2008). Loss of effective connectivity during general anesthesia. *International anesthesiology clinics, 46*(3), 55-73. doi: 10.1097/AIA.0b013e3181755dc6

Alkire, M. T., Hudetz, A. G., & Tononi, G. (2008). Consciousness and anesthesia. *Science, 322*(5903), 876-880. doi: 10.1126/science.1149213

Alkire, M. T., & Miller, J. (2005). General anesthesia and the neural correlates of consciousness. *Prog Brain Res, 150*, 229-244. doi: 10.1016/S0079-6123(05)50017-7

Antkowiak, B., & Helfrich-Forster, C. (1998). Effects of small concentrations of volatile anesthetics on action potential firing of neocortical neurons in vitro. *Anesthesiology, 88*(6), 1592-1605.

Anton-Erxleben, K., Stephan, V. M., & Treue, S. (2009). Attention reshapes center-surround receptive field structure in macaque cortical area MT. *Cereb Cortex, 19*(10), 2466-2478. doi: 10.1093/cercor/bhp002

Binzegger, T., Douglas, R. J., & Martin, K. A. (2009). Topology and dynamics of the canonical circuit of cat V1. *Neural networks : the official journal of the International Neural Network Society, 22*(8), 1071-1078. doi: 10.1016/j.neunet.2009.07.011

Bonhomme, V., Boveroux, P., Brichant, J. F., Laureys, S., & Boly, M. (2012). Neural correlates of consciousness during general anesthesia using functional magnetic resonance imaging (fMRI). *Arch Ital Biol, 150*(2-3), 155-163. doi: 10.4449/aib.v150i2.1242

Boveroux, P., Vanhaudenhuyse, A., Bruno, M. A., Noirhomme, Q., Lauwick, S., Luxen, A., . . . Boly, M. (2010). Breakdown of within- and between-network resting state functional magnetic resonance imaging connectivity during propofol-induced loss of consciousness. *Anesthesiology, 113*(5), 1038-1053. doi: 10.1097/ALN.0b013e3181f697f5

Brainard, D. H. (1997). The Psychophysics Toolbox. *Spatial vision, 10*(4), 433-436.

Brown, E. N., Lydic, R., & Schiff, N. D. (2010). General anesthesia, sleep, and coma. *The New England journal of medicine, 363*(27), 2638-2650. doi: 10.1056/NEJMra0808281

Brown, E. N., Purdon, P. L., & Van Dort, C. J. (2011). General Anesthesia and Altered States of Arousal: A Systems Neuroscience Analysis. *Annual Review of Neuroscience, Vol 34, 34*, 601-628. doi: DOI 10.1146/annurev-neuro-060909-153200

Buschman, T. J., & Miller, E. K. (2007). Top-down versus bottom-up control of attention in the prefrontal and posterior parietal cortices. *Science, 315*(5820), 1860-1862. doi: 10.1126/science.1138071

Campagna, J. A., Miller, K. W., & Forman, S. A. (2003). Mechanisms of actions of inhaled anesthetics. *The New England journal of medicine, 348*(21), 2110-2124. doi: 10.1056/NEJMra021261

Cantone, G., Xiao, J., McFarlane, N., & Levitt, J. B. (2005). Feedback connections to ferret striate cortex: direct evidence for visuotopic convergence of feedback inputs. *The Journal of comparative neurology, 487*(3), 312-331. doi: 10.1002/cne.20570

Chandler, D. J., Lamperski, C. S., & Waterhouse, B. D. (2013). Identification and distribution of projections from monoaminergic and cholinergic nuclei to functionally differentiated subregions of prefrontal cortex. *Brain Res, 1522*, 38-58. doi: 10.1016/j.brainres.2013.04.057

Davidson, G., & Plumb, D. C. (2003). *Veterinary drug handbook* (Client information ed.). Ames, Iowa: Distributed by Iowa State Press.

Detsch, O., Vahle-Hinz, C., Kochs, E., Siemers, M., & Bromm, B. (1999). Isoflurane induces dose-dependent changes of thalamic somatosensory information transfer. *Brain Res, 829*(1-2), 77-89.

Devonshire, I. M., Grandy, T. H., Dommett, E. J., & Greenfield, S. A. (2010). Effects of urethane anaesthesia on sensory processing in the rat barrel cortex revealed by combined optical imaging and electrophysiology. *Eur J Neurosci, 32*(5), 786-797. doi: 10.1111/j.1460-9568.2010.07322.x

Duque, A., & McCormick, D. A. (2010). Circuit-based localization of ferret prefrontal cortex. *Cereb Cortex, 20*(5), 1020-1036. doi: 10.1093/cercor/bhp164

Eckle, V. S., Digruccio, M. R., Uebele, V. N., Renger, J. J., & Todorovic, S. M. (2012). Inhibition of T-type calcium current in rat thalamocortical neurons by isoflurane. *Neuropharmacology, 63*(2), 266-273. doi: 10.1016/j.neuropharm.2012.03.018

Erchova, I. A., Lebedev, M. A., & Diamond, M. E. (2002). Somatosensory cortical neuronal population activity across states of anaesthesia. *Eur J Neurosci, 15*(4), 744-752.

Esser, S. K., Hill, S., & Tononi, G. (2009). Breakdown of effective connectivity during slow wave sleep: investigating the mechanism underlying a cortical gate using large-scale modeling. *Journal of neurophysiology, 102*(4), 2096-2111. doi: 10.1152/jn.00059.2009

Ferrarelli, F., Massimini, M., Sarasso, S., Casali, A., Riedner, B. A., Angelini, G., . . . Pearce, R. A. (2010). Breakdown in cortical effective connectivity during midazolam-induced loss of consciousness. *Proceedings of the National Academy of Sciences of the United States of America, 107*(6), 2681-2686. doi: 10.1073/pnas.0913008107

Fries, P., Reynolds, J. H., Rorie, A. E., & Desimone, R. (2001). Modulation of oscillatory neuronal synchronization by selective visual attention. *Science, 291*(5508), 1560-1563. doi: 10.1126/science.291.5508.1560

Fritz, J., Shamma, S., Elhilali, M., & Klein, D. (2003). Rapid task-related plasticity of spectrotemporal receptive fields in primary auditory cortex. *Nat Neurosci, 6*(11), 1216-1223. doi: 10.1038/nn1141

Fritz, J. B., David, S. V., Radtke-Schuller, S., Yin, P., & Shamma, S. A. (2010). Adaptive, behaviorally gated, persistent encoding of task-relevant auditory information in ferret frontal cortex. *Nat Neurosci, 13*(8), 1011-1019. doi: 10.1038/nn.2598

Gabernet, L., Jadhav, S. P., Feldman, D. E., Carandini, M., & Scanziani, M. (2005). Somatosensory integration controlled by dynamic thalamocortical feed-forward inhibition. *Neuron, 48*(2), 315-327. doi: 10.1016/j.neuron.2005.09.022

Gaese, B. H., & Ostwald, J. (2001). Anesthesia changes frequency tuning of neurons in the rat primary auditory cortex. *J Neurophysiol, 86*(2), 1062-1066.

Gilbert, C. D. (1977). Laminar differences in receptive field properties of cells in cat primary visual cortex. *J Physiol, 268*(2), 391-421.

Goupillaud, P., Grossmann, A., & Morlet, J. (1984). Cycle-Octave and Related Transforms in Seismic Signal Analysis. *Geoexploration, 23*(1), 85-102. doi: Doi 10.1016/0016-7142(84)90025-5

Greenberg, D. S., Houweling, A. R., & Kerr, J. N. (2008). Population imaging of ongoing neuronal activity in the visual cortex of awake rats. *Nat Neurosci, 11*(7), 749-751. doi: 10.1038/nn.2140

Gregoriou, G. G., Gotts, S. J., Zhou, H., & Desimone, R. (2009). High-frequency, long-range coupling between prefrontal and visual cortex during attention. *Science, 324*(5931), 1207-1210. doi: 10.1126/science.1171402

Haider, B., Duque, A., Hasenstaub, A. R., & McCormick, D. A. (2006). Neocortical network activity in vivo is generated through a dynamic balance of excitation and inhibition. *J Neurosci, 26*(17), 4535-4545. doi: 10.1523/JNEUROSCI.5297-05.2006

Haider, B., Hausser, M., & Carandini, M. (2013). Inhibition dominates sensory responses in the awake cortex. *Nature, 493*(7430), 97-100. doi: 10.1038/nature11665

Heinke, W., & Koelsch, S. (2005). The effects of anesthetics on brain activity and cognitive function. *Current opinion in anaesthesiology, 18*(6), 625-631. doi: 10.1097/01.aco.0000189879.67092.12

Heinke, W., & Schwarzbauer, C. (2001). Subanesthetic isoflurane affects task-induced brain activation in a highly specific manner: a functional magnetic resonance imaging study. *Anesthesiology, 94*(6), 973-981.

Heinke, W., & Schwarzbauer, C. (2002). In vivo imaging of anaesthetic action in humans: approaches with positron emission tomography (PET) and functional magnetic resonance imaging (fMRI). *British journal of anaesthesia, 89*(1), 112-122.

Hemmings, H. C., Jr. (2009). Sodium channels and the synaptic mechanisms of inhaled anaesthetics. *Br J Anaesth, 103*(1), 61-69. doi: 10.1093/bja/aep144

Hemmings, H. C., Jr., Akabas, M. H., Goldstein, P. A., Trudell, J. R., Orser, B. A., & Harrison, N. L. (2005). Emerging molecular mechanisms of general anesthetic action. *Trends Pharmacol Sci, 26*(10), 503-510. doi: 10.1016/j.tips.2005.08.006

Hentschke, H., Schwarz, C., & Antkowiak, B. (2005). Neocortex is the major target of sedative concentrations of volatile anaesthetics: strong depression of firing rates and increase of GABAA receptor-mediated inhibition. *Eur J Neurosci, 21*(1), 93-102.

Higley, M. J., & Contreras, D. (2006). Balanced excitation and inhibition determine spike timing during frequency adaptation. *The Journal of neuroscience : the official journal of the Society for Neuroscience, 26*(2), 448-457. doi: 10.1523/JNEUROSCI.3506-05.2006

Hirsch, J. A., & Martinez, L. M. (2006). Laminar processing in the visual cortical column. *Curr Opin Neurobiol, 16*(4), 377-384. doi: 10.1016/j.conb.2006.06.014

Hubel, D. H., & Wiesel, T. N. (1959). Receptive fields of single neurones in the cat's striate cortex. *The Journal of physiology, 148*, 574-591.

Hudetz, A. G., & Imas, O. A. (2007). Burst activation of the cerebral cortex by flash stimuli during isoflurane anesthesia in rats. *Anesthesiology, 107*(6), 983-991. doi: 10.1097/01.anes.0000291471.80659.55

Hudetz, A. G., Vizuete, J. A., & Imas, O. A. (2009). Desflurane selectively suppresses long-latency cortical neuronal response to flash in the rat. *Anesthesiology, 111*(2), 231-239. doi: 10.1097/ALN.0b013e3181ab671e

Imas, O. A., Ropella, K. M., Ward, B. D., Wood, J. D., & Hudetz, A. G. (2005). Volatile anesthetics enhance flash-induced gamma oscillations in rat visual cortex. *Anesthesiology, 102*(5), 937-947.

Imas, O. A., Ropella, K. M., Wood, J. D., & Hudetz, A. G. (2006). Isoflurane disrupts anterio-posterior phase synchronization of flash-induced field potentials in the rat. *Neurosci Lett, 402*(3), 216-221.

John, E. R., Prichep, L. S., Kox, W., Valdes-Sosa, P., Bosch-Bayard, J., Aubert, E., . . . Gugino, L. D. (2001). Invariant reversible QEEG effects of anesthetics. *Consciousness and Cognition, 10*(2), 165-183. doi: DOI 10.1006/ccog.2001.0507

Jordan, D., Ilg, R., Riedl, V., Schorer, A., Grimberg, S., Neufang, S., . . . Schneider, G. (2013). Simultaneous electroencephalographic and functional magnetic resonance imaging indicate impaired cortical top-down processing in association with anesthetic-induced unconsciousness. *Anesthesiology, 119*(5), 1031-1042. doi: 10.1097/ALN.0b013e3182a7ca92

Katoh, T., Suzuki, A., & Ikeda, K. (1998). Electroencephalographic derivatives as a tool for predicting the depth of sedation and anesthesia induced by sevoflurane. *Anesthesiology, 88*(3), 642-650.

Kayser, C., Logothetis, N. K., & Panzeri, S. (2010). Millisecond encoding precision of auditory cortex neurons. *Proceedings of the National Academy of Sciences of the United States of America, 107*(39), 16976-16981. doi: 10.1073/pnas.1012656107

Kimura, R., Safari, M. S., Mirnajafi-Zadeh, J., Kimura, R., Ebina, T., Yanagawa, Y., . . . Tsumoto, T. (2014). Curtailing effect of awakening on visual responses of cortical neurons by cholinergic activation of inhibitory circuits. *The Journal of neuroscience : the official journal of the Society for Neuroscience, 34*(30), 10122-10133. doi: 10.1523/JNEUROSCI.0863-14.2014

Kohn, D. F. (1997). *Anesthesia and analgesia in laboratory animals*. San Diego: Academic Press.

Kreuzer, M., Hentschke, H., Antkowiak, B., Schwarz, C., Kochs, E. F., & Schneider, G. (2010). Cross-approximate entropy of cortical local field potentials quantifies effects of anesthesia--a pilot study in rats. *BMC Neurosci, 11*, 122. doi: 10.1186/1471-2202-11-122

Krieg, J., Trebuchon-Da Fonseca, A., Martinez-Montes, E., Marquis, P., Liegeois-Chauvel, C., & Benar, C. G. (2011). A comparison of methods for assessing alpha phase resetting in electrophysiology, with application to intracerebral EEG in visual areas. *Neuroimage, 55*(1), 67-86. doi: 10.1016/j.neuroimage.2010.11.058

Lachaux, J. P., Rodriguez, E., Martinerie, J., & Varela, F. J. (1999). Measuring phase synchrony in brain signals. *Hum Brain Mapp, 8*(4), 194-208.

Lamme, V. A., Zipser, K., & Spekreijse, H. (1998). Figure-ground activity in primary visual cortex is suppressed by anesthesia. *Proc Natl Acad Sci U S A, 95*(6), 3263-3268.

Land, R., Engler, G., Kral, A., & Engel, A. K. (2012). Auditory evoked bursts in mouse visual cortex during isoflurane anesthesia. *PLoS One, 7*(11), e49855. doi: 10.1371/journal.pone.0049855

Lee, U., Ku, S., Noh, G., Baek, S., Choi, B., & Mashour, G. A. (2013). Disruption of frontal-parietal communication by ketamine, propofol, and sevoflurane. *Anesthesiology, 118*(6), 1264-1275. doi: 10.1097/ALN.0b013e31829103f5

Lennox, W. G. (1949). Influence of drugs on the human electroencephalogram. *Electroencephalography and clinical neurophysiology, 1*, 45-51. doi: 10.1016/0013-4694(49)90162-5

Lewis, L. D., Weiner, V. S., Mukamel, E. A., Donoghue, J. A., Eskandar, E. N., Madsen, J. R., . . . Purdon, P. L. (2012). Rapid fragmentation of neuronal networks at the onset of propofol-induced unconsciousness. *Proceedings of the National Academy of Sciences, 109*, E3377-E3386. doi: 10.1073/pnas.1210907109

Lewis, L. D., Weiner, V. S., Mukamel, E. A., Donoghue, J. A., Eskandar, E. N., Madsen, J. R., . . . Purdon, P. L. (2012). Rapid fragmentation of neuronal networks at the onset of propofol-induced unconsciousness. *Proc Natl Acad Sci U S A, 109*(49), E3377-3386. doi: 10.1073/pnas.1210907109

Liu, X., Lauer, K. K., Ward, B. D., Rao, S. M., Li, S. J., & Hudetz, A. G. (2012). Propofol disrupts functional interactions between sensory and high-order processing of auditory verbal memory. *Hum Brain Mapp, 33*(10), 2487-2498. doi: 10.1002/hbm.21385

Lu, T., Liang, L., & Wang, X. (2001). Temporal and rate representations of time-varying signals in the auditory cortex of awake primates. *Nature neuroscience, 4*(11), 1131-1138. doi: 10.1038/nn737

Madler, C., Keller, I., Schwender, D., & Poppel, E. (1991). Sensory information processing during general anaesthesia: effect of isoflurane on auditory evoked neuronal oscillations. *British journal of anaesthesia, 66*(1), 81-87.

Martinez-Montes, E., Cuspineda-Bravo, E. R., El-Deredy, W., Sanchez-Bornot, J. M., Lage-Castellanos, A., & Valdes-Sosa, P. A. (2008). Exploring event-related brain dynamics with tests on complex valued time-frequency representations. *Stat Med, 27*(15), 2922-2947. doi: 10.1002/sim.3132

Mashour, G. A. (2004). Consciousness unbound: toward a paradigm of general anesthesia. *Anesthesiology, 100*(2), 428-433.

Mashour, G. A. (2013). Consciousness and the 21st century operating room. *Anesthesiology, 119*(5), 1003-1005. doi: 10.1097/ALN.0b013e3182a7cad1

Miller, E. K., & Buschman, T. J. (2012). Cortical circuits for the control of attention. *Curr Opin Neurobiol*. doi: 10.1016/j.conb.2012.11.011

Moeller, S., Nallasamy, N., Tsao, D. Y., & Freiwald, W. A. (2009). Functional connectivity of the macaque brain across stimulus and arousal states. *J Neurosci, 29*(18), 5897-5909. doi: 10.1523/JNEUROSCI.0220-09.2009

Morishima, Y., Akaishi, R., Yamada, Y., Okuda, J., Toma, K., & Sakai, K. (2009). Task-specific signal transmission from prefrontal cortex in visual selective attention. *Nat Neurosci, 12*(1), 85-91. doi: 10.1038/nn.2237

Nallasamy, N., & Tsao, D. Y. (2011). Functional connectivity in the brain: effects of anesthesia. *The Neuroscientist : a review journal bringing neurobiology, neurology and psychiatry, 17*(1), 94-106. doi: 10.1177/1073858410374126

Okun, M., & Lampl, I. (2008). Instantaneous correlation of excitation and inhibition during ongoing and sensory-evoked activities. *Nature neuroscience, 11*(5), 535-537. doi: 10.1038/nn.2105

Opris, I., Hampson, R. E., Stanford, T. R., Gerhardt, G. A., & Deadwyler, S. A. (2011). Neural activity in frontal cortical cell layers: evidence for columnar sensorimotor processing. *J Cogn Neurosci, 23*(6), 1507-1521. doi: 10.1162/jocn.2010.21534

Oram, M. W., Wiener, M. C., Lestienne, R., & Richmond, B. J. (1999). Stochastic nature of precisely timed spike patterns in visual system neuronal responses. *Journal of neurophysiology, 81*(6), 3021-3033.

Pack, C. C., Berezovskii, V. K., & Born, R. T. (2001). Dynamic properties of neurons in cortical area MT in alert and anaesthetized macaque monkeys. *Nature, 414*(6866), 905-908. doi: Doi 10.1038/414905a

Patel, A. J., Honore, E., Lesage, F., Fink, M., Romey, G., & Lazdunski, M. (1999). Inhalational anesthetics activate two-pore-domain background K+ channels. *Nat Neurosci, 2*(5), 422-426. doi: 10.1038/8084

Petersen, R. S., Panzeri, S., & Diamond, M. E. (2001). Population coding of stimulus location in rat somatosensory cortex. *Neuron, 32*(3), 503-514.

Pinaud, R., Tremere, L. A., & De Weerd, P. (2006). *Plasticity in the visual system : from genes to circuits*. New York: Springer.

Purdon, P. L., Pierce, E. T., Bonmassar, G., Walsh, J., Harrell, P. G., Kwo, J., . . . Brown, E. N. (2009). Simultaneous electroencephalography and functional magnetic resonance imaging of general anesthesia. *Annals of the New York Academy of Sciences, 1157*, 61-70. doi: 10.1111/j.1749-6632.2008.04119.x

Rampil, I. J. (1998). A primer for EEG signal processing in anesthesia. *Anesthesiology, 89*(4), 980-1002.

Rasmusson, D. D., Smith, S. A., & Semba, K. (2007). Inactivation of prefrontal cortex abolishes cortical acetylcholine release evoked by sensory or sensory pathway stimulation in the rat. *Neuroscience, 149*(1), 232-241. doi: 10.1016/j.neuroscience.2007.06.057

Raz, A., Grady, S. M., Krause, B. M., Uhlrich, D. J., Manning, K. A., & Banks, M. I. (2014). Preferential effect of isoflurane on top-down vs. bottom-up pathways in sensory cortex. *Front Syst Neurosci, 8*, 191. doi: 10.3389/fnsys.2014.00191

Rojas, M. J., Navas, J. A., Greene, S. A., & Rector, D. M. (2008). Discrimination of auditory stimuli during isoflurane anesthesia. *Comparative medicine, 58*(5), 454-457.

Rudolph, M., Pospischil, M., Timofeev, I., & Destexhe, A. (2007). Inhibition determines membrane potential dynamics and controls action potential generation in awake and sleeping cat cortex. *The Journal of neuroscience : the official journal of the Society for Neuroscience, 27*(20), 5280-5290. doi: 10.1523/JNEUROSCI.4652-06.2007

Rudolph, U., & Antkowiak, B. (2004). Molecular and neuronal substrates for general anaesthetics. *Nat Rev Neurosci, 5*(9), 709-720. doi: 10.1038/nrn1496

Schrouff, J., Perlbarg, V., Boly, M., Marrelec, G., Boveroux, P., Vanhaudenhuyse, A., . . . Benali, H. (2011). Brain functional integration decreases during propofol-induced loss of consciousness. *NeuroImage, 57*(1), 198-205. doi: 10.1016/j.neuroimage.2011.04.020

Schumacher, J. W., Schneider, D. M., & Woolley, S. M. (2011). Anesthetic state modulates excitability but not spectral tuning or neural discrimination in single auditory midbrain neurons. *J Neurophysiol, 106*(2), 500-514. doi: 10.1152/jn.01072.2010

Sebel, P. S., Ingram, D. A., Flynn, P. J., Rutherfoord, C. F., & Rogers, H. (1986). Evoked potentials during isoflurane anaesthesia. *British journal of anaesthesia, 58*(6), 580-585.

Sellers, K. K., Bennett, D. V., & Frohlich, F. (2015). Frequency-band signatures of visual responses to naturalistic input in ferret primary visual cortex during free viewing. *Brain Res, 1598*, 31-45. doi: 10.1016/j.brainres.2014.12.016

Sellers, K. K., Bennett, D. V., Hutt, A., & Frohlich, F. (2013). Anesthesia differentially modulates spontaneous network dynamics by cortical area and layer. *Journal of neurophysiology, 110*(12), 2739-2751. doi: 10.1152/jn.00404.2013

Shu, Y., Hasenstaub, A., & McCormick, D. A. (2003). Turning on and off recurrent balanced cortical activity. *Nature, 423*(6937), 288-293. doi: 10.1038/nature01616

Takagaki, K., Zhang, C., Wu, J. Y., & Lippert, M. T. (2008). Crossmodal propagation of sensory-evoked and spontaneous activity in the rat neocortex. *Neuroscience letters, 431*(3), 191-196. doi: 10.1016/j.neulet.2007.11.069

Tallon-Baudry, C., Bertrand, O., Delpuech, C., & Pernier, J. (1996). Stimulus specificity of phase-locked and non-phase-locked 40 Hz visual responses in human. *J Neurosci, 16*(13), 4240-4249.

Tiesinga, P., Fellous, J. M., & Sejnowski, T. J. (2008). Regulation of spike timing in visual cortical circuits. *Nature reviews. Neuroscience, 9*(2), 97-107. doi: 10.1038/nrn2315

Ulbert, I., Halgren, E., Heit, G., & Karmos, G. (2001). Multiple microelectrode-recording system for human intracortical applications. *Journal of neuroscience methods, 106*(1), 69-79.

van Vugt, M. K., Sederberg, P. B., & Kahana, M. J. (2007). Comparison of spectral analysis methods for characterizing brain oscillations. *J Neurosci Methods, 162*(1-2), 49-63. doi: 10.1016/j.jneumeth.2006.12.004

Villeneuve, M. Y., & Casanova, C. (2003). On the use of isoflurane versus halothane in the study of visual response properties of single cells in the primary visual cortex. *J Neurosci Methods, 129*(1), 19-31.

Vincent, J. L., Patel, G. H., Fox, M. D., Snyder, A. Z., Baker, J. T., Van Essen, D. C., . . . Raichle, M. E. (2007). Intrinsic functional architecture in the anaesthetized monkey brain. *Nature, 447*(7140), 83-86. doi: 10.1038/nature05758

Vincis, R., Gschwend, O., Bhaukaurally, K., Beroud, J., & Carleton, A. (2012). Dense representation of natural odorants in the mouse olfactory bulb. *Nat Neurosci, 15*(4), 537-539. doi: 10.1038/nn.3057

W. B. Saunders Company. Veterinary Clinics of North America. Food animal practice. Philadelphia ; London. Philadelphia, PA.

Waterhouse, B. D., Azizi, S. A., Burne, R. A., & Woodward, D. J. (1990). Modulation of rat cortical area 17 neuronal responses to moving visual stimuli during norepinephrine and serotonin microiontophoresis. *Brain Res, 514*(2), 276-292.

Wehr, M., & Zador, A. M. (2003). Balanced inhibition underlies tuning and sharpens spike timing in auditory cortex. *Nature, 426*(6965), 442-446. doi: 10.1038/nature02116

White, N. S., & Alkire, M. T. (2003). Impaired thalamocortical connectivity in humans during general-anesthetic-induced unconsciousness. *Neuroimage, 19*(2 Pt 1), 402-411.

Yang, W., Carrasquillo, Y., Hooks, B. M., Nerbonne, J. M., & Burkhalter, A. (2013). Distinct balance of excitation and inhibition in an interareal feedforward and feedback circuit of mouse visual cortex. *J Neurosci, 33*(44), 17373-17384. doi: 10.1523/JNEUROSCI.2515-13.2013

Zhan, Y., Halliday, D., Jiang, P., Liu, X., & Feng, J. (2006). Detecting time-dependent coherence between non-stationary electrophysiological signals--a combined statistical and time-frequency approach. *J Neurosci Methods, 156*(1-2), 322-332. doi: 10.1016/j.jneumeth.2006.02.013

CHAPTER 6: FREQUENCY-BAND SIGNATURES OF VISUAL RESPONSES TO NATURALISTIC INPUT IN FERRET PRIMARY VISUAL CORTEX DURING FREE VIEWING[5]

INTRODUCTION

Encoding of sensory stimuli in cortex represents the process of transforming external physical signals into neuronal activity patterns that reduce the redundancy of the sensory input (Barlow, 1961; E P Simoncelli & B A Olshausen, 2001). In primary visual cortex (V1), the responses of individual neurons and networks of neurons to synthetic visual stimuli measured by changes in action-potential firing are well characterized (Hubel & Wiesel, 1959; but see Olshausen & Field, 2005). These "artificial" stimuli have been optimized to elicit neuronal spiking responses as a function of basic input properties such as orientation, contrast, and spatial frequency. Recently, it has been proposed that synthetic stimuli modulate neuronal activity differently than naturalistic visual stimuli (Felsen & Dan, 2005; Smyth, Willmore, Baker, Thompson, & Tolhurst, 2003a) due to the different image statistics of synthetic laboratory stimuli and real-world visual input (E P Simoncelli & B A Olshausen, 2001). Specifically, naturalistic stimuli exhibit a characteristic $1/f$ to $1/f^2$ power distribution as a function of spatial frequency f (Ruderman & Bialek, 1994; E. P. Simoncelli & B. A. Olshausen, 2001; Tolhurst, Tadmor, & Chao, 1992; van der Schaaf & van Hateren, 1996). Studies that employed naturalistic images and movie segments to investigate neuronal responses have revealed sparse coding in V1 (e.g. Baddeley et al., 1997; Froudarakis et al., 2014; Haider et al., 2010; Vinje & Gallant, 2000; Weliky, Fiser, Hunt, & Wagner, 2003; Willmore, Mazer, & Gallant, 2011) that facilitated decoding, maximized coding capacity, and was driven by higher-order statistics of the stimulus. Sensory-evoked activity has been recognized to closely relate to

[5] This chapter previously appeared as an article in Brain Research; doi: 10.1016/j.brainres.2014.12.016 (http://www.sciencedirect.com/science/article/pii/S0006899314016850). The original citation is as follows: **Kristin K. Sellers**, Davis V. Bennett, Flavio Frohlich (2015). Frequency-band signatures of visual responses to naturalistic input in ferret primary visual cortex during free viewing. Brain Research, 1598:31-45.

the ongoing spontaneous activity (Berkes, Orban, Lengyel, & Fiser, 2011; Luczak, Bartho, & Harris, 2013; Scholvinck, Friston, & Rees, 2011; Tsodyks, Kenet, Grinvald, & Arieli, 1999). For example, the structure of spontaneous network dynamics was only modestly altered by naturalistic visual input as determined by similarity in correlation structure of spiking activity (J. Fiser, C. Y. Chiu, & M. Weliky, 2004). Recently, sparse coding of naturalistic visual input was demonstrated to be state-dependent such that the quiet waking animal employed a less sparse code than the alert animal (Froudarakis et al., 2014). In general, visual responses depend on overall state (Bennett, Arroyo, & Hestrin, 2013; Niell & Stryker, 2010; Polack, Friedman, & Golshani, 2013). Also, in theoretical models, overall state-defining fluctuations explain response distributions (Goris, Movshon, & Simoncelli, 2014). Together, these results point towards a model of sensory processing of naturalistic input in which visual responses (1) are sparse and reliable, and (2) emerge from the modulation of ongoing endogenous network dynamics that depend on overall behavioral state. Yet, a limited number of studies have considered the local field potential (LFP) dynamics of naturalistic vision in the awake animal (Brunet et al., 2013; Ito, Maldonado, Singer, & Grün, 2011; Kayser, Salazar, & Konig, 2003; Whittingstall & Logothetis, 2009) and very little is known about the temporal structure of mesoscale network dynamics in V1 across cortical layers measured by the LFP and its relationship to the microscale spiking activity in the awake, freely viewing animal.

Given the recent description of different activity states characterized by the relative presence or absence of slow rhythmic activity in the cortical LFP of awake animals (Harris & Thiele, 2011; Poulet & Petersen, 2008), we here asked (1) how naturalistic visual input modulated the mesoscale V1 activity structure during free viewing in the awake animal, and (2) how the mesoscale activity structure related to the microscopic spiking response. We used the well-known trial-to-trial variability of sensory responses (Tolhurst, Movshon, & Dean, 1983) as a tool to answer these questions and thereby fill a key gap in our understanding of how sensory input interacts with ongoing network dynamics in the awake animal. In this study, we used the ferret animal model due to its well-studied visual system (Law, Zahs, & Stryker, 1988) and primate-like columnar architecture of V1 (Chapman & Stryker, 1993). We presented full-field nature movie clips to awake, head-fixed ferrets and determined the rhythmic architecture of the LFP before and during visual stimulation (corresponding to spontaneous and sensory-evoked activity) and how these

mesoscale network dynamics related to the multiunit spiking response elicited by the visual stimulus as a function of cortical layer.

METHODS

Acclimation and Surgery

Female ferrets (*Mustela putoris furo*, supplied by Marshall BioResources, 15-20 weeks old at study onset, 750-1000g, n = 3) were used in this study. Surgical and electrophysiological recording procedures were described in detail previously (Sellers, Bennett, Hutt, & Frohlich, 2013). The growth of female ferrets plateaus prior to the age used here, making females more suited than males for chronic chamber implants. All animals were spayed by the vendor in case they were kept past the age of sexual maturity; in this study, all animals were used prior to the age of sexual maturity. Animals were acclimated to be calmly restrained for up to two hours. Subsequently, animals underwent aseptic surgery in preparation for electrophysiological recordings in primary visual cortex (V1). An initial intramuscular injection of ketamine (30 mg/kg) and xylazine (1-2 mg/kg) was used for anesthesia induction. Deep anesthesia was maintained for the duration of the surgery with supplemental intramuscular injections of ketamine and xylazine, approximately every 40 minutes. This anesthesia paradigm was designed to achieve general anesthesia throughout surgery, and was assayed by complete absence of withdrawal response to toe pinch. Physiologic monitors included electrocardiogram, pulse oxygen level, and rectal body temperature. Animals were warmed with a water heating blanket to maintain rectal body temperature of 38.0-39.0°C. The animal's eyes were protected with paralube for the duration of surgery.

Surgical procedures consisted of an initial midline incision of the scalp, retraction of the soft tissue, and a circular craniotomy located over V1 (approximately 3 mm anterior to lambda and 9 mm lateral to the midline). The potential for swelling was reduced with an injection of furosemide (1mg/kg, IM). After removal of dura, the brain was covered with warm sterile 4% agar. A custom-fabricated cylindrical chamber with a removable cap (material: Ultem 1000) was cemented to the skull in order to allow subsequent access to the craniotomy for recordings. Additionally, a stainless steel head post was implanted with bone screws and dental cement. Upon completion of these surgical procedures, the incision was closed with sutures and treated with antibiotic cream. Yohimbine (0.25-0.5mg/kg, IM) was

administered to reverse anesthesia. The animal was kept warm with a heating blanket and observed during recovery from anesthesia. Meloxicam (0.2mg/kg, IM) and enrofloxacin (5mg/kg, IM) were administered to prevent infection and to minimize post-surgical discomfort for five days post-surgery. Animals were allowed to fully recover from surgery (at least 7 days) before the first recording session. All procedures were approved by the UNC- Chapel Hill IACUC and exceed guidelines set forth by the NIH and USDA.

Multichannel Extracellular Recordings

Local field potential (LFP) and multiunit activity (MUA) were recorded during spontaneous activity and presentation of naturalistic visual stimuli. During each recording session, animals were restrained, head-fixed, and the recording chamber was opened. After rinsing the craniotomy site with sterile saline, a linear 32-channel depth probe (Neuronexus, Ann Arbor, MI) was acutely inserted perpendicular to the surface of cortex to record from all cortical layers simultaneously. Recording sites were spaced 50µm apart along the z-axis, with the reference electrode located on the same shank (0.5mm above the top recording site). Probes were slowly advanced into cortex using a micromanipulator (Narishige, Tokyo, Japan), and correct depth placement was determined by small amplitude deflections of the LFP at superficial electrode sites and large amplitude deflections of the LFP at deeper electrode sites. Current source density (CSD) analysis was conducted offline to determine location of recording electrode relative to cortical layer IV (see Data Analysis). All electrode penetrations were made within 1mm of the same location in V1, corresponding to 5 degrees visual field in azimuth and 4.8 degrees visual field in elevation (given magnification factors in area 17 of 0.2mm in cortex/degrees of visual space in the azimuth, and 0.207mm in cortex/degrees of visual space in elevation) (Cantone, Xiao, McFarlane, & Levitt, 2005).

Raw signals were first amplified with MPA8I head-stages with gain 10 (Multichannel Systems, Reutlingen, Germany) and then further amplified with gain 500, (Model 3500, A-M Systems, Carlsborg, WA), digitized at 20 kHz (Power 1401, Cambridge Electronic Design, Cambridge, UK), and digitally stored using Spike2 software (Cambridge Electronic Design). All recordings were conducted with room lights off and with minimal acoustic noise to prevent contamination of the recording with neuronal responses to extraneous stimuli.

Upon correct depth placement of the electrode, the animal was presented with naturalistic visual stimuli (four different movie clips from Planet Earth, BBC, London, UK) on a 52 x 29 cm monitor with 120Hz refresh rate and full high definition resolution (1,920 x 1,080 pixels, GD235HZ, Acer Inc., New Taipei City, Taiwan) at 47cm distance from the animal. Visual stimuli filled 58 degrees of the visual field horizontally, 33 degrees of the visual field vertically, and was controlled by the Psychophysics toolbox (Brainard, 1997) for MATLAB and a GeForce580 GPU (NVIDIA, Santa Clara, CA). Correct timing of individual display frames was ascertained by a photodiode covering a small flashing square in the corner of the monitor. Each trial of visual stimulation contained 10 seconds of dark control before visual stimulation (to record spontaneous activity), 10 seconds of Planet Earth footage (movie of animals moving across the screen), and 10 seconds dark control after visual stimulation. For a few sessions, only a subset of stimuli was used to shorten the duration of the head-restraint. Continuous video recording with an infrared sensitive camera (Handycam HDR-cx560v, Sony, Tokyo, Japan) and LED infrared illumination was used to document that the animal was fully awake during recordings as evidenced by whisking and noise twitching. At the conclusion of the study, all animals were humanely killed with an overdose of sodium pentobarbital and immediately perfused with 4% formaldehyde in 0.1M phosphate buffered saline for subsequent histological verification of recording locations.

Data Analysis

Recorded signals were processed offline with custom-written scripts in MATLAB (Mathworks, Natick, MA). Current source density (CSD) was calculated in order to determine the location of the 32-channel probes relative to cortical layers. Cortical layers were aligned across different electrode penetrations according to putative granular layer IV. CSD was determined by calculating the second spatial derivative of the low-pass filtered and smoothed LFP in response to full-field flashes (white screen) of duration 32ms, presented at a rate of 1Hz. The first stimulus-evoked sink in the laminar profile is indicative of layer IV (Mitzdorf, 1985). As additional verification of probe placement, MU firing rate was calculated for 30-50ms post stimulus onset. A subset of trials was manually excluded due to motion artifacts in the LFP signal, determined by extreme values in the raw traces. In order to calculate the spatial frequency of the visual stimuli, the video was converted to gray scale and a two-dimensional

discrete Fourier transform was calculated on a square region of each frame. Rotational averaging was used to reduce the two dimensional power spectrum to one dimension. The same procedure was conducted to calculate spatial frequency of a stock image of a naturalistic visual stimulus (from the point-of-view of an animal) and for two artificial visual stimuli (black and white checkerboard noise and luminance gratings). Data from different naturalistic visual stimulus movies were pooled (n = 578 trials). Data are presented per trial, averaged across electrodes, unless otherwise noted. Values are reported as median ± sem (standard error of the mean). The spectral content of the LFP was determined by convolving the raw extracellular voltage signals with a family of Morlet wavelets (0.5Hz – 40Hz, step-width 0.5Hz) with normalized amplitude, providing an optimal trade-off between time and frequency uncertainty (Goupillaud, Grossmann, & Morlet, 1984). Power in each frequency band (delta = 0.5-4Hz, theta = 4-8Hz, alpha = 8-12Hz, beta = 12-20Hz, gamma = 20-40Hz) was calculated for each trial. Relative power was determined by calculating the percent of total power in each frequency band, on a trial-by-trial basis. Relative power enhancement was calculated by dividing the relative power during visual stimulation by the relative power during spontaneous activity before stimulation, on a trial-by-trial basis. We wanted to test if observed spectral modulation of the LFP was induced by spectral properties of the visual stimulus. To do so, we employed a linear-nonlinear model of V1 spatio-temporal receptive fields and used these as spatial and temporal filters of the 10 second movie clips (Mante, Bonin, & Carandini, 2008; Ringach, 2004). Modeled MU activity was peak-normalized, and the spectrum was calculated using the fast Fourier transform. MU action potential firing was detected by high-pass filtering the data (4th order Butterworth filter, 300Hz cutoff) and imposing a threshold of -3*std. MU firing rate enhancement was calculated by dividing MU firing rate during visual stimulation by MU firing rate during spontaneous activity before stimulation, on a trial-by-trial basis. Correlation coefficients were calculated using MATLAB function corrcoef, and significance was calculated by using the Fisher r-to-z transformation.

To determine the preferred phase-of-firing of MUA for each frequency band, the instantaneous phase was calculated using the Hilbert transform on band-pass filtered data (delta = 0.5-4Hz, theta = 4-8Hz, alpha = 8-12Hz, beta = 12-20Hz, gamma = 20-40Hz). Peak phase-of-firing was determined as the phase with the highest probability of spiking. Kullback-Leibler (KL) divergence was used to determine the difference of the resulting preferred phase-of-firing histograms from a flat distribution. To determine the

time-course of the band-limited power in the five frequency bands, we used the Hilbert transform on band-pass filtered data (delta = 0.5-4Hz, theta = 4-8Hz, alpha = 8-12Hz, beta = 12-20Hz, gamma = 20-40Hz) to determine the instantaneous amplitude in each frequency band. This allowed for trajectory plots of the oscillatory activity in frequency-band pairs of interest (phase space plots of instantaneous amplitudes in frequency bands of interest). We conducted k-means clustering of normalized amplitudes (at all time-steps) in order to quantify if behavioral states could be differentiated based on oscillatory activity. We requested clustering into two clusters based on visual inspection of the phase-space plots. We did not include the one second of data immediately following onset and offset of the stimulus in k-means clustering, as we were interested in the equilibrium states corresponding to spontaneous activity and visual stimulation rather than transients at stimulation onset and offset. Correctly clustered refers to trials which were categorized correctly based on if the data originated from a spontaneous activity or visually-evoked data point. Phase-amplitude coupling was calculated between the phase of low frequencies (delta or alpha) and the amplitude of the gamma oscillation, according to (Voytek et al., 2010). Briefly, the raw signal was band pass filtered at the low frequency of interest (delta or alpha) and the gamma frequency. The amplitude of the gamma-filtered signal was extracted, and then filtered at the lower frequency of interest. The phase of both signals was extracted and phase-amplitude coupling was calculated as the mean vector between the angles.

Bootstrapping with 100 iterations of resampling with replacement, a distribution-independent method, was used to calculate standard errors when parametric models were inappropriate. The non-parametric Kruskall-Wallis test was used to determine statistical significance (if the samples of interest came from the same distribution) and multiple comparisons were corrected for using Tukey's honestly significant difference criterion.

RESULTS

Little is known about the mesoscale network dynamics in V1 of awake animals in absence of experimental constraints such as anesthesia or reward-driven attentional processes that define cortical state by shaping the overall network dynamics. In order to characterize how naturalistic visual input modulates local network activity in the freely-viewing animal, we presented fullfield (58 x 33 degrees

visual field) movie clips displaying nature scenes to awake, head-fixed ferrets. The presentation of the movie clips was interleaved with periods of no visual stimulation (spontaneous activity). The visual stimuli exhibited the characteristic 1/f to $1/f^2$ spatial frequency structure of naturalistic stimuli (Figure 6.1A, left), which is comparable to the spectra of a point-of-view naturalistic visual stimulus (Figure 6.1A, left middle). Traditionally used synthetic visual stimuli (checkerboard noise pattern, luminance grating) exhibited characteristically different spectra (Figure 6.1A, right). The animals were acclimated to restraint but did not receive any other behavioral training and the recording sessions did not include any reward contingencies. We verified that the animals were awake during the entirety of the recording sessions by reviewing infrared videography for open eyes and minor movements. Local field potential (LFP) and multiunit activity (MUA) were recorded with multichannel depth probes in V1 (N = 3 animals). Raw LFP traces revealed strikingly different network dynamics for periods of spontaneous activity and visual stimulation (Figure 6.1B). Prominent high amplitude, low frequency oscillations often occurred during periods of spontaneous network activity; this slow rhythmic activity was typically suppressed for the duration of the visual stimulus. Full-field naturalistic visual input therefore altered overall mesoscale activity in structure in V1, with the most obvious difference present in the low frequencies. Spectral analysis averaged across trials (N = 578) and cortical depth revealed that visual stimulation modulated the power in the entire spectrum included in the analysis (Figure 6.2A, 0.5 Hz-40 Hz, change in power determined by subtraction of spectra during and before visual stimulation). In particular, power at low frequencies (with the exception of a narrow peak around 6 Hz) was lower during visual stimulation and power at higher frequencies was enhanced with a cross-over frequency of suppression and enhancement around 18 Hz. We mapped this broadband modulation of oscillatory activity onto the standard frequency bands as determined by the percent of total power for any given frequency band. This provided a measure of the relative presence of oscillations in difference frequency bands (El Boustani et al., 2009). When comparing spontaneous activity (Figure 6.2B left, median percent ± sem, delta = 31% ± 0.34, theta = 16% ± 0.10, alpha = 13% ± 0.12, beta = 19% ± 0.18, gamma = 21% ± 0.23, n = 578 trials) with visually-driven activity (Figure 6.2B right, median percent ± sem, delta = 28% ± 0.29, theta = 17% ± 0.11, alpha = 12% ± 0.10, beta = 17% ± 0.12, gamma = 26% ± 0.22, n = 578 trials), delta, alpha, and beta band activity decreased with presentation of visual input and theta and gamma band increased. The mean ranks

comparing spontaneous and evoked activity for each of the frequency bands were significantly different (delta: df = 1, H = 29.67, p<0.0001; theta: df = 1, H = 10.85, p=0.001; alpha: df=1, H = 43.33, p<0.0001; beta: df = 1, H = 47.98, p<0.0001; gamma: df = 1, H = 190.3, p<0.0001; n = 578 trials, Kruskal-Wallis test). Thus, naturalistic visual input caused heterogeneous spectral modulation across all cortical oscillation frequencies, suggesting that naturalistic visual input elicits comprehensive modulation of the overall activity structure in the awake, freely viewing animal presented with full-field naturalistic visual input. Importantly, visual stimulation not only increased fast cortical oscillations but also decreased the presence of slow oscillatory activity both on absolute (Figure 6.2A) and relative (Figure 6.2B) scales. To verify that this spectral modulation was not induced by spectral components of the visual stimulus itself, we modeled the spectral properties of responses to the naturalistic videos (Figure 6.2C). Briefly, we created spatio-temporal receptive fields characteristic of V1, modeled MU responses using these receptive fields as spatial and temporal filters of the visual stimulus, and extracted the frequency information of this MU activity. Indeed, we found that the spectral modulation measured in ferret V1 could not be explained by these modeled responses to the visual stimulus.

We then asked how these changes in mesoscopic network dynamics related to the MUA in response to the visual stimulus. In principle, modulation of mesoscopic LFP activity and microscopic MUA by visual input could reflect two distinct processes. Alternatively, changes in oscillatory activity could define excitability of the local circuitry in V1 and therefore be closely related to the MUA response to the visual input. To disambiguate between these two scenarios, we asked to what extent the trial-to-trial variability of MUA visual responses to the naturalistic visual input was captured by the trial-to-trial variability of the stimulus-induced changes to the oscillation power in the different frequency bands. In one extreme scenario, the trial-to-trial fluctuation in change of LFP power to the visual input would not correlate with the MU trial-to-trial variability, suggesting a decoupling of overall oscillatory tone at the mesoscale and sensory processing at the microscale. Alternatively, changes in LFP power could closely relate to changes in MU responses and therefore be another representation of the same underlying process. In particular, it has long been known that engagement of sensory systems measured by MUA co-occurred with increases in gamma oscillations in the anesthetized animal. We here asked, given the broad spectral modulation that we found at the LFP level in the awake, freely-viewing animal, if and how

the classical frequency bands related to the MU response in average across all cortical layers. For each frequency band, we correlated the normalized visual response to the entire stimulus (spike count) with the change in relative LFP power in that given frequency band. For the delta oscillation, we found a negative correlation, indicating that a stimulus-induced decrease in delta power was associated with a stronger MU responses to the stimulus (Figure 6.3A, sample LFP and MUA traces; Figure 6.3B, R = -0.15, 95% CI [-0.23, -0.07], n = 578 trials; correlation coefficient significantly different from 0, $p < 0.001$). In contrast, we found no significant correlation for the theta band (Figure 6.3C, R = 0.004, 95% CI [-0.078, 0.085], n = 578 trials; correlation coefficient not significantly different from 0, $p = 0.93$. The alpha oscillation power was also negatively correlated with the MU response, again indicating that the LFP state dynamics were related to the network MU response (Figure 6.3D, R = -0.24, 95% CI [-0.31, -0.16], n = 578 trials; correlation coefficient significantly different from 0, $p < 0.001$). This correlation coefficient was not statistically different from the corresponding measure for the delta band (Fisher r-to-z transformation, $p=0.11$). For the beta band, we found a small negative correlation (Figure 6.3E, R = -0.09, 95% CI [-0.17, -0.008], n = 578 trials; correlation coefficient significantly different from 0, $p = 0.03$). MU response exhibited a positive correlation with gamma oscillation power (Figure 6.3F, R = 0.37, 95% CI [0.30, 0.44], n = 578 trials; correlation coefficient significantly different from 0, $p < 0.001$). This correlation coefficient was significantly different from the corresponding measures in the delta (Fisher r-to-z transformation, $p<0.001$) and alpha (Fisher r-to-z transformation, $p<0.001$) frequency bands. Together, these results propose that measurements in LFP power in different frequency bands relate to the MUA such that low frequencies (delta and alpha) correspond to decreased response to visual input whereas increase in the gamma frequency reflects an increased response to the visual stimulus. Importantly, these results suggest that the bidirectional modulation of the oscillatory activity found here directly relates to the microscopic spiking response.

We then asked if the relationship between modulation of oscillation power in individual frequency bands and MUA visual responses exhibited a layer-specific fine-structure. To answer this question, we computed the same correlation coefficients separately for supragranular (LI-LII/III), granular (LIV), and infragranular (LV-VI) layers (Figure 6.4). Again, the delta, alpha, and gamma bands exhibited the most pronounced correlations with MUA visual responses. The relationship between oscillation recruitment and

MUA responses was quite uniform across layers for the alpha (supragranular: R = -0.16, 95% CI [-0.26 -0.061]; granular: R = - 0.18, 95% CI [-0.26 -0.96]; infragranular: R= -0.14, 95% CI [-0.22 -0.054]) and gamma (supragranular: R = 0.29, 95% CI [0.19 0.38]; granular: R = 0.31, 95% CI [0.23 0.39]; infragranular: R= 0.30, 95% CI [0.23 0.38]) frequency bands. However, several interesting additional features became apparent in this analysis. First, the negative correlation between recruitment of delta oscillation and MUA response was absent for supragranular layers (R = -0.073, 95% CI: [-0.18 0.031]) but not for granular (R = -0.20, 95% CI: [-0.28 -0.11]) and infragranular (R = -0.16, 95% CI: [-0.24 -0.076]) layers. Theta oscillation recruitment weakly correlated with MUA responses exclusively in the granular layer (R = 0.086, 95% CI [0.0019 0.17]; supragranular: R = 0.02, 95% CI [-0.084 0.12]; infragranular: R = 0.0047, 95% CI [-0.087 0.078]). Beta oscillation recruitment was negatively correlated with MUA responses only in the supragranular layers (R = -0.12, 95% CI [-0.22 -0.017]; granular: R = -0.062, 95% CI [-0.15 .022]; infragranular: R = 0.026, 95% CI [-0.057 0.11]). This layer-specific fine structure may reflect local differences in the functional role of oscillatory activity within the V1 microcircuit or the preferential target layers of incoming connections that use specific oscillation frequencies as their signal. Thus, these data suggest the presence of an endogenous trade-off between slow (delta and alpha) and fast (gamma) oscillation power that is modulated by visual input and shapes the spiking response to naturalistic visual input.

In addition to the relationship between time-averaged MUA and oscillatory power, MUA has been shown to exhibit preferred phase-of-firing according to the ongoing oscillation in different frequencies (Masquelier, Hugues, Deco, & Thorpe, 2009). Therefore, we next asked if MUA exhibited a preferred phase-of-firing, and if these faster timescale dynamics were also modulated by presentation of naturalistic visual stimuli. We found that MUA exhibited the strongest preferred phase-of-firing for the delta oscillation both during spontaneous activity and visual stimulation (Figure 6.5A, example high-pass filtered trace and delta-frequency band-pass filtered LFP trace. Figure 6.5B and 6.5C, left: preferred phase of firing for delta oscillation = -2.83 radians). Kullback-Leibler (KL) divergence was calculated as a metric of non-uniformity of MUA phase distribution (Figure 6.5D, median KL divergence and 95% CI: spontaneous activity, delta = 0.0068 [0.0066 0.0070]; visual stimulation, delta = 0.0023 [0.0022 0.0024]). Naturalistic visual stimulation decreased the strength of preference for phase-of-firing, particularly in the lower frequencies (Figure

6.5D, median KL divergence during spontaneous activity and 95 % CI: theta = 0.0037 [0.0035 0.0038], alpha = 0.0018 [0.0017 0.0019], beta = 0.0005 [0.0004 0.0005], gamma = 0.0002 [0.0002 0.0002], median KL divergence during visual stimulation and 95% CI: theta = 0.0008 [0.0007 0.0009], alpha = 0.0005 [0.0005 0.0006], beta = 0.0004 [0.0003 0.0004], gamma = 0.0002 [0.0002 0.0002]). Therefore, naturalistic visual input weakened the strength of coupling between MUA and phase of the ongoing oscillation. Together, these data suggest that the low frequency oscillations are not only decreased in amplitude but also had less influence on spike-timing during presentation of naturalistic visual input.

We next investigated the time-course of the modulation of the LFP spectrum, in particular of the delta, alpha, and gamma bands that we found to be correlated with the MUA response. In order to gain resolution in the time-domain, we used the Hilbert transformation to extract the time-course of the power in the different frequency bands for LFP activity in three groups of cortical layers (supragranular: LI-LII/III, granular: LIV, and infragranular: LV-VI). We used a two-dimensional state-space representation defined by delta and gamma power (averaged across trials) to characterize the dynamics of the band-limited oscillation power. Trajectories in state space that separate into two clusters, connected by transients at stimulation onset and offset, would indicate that presentation of naturalistic visual input switched the V1 network between two states. Alternatively, lack of separation of the epochs corresponding to spontaneous activity and visual stimulation would support a model in which relative oscillation strength in different frequencies occurs on a continuum without clear separation into distinct network states. In agreement with the former model of distinct states, the delta-gamma phase plots demonstrated clear clustering into two relatively distinct states with transitions at stimulus onset and offset for all three groups of cortical layers (Figure 6.6). At stimulation onset, an initially transient (light blue) characterized by an increase in both gamma and delta power was followed by a state switch that corresponded to a reduction of delta power and a concomitant increase of gamma power. Importantly, the transients between the two states were quite pronounced and lasted up to several seconds, in particular at the offset of the stimulus (orange time points). Although the offset transient quickly moved the trajectory back to the state corresponding to spontaneous activity (marked as “I” in Figure 6.6C), an extra “rebound detour” occurred before final convergence (marked as “II”), in particular for deep layers. Similarly, for the state space representation of the alpha-gamma power pair, we again found two distinct clusters (Figure 6.7). Stimulus onset induced a

switch from a high alpha, low gamma power state to a low alpha, high gamma power state. Interestingly, the offset transient lasted several seconds and mostly corresponded to a recovery of the spontaneous alpha oscillation levels (near horizontal orange part of the trajectories). Together, this state-space analysis proposes that free viewing of naturalistic stimuli induced a state transition from a cortical state characterized by relative dominance of delta and alpha oscillations to a cortical state characterized by the relative dominance of the gamma oscillation. To test this model, we used k-means clustering to assay for the presence of two distinct clusters and measured the number of misclassification as an indicator for poorly captured structure by two clusters. Mostly, the two clusters determined by k-means clustering indeed corresponded to spontaneous and evoked activity. We quantified the percent of data points which were incorrectly clustered for each group of cortical layers. For both delta-gamma and alpha-gamma trajectories, supragranular layers exhibited less accurate clustering, with significantly more incorrectly clustered data points than granular or infragranular layers (Figure 6.8, percent incorrectly clustered ± sem for supragranular, granular, and infragranular respectively; bars represent medians across 100 iterations of bootstrapping. Delta-gamma: 6.78% ± 0.24, 0.69% ± 0.07, 1.03% ± 0.08; Alpha-gamma: 6.42% ± 0.25, 2.28% ± 0.15, 3.48% ± 0.12, comparisons significant at $p < 0.05$ are noted). These results further support the presence of two distinct states that are governed by the same trade-off of delta and alpha versus gamma band activity. Transitions for gamma oscillation power were relatively fast but the delta and alpha oscillation power transients lasted up to several seconds, suggesting a slow transition between the two states.

The distinct states described above were described by the relative power between slow and fast frequency oscillations. Substantial work has demonstrated the importance of coordination between the phase of low frequencies and amplitude of higher frequency oscillations (Canolty & Knight, 2010). Thus, we asked whether the two distinct states defined by delta or alpha power vs gamma power also exhibited differences in the phase-amplitude coupling (PAC) of slow and fast frequencies. Indeed, we found that both delta-gamma and alpha-gamma PAC were lower during the state elicited by presentation of naturalistic visual stimuli compared to spontaneous activity (Figure 6.9). Interestingly delta-gamma PAC differed less between the two states, particularly in the granular layer (Figure 6.9B, right). In other words, alpha-gamma PAC was more strongly modulated by visual stimulation. This result is in agreement with

our finding that alpha power is more highly correlated with MU spiking activity, compared to delta power. Together, these results demonstrate that the state change induced by visual stimulation is characterized by a change in the balance between low and high frequencies and also by a decoupling of slow and fast oscillations.

DISCUSSION

Our understanding of the visual system is mostly based on the neuronal responses to synthetic, optimized stimuli presented to anesthetized animals. Recent work that employed naturalistic visual input provided a new perspective on visual coding and the modulatory rather than driving nature of sensory input both in animal models (Belitski et al., 2008; Besserve, Scholkopf, Logothetis, & Panzeri, 2010; Dan, Atick, & Reid, 1996; David, Vinje, & Gallant, 2004; J. Fiser, C. Chiu, & M. Weliky, 2004; Gallant, Connor, & Van Essen, 1998; Ito et al., 2011; MacEvoy, Hanks, & Paradiso, 2008; A. Mazzoni, N. Brunel, S. Cavallari, N. K. Logothetis, & S. Panzeri, 2011; Alberto Mazzoni, Nicolas Brunel, Stefano Cavallari, Nikos K Logothetis, & Stefano Panzeri, 2011; Mazzoni, Panzeri, Logothetis, & Brunel, 2008; Montemurro, Rasch, Murayama, Logothetis, & Panzeri, 2008; Reinagel, 2001; Smyth, Willmore, Baker, Thompson, & Tolhurst, 2003b; Vinje & Gallant, 2000; Wang et al., 2007; Weliky et al., 2003; Whittingstall & Logothetis, 2009) and in human imaging studies (e.g. Betti et al., 2013). However, surprisingly little is known about network dynamics in absence of experimentally induced constraints such as anesthesia, which selectively increase delta oscillations and suppress alpha oscillation in visual cortex (Purdon et al., 2013), or attention paradigms that use reward-based approaches that selectively modulate gamma oscillations as a function of the specific attentional demands (Buschman & Miller, 2007). We here sought to fill in this gap of knowledge about the mesoscale network dynamics in V1 during free viewing of naturalistic visual input.

We found that free viewing of naturalistic visual stimuli (movie clips of nature scenes) modulated cortical oscillations in all frequency bands; most prominently, the delta and alpha frequency bands were suppressed and the gamma frequency band was enhanced. Analysis of the time-course of the instantaneous power in these frequency bands demonstrated that visual stimuli switched the overall network between two distinct states at the onset and offset of the stimulus, respectively. These LFP dynamics were related to the microscopic MUA responses to the visual stimuli. Both the delta and alpha

frequency bands negatively correlated with the MU responses and explained a moderate amount of the trial-to-trial variability of the MU response. Stimulus-elicited changes in the gamma frequency band positively correlated with the MU response. Together, these data propose that V1 switches between distinct states that are defined by the relative presence of delta and alpha oscillations on the one hand side and gamma oscillations on the other hand side.

Our data agree with previous studies that consistently found gamma oscillations to be a marker of visual processing for a large number of different visual stimuli and experimental conditions. Most importantly in the context of our results, naturalistic visual input increased gamma oscillations in awake primates (Brunet et al., 2013; Ito et al., 2011; Whittingstall & Logothetis, 2009) and cats (Kayser et al., 2003). Similar to our results, recruitment of gamma oscillations correlated with MU responses in the awake, fixating primate (Whittingstall & Logothetis, 2009). Gamma oscillations arise from local circuit interactions, specifically from the dynamic interaction of principle cells and parvalbumin-positive, fast-spiking inhibitory interneurons (Cardin et al., 2009; Sohal, Zhang, Yizhar, & Deisseroth, 2009). Likely, excitatory afferent drive caused by the visual stimulation increased spiking activity in V1 and concomitantly the power in the gamma band. In contrast to our results, previous studies (e.g. Belitski et al., 2008) reported a stimulus-induced increase in the low frequencies (but see: Kayser et al., 2003) and found a positive correlation between low frequency activity and spiking response (Whittingstall & Logothetis, 2009). These differences may be explained by the fact that our paradigm did not include application of anesthetics or behavioral contingencies that would have shaped the behavioral state of the animal and might have suppressed the state transitions with visual stimulation as found in our study.

At the macroscopic level of human electroencephalograms (EEGs), both alpha and delta oscillations have emerged as regulators of overall network excitability. Specifically, human studies have consistently found that the power and phase of the alpha oscillation measured with EEG or MEG modulated threshold sensory responses (Busch, Dubois, & VanRullen, 2009; Ergenoglu et al., 2004; Hanslmayr et al., 2007; Palva & Palva, 2007; van Dijk, Schoffelen, Oostenveld, & Jensen, 2008). Our results of stronger visual responses on trials with more stimulus-induced suppression of the delta and alpha frequency band conceptually agree with the functional role of these macroscopic network dynamics. Importantly, however, we did not employ threshold sensory stimuli nor did we require specific

behavioral responses. Rather, we used naturalistic full-field visual input without any experimental contingencies. Our results therefore propose that (1) the functional roles of these mesoscale oscillations relate to the macroscopic dynamics in human EEG studies and (2) that the regulation of MUA in V1 reflects the underlying mechanism of differential responses as a function of delta and alpha oscillations measured by EEG.

Sensory responses not only reflect the properties of the physical input but also the state of the sensory system before and during the receipt of incoming information. Separation of endogenous state dynamics of neuronal networks and sensory responses is fundamentally difficult to achieve since any input – at least in theory - perturbs the state of the system. To mitigate this confound, studies of state-dependent sensory processing typically employ brief, weak stimuli (Castro-Alamancos, 2004; Curto, Sakata, Marguet, Itskov, & Harris, 2009; Haider, Duque, Hasenstaub, Yu, & McCormick, 2007; Hasenstaub, Sachdev, & McCormick, 2007; Worgotter et al., 1998) and implicitly assume that the stimulus itself does not change global brain state. These studies demonstrated the role of oscillatory activity in regulating excitability and therefore sensory responses. In contrast, our study provides a different perspective in which the sensory stimulus itself (10 sec of full-field naturalistic visual input) switches overall cortical state. Such state transitions between slow rhythmic and desynchronized states have been recently reported to spontaneously occur in both the somatosensory and the auditory system of rodents (Luczak et al., 2013; Poulet & Petersen, 2008). Our study shows a similar presence of slow rhythmic activity in the awake, resting ferret. Of note, not all recent work in awake animals found such rhythmic structure. These differences may be due to different experimental conditions where for example, animals received intermittent rewards during head fixation (Haider, Hausser, & Carandini, 2013) and therefore assumed an anticipatory behavioral state, or where animals exhibited heightened, experimentally-induced noradrenergic tone (Constantinople & Bruno, 2011). Together, our findings support the existence of a state characterized by the relative dominance of delta and alpha oscillations and a state characterized by the relative dominance of the gamma oscillation (as identified by the trial-averaged phase-space representation and the subsequent k-means clustering).

As a notable limitation, our study did not probe the underlying mechanism for the meso- and microscale dynamics described here. Likely candidate mechanisms are modulation of neuromodulatory

tone, top-down modulation by higher-order cortical areas such as prefrontal cortex, and state switching in thalamo-cortical loops due to increased depolarization by the afferent visual input from the retina to the thalamus. Each of these mechanisms may individually or together contribute to the dynamics described here. Changes in cholinergic tone are associated with changes in attentional state (Harris & Thiele, 2011; Lee & Dan, 2012); increased cholinergic tone has broad effects on intrinsic and synaptic properties, with the main effect at the meso- and macroscale being a desynchronization that typically corresponds to a selective suppression of low frequency network activity (Metherate, Cox, & Ashe, 1992). Stimulation of brainstem cholinergic centers leads to tonic depolarization of cortical neurons (Steriade, Amzica, & Nunez, 1993; Steriade, McCormick, & Sejnowski, 1993), and stimulation of cortical sources of cholinergic innervation produces awake-like cortical activity in anesthetized animals (Goard & Dan, 2009; Metherate et al., 1992; Steriade, Amzica, et al., 1993; Steriade, McCormick, et al., 1993). Release of neocortical acetylcholine shifted subthreshold membrane potential fluctuations from slow, delta oscillations to low-amplitude, gamma frequency oscillation (Metherate et al., 1992). Although no experimental contingency provided an incentive for the animals in our study to pay attention to the visual stimulus, the onset of the visual stimuli in absence of other salient sensory input may still have recruited cholinergic modulation by means of sensory-driven, bottom-up attention. Top-down modulation from higher order cortical areas could also provide (possible concomitantly or synergistically with changes in neuromodulatory tone) different network set-points as recently described in the somatosensory system (Zagha, Casale, Sachdev, McGinley, & McCormick, 2013). Third and last, cortical activity arises from the thalamocortical interaction in the canonical circuit that consists of the primary thalamic nucleus (in case of the visual system the lateral geniculate nucleus, LGN), the primary cortical target, here V1, and the reticular nucleus. Thalamo-cortical relay cells exhibit bistable behavior in which, as a result of depolarization and overall neuromodulatory tone, neurons either exhibit burst firing that facilitates slow rhythmic activity in the thalamo-cortical loop or tonic spiking that corresponds to an “activated” or desynchronized cortex (Steriade, McCormick, et al., 1993). In this scenario, afferent sensory input would provide the necessary drive to induce such transitions between the two states. Related to this, it remains to be studied if the network dynamics described here are unique to V1, or if these properties are more ubiquitous throughout cortical regions. Specific parameters which may affect the network dynamics described here may include

cell populations, innervation by other brain regions, and feedback within a given brain region and with other brain regions (e.g. thalamocortical loops).

Together, our work provides a novel perspective on the mesoscale network dynamics in V1 of the awake, freely viewing animal. We found that naturalistic visual input switched cortical state in the freely viewing animal and that the balance between delta and alpha oscillations on the one hand side and gamma oscillations on the other hand side may provide a mechanism by which sensory responsiveness is adjusted on a trial-to-trial basis. Our work therefore proposes that using more naturalistic experimental approaches to visual stimulation offers an important, complementary perspective on how mesoscopic state dynamics mediate sensory processing. Eventually, such insights could provide a network-level understanding of sensory processing deficits in patients with schizophrenia and autism, disease state that have been recently associated deficits in cortical oscillatory activity (Uhlhaas & Singer, 2012).

FIGURES

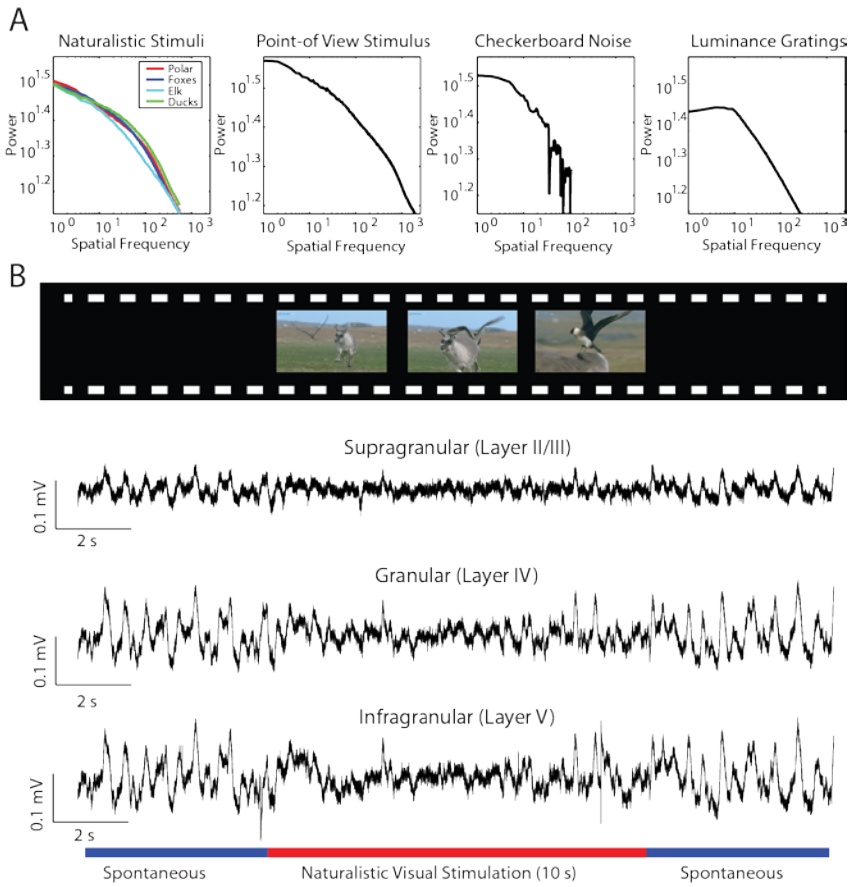

Figure 6.1. Naturalistic visual stimuli exhibit characteristic spectral properties and modulate LFP dynamics.

(A) The spatial frequency of the naturalistic videos used for visual stimulation (far left) and a point-of-view naturalistic image (middle left) exhibit the characteristic 1/f to $1/f^2$ spatial frequency distribution of naturalistic stimuli. Artificial stimuli of black and white checkerboard noise (middle right) and luminance gratings (far right) do not exhibit this spatial frequency structure.

(B) Trials consisted of 10 sec of spontaneous activity (screen dark), followed by 10 sec of naturalistic movie clip, followed by 10 sec of spontaneous activity. Representative local field potential traces simultaneously recorded on electrode contact sites in supragranular (top), granular (middle), and infragranular (bottom) layers of ferret V1.

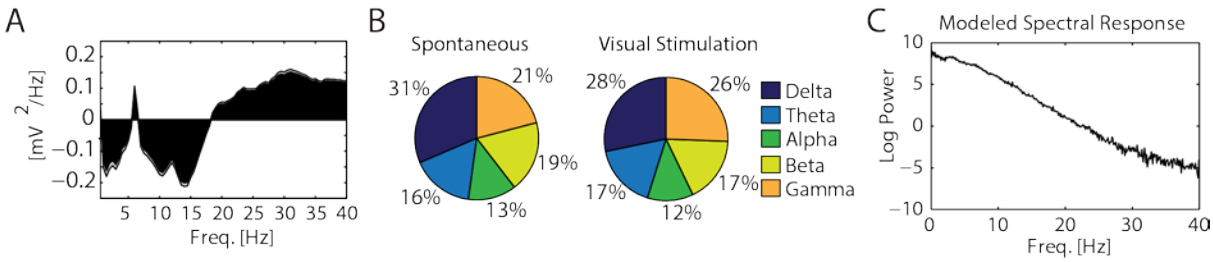

Figure 6.2. Modulation of mesoscopic network dynamics in V1 by naturalistic visual input during free viewing.

(A) Group averaged difference in power spectrum of LFP between spontaneous and visually-evoked activity. Low frequencies exhibited downregulation (with the exception of a small peak in the theta range) and higher frequencies exhibited an upregulation of oscillation power. Gray line indicates ± 1 sem.

(B) Relative power for each frequency band during spontaneous activity (left) and during visual stimulation (right). Relative power was calculated by dividing power in each frequency band by total power, on a trial-by-trial basis. The medians across all trials are plotted.

(C) The LFP spectral modulation is not explained by modeled physiological responses to the naturalistic videos, using spatio-temporal receptive fields characteristic of V1.

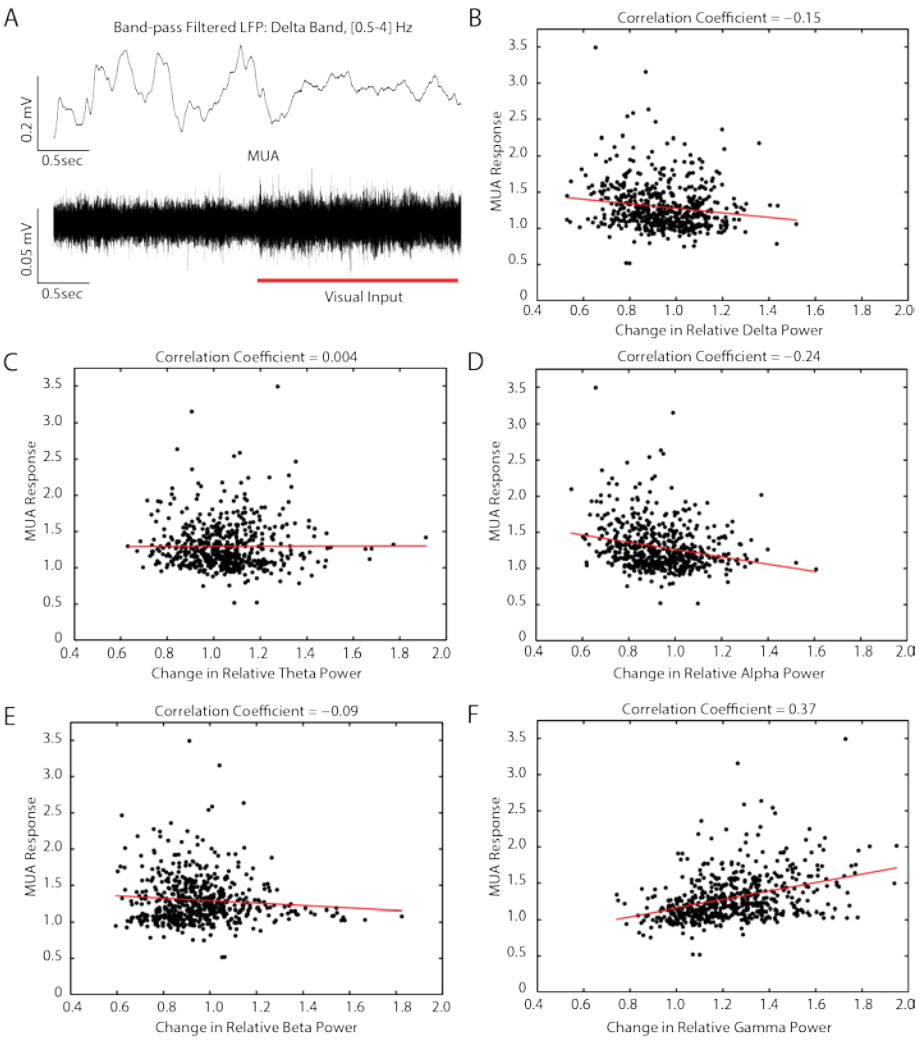

Figure 6.3. Relationship between mesoscale (LFP) and microscale activity (MUA) during free viewing of naturalistic visual input

(A) Representative sample traces (2 sec of spontaneous activity followed by 2 sec of visual response). Top: band-limited LFP in delta band. Bottom: MUA. Stimulus suppressed power in delta frequency bands and increased MUA.

(B) Enhancement in relative delta power exhibited a negative correlation with enhancement of MUA in response to stimulus. Enhancement in relative delta power was calculated for each trial by dividing the relative power during visual stimulation by the relative power during rest before visual stimulation. MUA enhancement was calculated for each trial by dividing MUA firing rate during visual stimulation by MUA firing rate during spontaneous activity before stimulation. Each data point represents one trial. Best fit line is plotted in red (y = -0.31x + 1.59).

(C) Enhancement in relative theta power exhibited a near zero correlation with enhancement of MUA. Each data point represents one trial. Best fit line is plotted in red (y = 0.007x + 1.29).

(D) Enhancement in relative alpha power exhibited a negative correlation with enhancement of MUA. Each data point represents one trial. Best fit line is plotted in red (y = -0.51x + 1.77).

(E) Enhancement in relative beta power exhibited a near zero negative correlation with enhancement of MUA. Each data point represents one trial. Best fit line is plotted in red (y = -0.17 + 1.45).

(F) Enhancement of relative gamma power exhibited a positive correlation with enhancement of MUA. Each data point represents one trial. Best fit line is plotted in red (y = 0.58x + 0.57).

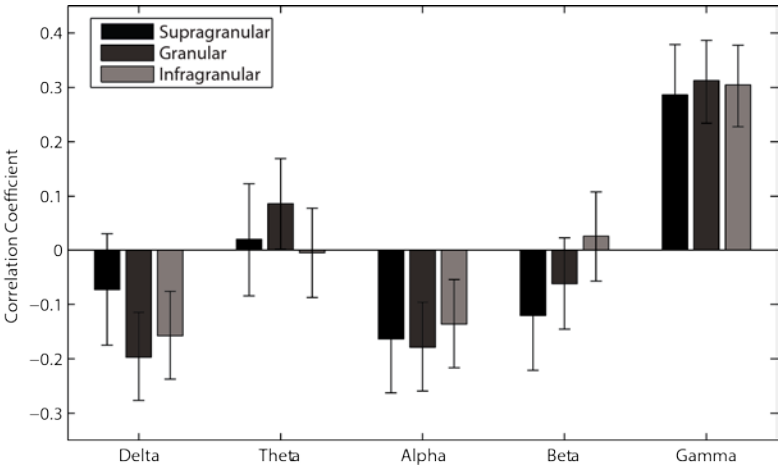

Figure 6.4. Relationship between mesoscale (LFP) and microscale activity (MUA) during free viewing of naturalistic visual input as a function of supragranular, granular, and infragranular electrode site locations

.

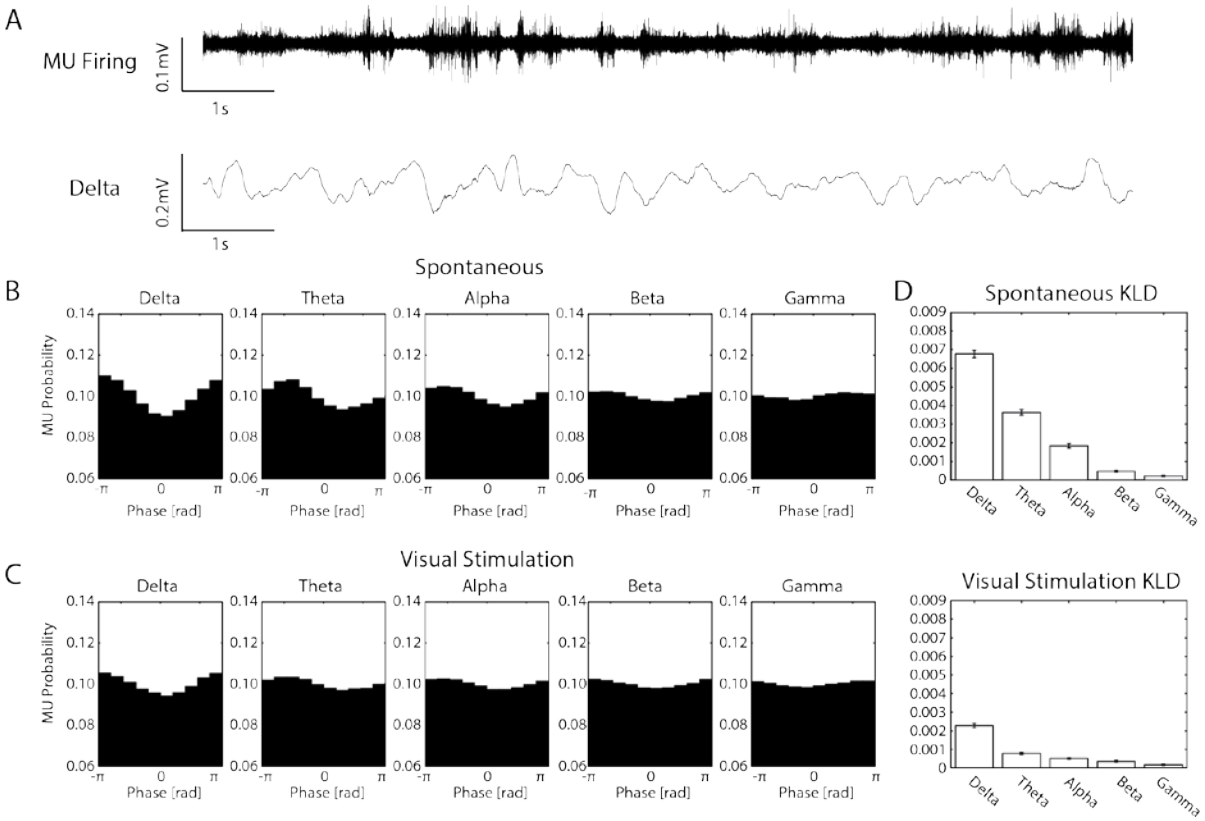

Figure 6.5. MUA exhibited the strongest preferred phase-of-firing to the delta oscillation; naturalistic visual stimulation decreased MUA preferred phase-of-firing in low frequencies.

(A) Simultaneous sample traces during spontaneous activity. High-pass filtered data (top) shows MUA which is phase aligned to the delta phase band-pass filtered LFP (bottom).

(B) Preferred phase-of-firing for all MUA during spontaneous activity, according to the phase of individual frequency bands.

(C) Preferred phase-of-firing for MUA during visual stimulation, according to the phase of each frequency band.

(D) The Kullback-Leibler divergence was used as a metric of non-uniformity of MUA. MUA showed the strongest phase-of-firing preference according to the phase of the delta oscillation. MUA exhibited stronger preferred phase-of-firing during spontaneous activity (top) compared to during visual stimulation (bottom). Plots show median and 95% CI.

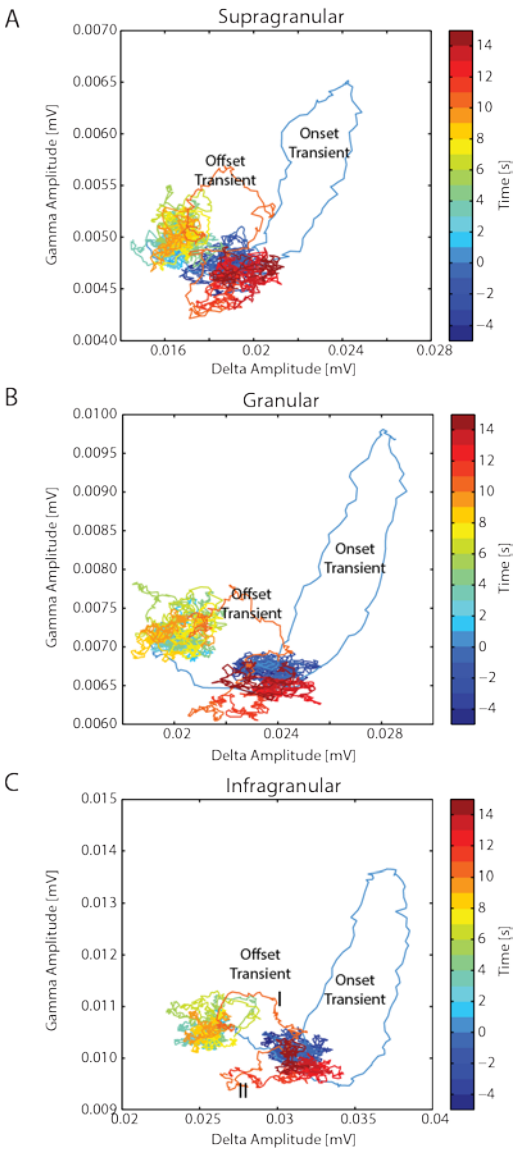

Figure 6.6. Phase-space representation of instantaneous amplitudes of delta and gamma oscillations

(A) Left: Trajectory of instantaneous delta and gamma amplitudes in supragranular layers, color-coded in 1 second increments. Periods of spontaneous activity are plotted in dark blue (before visual stimulation) and red (after visual stimulation), while periods of visual stimulation are plotted in intermediate colors. Onset and offset of the visual stimulation caused a transient change in both delta and gamma amplitudes.

(B) Same representations as in (A) but for granular layer.

(C) Same representations as in (A) but for infragranular layer.

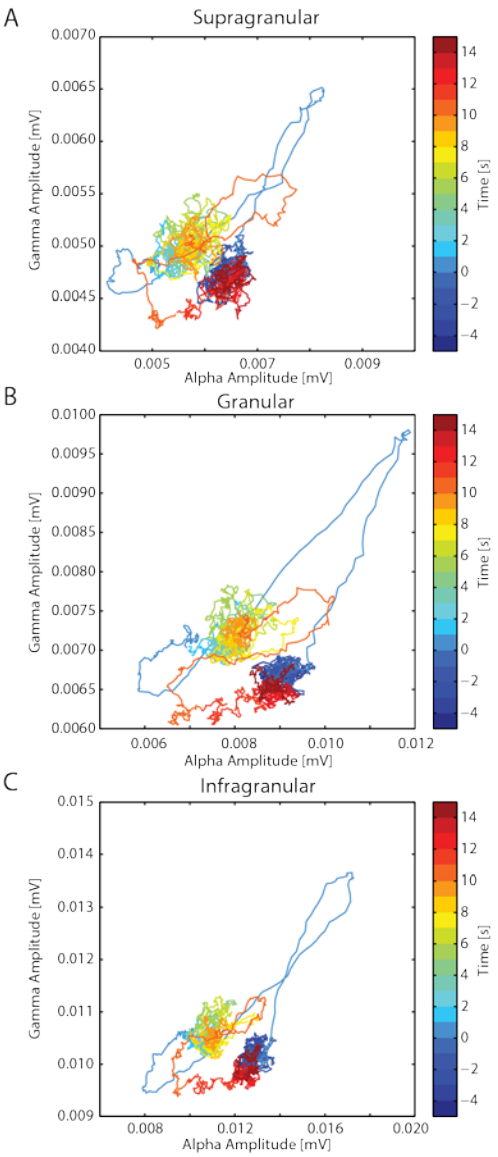

Figure 6.7. Phase-space representation of instantaneous amplitudes of alpha and gamma oscillations. Same representations as in Figure 6.6 but for different pair of frequency bands

(A) Left: Trajectory of instantaneous delta and gamma amplitudes in supragranular layers, color-coded in 1 second increments.

(B) Same representations as in (A) but for granular layer.

(C) Same representations as in (A) but for infragranular layer.

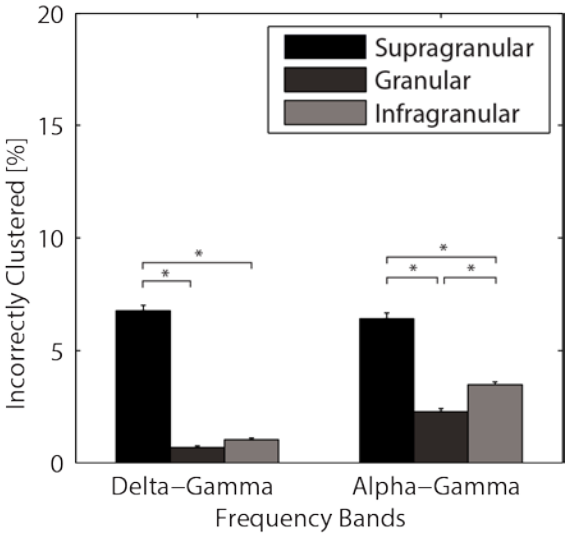

Figure 6.8. Percent of incorrectly clustered data points for delta-gamma and alpha-gamma trajectories, respectively.

100 iterations of bootstrapping were conducted to calculate standard error of the mean. Error bars indicate ± 1 sem, * indicates significantly different at $p < 0.05$.

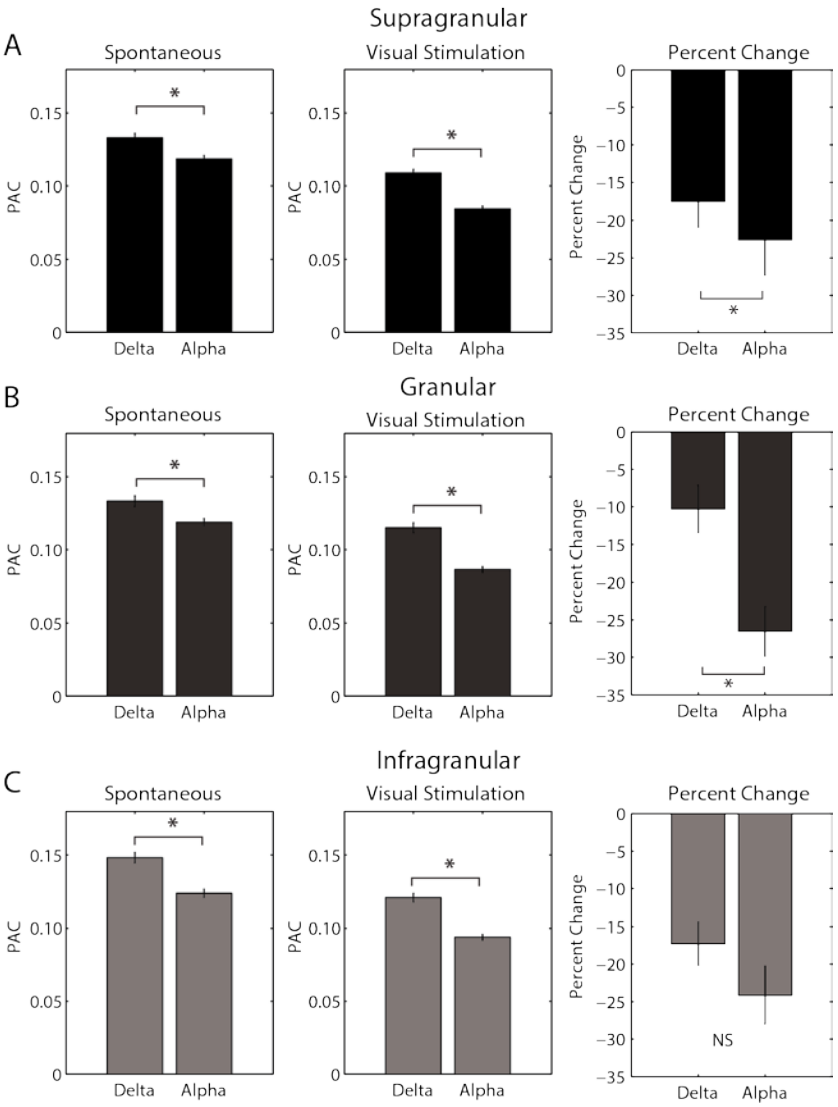

Figure 6.9. Phase-amplitude coupling (PAC) of low frequency phases and gamma amplitude was decreased by presentation of the naturalistic visual stimulus.

(A) PAC during spontaneous activity (left) between delta or alpha phase and gamma amplitude was decreased by presentation of the visual stimulus (middle, right). Coupling between delta phase and gamma amplitude was stronger than alpha-gamma PAC, and was less affected by visual stimulation.

(B) Same representations as in (A) but for granular layer.

(C) Same representations as in (A) but for infragranular layer

REFERENCES

Baddeley, R., Abbott, L. F., Booth, M. C. A., Sengpiel, F., Freeman, T., Wakeman, E. A., & Rolls, E. T. (1997). Responses of neurons in primary and inferior temporal visual cortices to natural scenes. *Proceedings of the Royal Society of London. Series B: Biological Sciences, 264*, 1775-1783. doi: 10.1098/rspb.1997.0246

Barlow, H. (1961). Possible principles underlying the transformations of sensory messages. In W. Rosenblith (Ed.), *Sensory Communication* (pp. 217-234): MIT Press.

Belitski, A., Gretton, A., Magri, C., Murayama, Y., Montemurro, M. a., Logothetis, N. K., & Panzeri, S. (2008). Low-frequency local field potentials and spikes in primary visual cortex convey independent visual information. *The Journal of neuroscience : the official journal of the Society for Neuroscience, 28*(22), 5696-5709. doi: 10.1523/JNEUROSCI.0009-08.2008

Bennett, C., Arroyo, S., & Hestrin, S. (2013). Subthreshold mechanisms underlying state-dependent modulation of visual responses. *Neuron, 80*(2), 350-357. doi: 10.1016/j.neuron.2013.08.007

Berkes, P., Orban, G., Lengyel, M., & Fiser, J. (2011). Spontaneous cortical activity reveals hallmarks of an optimal internal model of the environment. *Science, 331*(6013), 83-87. doi: 10.1126/science.1195870

Besserve, M., Scholkopf, B., Logothetis, N. K., & Panzeri, S. (2010). Causal relationships between frequency bands of extracellular signals in visual cortex revealed by an information theoretic analysis. *Journal of computational neuroscience, 29*(3), 547-566. doi: 10.1007/s10827-010-0236-5

Betti, V., Della Penna, S., de Pasquale, F., Mantini, D., Marzetti, L., Romani, G. L., & Corbetta, M. (2013). Natural scenes viewing alters the dynamics of functional connectivity in the human brain. *Neuron, 79*, 782-797. doi: 10.1016/j.neuron.2013.06.022

Brainard, D. H. (1997). The Psychophysics Toolbox. *Spatial vision, 10*(4), 433-436.

Brunet, N., Bosman, C. A., Roberts, M., Oostenveld, R., Womelsdorf, T., De Weerd, P., & Fries, P. (2013). Visual Cortical Gamma-Band Activity During Free Viewing of Natural Images. *Cerebral cortex*. doi: 10.1093/cercor/bht280

Busch, N. A., Dubois, J., & VanRullen, R. (2009). The phase of ongoing EEG oscillations predicts visual perception. *The Journal of neuroscience : the official journal of the Society for Neuroscience, 29*(24), 7869-7876. doi: 10.1523/JNEUROSCI.0113-09.2009

Buschman, T. J., & Miller, E. K. (2007). Top-down versus bottom-up control of attention in the prefrontal and posterior parietal cortices. *Science, 315*(5820), 1860-1862. doi: 10.1126/science.1138071

Canolty, R. T., & Knight, R. T. (2010). The functional role of cross-frequency coupling. *Trends in cognitive sciences, 14*(11), 506-515. doi: 10.1016/j.tics.2010.09.001

Cantone, G., Xiao, J., McFarlane, N., & Levitt, J. B. (2005). Feedback connections to ferret striate cortex: direct evidence for visuotopic convergence of feedback inputs. *The Journal of comparative neurology, 487*(3), 312-331. doi: 10.1002/cne.20570

Cardin, J. A., Carlen, M., Meletis, K., Knoblich, U., Zhang, F., Deisseroth, K., . . . Moore, C. I. (2009). Driving fast-spiking cells induces gamma rhythm and controls sensory responses. *Nature, 459*(7247), 663-667. doi: 10.1038/nature08002

Castro-Alamancos, M. A. (2004). Absence of rapid sensory adaptation in neocortex during information processing states. *Neuron, 41*(3), 455-464.

Chapman, B., & Stryker, M. P. (1993). Development of orientation selectivity in ferret visual cortex and effects of deprivation. *The Journal of neuroscience : the official journal of the Society for Neuroscience, 13*(12), 5251-5262.

Constantinople, C. M., & Bruno, R. M. (2011). Effects and mechanisms of wakefulness on local cortical networks. *Neuron, 69*(6), 1061-1068. doi: 10.1016/j.neuron.2011.02.040

Curto, C., Sakata, S., Marguet, S., Itskov, V., & Harris, K. D. (2009). A simple model of cortical dynamics explains variability and state dependence of sensory responses in urethane-anesthetized auditory cortex. *The Journal of neuroscience : the official journal of the Society for Neuroscience, 29*(34), 10600-10612. doi: 10.1523/JNEUROSCI.2053-09.2009

Dan, Y., Atick, J. J., & Reid, R. C. (1996). Efficient coding of natural scenes in the lateral geniculate nucleus: experimental test of a computational theory. *The Journal of neuroscience: the official journal of the Society for Neuroscience, 16*, 3351-3362.

David, S. V., Vinje, W. E., & Gallant, J. L. (2004). Natural Stimulus Statistics Alter the Receptive Field Structure of V1 Neurons. *The Journal of Neuroscience, 24*, 6991-7006. doi: 10.1523/JNEUROSCI.1422-04.2004

El Boustani, S., Marre, O., Behuret, S., Baudot, P., Yger, P., Bal, T., . . . Fregnac, Y. (2009). Network-state modulation of power-law frequency-scaling in visual cortical neurons. *PLoS Comput Biol, 5*(9), e1000519. doi: 10.1371/journal.pcbi.1000519

Ergenoglu, T., Demiralp, T., Bayraktaroglu, Z., Ergen, M., Beydagi, H., & Uresin, Y. (2004). Alpha rhythm of the EEG modulates visual detection performance in humans. *Brain Res Cogn Brain Res, 20*(3), 376-383. doi: 10.1016/j.cogbrainres.2004.03.009

Felsen, G., & Dan, Y. (2005). A natural approach to studying vision. *Nat Neurosci, 8*(12), 1643-1646. doi: 10.1038/nn1608

Fiser, J., Chiu, C., & Weliky, M. (2004). Small modulation of ongoing cortical dynamics by sensory input during natural vision. *Nature, 431*, 573-578. doi: 10.1038/nature02907

Fiser, J., Chiu, C. Y., & Weliky, M. (2004). Small modulation of ongoing cortical dynamics by sensory input during natural vision. *Nature, 431*(7008), 573-578. doi: Doi 10.1038/Nature02907

Froudarakis, E., Berens, P., Ecker, A. S., Cotton, R. J., Sinz, F. H., Yatsenko, D., . . . Tolias, A. S. (2014). Population code in mouse V1 facilitates readout of natural scenes through increased sparseness. *Nature neuroscience, 17*(6), 851-857. doi: 10.1038/nn.3707

Gallant, J. L., Connor, C. E., & Van Essen, D. C. (1998). Neural activity in areas V1, V2 and V4 during free viewing of natural scenes compared to controlled viewing:. *Neuroreport, 9*, 2153-2158. doi: 10.1097/00001756-199806220-00045

Goard, M., & Dan, Y. (2009). Basal forebrain activation enhances cortical coding of natural scenes. *Nat Neurosci, 12*(11), 1444-1449. doi: 10.1038/nn.2402

Goris, R. L. T., Movshon, J. A., & Simoncelli, E. P. (2014). Partitioning neuronal variability. *Nature neuroscience, 17*, 858-865. doi: 10.1038/nn.3711

Goupillaud, P., Grossmann, A., & Morlet, J. (1984). Cycle-Octave and Related Transforms in Seismic Signal Analysis. *Geoexploration, 23*(1), 85-102. doi: Doi 10.1016/0016-7142(84)90025-5

Haider, B., Duque, A., Hasenstaub, A. R., Yu, Y., & McCormick, D. A. (2007). Enhancement of visual responsiveness by spontaneous local network activity in vivo. *Journal of neurophysiology, 97*(6), 4186-4202. doi: 10.1152/jn.01114.2006

Haider, B., Hausser, M., & Carandini, M. (2013). Inhibition dominates sensory responses in the awake cortex. *Nature, 493*(7430), 97-100. doi: 10.1038/nature11665

Haider, B., Krause, M. R., Duque, A., Yu, Y., Touryan, J., Mazer, J. A., & McCormick, D. A. (2010). Synaptic and network mechanisms of sparse and reliable visual cortical activity during nonclassical receptive field stimulation. *Neuron, 65*(1), 107-121. doi: 10.1016/j.neuron.2009.12.005

Hanslmayr, S., Aslan, A., Staudigl, T., Klimesch, W., Herrmann, C. S., & Bäuml, K.-H. (2007). Prestimulus oscillations predict visual perception performance between and within subjects. *NeuroImage, 37*(4), 1465-1473. doi: 10.1016/j.neuroimage.2007.07.011

Harris, K. D., & Thiele, A. (2011). Cortical state and attention. *Nat Rev Neurosci, 12*(9), 509-523. doi: 10.1038/nrn3084

Hasenstaub, A., Sachdev, R. N., & McCormick, D. A. (2007). State changes rapidly modulate cortical neuronal responsiveness. *The Journal of neuroscience : the official journal of the Society for Neuroscience, 27*(36), 9607-9622. doi: 10.1523/JNEUROSCI.2184-07.2007

Hubel, D. H., & Wiesel, T. N. (1959). Receptive fields of single neurones in the cat's striate cortex. *The Journal of physiology, 148*, 574-591.

Ito, J., Maldonado, P., Singer, W., & Grün, S. (2011). Saccade-Related Modulations of Neuronal Excitability Support Synchrony of Visually Elicited Spikes. *Cerebral cortex, 21*, 2482-2497. doi: 10.1093/cercor/bhr020

Kayser, C., Salazar, R. F., & Konig, P. (2003). Responses to natural scenes in cat V1. *Journal of neurophysiology, 90*, 1910-1920. doi: 10.1152/jn.00195.2003

Law, M. I., Zahs, K. R., & Stryker, M. P. (1988). Organization of primary visual cortex (area 17) in the ferret. *The Journal of comparative neurology, 278*(2), 157-180. doi: 10.1002/cne.902780202

Lee, S. H., & Dan, Y. (2012). Neuromodulation of brain states. *Neuron, 76*(1), 209-222. doi: 10.1016/j.neuron.2012.09.012

Luczak, A., Bartho, P., & Harris, K. D. (2013). Gating of sensory input by spontaneous cortical activity. *The Journal of neuroscience : the official journal of the Society for Neuroscience, 33*(4), 1684-1695. doi: 10.1523/JNEUROSCI.2928-12.2013

MacEvoy, S. P., Hanks, T. D., & Paradiso, M. A. (2008). Macaque V1 Activity During Natural Vision: Effects of Natural Scenes and Saccades. *Journal of neurophysiology, 99*, 460-472. doi: 10.1152/jn.00612.2007

Mante, V., Bonin, V., & Carandini, M. (2008). Functional mechanisms shaping lateral geniculate responses to artificial and natural stimuli. *Neuron, 58*(4), 625-638. doi: 10.1016/j.neuron.2008.03.011

Masquelier, T., Hugues, E., Deco, G., & Thorpe, S. J. (2009). Oscillations, phase-of-firing coding, and spike timing-dependent plasticity: an efficient learning scheme. *The Journal of neuroscience : the official journal of the Society for Neuroscience, 29*(43), 13484-13493. doi: 10.1523/JNEUROSCI.2207-09.2009

Mazzoni, A., Brunel, N., Cavallari, S., Logothetis, N. K., & Panzeri, S. (2011). Cortical dynamics during naturalistic sensory stimulations: experiments and models. *Journal of physiology, Paris, 105*(1-3), 2-15. doi: 10.1016/j.jphysparis.2011.07.014

Mazzoni, A., Brunel, N., Cavallari, S., Logothetis, N. K., & Panzeri, S. (2011). Cortical dynamics during naturalistic sensory stimulations: experiments and models. *Journal of physiology, Paris, 105*, 2-15. doi: 10.1016/j.jphysparis.2011.07.014

Mazzoni, A., Panzeri, S., Logothetis, N. K., & Brunel, N. (2008). Encoding of naturalistic stimuli by local field potential spectra in networks of excitatory and inhibitory neurons. *PLoS computational biology, 4*(12), e1000239-e1000239. doi: 10.1371/journal.pcbi.1000239

Metherate, R., Cox, C. L., & Ashe, J. H. (1992). Cellular bases of neocortical activation: modulation of neural oscillations by the nucleus basalis and endogenous acetylcholine. *The Journal of neuroscience : the official journal of the Society for Neuroscience, 12*(12), 4701-4711.

Mitzdorf, U. (1985). Current source-density method and application in cat cerebral cortex: investigation of evoked potentials and EEG phenomena. *Physiological reviews, 65*(1), 37-100.

Montemurro, M. a., Rasch, M. J., Murayama, Y., Logothetis, N. K., & Panzeri, S. (2008). Phase-of-firing coding of natural visual stimuli in primary visual cortex. *Current biology : CB, 18*(5), 375-380. doi: 10.1016/j.cub.2008.02.023

Niell, C. M., & Stryker, M. P. (2010). Modulation of visual responses by behavioral state in mouse visual cortex. *Neuron, 65*(4), 472-479. doi: 10.1016/j.neuron.2010.01.033

Olshausen, B. A., & Field, D. J. (2005). How close are we to understanding v1? *Neural computation, 17*(8), 1665-1699. doi: 10.1162/0899766054026639

Palva, S., & Palva, J. M. (2007). New vistas for α-frequency band oscillations. *Trends in neurosciences, 30*(4), 150-158.

Polack, P. O., Friedman, J., & Golshani, P. (2013). Cellular mechanisms of brain state-dependent gain modulation in visual cortex. *Nature neuroscience, 16*(9), 1331-1339. doi: 10.1038/nn.3464

Poulet, J. F., & Petersen, C. C. (2008). Internal brain state regulates membrane potential synchrony in barrel cortex of behaving mice. *Nature, 454*(7206), 881-885. doi: 10.1038/nature07150

Purdon, P. L., Pierce, E. T., Mukamel, E. A., Prerau, M. J., Walsh, J. L., Wong, K. F., . . . Brown, E. N. (2013). Electroencephalogram signatures of loss and recovery of consciousness from propofol. *Proc Natl Acad Sci U S A, 110*(12), E1142-1151. doi: 10.1073/pnas.1221180110

Reinagel, P. (2001). How do visual neurons respond in the real world? *Current opinion in neurobiology, 11*, 437-442. doi: 10.1016/S0959-4388(00)00231-2

Ringach, D. L. (2004). Mapping receptive fields in primary visual cortex. *The Journal of physiology, 558*(Pt 3), 717-728. doi: 10.1113/jphysiol.2004.065771

Ruderman, D. L., & Bialek, W. (1994). Statistics of natural images: Scaling in the woods. *Phys Rev Lett, 73*(6), 814-817.

Scholvinck, M. L., Friston, K. J., & Rees, G. (2011). The influence of spontaneous activity on stimulus processing in primary visual cortex. *NeuroImage*. doi: 10.1016/j.neuroimage.2011.10.066

Sellers, K. K., Bennett, D. V., Hutt, A., & Frohlich, F. (2013). Anesthesia differentially modulates spontaneous network dynamics by cortical area and layer. *Journal of neurophysiology, 110*(12), 2739-2751. doi: 10.1152/jn.00404.2013

Simoncelli, E. P., & Olshausen, B. A. (2001). Natural image statistics and neural representation. *Annual review of neuroscience, 24*, 1193-1216. doi: 10.1146/annurev.neuro.24.1.1193

Simoncelli, E. P., & Olshausen, B. A. (2001). Natural image statistics and neural representation. *Annual review of neuroscience, 24*, 1193-1216. doi: 10.1146/annurev.neuro.24.1.1193

Smyth, D., Willmore, B., Baker, G. E., Thompson, I. D., & Tolhurst, D. J. (2003a). The receptive-field organization of simple cells in primary visual cortex of ferrets under natural scene stimulation. *The Journal of neuroscience : the official journal of the Society for Neuroscience, 23*(11), 4746-4759.

Smyth, D., Willmore, B., Baker, G. E., Thompson, I. D., & Tolhurst, D. J. (2003b). The receptive-field organization of simple cells in primary visual cortex of ferrets under natural scene stimulation. *The Journal of neuroscience : the official journal of the Society for Neuroscience, 23*(11), 4746-4759.

Sohal, V. S., Zhang, F., Yizhar, O., & Deisseroth, K. (2009). Parvalbumin neurons and gamma rhythms enhance cortical circuit performance. *Nature, 459*(7247), 698-702. doi: 10.1038/nature07991

Steriade, M., Amzica, F., & Nunez, A. (1993). Cholinergic and noradrenergic modulation of the slow (approximately 0.3 Hz) oscillation in neocortical cells. *J Neurophysiol, 70*(4), 1385-1400.

Steriade, M., McCormick, D. A., & Sejnowski, T. J. (1993). Thalamocortical oscillations in the sleeping and aroused brain. *Science, 262*(5134), 679-685.

Tolhurst, D. J., Movshon, J. A., & Dean, A. F. (1983). The statistical reliability of signals in single neurons in cat and monkey visual cortex. *Vision research, 23*(8), 775-785.

Tolhurst, D. J., Tadmor, Y., & Chao, T. (1992). Amplitude spectra of natural images. *Ophthalmic Physiol Opt, 12*(2), 229-232.

Tsodyks, M., Kenet, T., Grinvald, A., & Arieli, A. (1999). Linking spontaneous activity of single cortical neurons and the underlying functional architecture. *Science, 286*(5446), 1943-1946.

Uhlhaas, P. J., & Singer, W. (2012). Neuronal dynamics and neuropsychiatric disorders: toward a translational paradigm for dysfunctional large-scale networks. *Neuron, 75*(6), 963-980. doi: 10.1016/j.neuron.2012.09.004

van der Schaaf, A., & van Hateren, J. H. (1996). Modelling the power spectra of natural images: statistics and information. *Vision Res, 36*(17), 2759-2770.

van Dijk, H., Schoffelen, J.-M., Oostenveld, R., & Jensen, O. (2008). Prestimulus oscillatory activity in the alpha band predicts visual discrimination ability. *The Journal of neuroscience : the official journal of the Society for Neuroscience, 28*(8), 1816-1823. doi: 10.1523/JNEUROSCI.1853-07.2008

Vinje, W. E., & Gallant, J. L. (2000). Sparse coding and decorrelation in primary visual cortex during natural vision. *Science (New York, N.Y.), 287*, 1273-1276.

Voytek, B., Canolty, R. T., Shestyuk, A., Crone, N. E., Parvizi, J., & Knight, R. T. (2010). Shifts in gamma phase-amplitude coupling frequency from theta to alpha over posterior cortex during visual tasks. *Front Hum Neurosci, 4*, 191. doi: 10.3389/fnhum.2010.00191

Wang, X., Wei, Y., Vaingankar, V., Wang, Q., Koepsell, K., Sommer, F. T., & Hirsch, J. A. (2007). Feedforward Excitation and Inhibition Evoke Dual Modes of Firing in the Cat's Visual Thalamus during Naturalistic Viewing. *Neuron, 55*, 465-478. doi: 10.1016/j.neuron.2007.06.039

Weliky, M., Fiser, J., Hunt, R. H., & Wagner, D. N. (2003). Coding of Natural Scenes in Primary Visual Cortex. *Neuron, 37*, 703-718. doi: 10.1016/S0896-6273(03)00022-9

Whittingstall, K., & Logothetis, N. K. (2009). Frequency-Band Coupling in Surface EEG Reflects Spiking Activity in Monkey Visual Cortex. *Neuron, 64*, 281-289. doi: 10.1016/j.neuron.2009.08.016

Willmore, B. D. B., Mazer, J. A., & Gallant, J. L. (2011). Sparse coding in striate and extrastriate visual cortex. *Journal of neurophysiology, 105*, 2907-2919. doi: 10.1152/jn.00594.2010

Worgotter, F., Suder, K., Zhao, Y., Kerscher, N., Eysel, U. T., & Funke, K. (1998). State-dependent receptive-field restructuring in the visual cortex. *Nature, 396*(6707), 165-168. doi: 10.1038/24157

Zagha, E., Casale, A. E., Sachdev, R. N. S., McGinley, M. J., & McCormick, D. a. (2013). Motor cortex feedback influences sensory processing by modulating network state. *Neuron, 79*(3), 567-578. doi: 10.1016/j.neuron.2013.06.008

CHAPTER 7: OSCILLATORY INTERACTION DYNAMICS IN THE FRONTOPARIETAL ATTENTION NETWORK DURING SUSTAINED ATTENTION IN THE FERRET

INTRODUCTION

Numerous studies in both humans and animal models have reported frequency-specific modulation of cortical oscillations as a function of overall state and behavioral demands (Buzsaki & Draguhn, 2004; Engel, Fries, & Singer, 2001). Given the ubiquitous nature of oscillatory activity patterns in cortex, oscillations at specific frequencies cannot be associated with a single cognitive demand or behavior but are rather involved in a range of behaviors (Fries, 2005; Voytek & Knight, 2015). Yet there may be overarching principles which guide the presence of specific oscillations (Siegel, Warden, & Miller, 2009; von Stein & Sarnthein, 2000; Womelsdorf & Fries, 2007). For example, oscillations may enable the coordination of activity within and across multiple brain regions (Canolty et al., 2010; Fries, 2009; Sarnthein, Petsche, Rappelsberger, Shaw, & von Stein, 1998; Totah, Jackson, & Moghaddam, 2013; Varela, Lachaux, Rodriguez, & Martinerie, 2001). Overall, there is growing evidence that low-frequency oscillations generally mediate long-range local field potential (LFP) organization while higher-frequency gamma oscillations organize local activity (Kopell, Ermentrout, Whittington, & Traub, 2000; von Stein, Chiang, & Konig, 2000).

Visual attention is ideal for investigating such organization of inter-area interaction dynamics since it requires coordination of activity within and across brain regions (Clayton, Yeung, & Cohen Kadosh, 2015; Posner & Petersen, 1990). Substantial work conducted using fMRI has demonstrated that visual attention is correlated with activation of a number of cortical (frontal, parietal, temporal, occipital) as well as subcortical (thalamic and midbrain) regions (Corbetta & Shulman, 2002; Langner & Eickhoff, 2013; Petersen & Posner, 2012; Scolari, Seidl-Rathkopf, & Kastner, 2015). In particular, the frontoparietal attention network is activated during attention-demanding visuospatial tasks (Katsuki & Constantinidis, 2012). However, the finer-time scale electrophysiological correlates of sustained attention are less clear.

Limited work has shown that prefrontal and posterior parietal cortices exhibit LFP synchrony in lower and middle gamma frequencies during top-down and bottom-up attention, respectively (Buschman & Miller, 2007). During the preparatory attention period of a task-switching paradigm, frontoparietal networks in monkeys exhibited increased 5 to 10Hz phase synchronization in trials which required a top-down behavioral strategy (Phillips, Vinck, Everling, & Womelsdorf, 2014). However, it remains poorly understood how spiking activity in the frontoparietal network is organized by oscillatory structure locally and long-range during sustained attention. To fill this gap, we investigated LFP oscillations and SU spiking activity and their relationship both within and between PFC and PPC during a task that requires sustained attention, the 5-choice serial reaction time task (5-CSRTT). We hypothesized that local organization of spiking activity is mediated by high frequency oscillatory activity, while long-range organization relies on low-frequency oscillations.

METHODS

Behavioral Training

Spayed female ferrets (*Mustela putorius furo,* ~17 weeks old at study onset) were used in this study. 3 animals were trained to perform a sustained visual attention task. 4 additional animals were used for anatomical studies. All animal procedures were approved by the Institutional Animal Care and Use Committee of the University of North Carolina at Chapel Hill, and complied with guidelines set by the National Institute of Health.

We adapted the 5-choice serial reaction time task with touch screen implementation for this study (Bari, Dalley, & Robbins, 2008). An enclosed and sound-insulated custom-built behavioral box (interior box = 50 x 60 cm, exterior box = 83 x 91 x 110 cm) was used for training and testing sessions. A capacitive touch screen (Acer T232HL bmidz 23-inch touch screen LCD display) was secured behind a plexiglass mask with 5 squares (7 x 7 cm) to allow for response touches at one end of the box, and a spout for water delivery with infrared sensor and LED illumination was positioned near the floor on the opposing wall. Auditory cues were delivered through speakers (HP Compact 2.0 speaker), a houselight was mounted above the animal, and infrared videography was conducted during each session (Microsoft LifeCam Cinema 720p HD Webcam). Training was conducted in successive levels in order to train the

animal to associate the lick spout with reward, initiate trials at the lick spout, touch the screen, and touch the screen only following stimulus presentation.

Successful trial initiation was indicated by a beep (0.1s duration) and the lick spout light turning off. Following a 5 second delay period ('sustained attention'), one of the five windows displayed a white square filling the response area for 3.5 seconds. Correct responses could be indicated by touching this window during this 3.5 second period or for the 2 seconds following. Correct touches were indicated by immediate disappearance of the stimulus, a tone (0.5s duration), and the release of a water reward at the lick spout. Responses prior to the stimulus onset (premature), touch of one of the 4 unlit squares (incorrect), and lack of any touch response (omission) were indicated by a white noise stimulus (1s duration), illumination of the house light, and the start of a 6 second time-out period. Following the time-out period or 8 seconds after a correct response (sufficient time for the animal to retrieve water reward), the lick spout light re-illuminated to indicate the next trial could be initiated. Control of the behavior session was conducted using custom-written MATLAB code (MathWorks, Natick, MA) and a data acquisition device (USB 6212, National Instruments, Austin, TX). Each recording session consisted of 100 trials, although some sessions were terminated early if the animal stopped initiating trials.

Animals were trained and tested once daily on a 5 days on / 2 days off schedule. During training and testing, animals were water restricted to enhance participation in the behavioral task. Training/testing was conducted in the mornings, during which time animals received water for correct responses. Supplemental water was provided in the afternoon such that each animal had access to 60mL/kg/day. Ad lib water was provided during the 2 days off. Animal weight was monitored daily to ensure sufficient hydration.

Microelectrode Array Implantation Surgery

Upon meeting training criterion (5 consecutive days of at least 60 trials completed with less than 30% omission), animals were implanted with microelectrode arrays in PFC and PPC. Aseptic surgical procedures were used, as previously described (Sellers, Bennett, Hutt, & Frohlich, 2013; Sellers, Bennett, Hutt, Williams, & Frohlich, 2015). After anesthesia induction using an intramuscular (IM) injection of ketamine/xylazine (30 mg/kg of ketamine, 1-2 mg/kg of xylazine), ferrets were intubated and deep

anesthesia was maintained with isoflurane (1-2%) in 100% oxygen. Throughout surgery, end-tidal CO_2, electrocardiogram, partial oxygen saturation, and rectal body temperature were monitored. Body temperature was maintained between 38-39°C with a water heating blanket and end-tidal CO_2 was between 30-50 mmHg. Tissue and muscle were retraced to expose the skull surface. Two small craniotomies were made to access right hemisphere PFC (5 mm anterior to bregma and 2 mm lateral to the midline) and PPC (3.5 mm lateral to the midline and midway between bregma and lambda). 32-channel microelectrode arrays (tungsten electrodes oriented 4 x 8, 200µm spacing, low impedance reference electrode 1mm shorter on the same array, Innovative Neurophysiology, Durham, NC) were positioned above each craniotomy using a stereotaxic arm and slowly inserted into deep layers of cortex. Arrays were secured using dental cement, muscle and skin were sutured, and anesthesia was reversed. Animals were allowed to recover in their home cages for at least 7 days prior to reintroduction to water restriction and recording sessions. During recovery, meloxicam was administered for pain relief (0.2 mg/kg IM injection) and clavamox was administered to prevent infection (12.5-13mg/kg, PO).

In Vivo Electrophysiological Recordings

Continuous electrophysiological data was acquired during behavior at a sampling rate of 20kHz with a bandwidth of 0.1Hz to 5kHz using headstages (RHD2132 amplifier board, Intan Technologies, Los Angeles, CA) which amplified and digitized the signal and then transmitted via a cable to a control board (RHD2000 USB Interface Board, Intan Technologies, Los Angeles, CA). Behavioral responses were recorded as digital inputs together with the electrophysiology to ensure proper synchronization of neuronal activity and behavior. Because the task was self-paced, we selected behavioral responses to align the trials. Specifically, trial initiation was used for alignment, and 5 second before and 7 seconds after this time point were analyzed. The 5 seconds following initiation represent the sustained attention period. We only analyzed trials with correct responses, in which the animal was facing the screen at the time of stimulus onset. In order to select only trials in which the animal was facing the screen prior to stimulus onset, we manually reviewed video recordings and coded the orientation of the animal immediately prior to the stimulus onset as facing or not facing the screen. A small subset of trials with

signal artifacts, identified as simultaneous large amplitude deflections across channels, were excluded from analysis.

Data Analysis

The local field potential (LPF) was extracted by applying a low-pass filter (2^{nd} order Butterworth filter with cutoff at 300Hz) to the raw data. Spectral analysis was performed by convolving the LFP signals with a family of Morlet wavelets (0.5 to 120Hz, step width of 0.5Hz; or 0.2 to 10Hz, step width of 0.2Hz). Spectral analysis was conducted at standard frequency bands (delta = 0.5-4Hz, theta = 4- 8Hz, alpha = 8-12Hz, beta = 12-30Hz, gamma = 30-80Hz, high gamma = 80-120Hz). We found that all animals exhibited a local peak at 5Hz, and thus used this frequency for subsequent theta analysis. We also found that each animal exhibited a local peak in approximately the gamma frequency range (29Hz, 34Hz, and 33Hz, respectively) in PPC during the sustained attention period, and thus centered a 10Hz band around this local peak for each animal for analysis of PPC gamma. To assess difference in spectral power before and after trial initiation, the power within each frequency band was averaged for the 5 seconds prior to initiation and the 5 seconds after initiation (the sustained attention period).

Spikes were sorted into putative single units (SU) using standard methods (Offline Sorter, Plexon Inc, Dallas, TX). Briefly, spikes were detected by applying a high-pass filter (2^{nd} order butterworth filter with cutoff at 300Hz) to raw traces and a threshold of -4*standard deviation (750 µs deadtime); waveforms of 1600µs were extracted. The T-distribution expectation maximization algorithm was used to sort spikes from the first 300 seconds of recordings in order to create unit templates. Spikes were then matched to these templates. Outlier waveforms were removed through manual inspection. Spikes with shorter than 1ms refractory period were removed.

A structural change test (Chow, 1960) was used to assess if spiking activity was significantly modulated over the course of the peristimulus time period. Methods were adopted from (Kimchi & Laubach, 2009) and use the strucchange library (Zeileis, Leisch, Hornik, & Kleiber, 2002) for R (https://www.r-project.org/). Briefly, a PSTH was calculated for each unit with bin width of 1ms and convolved with a Gaussian window; a linear model was fit to the full data window, and a series of linear models were fit to smaller data windows. An F-statistic was calculated and evaluated with a criterion of p

< 0.05 to determine if the coefficients from the linear regressions based on the full series and the local segment were significantly different. In the case of significant differences between the linear regressions, the point with the largest change was indicated (breakpoint).

Phase locking values between LFP signals in the two brain regions were calculated as previously described (Lachaux, Rodriguez, Martinerie, & Varela, 1999; Liebe, Hoerzer, Logothetis, & Rainer, 2012). For every possible channel pair between PFC and PPC (*m* and *n*, respectively) a value for phase locking between 0 and 1 was calculated as

$$PLV_{mn}(t, f_0) = \frac{1}{K}\left|\sum_{k=1}^{K} e^{i(\varphi_k^m(t,f_0) - \varphi_k^n(t,f_0))}\right|$$

where *K* indicates trials, and $\varphi_k^m(t, f_0)$ and $\varphi_k^n(t, f_0)$ indicate the instantaneous phases of the two channels at frequency f_0 calculated using the Morlet wavelet transform. Significance was determined by the Rayleigh statistic at a significance level of p < 0.05 (Fisher, 1993). Summary figures show the average of significant PLV across channels pairs.

In order to assess the degree of phase-locking of single units, as a function of time and frequency, we calculated spike-LFP synchrony according to methods previously described (Totah et al., 2013). For the 12 second trials aligned by trial initiation, spike-LFP phase locking was calculated in 2s sliding windows with 200ms increments. Specifically, for each time window, LFP phase angles were extracted using the wavelet transform at each spike time across trials. The circular statistics toolbox for MATLAB was used for statistical analysis of spike-LFP phase synchrony (Berens, 2009). If any time window had fewer than 50 spikes, the unit was removed from analysis. Prior to calculating strength of phase locking, differences in spike rate across time for each unit were corrected for by subsampling the number of spikes in each window such that all windows had the same number of spikes. For analysis of spike-LFP phase locking within area, the phase was taken from a neighboring electrode in order to avoid potential bleed-through of spiking activity in the LFP. For analysis of spike-LFP phase locking across areas (phase from PFC, spiking in PPC, and vice versa), the LFP was averaged across channels in the phase-providing brain region and the wavelet transform was conducted on this averaged signal. The strength of spike-LFP phase locking was then calculated using Rayleigh's Z,

$$Z = nR^2$$

where n spikes contribute to the mean resultant phase vector length, R. The p-value at a significance level of 0.05 was computed using the approximation

$$p = e^{\left[\sqrt{(1+4N+4(N^2-R_n^2))}-(1+2n)\right]}$$

where $R_n = R \times n$ (Zar, 1999). The fraction of units exhibiting significant spike-LFP phase locking was determined by a significant estimated p-value for at least 20% of the trial.

Phase-amplitude coupling (PAC) (Voytek et al., 2010) was used to assess the relationship of activity in two different frequencies. We were specifically interested in the relationship of theta phase (centered at 5Hz) and high gamma amplitude (80-120Hz). The LFP was bandpass filtered separately in each of these frequency ranges. The high-gamma analytic amplitude signal was then filtered at the theta frequency band. The Hilbert transform was used to extract the phase of both signals (alpha-filtered, alpha-filtered high-gamma amplitude) and PAC was calculated as the mean vector between the angles. A Fisher's z-transform was used to normalize the data to an approximately Gaussian distribution, and the Kolmogorov-Smirnov test was used to assess if PAC values were significantly different from zero.

Tracing Studies

Two types of tracer studies were conducted to determine direct anatomical projections from PFC to PPC. Anterograde virus, rAAV5-CamKII-GFP (titer of 6 x 1012 vg/ml; dialyzed with 350 nM NaCl and 5% D-sorbitol in PBS, UNC Vector Core, Chapel Hill, NC), was injected in PFC (n = 2 animals) and retrograde tracer Alexa 488-conjugated cholera toxin subunit B (CTB, 1% CTB in phosphate buffer, Invitrogen) was injected in PPC (n = 2 animals) (Conte, Kamishina, & Reep, 2009). Similar aseptic surgical procedures were used as described above. rAAV5-CamKII-GFP or Alexa 488-conjugated cholera toxin subunit B were prepared in a 1 µL Hamilton syringe (Hamilton Company, Reno, NV). In the case of GFP injection, 1 µL of virus was delivered (0.1 µL/min) bilaterally in PFC at a depth of 0.9mm below the surface of cortex. In the case of CTB injection, 0.1 and 0.6µL was delivered (0.1 µL/min) bilaterally in PPC at a depth of 1-1.5mm below the surface of cortex. Following injection, the syringe was left in place for 10 minutes before being slowly removed. The craniotomy was covered with bone wax, and the tissue was sutured as described above. Virus was allowed to express for 10 weeks and CTB was allowed to traffic for 7 days.

Histological Procedures

Upon reaching scientific endpoint, electrolytic lesions were conducted in implanted animals by passing current through the four corner electrodes of the microelectrode array (5 µA, 10s, unipolar). Animals were humanely euthanized with an overdose of sodium pentobarbital and immediately perfused with 0.1M PBS and 4% paraformaldehyde solution in 0.1M PBS. 60 µm coronal sections of the fixed brain were prepared with a cryostat (CM3050S, Leica Microsystems). Sections from animals implanted with microarrays were separated into series and stained for cytochrome oxidase or Nissl (Yu et al., 2016). Sections from animals used in tracing studies were separated into series and cover-slipped unstained with DAPI mounting medium (Sigma-Aldrich, St. Louis, MO), or stained for cytochrome oxidase or Nissl. Slides were imaged using either a widefield microscope (Nikon Eclipse 80i, Nikon Instruments, Melville, NY) or a confocal microscope with 10x objective (Zeiss LSM, Zeiss, Jena, Germany).

RESULTS

Animals performed a sustained attention task, the 5-CSRTT, during simultaneous recording of LFP and spiking activity in PFC and PPC (Figure 7.1). In this self-paced task, animals initiated trials to start a 5-second sustained attention period, at the end of which a white square was displayed in one of five windows on a touchscreen for 3.5 seconds. Correct responses of the animal touching the window in which the stimulus was presented resulted in water reward, while other responses (premature: touching any window prior to stimulus presentation, incorrect: touching one of the other four windows, or omission: not touching any window) resulted in a time-out and no water reward. Animals performed this task with high accuracy (Figure 7.1C, performance of Animal C; Supplementary Figure 7.A). We focused on the time period 5 seconds prior to initiation to 7 seconds after initiation, which encompassed the 5-second sustained attention period of interest; subsequent analyses was conducted only on trials with correct behavioral responses in which the animal was facing the screen at the time of stimulus onset (verified by reviewing video). In total, we analyzed 42 sessions (Animal A = 7 sessions, Animal B = 16 sessions, Animal C = 19 sessions) with a total of 2418 trials (mean number of correct trials for each recording ± std: Animal A = 35.14 ± 7.47 trials, Animal B = 50.88 ± 22.27 trials, Animal C = 71.47 trials ± 9.06). After spike

sorting, we analyzed 458 single units in PFC (Animal A = 155, Animal B = 172, Animal C = 131) and 397 single units in PPC (Animal A = 193, Animal B =142, Animal C = 62).

The frontoparietal attention network in humans and monkeys exhibits rich anatomical connectivity (Cavada & Goldman-Rakic, 1989; Szczepanski, Pinsk, Douglas, Kastner, & Saalmann, 2013). Because we were interested in the frontoparietal attention network in the ferret, we conducted a separate tracing study (n = 4 animals) to determine if PFC and PPC exhibit direct anatomical connectivity in this intermediate model species. We conducted anterograde tracing using CaMKII-GFP injected into PFC (Figures 7.2A-C) and retrograde tracing using CTB injected into PPC (Figures 7.2D-F). Results from both of these tracing methods were in agreement and demonstrated direct anatomical connections from PFC to PPC. This lends support that these regions of PFC and PPC in the ferret are part of the frontoparietal attention network. Recording locations were verified with histology (Figure 7.3), and correspond to the PFC and PPC locations from the tracing study.

Task-Modulated Spiking Activity and Spectral Power in Select Frequencies

We first investigated how spiking activity and spectral power were modulated during the sustained attention period (Figure 7.4). Because we were interested in activity of single units throughout this period, rather than just transient evoked response such as in response to a visual stimulus, we employed a structural change test to assess modulation of spiking activity (Kimchi & Laubach, 2009). We found a 86.7% of PFC units and 85.1% of PPC units were modulated during the peristimulus period (Figure 7.4A left, percent of PFC units for each animal which were significantly task-modulated shown in color: Animal A = 80.7%, Animal B = 89.5%, Animal C = 90.1%; Figure 7.4B left, percent of PPC units for each animal which were significantly task-modulated shown in color: Animal A = 77.2%, Animal B = 94.4%, Animal C = 88.7%). The largest breakpoints for each significantly modulated unit indicate at what time the greatest change in spiking activity structure occurred (Figures 7.4A and B, right). PFC exhibited changes in spiking activity structure throughout the sustained attention period, whereas PPC spiking modulation was more localized to the trial and stimulus onsets.

Next, we looked at modulation of spectral power during the task. There were no local peaks in the PFC spectra (Figure 7.4C, averaged across recording sessions for Animal C). However, PPC exhibited

local peaks in activity at 5Hz (theta) and in the gamma band (Figure 7.4D, averaged across recording sessions for Animal C). There was a modest increase in power during the sustained attention period at delta frequencies, 5Hz, gamma frequencies (defined as a 10Hz band centered at the individual animal's local gamma peak), and high gamma frequencies (80-120Hz) in PPC (delta: $t(41) = -5.35$, $p < 0.001$; 5Hz theta, $t(41) = -6.62$, $p < 0.001$; gamma: $t(41) = -10.30$, $p < 0.001$; high gamma: $t(41) = -6.73$, $p < 0.001$). There was no significant change in spectral power during the sustained attention period in PFC. Based on the task-modulated activation of theta, gamma, and high gamma oscillations in PPC during the sustained attention period, we focused our subsequent investigation of local and long-range activity organization on these frequencies.

Task-Modulated Theta Phase Synchronization between PFC and PPC

Having demonstrated that select frequencies exhibited task-dependent modulation, we next asked if activity in PFC and PPC was coordinated at these frequencies. To assess synchronization between these areas across time and frequency, we calculated PLV (Lachaux et al., 1999) between simultaneously recorded channel pairs in PFC and PPC (mean number of electrode pairs for each recording ± std: Animal A = 779.14 ± 131.76 pairs, Animal B = 683.53 ± 212.55 pairs, Animal C = 498.32 ± 221.31 pairs) for frequencies between 0.2 to 120Hz. We found prominent 5Hz theta phase synchronization before trial initiation and after trial initiation, but a disruption in this between-area communication at the time of trial initiation (Figure 7.5A, example phases at 5Hz from a single channel pair example; Figure 7.5C, significant PLV for Animal C, averaged across recordings; Supplemental Figure 7.B). For all animals, synchronization at 5Hz was the most prominent between-region communication frequency (Figure 7.5B). 76% of recordings showed decreased PLV at 5Hz during initiation compared to before and after initiation (defined as -3 to -1 seconds and 1 to 3 seconds relative to initiation, respectively). Phase-locking at 5Hz was significantly decreased during trial initiation (defined as 0.5 seconds before initiation to 0.5 second after initiation) compared to before or after initiation (Figure 7.5D, paired t-test, before vs during: $t(41) = 3.17$, $p = 0.003$; after vs during: $t(41) = 3.36$, $p = 0.002$). Average phase lags across all recordings (PFC phase minus PPC phase) were small for all three animals (Figure 7.5E).

Unidirectional Long-Range Theta Spike-LFP Phase Locking

Theta phase synchronization between PFC and PPC indicates that this low-frequency oscillation may serve as the substrate for long-range cortico-cortical communication in the state of sustained attention. To confirm that this rhythmic interaction guided the spiking activity, we next assessed if spiking activity across these brain areas was also organized by theta oscillations. Specifically, we tested if spike-timing in one area was influenced by the phase of the theta oscillation in the other area by calculating spike-LFP phase locking. For each unit, the instantaneous phase was extracted for each spike. Rayleigh's Z was used as a measure of the strength of phase locking, and only values which were significant as determined by an estimated p-value were included. Normalization was conducted for differences in firing rates prior to calculating spike-LFP phase locking. We calculated time- and frequency-resolved spike-LFP phase locking both across area (units from PFC, phase from PPC, and vice versa) (Liebe et al., 2012; Totah et al., 2013).

In keeping with the phase synchronization in the theta frequency band between PFC and PPC, we found that units in PFC were phase locked to the theta oscillation in PPC. Of the 449 PFC unit – PPC phase pairs analyzed (Animal A = 152 pairs, Animal B = 168 pairs, Animal C = 129 pairs), 30.5% exhibited theta spike-LFP locking (Animal A = 60.5%, Animal B = 13.7%, Animal C = 17.1%), as defined by significant theta spike-LFP phase locking for at least 20% of the trial (Figure 7.6B, fraction of significantly phase-locking units across time for Animal A; Supplementary Figure 7.C). As shown by an example unit from Animal A, the strength of spike-LFP phase locking is centered on a narrow band at 5Hz (Figure 7.6C). A polar histogram shows the distribution of phases of each spike. Interestingly, phase locking did not exhibit any significant fluctuations across the duration of the trial; there was no significant difference in the average strength of significant spike-PLF phase locking before initiation and during the sustained attention period (PFC units: $t(180) = 1.54$, $p = 0.13$). In contrast, there was no sizeable phase locking of PPC units to theta oscillations in PFC. Of the 393 PPC unit – PFC phase pairs analyzed (Animal A = 189 pairs, Animal B = 142 pairs, Animal C = 62 pairs), only 1.8% exhibited theta spike-LFP locking (Supplementary Figure 7.E; Animal A = 1.6%, Animal B = 2.1%, Animal C = 1.6%). This unidirectional coupling of spikes to the theta phase suggests that the theta oscillation organizes cortico-cortical long-range interaction.

Local Theta and High Gamma Spike-LFP Phase Locking in PFC

Having established the importance of theta oscillations for the long-range coupling of PFC and PPC, we next sought to investigate whether theta oscillations were also responsible for the organization of local processing within each brain area. In principle, both long-range and local processing could rely on the theta oscillation; however, an alternative possibility is that local and long-range synchronization are mediated by different frequencies. In order to disambiguate between these possibilities, we investigated within-area spike-LFP phase locking (phase and units from the same brain area, on neighboring electrodes) across a broad range of frequencies.

Based on the fraction of significantly locked units, both theta and broad high gamma (80-120Hz) are relevant for local organization of spiking activity in PFC (Figure 7.7A). In addition to a greater fraction of units being significantly phase-locked to theta and high gamma, the strength of spike-LFP phase locking was greater in these frequencies compared to alpha, beta, and gamma frequencies (Figure 7.7B, average strength of significant spike-LFP phase locking for Animal A). Of the PFC unit – PFC phase pairs analyzed (Animal A = 152 pairs, Animal B = 168 pairs, Animal C = 126 pairs), 26.2% percent exhibited theta spike-LFP locking (Supplementary Figure 7.D; Animal A = 52.0%, Animal B = 10.1%, Animal C = 16.7%) and 45.5% to 61.9% exhibited high gamma spike-LFP locking in the 80-120Hz range (Animal A = 59.9% to 76.3%, Animal B = 35.1% to 47.%, Animal C = 42.1% to 63.5%). One example unit shows strong spike-LFP phase locking at 5Hz (Figure 7.7D), while another example unit shows spike-LFP phase locking broadly in the high gamma frequencies (Figure 7.7F). Of the PFC units with significant spike-LFP phase locking, 59% exhibited significant spike-LFP phase locking to 5Hz oscillations both locally in PFC and long-range with oscillations in PPC, while 14% and 27% exhibited only local or long-range locking, respectively (Figure 7.7G).

High Gamma Spike-LFP Phase Locking Locally in PPC

We next asked if the phase-locking to the theta and the gamma oscillation is a general principle that is shared by PFC and PPC. To answer this question, we performed the same analysis as above but for the PPC units. In contrast to our findings in PFC, PPC units only showed strong spike-LFP phase

locking to high gamma phase. Of the PPC unit – PPC phase pairs analyzed (Animal A = 189 pairs, Animal B = 142 pairs, Animal C = 62 pairs), only 7.6% percent exhibited theta spike-LFP locking (Supplementary Figure 7.D; Animal A = 6.4%, Animal B = 9.9%, Animal C =6.5 %) while 44.5% to 57.0% exhibited high gamma spike-LFP locking in the 80-120Hz range (Figure 7.8A, Animal A = 60.3% to 72.0%, Animal B = 22.5% to 30.1%, Animal C = 46.8% to 71.0%). Similar to the example unit in PFC, spike-LFP phase locking across broad high gamma frequencies is apparent in an example PPC unit (Figure 7.8C).

Theta and High Gamma Oscillations Organize Locally Through Phase-Amplitude Coupling

Given the prominent role of theta and gamma rhythms for organizing local and long-range synchrony, we next asked if and how theta and gamma coordinate locally. To answer this question, we calculated the phase-amplitude coupling of these two oscillations. Indeed, we found theta-high gamma phase-amplitude coupling in both PFC and PPC (Figure 7.9, Supplementary Figure 7.E). Theta-high gamma PAC was significant for each animal (Kolmogorov-Smirnov test was used to assess if PAC values were significantly different from zero, PAC in PFC and PPC for all animals $p < 0.001$).

Taken together, this work points to the coordination of low-frequency (theta) and high-frequency (high gamma, 80-120Hz) oscillations in organizing spiking activity long-range and locally. Figure 7.10 provides a summary of the local and long-range coordination within and between PFC and PPC elucidated in this study.

DISCUSSION

We found that PFC and PPC exhibited task-dependent synchronization at 5Hz during a sustained attention task. PFC spiking was organized locally by theta and high-gamma oscillations and long-range by PPC theta oscillations, while PPC spiking was only guided by local high-gamma oscillations. This suggests that overall regulation of neuronal processing during sustained attention is coordinated by a combination of local and long-range information integration, relying on different frequencies.

Relevance of PFC and PPC to Sustained Attention

Attention is a broad construct which has been defined as “the selective prioritization of the neural representations that are most relevant to one’s current behavioral goal” (Buschman & Kastner, 2015). Sustained attention, one facet of overall attention, involves focusing on one task for a continuous amount of time. The behavioral task used in this study, the 5-CSRTT, includes aspects of the continuous performance task used in humans and has been used extensively in assessing sustained attention in animals (Robbins, 1998). To our knowledge, this is the first investigation of neuronal networks underlying sustained visual attention in the ferret. We recorded from PFC in the rostral-most portion of the anterior sigmoid gyrus, similar to (Duque & McCormick, 2010; Fritz, David, Radtke-Schuller, Yin, & Shamma, 2010) and the caudal portion of PPC located on the suprasylvian gyrus. This area of PFC in ferrets has been shown to have reciprocal connections with thalamus (Duque & McCormick, 2010), and appears to be responsible for behaviorally-relevant selection of sensory stimuli (Fritz et al., 2010; Zhou, Yu, Sellers, & Frohlich, 2016). Our recording and tracer injection locations agreed with localization of PPC as defined by (Foxworthy, Allman, Keniston, & Meredith, 2013; Foxworthy & Meredith, 2011; Manger, Masiello, & Innocenti, 2002).

Through anterograde and retrograde tracing, we found that these areas in the ferret exhibit direct anatomical connections. In humans, direct frontoparietal connectivity assessed using diffusion tensor imaging found that the strength of white-matter fibers is related to the efficiency of attentional selection in visuospatial tasks (Tuch et al., 2005). The frontoparietal attention network in humans and monkeys incorporates multiple subdivisions of PFC and PPC which are strongly interconnected through fibers passing through the superior longitudinal fasciculus; regions in this network include but are not limited to the intraparietal sulcus, Areas 7a and 7b in the inferior parietal lobule, frontal eye field (FEF), and dorsal premotor cortex (Ptak, 2012). Taken together, our results suggest that in ferrets, these regions of PFC and PPC may be homologous to aspects of the frontoparietal attention network in the primate and human brain.

Extensive work in animals and humans has demonstrated the importance of the frontoparietal network, and in particular PFC and PPC, in mediating attention (Katsuki & Constantinidis, 2012). Inactivation of PFC in monkeys with muscimol injection resulted in a deficit in selective attention

performance (Iba & Sawaguchi, 2003), and deficits in visual attention in both FEF (Wardak, Ibos, Duhamel, & Olivier, 2006) and PPC (Wardak, Olivier, & Duhamel, 2004). Spiking activity is modulated during sustained attention in a number of brain areas, including PPC in rats (Broussard, Sarter, & Givens, 2006) and lateral intraparietal cortex (LIP) in rhesus macaques (Bendiksby & Platt, 2006). Lesion and imaging studies in humans have revealed that activation of frontal and parietal cortical areas are associated with performance on sustained attention tasks (Kastner & Ungerleider, 2000; Sarter, Givens, & Bruno, 2001). As further support of the importance of these brain regions in sustained attention, healthy control participants showed a task-related increase in theta activity primarily in frontal and parietal regions during sustained attention, which was absent in participants with attention-deficit/hyperactivity disorder; however, treatment with methylphenidate led to normalization of task-related theta enhancement (Skirrow et al., 2015). Our findings contribute to this body of work by elucidating similarities and differences in how activity in these brain areas is organized during sustained attention. The coordination of activity across these areas not only provides further support of the importance of coordinated activation of these brain regions for mediating attentional processing, but provides further insight into the mechanism of such communication.

Cognitive Importance of Theta and High Gamma Oscillations

A framework for the role of cortical oscillations in sustained attention with four components has recently been proposed: frontomedial theta oscillations mediate cognitive monitoring and control functions, low-frequency phase synchronization mediates communication across brain networks, gamma mediates excitation of task-relevant cortical areas, and alpha mediates inhibition of task-irrelevant cortical areas (Clayton et al., 2015). Our results provide further evidence for three of these organizing principles. We found that theta power increased during sustained attention in PPC. This further aligns with previous evidence that theta oscillations are involved in learning, attention, and memory (Kahana, Seelig, & Madsen, 2001). In addition to power increase, we found task-modulated phase-locking in the theta band between PFC and PPC. This finding may be expected, as long-range theta synchrony contributes to the coordination of goal-relevant information (Womelsdorf & Everling, 2015), and prefrontal-parietal networks in macaques have been found to phase synchronize at 5-10Hz during top-down controlled preparatory

states (Phillips et al., 2014). We also found increased power in gamma and high gamma frequency bands. Compared to lower-frequency oscillations, (high-) gamma is more spatially restricted and reflects more local processing (Canolty et al., 2007; Crone, Miglioretti, Gordon, & Lesser, 1998). Our results align with previous findings that Area V4 exhibits increased coherent gamma activity for attended vs non-attended stimuli during a selective attention task (Taylor, Mandon, Freiwald, & Kreiter, 2005).

It should be noted that substantial work conducted in the frontoparietal network has found beta synchronization to play an important role in long-range synchronization mediating attention (Gross et al., 2004; Hipp, Engel, & Siegel, 2011; Womelsdorf & Everling, 2015). In this study, we did not see beta synchronization of LFP activity between PFC and PPC. Selecting cutoffs to separate distinct frequency band is a topic of much debate, and there is presently a shift towards identifying the underlying generation mechanism for oscillations in order to separate functionally different rhythms. Nevertheless, future work will be needed to clarify modes of long-range synchronization as a function of specific brain networks, species, and behavioral demands.

While activity in individual frequency bands is important, the interaction of multiple-frequency bands has been found to mediate communication in a number of cognitive and behavioral paradigms. Overall, we found joint and distinct roles for theta and high-gamma activity in organizing local and long-range activity during sustained attention. Perhaps the most well-studied cross-frequency interaction is between theta and gamma oscillations in the hippocampus. Evidence indicates that nested oscillations allow for the representation of space for navigation (O'Keefe & Dostrovsky, 1971) as well as the ordered representation of multiple items relevant for working memory (Lisman & Jensen, 2013). However, the role of these oscillations in organizing the structure of activity in cortex is less well understood. Our findings aligned with (Lisman & Jensen, 2013) in demonstrating modulation of (high-)gamma amplitude by theta oscillations. Limited work has demonstrated that theta phase modulates high-gamma amplitude in humans in multiple tasks including non-visual verbal tasks, memory tasks, and motor tasks, as measured through electrocorticography (Canolty et al., 2006; Voytek et al., 2010). In macaques, an increase in phase-amplitude coupling between theta and gamma in anterior cingulate cortex and PFC was found with correct attentional shift but not before errors (Voloh, Valiante, Everling, & Womelsdorf, 2015). Work in primate visual cortex has found that feedforward communication utilizes theta and gamma frequency

bands, while feedback communication relies on the beta frequency band (Bastos et al., 2015). Other work indicates that theta synchronization across brain regions is characteristic of top down processes, incorporating expectations to coordinate lower level perception and encoding, while gamma synchronization reflects bottom up processing, in which interaction of perceptual inputs drive higher order mental activities (Kahana et al., 2001; von Stein & Sarnthein, 2000). While it must be fully tested if the same frequencies are implicated in other brain regions and species, brain function clearly exhibits multiplexing of activity across frequency bands.

O**rganization of Spiking Activity by Oscillations**

The organization of spiking activity by oscillations is critical for the effective integration of relevant task information. We found that PFC units were phase-locked to the 5Hz oscillation in PPC, whereas PPC units were not typically phase-locked to theta in PFC. This suggests that theta activity may be more prominent in PPC; indeed, we found a local peak in PPC spectral activity in the theta band that increased during the sustained attention period, while PFC showed no such spectral modulation. It remains an outstanding question why PPC units were only phase locked to local high-gamma activity but not the local theta oscillation. However, these findings align with previous theories that high-frequency oscillations in sensory areas reflect discrete sampling of the environment (Fiebelkorn et al., 2013); the activity of PPC units could be reflecting environmental sampling while the theta oscillation in PPC acts as a more global pacemaker, synchronizing with PFC to establish the PFC theta oscillation and guiding spiking activity in PFC. In a visual working memory task, single unit spiking activity was organized locally in V4 by theta oscillations (Lee, Simpson, Logothetis, & Rainer, 2005). Prior work conducted in monkeys during memory processing also found an asymmetric relationship in spike-LFP phase locking between PFC and V4. However, the authors reported stronger phase locking of V4 units to PFC oscillations (Liebe et al., 2012); the difference with our results may relate to the behavioral paradigm. Our sustained attention task was strongly dependent on the appearance of a visual stimulus, possibly relying on visually-responsive PPC, while the working memory task in the referenced study is a strongly top-down mediated behavior.

The specific cognitive demands of the attention task may elicit different network organization. Using a slightly different metric of assessing synchrony between areas, spike-field coherence, gamma

frequency coupling was found between FEF and V4 during a covert attention task (Gregoriou, Gotts, Zhou, & Desimone, 2009). Using the same method, greater gamma synchronization of spiking and oscillatory activity in monkey V4 was correlated with faster response times in a detection task (Womelsdorf, Fries, Mitra, & Desimone, 2006), suggesting that sensory changes are more efficiently processed by neurons with enhanced gamma-band synchronization.

Conclusions

Taken together, our findings suggest simultaneous organization of spiking activity by multiple frequencies mediating local and long-range connectivity during cognitively demanding behavior. Long-range organization of PFC and PPC was mediated by 5Hz activity. PFC exhibited local organization of spiking activity by both theta and high gamma oscillatory activity, while PPC spiking was locally organized only by high gamma oscillations. This work points to a unified yet distinct organization scheme for activity within and across cortical areas during sustained attention. Spiking activity in PPC may be encoding local sensory integration information, while low-frequency oscillatory activity mediates cross-area coupling for the execution of sustained attention given the processed sensory information.

FIGURES

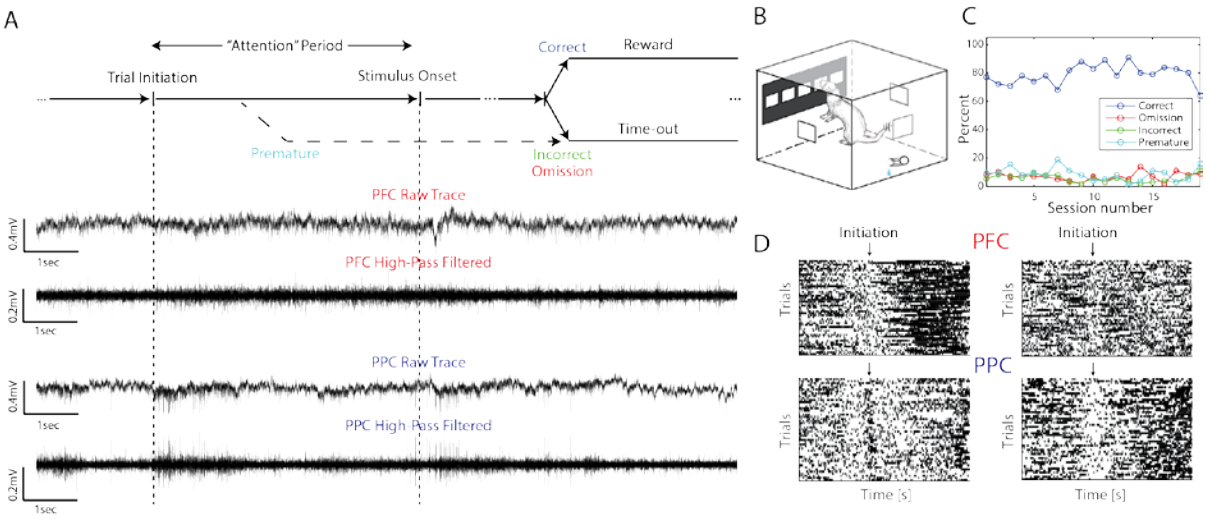

Figure 7.1. Animals performed a sustained visual attention task during simultaneous electrophysiological recordings in prefrontal cortex (PFC) and posterior parietal cortex (PPC).

(A) Top: The 5-choice serial reaction time task was a self-paced task; the animal initiated each trial, starting a 5 second sustained attention period, which terminated when a stimulus appeared in one of five windows. Bottom: Electrophysiological signals were continuously recorded during the task to provide information on LFP and spiking activity.

(B) Representation of the behavior chamber showing 5 response windows on a touch screen.

(C) After training, animals performed well in this task, answering approximately 80% of trials correctly per session. Figure shows sessions analyzed for Animal C. See Supplementary Figure 7.A for other animals.

(D) Spike sorting was conducted on high-pass filtered data. Single units in PFC and PPC aligned to trial initiation show task-modulation in firing rate. Different units showed heterogeneous changes in firing rate across time.

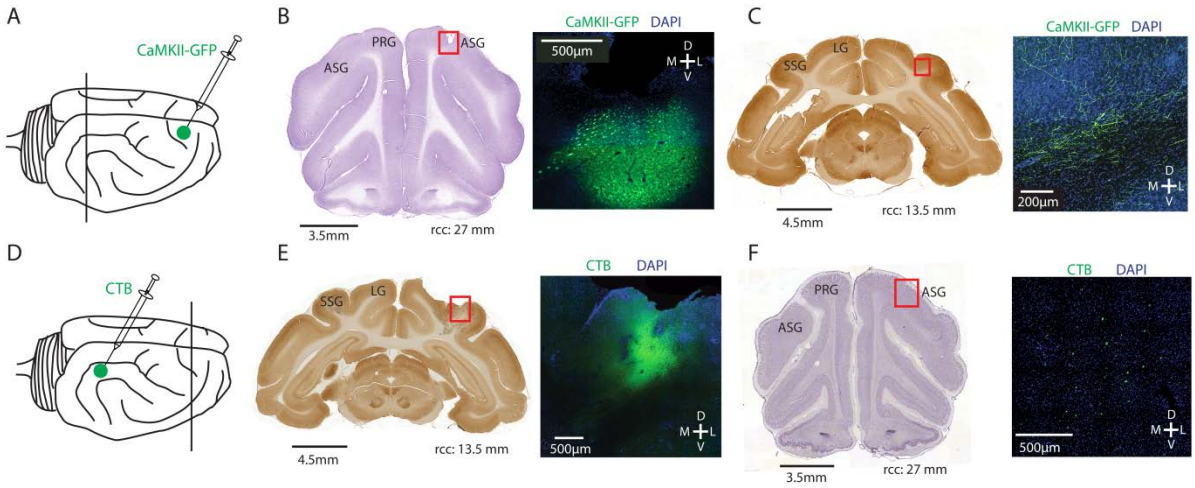

Figure 7.2. Anterograde and retrograde tracing demonstrate anatomical connectivity between PFC and PPC.

(A) rAAV5-CamKII-GFP was injected in PFC for anterograde tracing.

(B) GFP was injected in PFC at 27mm relative to caudal crest (rcc). Red square in neighboring Nissl stained section indicates location of fluorescent image on the right. Injection site in PFC shows robust labeling of cell bodies; green = GFP, blue = DAPI counterstain, ASG = anterior sigmoid gyrus, PRG = proreal gyrus.

(C) Cytochrome oxidase stained neighboring section in PPC (13.5mm rcc). Red square indicates location of fluorescent image on the right. Projections in PPC exhibit GFP labeling, indicating direct anatomical connections to the injection site location; green = GFP, blue = DAPI counterstain, SSG = suprasylvian gyrus, LG = lateral gyrus.

(D) CTB-488 was injected in PPC for retrograde tracing.

(E) CTB-488 was injected into PPC at 13.5mm rcc. Red square in neighboring section stained for cytochrome oxidase indicates location of fluorescent image on the right; green = CTB-488, blue = DAPI counterstain.

(F) PFC (27mm rcc) exhibits expression of CTB-488. Red square in neighboring section stained for Nissl indicates location of fluorescent image on the right; green = CTB-488, blue = DAPI counterstain.

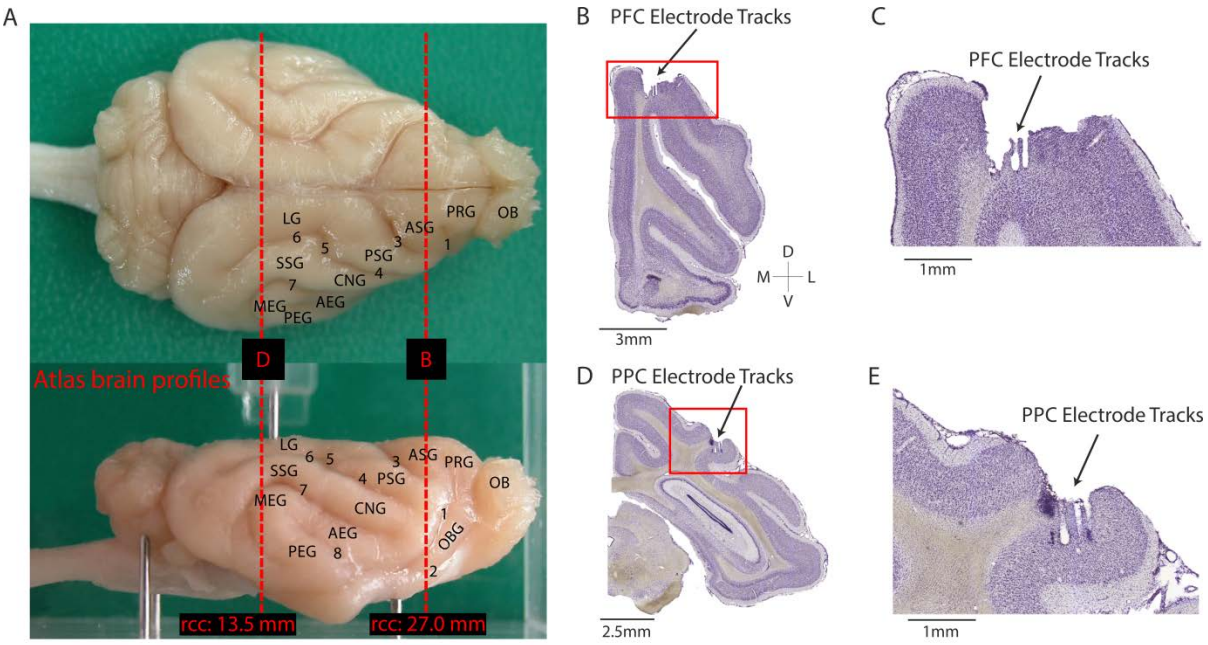

Figure 7.3. Recording locations in PFC and PPC

(A) Overview of electrode implantation locations and tracer injections from ferret atlas. PFC was 27mm rcc and PPC was 13.5mm rcc. OB = olfactory bulb, OBG = orbital gyrus, ASG = anterior sigmoid gyrus, PSG = posterior sigmoid gyrus, CNG = coronal gyrus, AEG = anterior ectosylvian gyrus, MEG = medial ectosylvian gyrus, PEG = posterior ectosylvian gyrus, SSG = suprasylvian gyrus, LG = lateral gyrus, PRG = proreal gyrus; 1 = prs presylvian sulcus, 2 = rf rhinal fissure, 3 = crs cruciate sulcus, 4 = cns coronal sulcus, 5 = as ansinate sulcus, 6 = ls lateral sulcus, 7 = sss suprasylvian sulcus, 8 = pss pseudosylvian sulcus.

(B) Nissl stained section in PFC showing electrode implantation location in Animal A indicated by electrolytic lesions.

(C) Area in red box from (B) showing electrode tracks.

(D) Nissl stained section in PPC showing electrode implantation location in Animal A.

(E) Area in red box from (D) showing electrode tracks

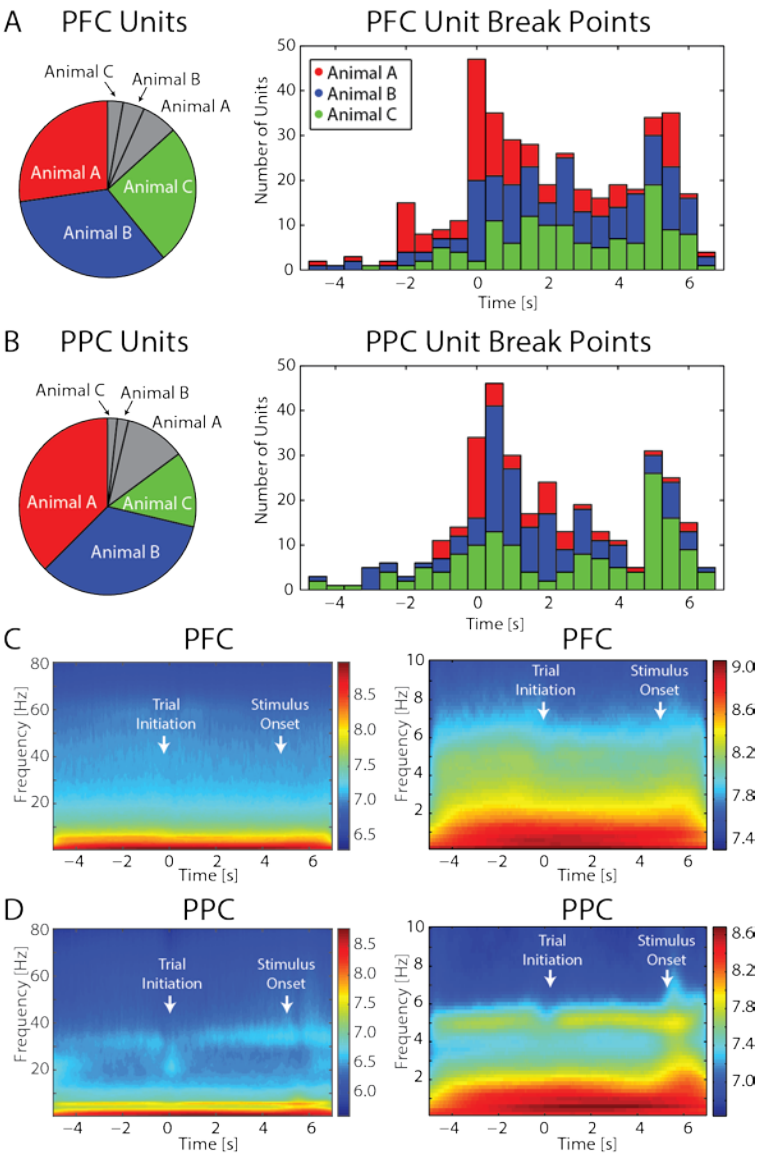

Figure 7.4. Task-dependent modulation of single unit spiking and spectral activity

(A) Left: 86.7% of PFC units across all animals showed significant modulation during the peristimulus period. Colored pie pieces indicate significantly modulated units for each animal, while gray pieces show units with non-significant modulation. Right: In PFC, the largest breakpoints for each significantly modulated unit indicate that structural change in spiking activity was most prominent during the sustained attention period.

(B) Left: 85.1% of PPC units across all animals exhibited significant modulation during the peristimulus period. Colored pie pieces indicate significantly modulated units for each animal, while gray pieces show units with non-significant modulation. Right: In PPC, the largest breakpoints for each

significantly modulated unit indicate that structural change in spiking activity was most prominent immediately following trial initiation and at stimulus onset.

(C) Spectrograms from PFC averaged across sessions in Animal C. Left: No prominent spectral modulation during trial. Right: No local spectral peak at 5Hz is evident

(D) Spectrograms from PPC averaged across sessions in Animal C Left: A narrow gamma band showed task-modulated changes in power. Right: A prominent 5Hz peak is evident in the spectra, again exhibiting task-modulation.

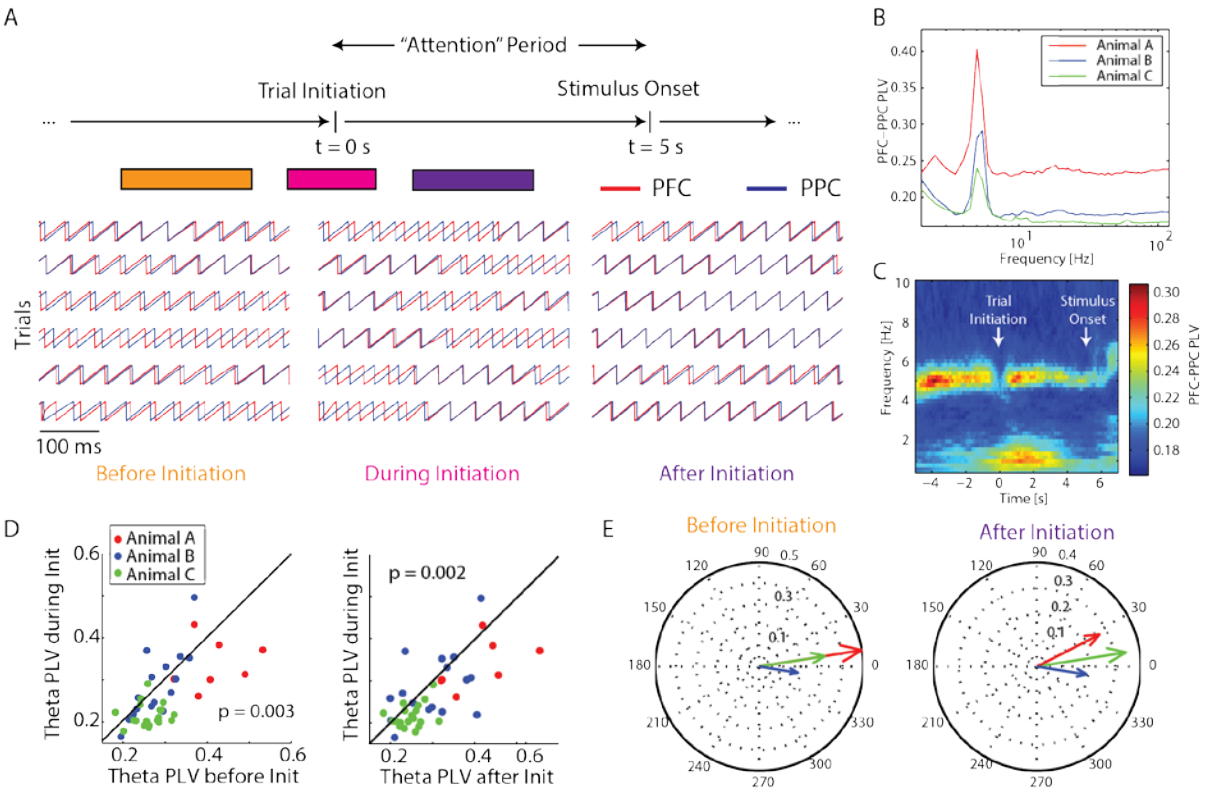

Figure 7.5. Task-dependent synchronization between PFC and PPC at 5Hz

(A) LFP-LFP phase locking was used to assess synchronization between PFC and PPC. At behaviorally-relevant periods during the behavior task (before initiation = 3 to 1 seconds before initiation, during initiation = 0.5 seconds before to 0.5 after, after initiation = 1 to 3 seconds after initiation) phases in PFC and PPC were assessed for consistent differences. Here, 5Hz phase is shown for one pair of channels across trials.

(B) Across all animals, phase locking value was highest at 5Hz.

(C) Averaged across all recordings for Animal C, phase locking between PFC and PPC was weakened during trial initiation and by stimulus onset. See Supplementary Figure 7.B for animals A and B.

(D) Across all recordings, phase locking values before initiation (left) and after initiation (right) were significantly greater than during initiation.

(E) Averaged across all recordings, the phase difference between PFC and PPC was near zero for all animals, both before initiation and after initiation.

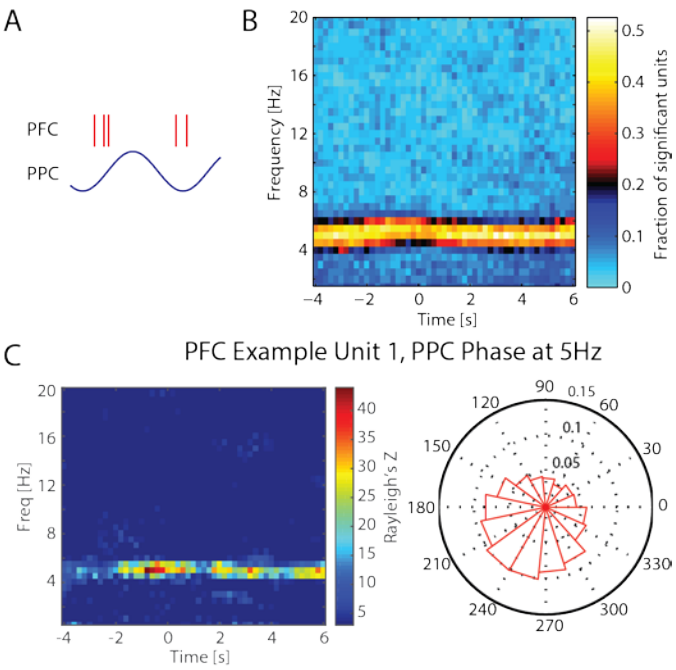

Figure 7.6. PPC 5Hz oscillation exerted long-range organization on spiking activity in PFC

(A) Spike-LFP phase locking was used to test if theta phase drove spiking activity across areas. Only a unidirectional long-range relationship was found, between PPC theta phase and PFC spiking activity.

(B) Averaged across recordings for Animal A, spike-LFP phase locking was most prominent at a narrow band centered on 5Hz. Spike-LFP phase locking was present throughout the duration of the trial, and did not exhibit task-dependent modulation in strength. See Supplementary Figure 7.C for Animals B and C.

(C) An example unit recorded in PFC exhibits phase-locking to PPC 5Hz activity. Polar plot indicates histogram of preferred phase of firing.

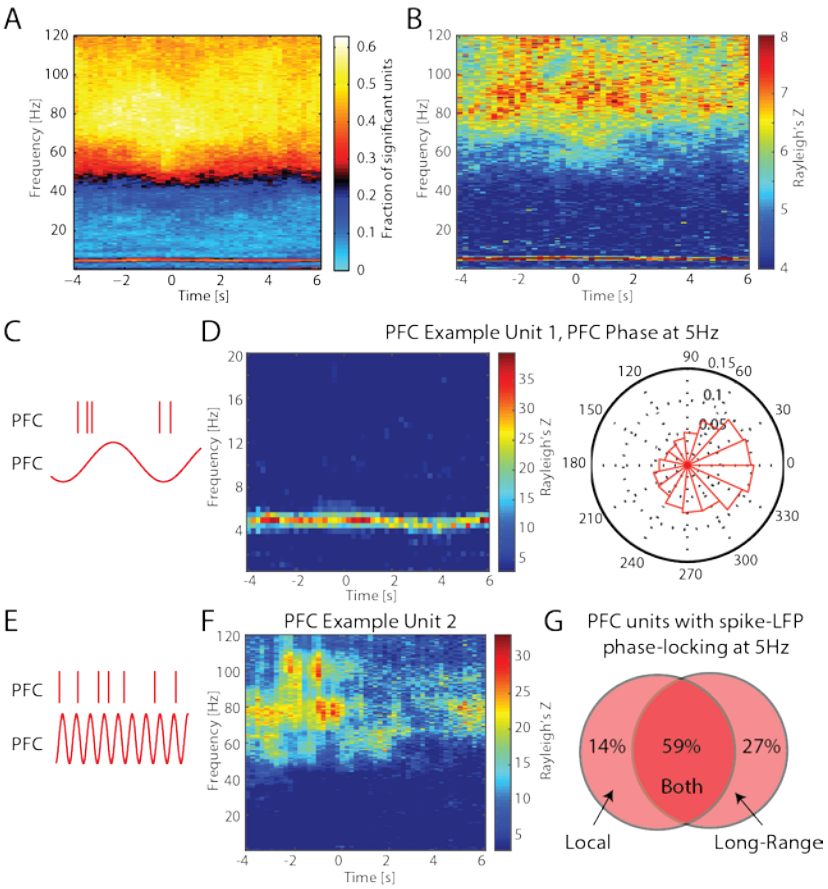

Figure 7.7. Both theta (5Hz) and high gamma (80-120Hz) oscillations are involved in the local organization of spiking activity in PFC

(A) Averaged across recordings for Animal A, units were predominantly phase-locked to oscillations at 5Hz and in the high gamma band.

(B) Averaged across recordings for Animal A, the average Rayleigh's Z for significantly locked units (a measure of the strength of phase locking) was also highest for spike-LFP phase locking at 5Hz and in the high gamma range.

(C) Spike-LFP phase locking was calculated between the 5Hz oscillation and spiking activity, both in PFC.

(D) An example unit recorded in PFC exhibits phase-locking to PFC 5Hz activity. The polar plot exhibits preferred phase of firing; same unit as Figure 7.6C.

(E) Spike-LFP phase locking was calculated between high-gamma oscillations and spiking activity, both in PFC.

(F) An example unit recorded in PFC exhibits phase locking to broad high-gamma activity.

(G) PFC units exhibited spike-LFP phase locking to the 5Hz oscillation both locally and long-range. Venn diagram indicates the percentage of units across all animals which exhibited local locking to PFC phase, long-range locking to PPC phase, or both local and long-range locking.

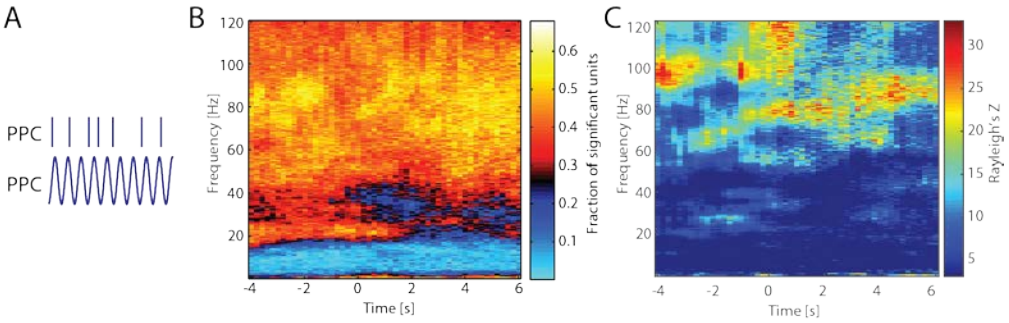

Figure 7.8. High gamma oscillations are responsible for the local organizing of spiking activity in PPC.

(A) Spike-LFP phase locking was calculated between high-gamma oscillations and spiking activity, both in PPC.

(B) Averaged across recordings in Animal C, units were predominantly phase-locked to high-gamma oscillations. In contrast to PPC, no prominent spike-LFP phase locking was seen at 5Hz.

(C) An example unit recorded in PPC exhibited phase locking to broad high-gamma activity.

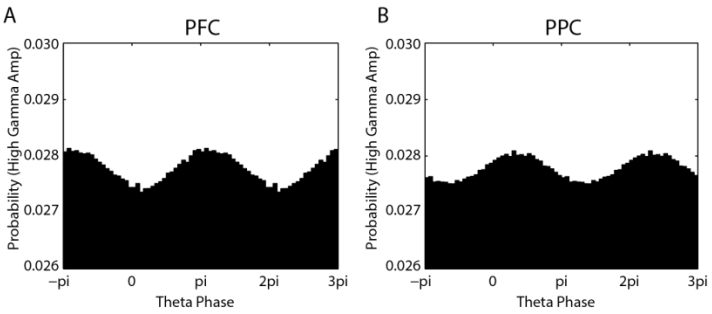

Figure 7.9. Theta and high-gamma activity are locally related through phase-amplitude coupling.

(A) In PFC, theta phase and high gamma amplitude show organizing through phase-amplitude coupling. Averaged across recordings for Animal C, two oscillation periods shown for visualization. See Supplementary Figure 7.E for Animals A and B.

(B) In PPC, theta phase and high gamma amplitude show organizing through phase-amplitude coupling. Averaged across recordings for Animal C, two oscillation periods shown for visualization.

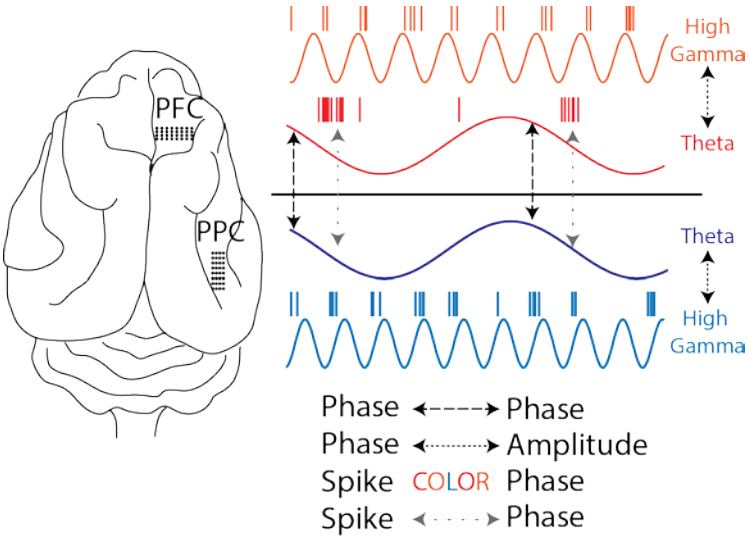

Figure 7.10. Cartoon illustrating organizational structure of activity within and between PFC and PPC.

Long-range, phase-phase synchronization in the theta frequency range was present between PFC and PPC. Spike-LFP phase synchronization was evident between PFC units and PPC theta phase. Locally in PFC, both theta and high gamma oscillations organized spiking activity while only high-gamma oscillations organized local spiking activity in PPC. Both PFC and PPC exhibited within area coordination of theta and high-gamma through phase-amplitude coupling.

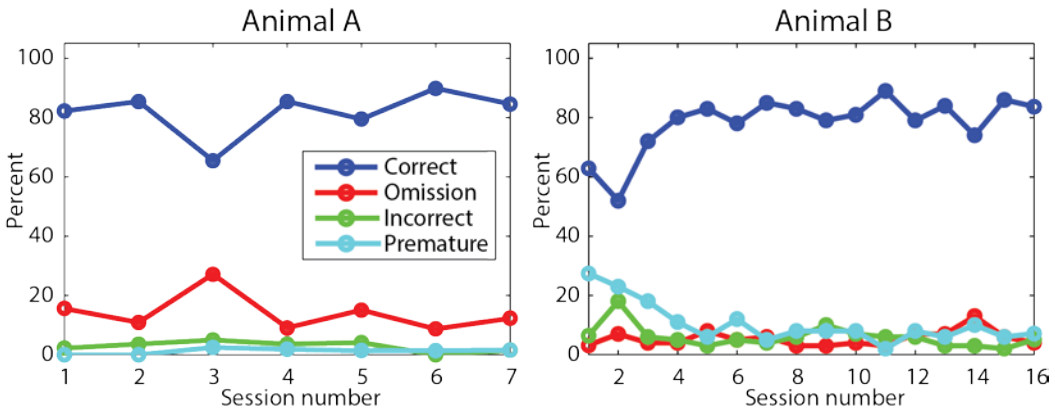

Figure 7.A. Behavioral performance for Animals A and B during recording sessions.

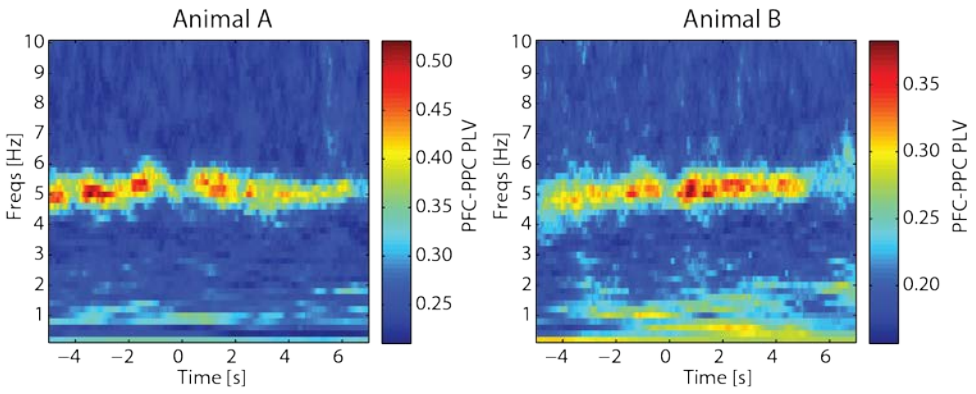

Figure 7.B. Phase locking between PFC and PPC for animals A and B

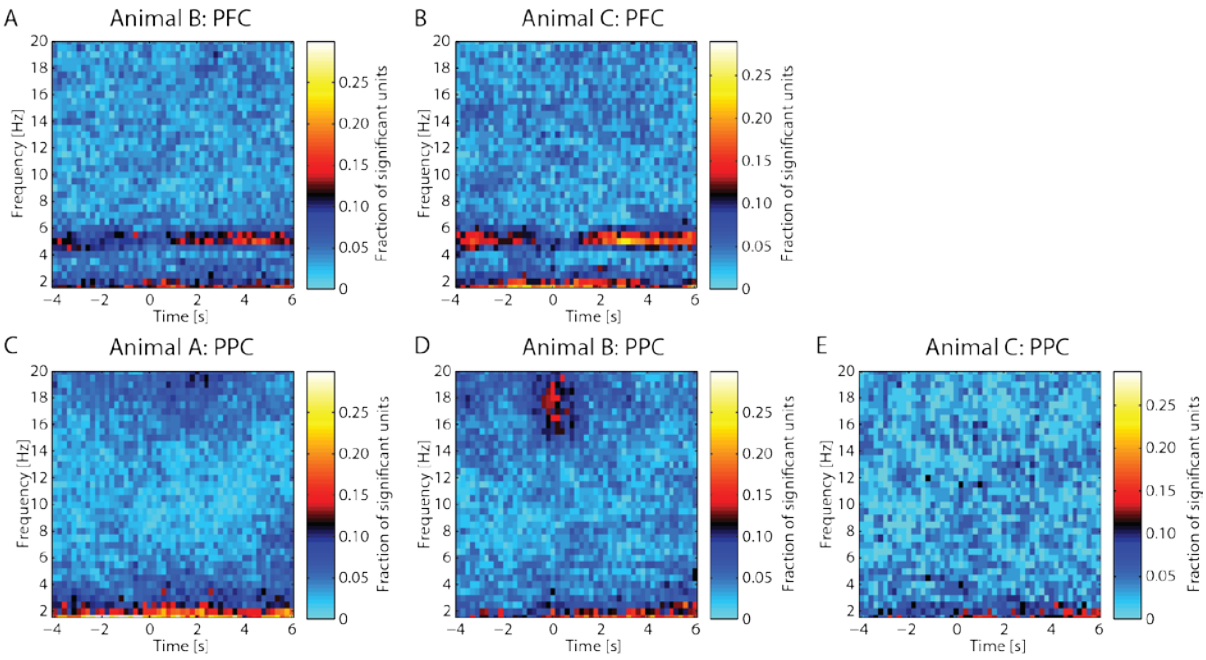

Figure 7.C. Fraction of units with significant spike-LFP phase locking between areas.

(A) Across recording sessions for Animal B, PFC units exhibited significant spike-LFP phase locking with PPC 5Hz oscillations.

(B) Same as A for Animal C.

(C) Across recording session for Animal A, no sizeable fraction of PPC units exhibited spike-LFP phase locking with PFC 5Hz oscillations.

(D) Same as C for Animal B.

(E) Same as C for Animal C.

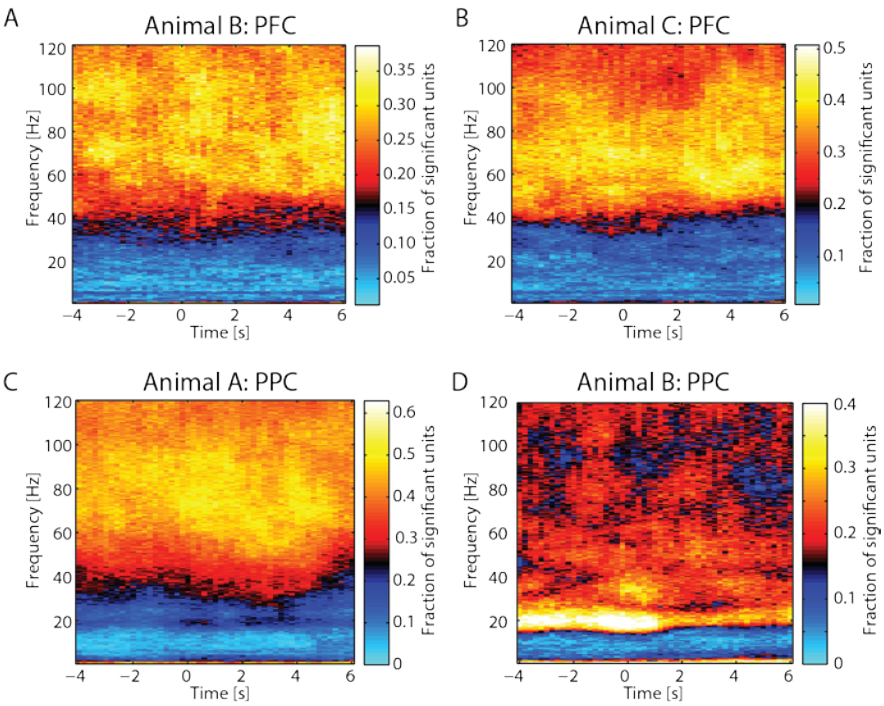

Figure 7.D. PFC and PPC units exhibit local spike-LFP phase locking at high-gamma frequencies.

(A) Averaged across recordings for Animal B, PFC units exhibited spike-LFP phase locking at high-gamma frequencies.

(B) Same as A for Animal C.

(C) Averaged across recordings for Animal A, PPC units exhibited spike-LFP phase locking at high-gamma frequencies.

(D) Same as C for Animal B.

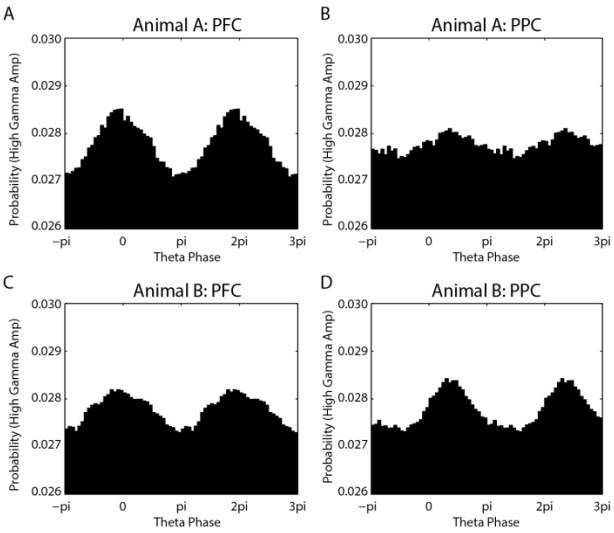

Figure 7.E. Local theta and high-gamma activity exhibit phase-amplitude coupling

(A) In PFC, theta phase and high gamma amplitude show organization through phase-amplitude coupling. Averaged across recordings for Animal A, two oscillation periods shown for visualization.

(B) Same as A for PPC in Animal A.

(C) Same as A for Animal B.

(D) Same as B for Animal B.

REFERENCES

Bari, A., Dalley, J. W., & Robbins, T. W. (2008). The application of the 5-choice serial reaction time task for the assessment of visual attentional processes and impulse control in rats. *Nat Protoc, 3*(5), 759-767. doi: 10.1038/nprot.2008.41

Bastos, A. M., Vezoli, J., Bosman, C. A., Schoffelen, J. M., Oostenveld, R., Dowdall, J. R., . . . Fries, P. (2015). Visual areas exert feedforward and feedback influences through distinct frequency channels. *Neuron, 85*(2), 390-401. doi: 10.1016/j.neuron.2014.12.018

Bendiksby, M. S., & Platt, M. L. (2006). Neural correlates of reward and attention in macaque area LIP. *Neuropsychologia, 44*(12), 2411-2420. doi: 10.1016/j.neuropsychologia.2006.04.011

Berens, P. (2009). CircStat: A MATLAB Toolbox for Circular Statistics. *Journal of Statistical Software, 31*(10), 1-21.

Broussard, J., Sarter, M., & Givens, B. (2006). Neuronal correlates of signal detection in the posterior parietal cortex of rats performing a sustained attention task. *Neuroscience, 143*(2), 407-417. doi: 10.1016/j.neuroscience.2006.08.030

Buschman, T. J., & Kastner, S. (2015). From Behavior to Neural Dynamics: An Integrated Theory of Attention. *Neuron, 88*(1), 127-144. doi: 10.1016/j.neuron.2015.09.017

Buschman, T. J., & Miller, E. K. (2007). Top-down versus bottom-up control of attention in the prefrontal and posterior parietal cortices. *Science, 315*(5820), 1860-1862. doi: 10.1126/science.1138071

Buzsaki, G., & Draguhn, A. (2004). Neuronal oscillations in cortical networks. *Science, 304*(5679), 1926-1929. doi: 10.1126/science.1099745

Canolty, R. T., Edwards, E., Dalal, S. S., Soltani, M., Nagarajan, S. S., Kirsch, H. E., . . . Knight, R. T. (2006). High gamma power is phase-locked to theta oscillations in human neocortex. *Science, 313*(5793), 1626-1628. doi: 10.1126/science.1128115

Canolty, R. T., Ganguly, K., Kennerley, S. W., Cadieu, C. F., Koepsell, K., Wallis, J. D., & Carmena, J. M. (2010). Oscillatory phase coupling coordinates anatomically dispersed functional cell assemblies. *Proc Natl Acad Sci U S A, 107*(40), 17356-17361. doi: 10.1073/pnas.1008306107

Canolty, R. T., Soltani, M., Dalal, S. S., Edwards, E., Dronkers, N. F., Nagarajan, S. S., . . . Knight, R. T. (2007). Spatiotemporal dynamics of word processing in the human brain. *Front Neurosci, 1*(1), 185-196. doi: 10.3389/neuro.01.1.1.014.2007

Cavada, C., & Goldman-Rakic, P. S. (1989). Posterior parietal cortex in rhesus monkey: II. Evidence for segregated corticocortical networks linking sensory and limbic areas with the frontal lobe. *J Comp Neurol, 287*(4), 422-445. doi: 10.1002/cne.902870403

Chow, G. (1960). Tests of equality between sets of coefficients in two linear regressions. *Econometrica, 28*, 591-605.

Clayton, M. S., Yeung, N., & Cohen Kadosh, R. (2015). The roles of cortical oscillations in sustained attention. *Trends Cogn Sci, 19*(4), 188-195. doi: 10.1016/j.tics.2015.02.004

Conte, W. L., Kamishina, H., & Reep, R. L. (2009). Multiple neuroanatomical tract-tracing using fluorescent Alexa Fluor conjugates of cholera toxin subunit B in rats. *Nat Protoc, 4*(8), 1157-1166. doi: 10.1038/nprot.2009.93

Corbetta, M., & Shulman, G. L. (2002). Control of goal-directed and stimulus-driven attention in the brain. *Nat Rev Neurosci, 3*(3), 201-215. doi: 10.1038/nrn755

Crone, N. E., Miglioretti, D. L., Gordon, B., & Lesser, R. P. (1998). Functional mapping of human sensorimotor cortex with electrocorticographic spectral analysis. II. Event-related synchronization in the gamma band. *Brain, 121 (Pt 12)*, 2301-2315.

Duque, A., & McCormick, D. A. (2010). Circuit-based localization of ferret prefrontal cortex. *Cereb Cortex, 20*(5), 1020-1036. doi: 10.1093/cercor/bhp164

Engel, A. K., Fries, P., & Singer, W. (2001). Dynamic predictions: oscillations and synchrony in top-down processing. *Nat Rev Neurosci, 2*(10), 704-716. doi: 10.1038/35094565

Fiebelkorn, I. C., Snyder, A. C., Mercier, M. R., Butler, J. S., Molholm, S., & Foxe, J. J. (2013). Cortical cross-frequency coupling predicts perceptual outcomes. *Neuroimage, 69*, 126-137. doi: 10.1016/j.neuroimage.2012.11.021

Fisher, N. I. (1993). *Statistical analysis of circular data*. Cambridge England ; New York, NY, USA: Cambridge University Press.

Foxworthy, W. A., Allman, B. L., Keniston, L. P., & Meredith, M. A. (2013). Multisensory and unisensory neurons in ferret parietal cortex exhibit distinct functional properties. *Eur J Neurosci, 37*(6), 910-923. doi: 10.1111/ejn.12085

Foxworthy, W. A., & Meredith, M. A. (2011). An examination of somatosensory area SIII in ferret cortex. *Somatosens Mot Res, 28*(1-2), 1-10. doi: 10.3109/08990220.2010.548465

Fries, P. (2005). A mechanism for cognitive dynamics: neuronal communication through neuronal coherence. *Trends Cogn Sci, 9*(10), 474-480. doi: 10.1016/j.tics.2005.08.011

Fries, P. (2009). Neuronal gamma-band synchronization as a fundamental process in cortical computation. *Annu Rev Neurosci, 32*, 209-224. doi: 10.1146/annurev.neuro.051508.135603

Fritz, J. B., David, S. V., Radtke-Schuller, S., Yin, P., & Shamma, S. A. (2010). Adaptive, behaviorally gated, persistent encoding of task-relevant auditory information in ferret frontal cortex. *Nat Neurosci, 13*(8), 1011-1019. doi: 10.1038/nn.2598

Gregoriou, G. G., Gotts, S. J., Zhou, H., & Desimone, R. (2009). High-frequency, long-range coupling between prefrontal and visual cortex during attention. *Science, 324*(5931), 1207-1210. doi: 10.1126/science.1171402

Gross, J., Schmitz, F., Schnitzler, I., Kessler, K., Shapiro, K., Hommel, B., & Schnitzler, A. (2004). Modulation of long-range neural synchrony reflects temporal limitations of visual attention in humans. *Proc Natl Acad Sci U S A, 101*(35), 13050-13055. doi: 10.1073/pnas.0404944101

Hipp, J. F., Engel, A. K., & Siegel, M. (2011). Oscillatory synchronization in large-scale cortical networks predicts perception. *Neuron, 69*(2), 387-396. doi: 10.1016/j.neuron.2010.12.027

Iba, M., & Sawaguchi, T. (2003). Involvement of the dorsolateral prefrontal cortex of monkeys in visuospatial target selection. *J Neurophysiol, 89*(1), 587-599. doi: 10.1152/jn.00148.2002

Kahana, M. J., Seelig, D., & Madsen, J. R. (2001). Theta returns. *Curr Opin Neurobiol, 11*(6), 739-744.

Kastner, S., & Ungerleider, L. G. (2000). Mechanisms of visual attention in the human cortex. *Annu Rev Neurosci, 23*, 315-341. doi: 10.1146/annurev.neuro.23.1.315

Katsuki, F., & Constantinidis, C. (2012). Unique and shared roles of the posterior parietal and dorsolateral prefrontal cortex in cognitive functions. *Front Integr Neurosci, 6*, 17. doi: 10.3389/fnint.2012.00017

Kimchi, E. Y., & Laubach, M. (2009). Dynamic encoding of action selection by the medial striatum. *J Neurosci, 29*(10), 3148-3159. doi: 10.1523/JNEUROSCI.5206-08.2009

Kopell, N., Ermentrout, G. B., Whittington, M. A., & Traub, R. D. (2000). Gamma rhythms and beta rhythms have different synchronization properties. *Proc Natl Acad Sci U S A, 97*(4), 1867-1872.

Lachaux, J. P., Rodriguez, E., Martinerie, J., & Varela, F. J. (1999). Measuring phase synchrony in brain signals. *Hum Brain Mapp, 8*(4), 194-208.

Langner, R., & Eickhoff, S. B. (2013). Sustaining attention to simple tasks: a meta-analytic review of the neural mechanisms of vigilant attention. *Psychol Bull, 139*(4), 870-900. doi: 10.1037/a0030694

Lee, H., Simpson, G. V., Logothetis, N. K., & Rainer, G. (2005). Phase locking of single neuron activity to theta oscillations during working memory in monkey extrastriate visual cortex. *Neuron, 45*(1), 147-156. doi: 10.1016/j.neuron.2004.12.025

Liebe, S., Hoerzer, G. M., Logothetis, N. K., & Rainer, G. (2012). Theta coupling between V4 and prefrontal cortex predicts visual short-term memory performance. *Nat Neurosci, 15*(3), 456-462, S451-452. doi: 10.1038/nn.3038

Lisman, J. E., & Jensen, O. (2013). The theta-gamma neural code. *Neuron, 77*(6), 1002-1016. doi: 10.1016/j.neuron.2013.03.007

Manger, P. R., Masiello, I., & Innocenti, G. M. (2002). Areal organization of the posterior parietal cortex of the ferret (Mustela putorius). *Cereb Cortex, 12*(12), 1280-1297.

O'Keefe, J., & Dostrovsky, J. (1971). The hippocampus as a spatial map. Preliminary evidence from unit activity in the freely-moving rat. *Brain Res, 34*(1), 171-175.

Petersen, S. E., & Posner, M. I. (2012). The attention system of the human brain: 20 years after. *Annu Rev Neurosci, 35*, 73-89. doi: 10.1146/annurev-neuro-062111-150525

Phillips, J. M., Vinck, M., Everling, S., & Womelsdorf, T. (2014). A long-range fronto-parietal 5- to 10-Hz network predicts "top-down" controlled guidance in a task-switch paradigm. *Cereb Cortex, 24*(8), 1996-2008. doi: 10.1093/cercor/bht050

Posner, M. I., & Petersen, S. E. (1990). The attention system of the human brain. *Annu Rev Neurosci, 13*, 25-42. doi: 10.1146/annurev.ne.13.030190.000325

Ptak, R. (2012). The frontoparietal attention network of the human brain: action, saliency, and a priority map of the environment. *Neuroscientist, 18*(5), 502-515. doi: 10.1177/1073858411409051

Robbins, T. W. (1998). Arousal and attention: psychopharmacological and neuropsychological studies in experimental animals. In R. Parasuraman (Ed.), *The Attentive Brain* (pp. 189-220). Cambridge: MIT Press.

Sarnthein, J., Petsche, H., Rappelsberger, P., Shaw, G. L., & von Stein, A. (1998). Synchronization between prefrontal and posterior association cortex during human working memory. *Proc Natl Acad Sci U S A, 95*(12), 7092-7096. doi: DOI 10.1073/pnas.95.12.7092

Sarter, M., Givens, B., & Bruno, J. P. (2001). The cognitive neuroscience of sustained attention: where top-down meets bottom-up. *Brain Res Brain Res Rev, 35*(2), 146-160.

Scolari, M., Seidl-Rathkopf, K. N., & Kastner, S. (2015). Functions of the human frontoparietal attention network: Evidence from neuroimaging. *Current Opinion in Behavioral Sciences*(1), 32-39.

Sellers, K. K., Bennett, D. V., Hutt, A., & Frohlich, F. (2013). Anesthesia differentially modulates spontaneous network dynamics by cortical area and layer. *J Neurophysiol, 110*(12), 2739-2751. doi: 10.1152/jn.00404.2013

Sellers, K. K., Bennett, D. V., Hutt, A., Williams, J. H., & Frohlich, F. (2015). Awake vs. anesthetized: layer-specific sensory processing in visual cortex and functional connectivity between cortical areas. *J Neurophysiol, 113*(10), 3798-3815. doi: 10.1152/jn.00923.2014

Siegel, M., Warden, M. R., & Miller, E. K. (2009). Phase-dependent neuronal coding of objects in short-term memory. *Proc Natl Acad Sci U S A, 106*(50), 21341-21346. doi: 10.1073/pnas.0908193106

Skirrow, C., McLoughlin, G., Banaschewski, T., Brandeis, D., Kuntsi, J., & Asherson, P. (2015). Normalisation of frontal theta activity following methylphenidate treatment in adult attention-deficit/hyperactivity disorder. *Eur Neuropsychopharmacol, 25*(1), 85-94. doi: 10.1016/j.euroneuro.2014.09.015

Szczepanski, S. M., Pinsk, M. A., Douglas, M. M., Kastner, S., & Saalmann, Y. B. (2013). Functional and structural architecture of the human dorsal frontoparietal attention network. *Proc Natl Acad Sci U S A, 110*(39), 15806-15811. doi: 10.1073/pnas.1313903110

Taylor, K., Mandon, S., Freiwald, W. A., & Kreiter, A. K. (2005). Coherent oscillatory activity in monkey area v4 predicts successful allocation of attention. *Cereb Cortex, 15*(9), 1424-1437. doi: 10.1093/cercor/bhi023

Totah, N. K., Jackson, M. E., & Moghaddam, B. (2013). Preparatory attention relies on dynamic interactions between prelimbic cortex and anterior cingulate cortex. *Cereb Cortex, 23*(3), 729-738. doi: 10.1093/cercor/bhs057

Tuch, D. S., Salat, D. H., Wisco, J. J., Zaleta, A. K., Hevelone, N. D., & Rosas, H. D. (2005). Choice reaction time performance correlates with diffusion anisotropy in white matter pathways supporting visuospatial attention. *Proc Natl Acad Sci U S A, 102*(34), 12212-12217. doi: 10.1073/pnas.0407259102

Varela, F., Lachaux, J. P., Rodriguez, E., & Martinerie, J. (2001). The brainweb: phase synchronization and large-scale integration. *Nat Rev Neurosci, 2*(4), 229-239. doi: 10.1038/35067550

Voloh, B., Valiante, T. A., Everling, S., & Womelsdorf, T. (2015). Theta-gamma coordination between anterior cingulate and prefrontal cortex indexes correct attention shifts. *Proc Natl Acad Sci U S A, 112*(27), 8457-8462. doi: 10.1073/pnas.1500438112

von Stein, A., Chiang, C., & Konig, P. (2000). Top-down processing mediated by interareal synchronization. *Proc Natl Acad Sci U S A, 97*(26), 14748-14753. doi: 10.1073/pnas.97.26.14748

von Stein, A., & Sarnthein, J. (2000). Different frequencies for different scales of cortical integration: from local gamma to long range alpha/theta synchronization. *Int J Psychophysiol, 38*(3), 301-313.

Voytek, B., Canolty, R. T., Shestyuk, A., Crone, N. E., Parvizi, J., & Knight, R. T. (2010). Shifts in gamma phase-amplitude coupling frequency from theta to alpha over posterior cortex during visual tasks. *Front Hum Neurosci, 4*, 191. doi: 10.3389/fnhum.2010.00191

Voytek, B., & Knight, R. T. (2015). Dynamic network communication as a unifying neural basis for cognition, development, aging, and disease. *Biol Psychiatry, 77*(12), 1089-1097. doi: 10.1016/j.biopsych.2015.04.016

Wardak, C., Ibos, G., Duhamel, J. R., & Olivier, E. (2006). Contribution of the monkey frontal eye field to covert visual attention. *J Neurosci, 26*(16), 4228-4235. doi: 10.1523/JNEUROSCI.3336-05.2006

Wardak, C., Olivier, E., & Duhamel, J. R. (2004). A deficit in covert attention after parietal cortex inactivation in the monkey. *Neuron, 42*(3), 501-508.

Womelsdorf, T., & Everling, S. (2015). Long-Range Attention Networks: Circuit Motifs Underlying Endogenously Controlled Stimulus Selection. *Trends Neurosci, 38*(11), 682-700. doi: 10.1016/j.tins.2015.08.009

Womelsdorf, T., & Fries, P. (2007). The role of neuronal synchronization in selective attention. *Curr Opin Neurobiol, 17*(2), 154-160. doi: 10.1016/j.conb.2007.02.002

Womelsdorf, T., Fries, P., Mitra, P. P., & Desimone, R. (2006). Gamma-band synchronization in visual cortex predicts speed of change detection. *Nature, 439*(7077), 733-736. doi: 10.1038/nature04258

Yu, C. X., Sellers, K. K., Radtke-Schuller, S., Lu, J. H., Xing, L., Ghukasyan, V., . . . Frohlich, F. (2016). Structural and functional connectivity between the lateral posterior-pulvinar complex and primary visual cortex in the ferret. *European Journal of Neuroscience, 43*(2), 230-244. doi: 10.1111/ejn.13116

Zar, J. H. (1999). *Biostatistical analysis* (4th ed.). Upper Saddle River, N.J.: Prentice Hall.

Zeileis, A., Leisch, F., Hornik, K., & Kleiber, C. (2002). strucchange: An R Package for Testing for Structural Change in Linear Regression Models. *Journal of Statistical Software, 7*(2).

Zhou, Z. C., Yu, C., Sellers, K. K., & Frohlich, F. (2016). Dorso-Lateral Frontal Cortex of the Ferret Encodes Perceptual Difficulty during Visual Discrimination. *Scientific Reports*.

CHAPTER 8: DISCUSSION

The studies described in this dissertation provide insight in the physiological organization of network dynamics at the level of LFP and action potential firing. A deeper understanding of network organization is critical for the rational design of non-invasive brain stimulation techniques to target perturbed network activity in patients with neuropsychiatric disorders. The studies here were conducted in both an intermediate animal model species and healthy human participants. Electrophysiology and behavior/psychophysics were combined to assess cortical network dynamics across a variety of states and in the context of specific cognitive functions.

In Chapter 2, I demonstrated that tDCS can be detrimental to cognitive processes. This non-invasive brain stimulation modality using a constant current decreased performance on an IQ test when applied either bilaterally or unilaterally, compared to sham stimulation. Based on work conducted in the motor cortex, tDCS is believed to increase or decrease excitability of neurons depending on the polarity of stimulation (Nitsche & Paulus, 2000). While some previous reports have demonstrated a positive effect of tDCS, the use of constant current may be better served when there is a known deficit or excess of excitability. However, substantial work has demonstrated that the synchronization of rhythmic neuronal activity is critical to cognitive process. Thus, a promising alternative approach is the use of periodic waveforms, such the sine-wave stimulation employed in tACS.

In Chapter 3, I provide a review of studies which used tACS to assess the effects of periodic sine-wave stimulation on cognitive tasks. The goal of this review was to propose that tACS be used to elucidate the causal role of synchronization in cognition, with the aim of future work correcting pathological network synchrony and dynamics. Towards this goal, discussion was organized according to the cognitive systems domain of the RDoC framework established by the National Institute of Mental Health.

Starting in Chapter 4, I present a series of studies utilizing an animal model to study network dynamics within and across cortical areas. The use of an animal model was advantageous because of

the accessibility gained through invasive recordings and techniques which are not currently possible in humans (e.g. injection of tracers to determine direct anatomical connections). In Chapter 4, I showed that V1 and PFC have markedly different spontaneous network dynamics compared to each other and depending on state. Here, state was defined as animals being or anesthetized. In Chapter 5, I assessed differences in network dynamics during sensory processing in awake and anesthetized animals. Together, Chapter 4 and 5 emphasize the importance of considering state when assessing network dynamics. Anesthesia is commonly used in systems neuroscience because it decreases methodological difficulty and increases the yield of experiments. However, a theory of the network-level effect of anesthesia with substantial experimental support proposes that anesthetics induce cortical disintegration through loss of effective connectivity (Alkire, 2008; Hudetz, 2006, 2012) and disrupt long range corticocortical interactions (Mashour, 2004). In further support of this theory, I found that anesthesia reduced functional cortico-cortical connectivity between V1 and PFC, while stimulus-driven oscillatory activity was greatly enhanced in V1 during anesthesia. Thus, this system clearly may be suboptimal for studying network dynamics, which by definition incorporate the integration of information across multiple brain areas.

In Chapter 6, I present a study assessing state-dependent and state-independent differences in dynamics in V1 in awake animals either during resting condition or naturalistic visual stimulation. The use of naturalistic visual stimuli, with complex image features, has been shown to elicit different sensory responses compared to the traditional artificial stimuli originally designed to strongly drive visual responses (Felsen & Dan, 2005), although possibly not in the lateral geniculate nucleus (Mante, Bonin, & Carandini, 2008). We found that naturalistic stimuli modulated the full frequency spectrum in awake animals, with suppressed power of low frequency oscillations and enhanced power of high frequency oscillations. This bi-directional modulation was correlated with multiunit action potential firing, indicating relevance for encoding or processing of the visual stimuli.

In Chapter 7, animals were trained in a translational assay of sustained visual attention, the 5-choice serial reaction time task. Simultaneous recordings in PFC and PPC allowed for investigation of how oscillatory activity organized spiking activity locally and long-range during sustained attention. I found that long-range organization, assessed by both LFP-LFP phase locking and spike-LFP phase locking,

depended on low frequency theta oscillations, while local organization of spiking activity was primarily mediated by high-gamma oscillations.

Based on these results and previous work, a number of themes have emerged as particularly relevant for the organization of network activity. Specifically, I will briefly discuss the importance of cross-frequency coupling, the organization of spiking activity by oscillations, and state-dependent differences in responses.

Cross-frequency coupling refers to the association of multiple neuronal oscillations at different frequencies (Hyafil, Giraud, Fontolan, & Gutkin, 2015). Cross-frequency coupling can occur locally, in which the network generating the individual oscillations shares the same subpopulation of cells, or more long-range in which different populations of neurons generate the two different frequency oscillations. The coupling of these oscillations can happen between phase-frequency, phase-phase, phase-amplitude, and amplitude-amplitude (Canolty & Knight, 2010). The most well studied form of cross-frequency coupling is phase-phase coupling between theta and gamma oscillations in rodent hippocampus (Buzsaki & Moser, 2013; Tort, Rotstein, Dugladze, Gloveli, & Kopell, 2007). Theta and gamma oscillations allow for the representation of space in hippocampus for navigation, as well as the ordered representation of multiple items in working memory (J. E. Lisman & Jensen, 2013). Neuronal ensembles, comprised of groups of active neurons, represent particular mental items (or in the case of spatial encoding in hippocampus, particular regions in the environment). The timing of firing of cells in the ensembles relative to the gamma cycle allows for the organization of separate items; more specifically, the first item is represented by neurons which fire in the first gamma cycle, the second item is represented by firing during the second gamma cycle, etc. In order to recall these items in sequential order, the gamma oscillation is nested within a slower time-scale theta oscillation. Thus, each item is also encoded during a particular and unique phase of the theta cycle, providing an overall ordering (J. Lisman & Buzsaki, 2008). Cross-frequency coupling maybe particularly important for long-distance communication; slower oscillations can synchronize between brain areas because they are less sensitive to conduction delays (von Stein & Sarnthein, 2000), and coupling with higher frequency oscillations can then occur locally.

The organization of spiking activity by local and long-range oscillatory activity has also emerged as an important network principle. During short-term working memory, spiking in prefrontal cortex carried the

most information of the remembered objects when it occurred at particular phases of the dominant frequency oscillations (Siegel, Warden, & Miller, 2009). Furthermore, the strength of coupling between spiking and oscillatory activity in V4 and PFC was predictive of short-term memory performance (Liebe, Hoerzer, Logothetis, & Rainer, 2012). Single unit activity in extrastriate visual cortex also exhibited phase locking during a visual working memory task, indicating preferential encoding (Lee, Simpson, Logothetis, & Rainer, 2005). This is a refinement on previous theories which posited that increases in firing rate mediated remembering items in short term memory (Fuster & Alexander, 1971). Recordings of single unit and oscillatory activity during attention have demonstrated that spike-LFP phase locking is higher in prefrontal areas during trials when animals successfully recruited attention and made correct responses compared to error trials (Totah, Jackson, & Moghaddam, 2013). Experimental evidence has shown that incorporating multiple coding schemes, in particular both spike-train patterns and the phase of firing, provides more overall information and increases the fidelity of encoding sensory information (Kayser, Montemurro, Logothetis, & Panzeri, 2009; Montemurro, Rasch, Murayama, Logothetis, & Panzeri, 2008). Taken together, this body of research suggests that oscillations organize spiking activity in a behaviorally relevant manner. Oscillations may provide windows of increased excitability for the successful integration and organization of information encoded by spiking activity.

A recurring theme throughout this dissertation is the importance of state-dependent differences in network dynamics. Different levels of cortical synchrony are often used to classify states, ranging from sleep stages to findings that somatosensory barrel cortex exhibits desynchronized LFP activity during active whisking but higher amplitude low-frequency synchronized activity during quiet wakefulness (Crochet & Petersen, 2006; Poulet & Petersen, 2008). Differences in state, such as during passive and active behavioral conditions, can also modify properties of responses such as spectrotemporal response field in auditory cortex (Fritz, Shamma, Elhilali, & Klein, 2003). Visually evoked firing rate in V1 more than doubled when animals transited from standing to running with no changes in activity in LGN, indicating that state was strictly modulating cortical responses (Niell & Stryker, 2010). Changes in state induced by top-down control, such as through sustained or preparatory attention, also modify neuronal responses (Desimone & Duncan, 1995; Ghose & Maunsell, 2002; Harris & Thiele, 2011). Most studies have found a characteristic increase in responsiveness to attended stimuli (Moran & Desimone, 1985). Greater average

response enhancement was seen in progressively higher cortical hierarchy levels (Maunsell & Cook, 2002). However, task engagement in auditory cortex has also been shown to exert widespread and robust suppression of evoked responses (Otazu, Tai, Yang, & Zador, 2009). Of note, it has also been found that a large range of brain states are compatible with high performance in a relatively simple sensory perception task (Sachidhanandam, Sreenivasan, Kyriakatos, Kremer, & Petersen, 2013). Although state is often determined by ongoing activity in cortex and behavioral responses, other brain areas such as the thalamus are key in controlling cortical state (Poulet, Fernandez, Crochet, & Petersen, 2012).

There is growing evidence that disruption to communication and organization modes discussed here underlie a number of deficits found in neuropsychiatric disorders (Voytek & Knight, 2015). Disruption can result from oscillatory coupling which is too strong, leading to hyper-synchronicity of activity, or oscillatory coupling which is too weak, resulting in disorganized spike timing and lack of information integration. The studies included in this dissertation contribute to our understanding of the involvement of oscillatory activity and network dynamics in organizing cortical activity during rest, sensory processing, and sustained attention. Substantial work is still required to complete our understanding of the functional role of cortical oscillations and overall network dynamics in mediating cognitive and perceptual processing.

REFERENCES

Alkire, M. T. (2008). Loss of effective connectivity during general anesthesia. *International anesthesiology clinics, 46*(3), 55-73. doi: 10.1097/AIA.0b013e3181755dc6

Buzsaki, G., & Moser, E. I. (2013). Memory, navigation and theta rhythm in the hippocampal-entorhinal system. *Nat Neurosci, 16*(2), 130-138. doi: 10.1038/nn.3304

Canolty, R. T., & Knight, R. T. (2010). The functional role of cross-frequency coupling. *Trends Cogn Sci, 14*(11), 506-515. doi: 10.1016/j.tics.2010.09.001

Crochet, S., & Petersen, C. C. (2006). Correlating whisker behavior with membrane potential in barrel cortex of awake mice. *Nat Neurosci, 9*(5), 608-610. doi: 10.1038/nn1690

Desimone, R., & Duncan, J. (1995). Neural mechanisms of selective visual attention. *Annu Rev Neurosci, 18*, 193-222. doi: 10.1146/annurev.ne.18.030195.001205

Felsen, G., & Dan, Y. (2005). A natural approach to studying vision. *Nat Neurosci, 8*(12), 1643-1646. doi: 10.1038/nn1608

Fritz, J., Shamma, S., Elhilali, M., & Klein, D. (2003). Rapid task-related plasticity of spectrotemporal receptive fields in primary auditory cortex. *Nat Neurosci, 6*(11), 1216-1223. doi: 10.1038/nn1141

Fuster, J. M., & Alexander, G. E. (1971). Neuron activity related to short-term memory. *Science, 173*(3997), 652-654.

Ghose, G. M., & Maunsell, J. H. (2002). Attentional modulation in visual cortex depends on task timing. *Nature, 419*(6907), 616-620. doi: 10.1038/nature01057

Harris, K. D., & Thiele, A. (2011). Cortical state and attention. *Nat Rev Neurosci, 12*(9), 509-523. doi: 10.1038/nrn3084

Hudetz, A. G. (2006). Suppressing consciousness: Mechanisms of general anesthesia. *Seminars in Anesthsia, Perioperative Medicine and Pain, 25*, 196-204.

Hudetz, A. G. (2012). General anesthesia and human brain connectivity. *Brain connectivity, 2*(6), 291-302. doi: 10.1089/brain.2012.0107

Hyafil, A., Giraud, A. L., Fontolan, L., & Gutkin, B. (2015). Neural Cross-Frequency Coupling: Connecting Architectures, Mechanisms, and Functions. *Trends Neurosci, 38*(11), 725-740. doi: 10.1016/j.tins.2015.09.001

Kayser, C., Montemurro, M. A., Logothetis, N. K., & Panzeri, S. (2009). Spike-phase coding boosts and stabilizes information carried by spatial and temporal spike patterns. *Neuron, 61*(4), 597-608. doi: 10.1016/j.neuron.2009.01.008

Lee, H., Simpson, G. V., Logothetis, N. K., & Rainer, G. (2005). Phase locking of single neuron activity to theta oscillations during working memory in monkey extrastriate visual cortex. *Neuron, 45*(1), 147-156. doi: 10.1016/j.neuron.2004.12.025

Liebe, S., Hoerzer, G. M., Logothetis, N. K., & Rainer, G. (2012). Theta coupling between V4 and prefrontal cortex predicts visual short-term memory performance. *Nat Neurosci, 15*(3), 456-462, S451-452. doi: 10.1038/nn.3038

Lisman, J., & Buzsaki, G. (2008). A neural coding scheme formed by the combined function of gamma and theta oscillations. *Schizophr Bull, 34*(5), 974-980. doi: 10.1093/schbul/sbn060

Lisman, J. E., & Jensen, O. (2013). The theta-gamma neural code. *Neuron, 77*(6), 1002-1016. doi: 10.1016/j.neuron.2013.03.007

Mante, V., Bonin, V., & Carandini, M. (2008). Functional mechanisms shaping lateral geniculate responses to artificial and natural stimuli. *Neuron, 58*(4), 625-638. doi: 10.1016/j.neuron.2008.03.011

Mashour, G. A. (2004). Consciousness unbound: toward a paradigm of general anesthesia. *Anesthesiology, 100*(2), 428-433.

Maunsell, J. H., & Cook, E. P. (2002). The role of attention in visual processing. *Philos Trans R Soc Lond B Biol Sci, 357*(1424), 1063-1072. doi: 10.1098/rstb.2002.1107

Montemurro, M. A., Rasch, M. J., Murayama, Y., Logothetis, N. K., & Panzeri, S. (2008). Phase-of-firing codign of natural visual stimuli in primary visual cortex. *Current Biology, 18*(5), 375-380. doi: DOI 10.1016/j.cub.2008.02.023

Moran, J., & Desimone, R. (1985). Selective attention gates visual processing in the extrastriate cortex. *Science, 229*(4715), 782-784.

Niell, C. M., & Stryker, M. P. (2010). Modulation of visual responses by behavioral state in mouse visual cortex. *Neuron, 65*(4), 472-479. doi: 10.1016/j.neuron.2010.01.033

Nitsche, M. A., & Paulus, W. (2000). Excitability changes induced in the human motor cortex by weak transcranial direct current stimulation. *J Physiol, 527 Pt 3*, 633-639.

Otazu, G. H., Tai, L. H., Yang, Y., & Zador, A. M. (2009). Engaging in an auditory task suppresses responses in auditory cortex. *Nat Neurosci, 12*(5), 646-654. doi: 10.1038/nn.2306

Poulet, J. F., Fernandez, L. M., Crochet, S., & Petersen, C. C. (2012). Thalamic control of cortical states. *Nat Neurosci, 15*(3), 370-372. doi: 10.1038/nn.3035

Poulet, J. F., & Petersen, C. C. (2008). Internal brain state regulates membrane potential synchrony in barrel cortex of behaving mice. *Nature, 454*(7206), 881-885. doi: 10.1038/nature07150

Sachidhanandam, S., Sreenivasan, V., Kyriakatos, A., Kremer, Y., & Petersen, C. C. (2013). Membrane potential correlates of sensory perception in mouse barrel cortex. *Nat Neurosci, 16*(11), 1671-1677. doi: 10.1038/nn.3532

Siegel, M., Warden, M. R., & Miller, E. K. (2009). Phase-dependent neuronal coding of objects in short-term memory. *Proc Natl Acad Sci U S A, 106*(50), 21341-21346. doi: 10.1073/pnas.0908193106

Tort, A. B., Rotstein, H. G., Dugladze, T., Gloveli, T., & Kopell, N. J. (2007). On the formation of gamma-coherent cell assemblies by oriens lacunosum-moleculare interneurons in the hippocampus. *Proc Natl Acad Sci U S A, 104*(33), 13490-13495. doi: 10.1073/pnas.0705708104

Totah, N. K., Jackson, M. E., & Moghaddam, B. (2013). Preparatory attention relies on dynamic interactions between prelimbic cortex and anterior cingulate cortex. *Cereb Cortex, 23*(3), 729-738. doi: 10.1093/cercor/bhs057

von Stein, A., & Sarnthein, J. (2000). Different frequencies for different scales of cortical integration: from local gamma to long range alpha/theta synchronization. *Int J Psychophysiol, 38*(3), 301-313.

Voytek, B., & Knight, R. T. (2015). Dynamic network communication as a unifying neural basis for cognition, development, aging, and disease. *Biol Psychiatry, 77*(12), 1089-1097. doi: 10.1016/j.biopsych.2015.04.016